STUDIES OF BIOMASS PYROLYSIS AND GASIFICATION FOR FUEL PRODUCTION

Piyarat Weerachanchai

A Thesis Submitted in Partial Fulfillment of the Requirements for the
Degree of Doctor of Philosophy in Chemical Engineering
Suranaree University of Technology
Academic Year 2009

การศึกษากระบวนการไพโรไลซิสและแก๊สซิฟิเคชันของชีวมวลเพื่อการผลิตเชื้อเพลิง

นางสาวปิยรัตน์ วีระชาญชัย

วิทยานิพนธ์นี้เป็นส่วนหนึ่งของการศึกษาตามหลักสูตรปริญญาวิศวกรรมศาสตรดุษฎีบัณฑิต
สาขาวิชาวิศวกรรมเคมี
มหาวิทยาลัยเทคโนโลยีสุรนารี
ปีการศึกษา 2552

STUDIES OF BIOMASS PYROLYSIS AND GASIFICATION FOR FUEL PRODUCTION

Suranaree University of Technology has approved this thesis submitted in partial fulfillment of the requirements for the Degree of Doctor of Philosophy.

Thesis Examining Committee

(Dr. Terasut Sookkumnerd)
Chairperson

(Assoc. Prof. Dr. Chaiyot Tangsathitkulchai)
Member (Thesis Advisor)

(Dr. Atichat Wongkoblab)
Member

(Asst. Prof. Dr. Suneerat Pipatmanomai)
Member

(Dr. Nittaya Nugranad Milne)
Member

(Prof. Dr. Sukit Limpijumnong)
Vice Rector for Academic Affairs

(Assoc. Prof. Dr. Vorapot Khompis)
Dean of Institute of Engineering

ปิยรัตน์ วีระชาญชัย : การศึกษากระบวนการไพโรไลซิสและแก๊สซิฟิเคชันของชีวมวล
เพื่อการผลิตเชื้อเพลิง (STUDIES OF BIOMASS PYROLYSIS AND GASIFICATION
FOR FUEL PRODUCTION) อาจารย์ที่ปรึกษา : รศ. ดร.ชัยยศ ตั้งสถิตย์กุลชัย,
363 หน้า.

งานวิจัยนี้ศึกษากระบวนการไพโรไลซิสและแก๊สซิฟิเคชันของชีวมวลเพื่อศึกษาความเป็นไปได้ในการนำผลิตภัณฑ์ที่ได้จากทั้งสองกระบวนการนี้มาใช้เป็นแหล่งพลังงานที่มีศักยภาพ ขอบเขตของงานวิจัยนี้ได้ครอบคลุมถึงการวิเคราะห์ทางความร้อนของชีวมวลชนิดต่าง ๆ การศึกษาปัจจัยที่มีผลต่อผลิตภัณฑ์ต่าง ๆ ที่ได้จากกระบวนการไพโรไลซิสแบบใช้อัตราการให้ความร้อนต่ำ การปรับปรุงคุณภาพของน้ำมันชีวภาพที่ได้จากการไพโรไลซิสและการศึกษาปัจจัยที่มีผลต่อคุณภาพของแก๊สที่ได้จากกระบวนการแก๊สซิฟิเคชันด้วยไอน้ำ

ชีวมวลชนิดต่าง ๆ ได้แก่ กากมันสำปะหลัง เนื้อในเมล็ดปาล์มที่บีบน้ำมันออกแล้ว กะลาปาล์ม กะลามะพร้าวและเมล็ดลำไยถูกใช้ในการศึกษากระบวนการไพโรไลซิสด้วยเครื่องปฏิกรณ์แบบเบดนิ่งพบว่า ผลิตภัณฑ์ที่ได้จากกระบวนการไพโรไลซิสสามารถนำไปใช้เป็นเชื้อเพลิงในหลายรูปแบบหรือเป็นวัตถุดิบสำหรับการสังเคราะห์ผลิตภัณฑ์ต่าง ๆ ได้ น้ำมันชีวภาพจากการไพโรไลซิสของเนื้อในเมล็ดปาล์มซึ่งผ่านกระบวนการแยกน้ำแล้วมีศักยภาพเพื่อใช้ทดแทนเชื้อเพลิงปิโตรเลียมได้มากที่สุด เพราะน้ำมันชนิดนี้ให้ค่าความร้อนสูงถึง 40 เมกกะจูลต่อกิโลกรัม และมีช่วงอุณหภูมิของการกลั่นใกล้เคียงกับน้ำมันดีเซลมากที่สุด สำหรับน้ำมันชีวภาพที่ได้จากการไพโรไลซิสของชีวมวลชนิดอื่น ๆ ให้ค่าความร้อนน้อยกว่า อยู่ในช่วง 14-28 เมกกะจูลต่อกิโลกรัม และมีความเป็นกรดมากกว่าโดยมีค่าความเป็นกรด-เบสอยู่ในช่วง 2.1-4.1 สำหรับถ่านที่ได้จากกระบวนการไพโรไลซิสสามารถใช้เป็นเชื้อเพลิงแข็งซึ่งมีค่าความร้อนอยู่ในช่วง 29-35 เมกกะจูลต่อกิโลกรัมและพบว่าถ่านที่ได้จากเนื้อในเมล็ดปาล์มและกะลาปาล์มมีความพรุนสูงซึ่งสามารถนำไปกระตุ้นต่อเพื่อผลิตถ่านกัมมันต์ที่มีพื้นที่ผิวสูงได้ ผลิตภัณฑ์แก๊สที่ได้มีค่าความร้อน 1.14-4.42 เมกกะจูลต่อกิโลกรัมของชีวมวลและกากมันสำปะหลังและเมล็ดลำไยเป็นชีวมวลที่ให้ปริมาณแก๊สและค่าความร้อนของแก๊สสูงกว่าชีวมวลชนิดอื่น ๆ ที่ศึกษา

สำหรับการปรับปรุงคุณภาพน้ำมันชีวภาพที่ได้จากกระบวนการไพโรไลซิสโดยใช้รูปแบบที่แตกต่างกันทั้งหมดสามวิธีพบว่าทำให้คุณภาพของน้ำมันชีวภาพดีขึ้น โดยวิธีแรกน้ำมันชีวภาพที่ได้จากการไพโรไลซิสกากมันสำปะหลังถูกนำมาผสมกับถ่านที่บดละเอียดเพื่อผลิตเชื้อเพลิงแขวนลอย (slurry fuel) ที่ให้ค่าความร้อนสูงขึ้นและมีความเป็นกรดน้อยกว่าน้ำมันชีวภาพของมัน นอกจากนี้ยังคงคุณสมบัติของการไหลซึ่งสามารถนำไปประยุกต์ใช้งานได้เหมือนเชื้อเพลิงเหลวทั่วไป วิธีที่สองใช้การผสมน้ำมันชีวภาพที่ได้จากการไพโรไลซิสกากเนื้อในเมล็ดปาล์มกับน้ำมันดีเซล

และแอลกอฮอล์ช่วยให้ค่าความหนืดและปริมาณกากคาร์บอนของน้ำมันชีวภาพนี้ลดลงได้ และวิธีสุดท้ายทำโดยเปลี่ยนกรดคาร์บอกซาลิกในน้ำมันชีวภาพเป็นเอสเทอร์โดยปฏิกิริยาเอสเทอริฟิเคชันทำให้ความเป็นกรดของน้ำมันชีวภาพมีค่าลดลง

การศึกษาปัจจัยที่มีผลต่อคุณภาพแก๊สที่ได้จากกระบวนการแก๊สซิฟิเคชันของไม้สนโดยใช้ปฏิกรณ์ระบบฟลูอิไดซ์เบดพบว่า ชนิดของวัสดุเบด อุณหภูมิแก๊สซิฟิเคชันและชนิดของแก๊สในการทำปฏิกิริยาส่งผลโดยตรงต่อคุณภาพของแก๊สที่ได้ ผงหินปูนและคอนกรีตเหลือทิ้งซึ่งถูกใช้เป็นวัสดุเบดและผ่านการแคลซิเนชันแล้ว แสดงสมบัติของการเป็นตัวเร่งปฏิกิริยาและตัวดูดซับซึ่งช่วยให้ปริมาณแก๊สและค่าความร้อนของผลิตภัณฑ์แก๊สที่ได้มีค่าเพิ่มขึ้น และลดการปล่อยน้ำมันดินเมื่อเทียบกับการใช้ทรายเป็นวัสดุเบด นอกจากนี้ยังพบว่าเมื่ออุณหภูมิของการแก๊สซิฟิเคชันสูงขึ้นและการใช้ไอน้ำในกระบวนการแก๊สซิฟิเคชันทำให้สามารถผลิตแก๊สซึ่งมีค่าความร้อนสูงขึ้น อย่างไรก็ดี การใช้หินปูนซึ่งผ่านการแคลซิเนชัน ในกระบวนการแก๊สซิฟิเคชันด้วยไอน้ำที่อุณหภูมิของการแก๊สซิฟิเคชันที่สูงจะเพิ่มการแตกหัก การซินเทอริง และการรวมตัวของอนุภาคหินปูนทำให้เกิดการปิดกั้นการไหลของแก๊สได้ ในการแก้ปัญหานี้งานวิจัยนี้ได้ทดลองใช้หินปูนผสมกับคอนกรีตเหลือทิ้งในสัดส่วนที่เท่ากันเป็นวัสดุเบด ซึ่งพบว่าเบดผสมนี้สามารถช่วยลดปัญหาเหล่านี้ได้โดยแก๊สที่ผลิตได้ยังคงให้ค่าความร้อนค่อนข้างสูงและได้ค่าประสิทธิภาพการผลิตแก๊สเท่ากับ 75.88%.

สาขาวิชาวิศวกรรมเคมี ลายมือชื่อนักศึกษา ____________________
ปีการศึกษา 2552 ลายมือชื่ออาจารย์ที่ปรึกษา ______________
ลายมือชื่ออาจารย์ที่ปรึกษาร่วม ____________

PIYARAT WEERACHANCHAI : STUDIES OF BIOMASS PYROLYSIS AND GASIFICATION FOR FUEL PRODUCTION. THESIS ADVISOR : ASSOC. PROF. CHAIYOT TANGSATHITKULCHAI, Ph.D., 363 PP.

BIOMASS/PYROLYSIS/GASIFICATION/ENERGY/
FUEL PROPERTIES/CHEMICAL ANALYSIS

Pyrolysis and gasification of biomasses were investigated in this work to assess the possibility of using derived products as potential clean energy sources. The scope of research work covers thermal analysis of raw materials, studying effects of slow pyrolysis conditions on product yields and properties, improvements of bio-oil properties and studying effects of steam gasification conditions on syngas qualities. Five types of biomass including cassava pulp residue (CPR), palm kernel cake (PKC), palm shell (PS), coconut shell (CS) and longan fruit seed (LFS) were employed in the study of slow pyrolysis in a bench-scale fixed bed pyrolyzer. Products derived from pyrolysis can be used in various forms of energy sources or as valuable feedstocks for further product synthesis. Dewatered PKC bio-oil was the most promising liquid product to substitute a petroleum-based fuel because of its high heating value (40 MJ/kg) and giving boiling range distribution closest to that of diesel fuel. Dewatered bio-oils from pyrolysis of other biomasses had lower heating values varying in range of 14-28 MJ/kg and possessing higher acidity with pH in range of 2.1-4.1. Derived chars can be used as a solid fuel with heating value of 29-35 MJ/kg and the chars derived from PKC and PS showed a characteristic of reasonably high porosity material that could be used for production of good quality activated carbon. Pyrolysis gases possessed certain heating values from 1.14-4.42 MJ/kg-biomass and CPR and LFS gave higher gas yields and heating values of gas product compared with other biomasses.

For bio-oil upgrading, three different methods were successfully tested to improve different undesirable characteristics of the raw bio-oils. The first method involved preparation of slurry from a mixture of CPR oil and its co-product char to improve heat content and acidity of the raw bio-oil and yet maintaining flow properties similar to conventional liquid fuels. The second upgrading method was studied by blending dewatered PKC bio-oil with diesel and alcohol, giving lower values of viscosity and carbon residue content. Finally, the dewatered PS oil possessing high acidity was upgraded by converting its carboxylic acid contents to esters via esterification reaction. Finally, steam gasification of larch wood was performed in a shallow fluidized bed gasifier to study the influence of gasification conditions on properties of derived gas products. Type of bed material, gasification temperature and gasifying agent all played an important role in the steam gasification process. Calcined limestone and calcined waste concrete were capable of acting as both catalyst and adsorbent leading to increased gas yield and cold gas efficiency and lower tar production compared with those derived from using silica sand as bed material. The application of high gasification temperature and use of steam as gasifying agent gave much better gas qualities. However, the use of calcined limestone as a bed material in steam gasification process at a high temperature could enhance attrition, sintering, and agglomeration propensities of the bed material, resulting in blocking of gas flow. Combined use of calcined limestone and calcined waste concrete with equal proportion can mitigate this shortcoming and yet contributed relatively high cold gas efficiency of 75.88%LHV.

School of Chemical Engineering — Student's Signature__________________

Academic Year 2009 — Advisor's Signature _________________

Co-Advisor's Signature ______________

ACKNOWLEDGEMENTS

This thesis would not have been possible if Assoc. Prof. Dr. Chaiyot Tangsathitkulchai, my thesis advisor, has not provided me with the opportunity to undertake a Ph.D program. I felt indebted to his advice and guidance from the very early stage of this research as well as the continued support throughout my study. Thank is also due to my thesis co-advisor, Assoc. Prof. Dr. Malee Tangsathitkulchai for her valuable advice and criticism. My special thanks go to Prof. Dr. Masayuki Horio not only for being an excellent supervisor but also for taking care of my living during the research visit at Tokyo University of Agriculture and Technology (TUAT), Tokyo, Japan.

I would like to thank Dr. Terasut Sookkumnerd, Dr. Nittaya Nugranad Milne Asst. Prof. Dr. Suneerat Pipatmanomai and Dr. Atichat Wongkoblab for their many valuable comments and suggestions as thesis defense committee.

I am grateful to all of the lecturers at Suranaree University of Technology (SUT) for their educating. Also, my deep appreciation goes to all of the academic members in the School of Chemical Engineering, Assoc. Prof. Dr. Chaiyot Tangsathitkulchai, Asst. Prof. Dr. Chalongsri Flood and Assoc. Prof. Dr. Adrian E. Flood, Asst. Prof. Dr. Ratanawan Kiattikomol, Dr. Guntima Sirijeerachai, Dr. Terasut Sookkumnerd and Dr. Atichat Wongkoblab, not only for a good background of Chemical Engineering but also their encouragement and support.

During the course of this work, I was assisted by Mr. Saran Dokmaikul for guidelines of using laboratory equipment, Mrs. Amporn Ladnongkun for her skillful secretarial work and all of friends in the School of Chemical Engineering for sharing the experiences of experiments and graduate student life. Thanks are also extended to all the members of Horio laboratory and friends for assisting me during my time in Japan.

This thesis would not have been completed without the supports by SUT and TUAT, for the equipments required for the research. More importantly, I would like to acknowledge the financial support from the Royal Golden Jubilee Program (RGJ) of Thailand Research Fund (TRF) through the scholarship number 1.C.TS/46A.1.

Finally, I would like to express my gratitude to my family and friends. Their support, encouragement, quiet patience and unwavering love have been of great benefit to me over the course of this research.

Piyarat Weerachanchai

TABLE OF CONTENTS

Page

TABLE OF CONTENTS (Continued)

Page

TABLE OF CONTENTS (Continued)

Page

TABLE OF CONTENTS (Continued)

Page

TABLE OF CONTENTS (Continued)

TABLE OF CONTENTS (Continued)

Page

TABLE OF CONTENTS (Continued)

TABLE OF CONTENTS (Continued)

Page

TABLE OF CONTENTS (Continued)

Page

TABLE OF CONTENTS (Continued)

Page

TABLE OF CONTENTS (Continued)

Page

TABLE OF CONTENTS (Continued)

Page

LIST OF TABLES

Table **Page**

LIST OF TABLES (Continued)

LIST OF TABLES (Continued)

Table **Page**

LIST OF TABLES (Continued)

Table **Page**

LIST OF FIGURES

LIST OF FIGURES (Continued)

Figure **Page**

LIST OF FIGURES (Continued)

LIST OF FIGURES (Continued)

Figure **Page**

LIST OF FIGURES (Continued)

Figure **Page**

LIST OF FIGURES (Continued)

Figure **Page**

LIST OF FIGURES (Continued)

Figure **Page**

LIST OF FIGURES (Continued)

Figure **Page**

SYMBOLS AND VIATIONS

A = constant for Andrade equation
= frequency or pre-exponential factor, s^{-1}
= shear area, m^2
AAD = value of absolute average deviation
Al = alcohol (ethanol or butanol)
B = constant for Andrade equation
BET = Brunauer-Emmett-Teller equation
Bu = butanol
C = constant for Andrade equation
CCR = conradson carbon residue
CHP = combined heat and power
CPR = cassava pulp residue
CS = coconut shell
D = diesel
$D_{3,2}$ = volume-surface mean diameter, µm
DTG = first derivative curves
E = activation energy, kJ/mol
Et = ethanol
F = shearing force, N
FCC = fluidized catalytic cracking
G_{ij} = interaction parameter

SYMBOLS AND ABBRVIATIONS (Continued)

HHV = higher heating value

IGCC = integrated gasification combined cycle

IPCC = integrated pyrocycling combined cycle

k = rate constant

= size modulus

κ = consistency index, Pa·s

K_a = acid-ionization constant

L = calcined limestone

LFS = longan fruit seed

LHSV = liquid hourly space velocity

LHV = lower heating value

m = distribution modulus

m_f = final char yield

m_{f1} = final mass fractions of the first component

m_{f2} = final mass fractions of the second component

m_i = mass fraction or volume fraction of component

M = mass fractions of total residual weight

M_1 = residual weight of the first component

M_2 = residual weight of second component

MeOH = methanol

n = flow index

= reaction order

SYMBOLS AND ABBREVIATIONS (Continued)

N = total number of data points.

= number of experiment data

= number of atom

NA = Not analyzed

ND = Non detectable

N_{crit} = critical bob (inner cylinder) speed for the onset of turbulent flow

N_i = number of carbon atoms for component i

N_j = number of carbon atoms for component j

PAH = polycyclic aromatic hydrocarbon

PK = palm kernel bio-oil

PKC = palm kernel cake

PS = palm shell or palm shell oil

$P(x)$ = cumulative weight fraction less than a sieve size

R = universal gas constant, $\frac{J}{K \cdot mol}$

R = alkyl group

R_b = bob radius, m

S = bob-to-cup radius ratio

$SSRE$ = sum of square of relative error

t = time, s or min

T = absolute temperature, K

TG = weight remaining data

SYMBOLS AND ABBREVIATIONS (Continued)

U = weight fraction of raw material

U_0 = superficial gas velocity, m/s

U_{mf} = minimum fluidizing velocity, m/s

ν_i = volume fraction

V = flow velocity, m/s

$V_{KOH\text{-}cat}$ = volume of 0.1 M KOH titrated with water being contacted with pure catalyst, cm^3

$V_{KOH\text{-}raw}$ = volume of 0.1 M KOH titrated with the mixture of raw bio-oil and methanol, cm^3

$V_{KOH\text{-}upgraded}$ = volume of 0.1 M KOH titrated with the upgraded bio-oil after esterification, cm^3

$V_{NaHCO3\text{-}raw}$ = volume of 0.1 M $NaHCO_3$ titrated with the mixture of raw bio-oil and methanol, cm^3

W = actual weight of sample, mg

= weight fraction of solid char

W_0 = initial weight of sample, mg

WC = calcined waste concrete

W_f = final weight of sample, mg

x = stoichiometric coefficient

x_i = mole fraction

$X_{upgraded}$ = esterification conversion of upgraded bio-oil

y = stoichiometric coefficient

SYMBOLS AND ABBREVIATIONS (Continued)

Z = weight fraction of intermediate

%LHV = percentage of cold gas efficiency

α = residual weight fraction

$(\alpha_{exp})_i$ = experimental value for calculation of *SSRE*

$(\alpha_{cal})_i$ = calculated value for calculation of *SSRE*

β = constant heating rate, K/s

γ = shear rate or velocity gradient, s^{-1}

η = kinematic viscosity, mm^2/s

η_B = kinematic viscosity of blend, mm^2/s

η_i = kinematic viscosity of pure component *i,* mm^2/s

φ_B = property of the blend

φ_{Cal} = predicted value of the property

φ_{Exp} = experimental value of the measured property

φ_i = property of pure component

μ = coefficient of viscosity, Pa·s

μ_0 = limiting viscosity at zero shear rate, Pa·s

μ_a = apparent viscosity, Pa·s

μ_B = dynamic viscosity of mixture, Pa·s

μ_i = dynamic viscosity of pure *i* component, Pa·s

μ_L = medium viscosity, Pa·s

μ_s = slurry viscosity, Pa·s

SYMBOLS AND ABBREVIATIONS (Continued)

μ' = Bingham plastic viscosity, Pa·s

μ_∞ = limiting viscosity at infinite shear rate, Pa·s

ρ' = slurry density, kg/m^3

τ = shear stress, Pa

τ_o = yield stress, Pa

CHAPTER I

INTRODUCTION

1.1 Rationale of the Study

Nowadays increasing in energy demand but with dwindling supply of fossil fuel and in particular the price instability of petroleum-based fuels have threatened the sustainable world economic growth. Statistical review of world energy has demonstrated an increase of energy demand for all primary energy sources (oil, natural gas, nuclear energy, hydroelectricity and coal) with a projection of an increase from 8,888.5 million tonnes oil equivalent in 1998 to 11,294.9 million tonnes oil equivalent in 2008 (BP plc, 2009). Of these energy sources, oil remains the world's dominant fuel holding the leading share of consumption in almost all regions, though its market has steadily been lost to coal and natural gas in recent years (BP plc, 2009). However, burning of fossil fuels has caused the largest contribution of greenhouse effect due to CO_2 emission (Global Warming, 2007). The concern over global warming and climate changes has stimulated a search for alternative forms of energy that are renewable and environmentally friendly (Energy Information Administration, 2009). There are various forms of renewable energy that are abundantly available, including wind, solar, biomass, waste materials, geothermal, tidal wave, etc. All forms of renewable energy are an important contributor to the heat and power generation. The exploitation of these energy sources are growing in different parts of the world and its potential depends on such factors as energy policy target, renewable energy market, technology development and geographical regions (REN21, 2009).

As to biomass, it is a potentially important source of renewable energy in agriculture countries because of abundant supply and low prices. Biomass can be utilized in a number of ways such as direct combustion in boilers and furnaces, production of fuel gas by gasification for use as fuel in engines and vehicles or generation of electricity, and production of liquid bio-fuels (Babu, 2008). Thailand is an agriculture-based country that has a variety of agricultural products. The major ones are sugar cane, paddy, oil palm, maize, cassava, mungbean, soybean, and coconut residue. Their residues left after processing are plentiful and thus can be used as a viable source for energy production. Table 1.1 shows annual outputs of major crops, and amount of residue generated and used as a source of energy. From ten main agriculture products that have been assessed in year 2007, only 20 tonnes out of 87 tonnnes of these biomass residues were used as fuel with small amount of them being used for other purposes. Therefore, about 67 million tonnes of agriculture residues were not utilized (Srisovanna, P., 2004; Office of Agricultural Economics, 2009).

Table 1.1 Estimation of agricultural residues potential in year 2007 (Srisovanna P., 2004; Office of Agricultural Economics, 2009).

Major crops	**Crop output (ktonnes)**	**Types of residue**	**Residue ratio**	**Total amount of residue (ktonnes)**	**Energy use factor**	**Amount of residue used for energy (ktonnes)**
Sugar cane	64,365	bagasse	0.29	18,666	0.793	14,802
		top & trashes	0.30	19,310	-	-
Paddy	32,099	husk	0.23	7,383	0.507	3,743
		stalk	0.45	14,445	-	-
Maize	3,661	corn cob	0.27	988	0.193	191
Cassava	26,916	stalk	0.09	2,422	-	-
Palm Oil	6,390	empty bunches	0.43	2,748	0.030	82
		fiber	0.15	959	0.858	823
		shell	0.05	320	0.588	188
		frond	2.604	16,640	-	-
		male bunches	0.233	1,489	-	-
Coconut	1,722	husk	0.362	623	0.289	180
		shell	0.160	276	0.413	114
		bunches	0.049	84	0.144	12
		frond	0.225	387	0.159	62
Ground nut	54	shell	0.323	17	-	-
Cotton	15	stalk	3.232	48	-	-
Soybean	204	stalk, leave,shell	2.663	543	0.007	4
Sorghum	56	leave and stem	1.252	70	0.118	8
Total residues 135.5 (million tonnes)				87,418	-	20,209

A number of processes to produce energy from biomass are available through thermal conversion processes of combustion, gasification and pyrolysis as well as microorganism fermentation for production of alcohols and gas fuels (Demirbas, 2009). Of these processes, pyrolysis and gasification are most promising alternative routes to convert biomass to power/heat generation and production of transportation fuels and chemical feedstock (Pyne IEA Bioenergy, 2005). Pyrolysis is a viable process for efficient and economical transformation of biomass into solid char, bio-oil and gases. Especially, liquid product or bio-oil from pyrolysis process shows promise to be used as a liquid fuel due to its ease of handling, storage and transportation (Karaosmanoğlu *et al.*, 1999). Being more flexible than the direct combustion process, biomass gasification can be directly utilized in external and internal combustion engines or it can be converted via chemical processes to provide synthetic chemicals or liquid fuel. In addition, this process has added advantages of being a clean process (low emission of sulfur, nitrogen oxides, furan and dioxin compounds and particulates), high thermal efficiency and a good degree of control (Renewable Energy Technologies, 2001; Rezaiyan and Cheremisinoff, 2005).

Among various types of pyrolysis processes, fast pyrolysis is most commonly used to obtain high yield of liquid bio-oil (Meier and Faix, 1999). Nonetheless, the complexity of fast pyrolysis process that requires various auxiliary process technologies causes the increased cost of construction and operation. For this reason, the search for a less complicated type of pyrolysis should be a better alternative. Slow pyrolysis process which is capable of providing three simultaneous useful products (bio-oil, char and gases) plus its simpler operation and lower construction cost are the main impetus for studying slow pyrolysis in a fixed-bed mode in the present study. Various potential biomasses left from processing plants including cassava pulp residue, palm kernel cake, palm shell, coconut shell and longan fruit seed were chosen as starting materials for production of renewable fuels or valuable products via this pyrolysis process. The effects of pyrolysis conditions on product yields and properties were thoroughly examined. However, bio-oil derived from pyrolysis process shows undesirable fuel properties for applying in common combustion systems. Thus, study of various upgrading methods to improve bio-oil properties was also investigated.

In the study of biomass gasification, a number of previous works have been concentrated on optimizing gasification conditions to achieve high quality gas products for various applications. However, high tar emission is a major problem for using biomass as a precursor in the gasification process (El-Rub *et al.*, 2004; Han and Kim, 2008). Steam gasification has been known as a viable process to produce gaseous fuel with relatively high H_2 content and is highly effective for tar reduction and control (Corella *et al.*, 1991; Franco *et al.*, 2003; Kubiak and Muhlen, 1998). To enhance the efficiency of steam gasification, a search for effective catalysts should be a topic of research interest. Waste concrete abandoned from the disposal of residential structures was proposed in this study as a potential bed material in a steam gasification process. Containing active composition of CaO, waste concrete is expected to reduce tar emission and increase the yield of produced gases. In this work, the effects of all important gasifying conditions on distribution and properties of gasification products for steam gasification of larch wood were experimentally studied in a bubbling atmospheric fluidized-bed reactor.

1.2 Research Objectives

The overall objective of this thesis is to study pyrolysis and gasification processes for converting biomasses to potential fuels. The research scheme includes thermal analysis of raw materials, studying effect of process conditions on product yields and properties of products from pyrolysis and gasification processes as well as studying various upgrading techniques for improvement of bio-oil properties. The specific objectives of this research are as follows.

- To investigate the kinetic characteristics of thermal decomposition of various biomasses in a non-isothermal pyrolysis mode using thermogravimetric analysis (TGA).
- To study the influence of pyrolysis conditions on yields and physicochemical properties of pyrolysis products in a tubular fixed-bed reactor.
- To upgrade the qualities of bio-oils by blending the bio-oil with char to form a slurry fuel, preparing a mixture of bio-oil-diesel-alcohol and reducing bio-oil acidity through an esterification process.
- To study steam gasification of biomass performed in a bubbling fluidized bed reactor using calcined waste concrete as an alterative bed material and also study the effect of gasification conditions on gas yields and compositions.

1.3 Scope and Limitations

1.3.1 Characterizations and Pyrolysis Kinetic Studies of Raw Biomass Materials

1.3.1.1 Various biomasses including cassava pulp residue, palm kernel cake, palm shell, coconut shell and longan fruit seed were used as raw materials for pyrolysis studies and were characterized for their proximate analysis, elemental analysis and physical properties such as bulk and true densities and calorific values.

1.3.1.2 Non-isothermal pyrolysis characteristics of biomass raw materials were investigated in a thermogravimetric analyzer (TGA). The effects of biomass type, particle size and heating rate on pyrolysis decomposition behaviors were studied and the pyrolysis behaviors of cassava pulp residue at different heating rates and particle sizes were also tested with five different kinetic models.

1.3.2 Studying the Influence of Slow Pyrolysis Conditions and Product Characterizations

1.3.2.1 Slow pyrolysis studies of five biomasses including cassava pulp residue, palm kernel cake, palm shell, coconut shell and longan fruit seed were carried out in a fixed-bed reactor. The effect of pyrolysis conditions including biomass type, pyrolysis temperature, particle size, N_2 gas flow rate and heating rate on product yields of gas, bio-oil and char products were examined.

1.3.2.2 The derived products including solid (char), liquid (bio-oil) and gas from pyrolysis of various biomasses were characterized for their physicochemical properties. Pyrolysis liquids were analyzed for chemical functional groups by Fourier Transform Infrared Spectroscopy (FTIR), chemical compositions by Gas Chromatography-Mass Spectrometry (GC-MS), elemental analysis and fuel properties. Solid chars were examined for proximate and ultimate analyses, bulk and true densities, calorific value and porous properties. Finally, gas products were identified and quantified by Gas Chromatography (GC) and their heating values were determined.

1.3.3 Bio-oil Upgrading with Three Simple Methods for Three Bio-Oils

1.3.3.1 Rheology and fuel properties of char-bio-oil slurries - Bio-oil from pyrolysis of cassava pulp residue possessing single transparent phase of aqueous solution was used as a suspending medium for slurry preparation. The effects of solid concentration, particle size, temperature and shearing time on rheological behavior and fuel properties of the prepared slurries were examined and the rheological data were fitted by power law model with yield stress. Moreover, slurries prepared from palm shell oil and char were also studied to examine the effect of slurry type on the rheological behavior.

1.3.3.2 Phase behaviors and fuel properties of bio-oil-diesel-alcohol blends - High viscosity and high carbon residue content of dewatered palm kernel oil was proposed for studying the preparation of a blend of bio-oil-diesel-alcohol. Phase stability and fuel properties of binary system of bio-oil-alcohol and ternary system of bio-oil-diesel-alcohol were investigated. Furthermore, to estimate fuel properties of the fuel mixtures, Kay’s mixing rule, modified Grunberg-Nissan equation and Andrade equation were applied for this study.

1.3.3.3 Esterification of bio-oil and alcohol by acid catalysts - Dewatered palm shell oil which has high acidity and moderate heating value was upgraded by esterification process using acid catalysts. The effects of reaction temperature and time, types of alcohol and catalyst, amount of catalyst and weight ratio of alcohol and carboxylic acids in bio-oil on esterification conversion were studied and basic fuel properties of upgraded oils were measured.

1.3.4 Studying Effects of Gasifying Conditions and Bed Materials on Fluidized-Bed Steam Gasification of Wood Biomass

The study of steam gasification of biomass (larch) was performed in a bubbling fluidized bed reactor. Calcined waste concrete left from remnants of the residential structures was suggested as a promising bed material for steam gasification process. The influence of gasifying conditions (bed material type, temperature and gasifying agent) on gas yields and compositions were investigated. Moreover, the ability of CO_2 adsorption and physical deterioration of bed material at the end of gasification operation were also examined.

1.4 References

Babu, B. V. (2008). Biomass pyrolysis: a state-of-art review. **Biofuels, Bioproducts and Biorefining** 2: 393-414.

BP plc (2009). **BP Statistical Review of World Energy**. UK: Beacon Press.

Corella, J., Aznar, M., Delgado, J., and Aldea, E. (1991). Steam gasification of cellulosic wastes in a fluidized bed with downstream vessels. **Industrial Engineering and Chemistry Research** 30 (10): 2252-2262.

Demirbas, A. (2009). Biorefineries: Current activities and future developments. **Energy Conversion and Management** 50 (11): 2782-2801.

El-Rub, Z., Bramer, E., and Brem, G. (2004). Review of catalysts for tar elimination in biomass gasification processes. **Industrial & Engineering Chemistry Research** 43 (22): 6911-6919.

Energy Information Administration (2009). Annual energy outlook 2009 with projections to 2030 [On-line]. Available: **www.eia.doe.gov/oiaf/aeo/.**

Franco, C., Pinto, F., Gulyurtlu, I., and Cabrita, I., (2003). The study of reactions influencing the biomass steam gasification process. **Fuel** 82 (7), 835-842.

Global Warming (2007). Global Warming Causes [On-line]. Available: **http://www.globalwarming.org.in/**.

Han, J., and Kim, H. (2008). The reduction and control technology of tar during biomass gasification/pyrolysis: An overview. **Renewable and Sustainable Energy Reviews** 12 (2), 397-416.

Karaosmanoğlu, F., Tetik, E., and Göllü, E. (1999). Biofuel production using slow pyrolysis of the straw and stalk of the rapeseed plant. **Fuel Processing Technology** 59 (1): 1-12.

Kubiak, H., and Muhlen. H. J. (1998). Gas and electricity production from waste materials and biomass via allothermal gasification. In Kopetz, H., Weber, T., Palz, W., Chartier, P., and Ferrero, GL. (eds.). **Biomass for Energy and Industry** (Paper No. P.9.55). Proceedings of 10th European Conference and Technology Exhibition, Wurzburg.

Meier, D., and Faix, O. (1999). State of the art of applied fast pyrolysis of lignocellulosic materials-a review. **Bioresource Technology** 68 (1): 71-77.

Office of Agricultural Economics (2009). Agricultural Statistics [On-line]. Available: **http://www.oae.go.th/oae_report/stat_agri/main.php**.

Pyne IEA Bioenergy (2005). Applications [On-line]. Available: **http://www.pyne.co.uk/?_id=1**.

REN21 (2009). **Renewables Global Status Report: 2009 Update**. Deutsche Gesellschaft für Technische Zusammenarbeit (GTZ) GmbH.

Renewable Energy Technologies (2001). Biomass gasification [On-line]. Available: **http://www.cogeneration.net/biomass_gasification.htm**.

Rezaiyan, J. and Cheremisinoff, N. P. (2005). **Gasification technologies: a primer for engineers and scientists**. United State of America: Taylor & Francis Group.

Srisovanna, P. (2004). Thailand's Biomass Energy [On-line]. Available: **http://www.cogen3.net/doc/countryinfo/thailand/ThailandBiomassEnergy_report.pdf**.

CHAPTER II

GENERAL BACKGROUND

2.1 Biomass

Biomass is a renewable and alternative energy source. It can be utilized in many applications including direct combustion for heat and power generation, conversion by pyrolysis to liquid product for use as a liquid fuel or as a starting feedstock for recovering an array of valuable chemicals and production of syngas by process of gasification. The advantages of using biomass are numerous, for example, it is an environmentally friendly fuel, abundantly available on earth, low price in agricultural-based countries, and free from net carbon dioxide emission.

Biomass is defined as any organic matter of cellulosic or ligno-cellulosic matter which mainly consists of carbon, hydrogen, oxygen and nitrogen. It encompasses trees, plants and associated residues; plants fiber, poultry litter and animal wastes, industrial wastes, and municipal solid wastes (American Bioenergy Association, 2002).

2.1.1 Composition of Biomass

Biomass is very complex in composition consisting of many components. The three major components are cellulose, hemicellulose and lignin.

2.1.1.1 Cellulose

Cellulose is a polysaccharide having the general formula $(C_6H_{10}O_5)_n$ and it is a major component of wood with an average molecular weight ranging from 5,000-100,000 (Balat *et al.*, 2009). Cellulose is found in large amounts in nearly all plants. It constitutes approximately 40-60% of the dry substance in most wood species. Cellulose is the main component of plant cell walls and it is the basic building block for many textiles and paper. Cellulose is not only insoluble in water but also insoluble in most solvents and gives a low accessibility to acid and enzymatic hydrolysis (Balat *et al.*, 2009; Yaman, 2004). Monomeric component of cellulose is a homopolysaccharide of β-D-glucopyranose units which are linked together by (1-4)-glycosidic bonds (Figure 2.1). These groups form many hydrogen bonds with OH groups on adjacent chains. The chains also pack regularly in places to form hard, stable crystalline regions that give the bundled chains even more stability and strength (Sjostrom, 1993).

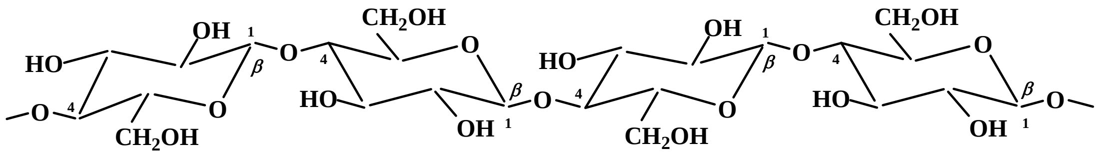

Figure 2.1 Structure of cellulose; linear chains of glucose linked by b-Glycosidic bonds (Sjostrom , 1993).

2.1.1.2 Hemicellulose

Hemicellulose is a term used to refer to a wide variety of heteropolysaccharides. The general formula is $(C_5H_8O_4)_n$ (Yaman, 2004). Hemicellulose consists of shorter repeating saccharide monomers (~150) than that of cellulose and highly branched chains of sugars (Balat *et al.*, 2009). The sugar composition varies with the plant species. It contains five-carbon sugars (usually D-xylose and L-arabinose) and six-carbon sugars (D-galactose, D-glucose and Dmannose) and uronic acid. The amount of hemicelluloses in dry wood is usually between 20 and 30% (Sjostrom, 1993). Hemicellulose acts as a supporting material in the cell walls in the same way as cellulose. The structure of hemicelluloses in the softwoods and hardwoods are different. Hemicellulose structure of softwood and hardwood are exemplified in Figures 2.2 (a) and (b), respectively. Hemicellulose is amorphous, and relatively easy to hydrolyze into its constituent sugars. It is also soluble in dilute alkali solutions (Yaman, 2004).

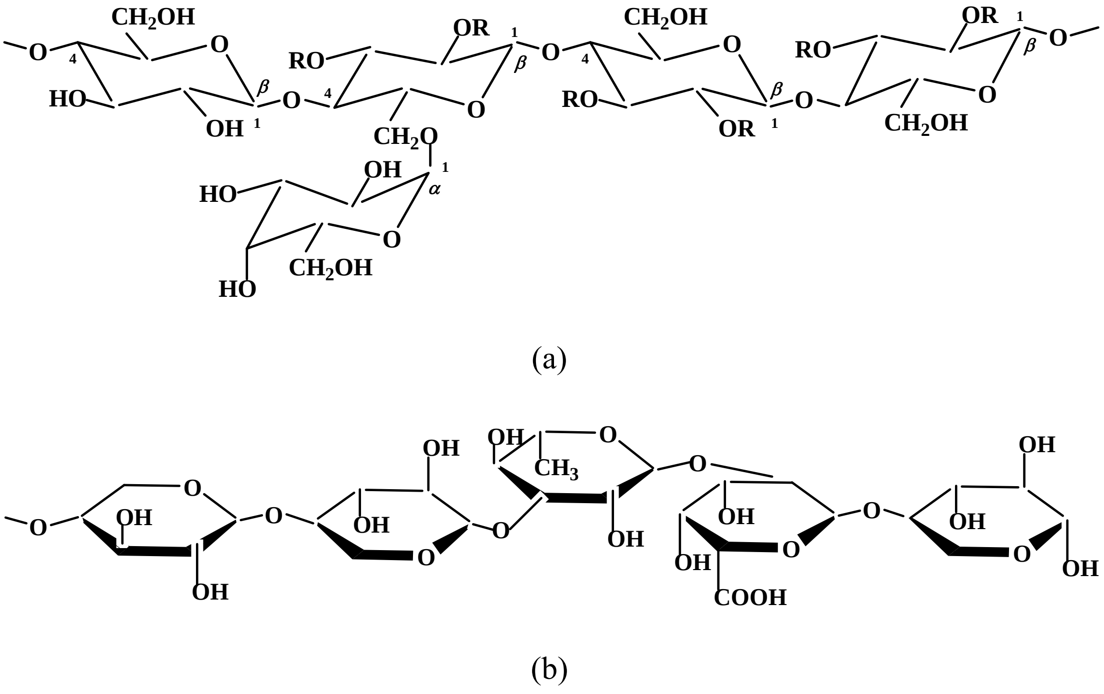

(a)

(b)

Figure 2.2 Structure of hemicellulose, (a) for softwood and (b) for hardwood (Sjostrom, 1993).

2.1.1.3 Lignin

Lignin is the second most abundant organic material on earth after cellulose. The strength of wood is a result of lignin, which makes up about one-quarter to one-third of the mass of dry wood. It is polymer of complex cross-linked phenolic compounds of which basic structural element is phenylpropane unit (Lemeune, 2005). Lignin is formed by removal of water from sugars to create aromatic structures. It is very suitable for production of oil because of its aromatic character and low oxygen content. Lignin cannot be depolymerized by hydrolysis (Yaman, 2004) and cleavage of the principal bonds in lignin requires oxidation (Jeffries, 1995). A general structure of lignin is shown in Figure 2.3. The typical compositions of various biomasses are presented in Table 2.1 (Demirbas, 2009).

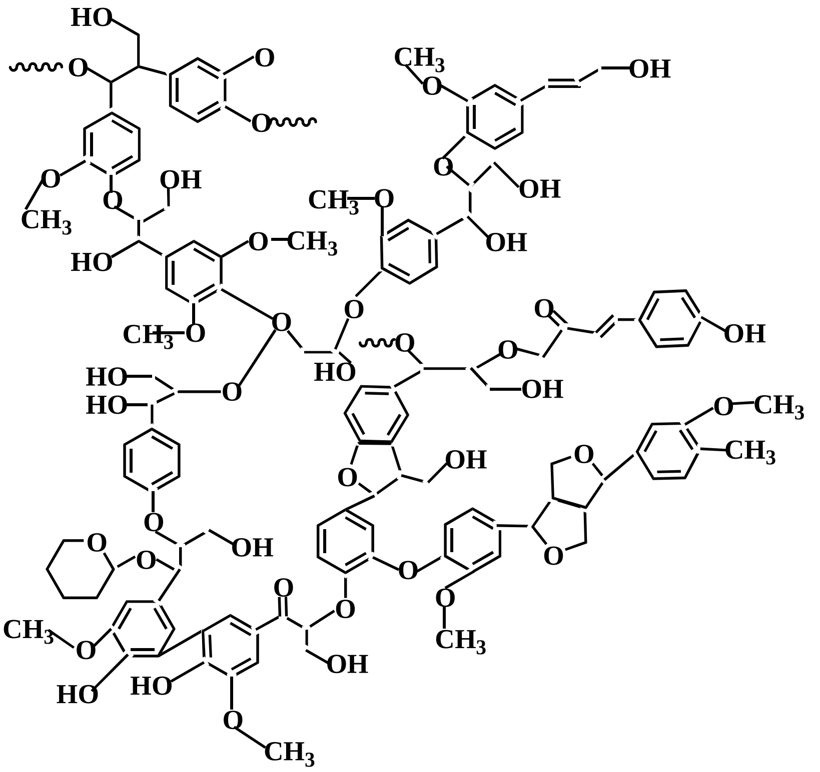

Figure 2.3 A general structure of lignin (Scanton Green Chemistry, 2005).

Table 2.1 Typical compositions (wt%) of some biomasses (Demirbas, 2009).

Spices	Cellulose	Hemicellulose	Lignin
Apricot stone	22.4	20.8	51.4
Beech wood	44.2	33.5	21.8
Birchwood	40.0	25.7	15.7
Hazelnut shell	25.2	28.2	42.1
Legume straw	28.1	34.1	34.0
Orchard grass	32.0	40.0	4.3
Pine sawdust	43.8	25.2	26.4
Rice straw	34.0	27.2	14.2
Spruce wood	43.0	29.4	27.6
Tea waste	31.2	22.8	40.3
Tobacco stalk	21.3	32.9	30.2

2.1.2 Potential Biomass for Pyrolysis Study

In this work, various biomasses were used as starting raw materials. They are agricultural waste or residues left from processing plants and a brief outline of these potential biomasses are as follows.

2.1.2.1 Cassava Pulp Residue

Cassava pulp residue is a solid residue produced from process of starch production. Presently, about 27 million tonnes of cassava are produced annually in Thailand (in 2007) with more than 50% of total production being from the northeast of Thailand, followed by the central and northern regions, respectively (Office of Agricultural Economics, 2009). For each tonne of cassava fed to the starch manufacturing process, about 0.28 tonnes of solid pulp residue is generated as a waste product (Nagatomi *et al.*, 2006). This implies that about 7.56 million tonnes of cassava pulp residue are produced each year. Cassava tubers comprise about 20-30% starch which is distributed in the cellulose matrix (Nanda *et al.*, 2005). After processing, cassava pulp residue still contains high starch content with cellulose and hemi-cellulose contributing about 25 and 7 wt%, respectively (Srinorakutara, T., *et al.*, 2006). Almost all of cassava pulp residue is utilized as a low-price carbohydrate source for veterinary food (Wattanachaisaereekul, S., 2001).

2.1.2.2 Palm Shell and Palm Kernel Cake

Palm shell and palm kernel cake are the solid wastes abandoned from palm oil milling processes. Annual output of oil palm fruit is about 6.4 million tonnes and more than 90% is from southern area of Thailand (Office of Agricultural Economics**,** 2009). The demand of palm oil has increased steadily for the manufactures of a variety of edible oils (especially margarines and fats), soap, laundry detergent, personal care products, lubricating greases, etc, as well as for the production of biodiesel (Index Mundi, 2009). According to the national biodiesel development plan, plantation area for oil palm will be doubled from the years 2008-2022 (Department of Alternative Energy Development and Efficiency, 2009). Palm shell and palm kernel cake left over by oil extraction process are estimated to be about 450 and 77 ktonnes per year, respectively (Pansamut, V., *et al.*, 2003). Palm shell is used as a boiler fuel in many industries; it consists of cellulose, hemicellulose and lignin in the proportion of 29.6%, 18.0% and 53.4%, respectively (Wan Daud and Wan Ali, 2004). Palm kernel cake, consisting of 14-35% cellulose, 19-37% hemicellulose and ~12% lignin, is employed in the animal feed factories but its use is rather limited due to low protein contents and its high fiber (Iluyemi *et al.*, 2006; Srinorakutara, T., *et al.*, 2006).

2.1.2.3 Coconut Shell

Approximately 1.7 million tonnes of coconut fruit are produced annually in Thailand and the major harvesting area is equally shared in the central and southern areas, 48.7 and 46.7%, respectively (Office of Agricultural Economics, 2009). Coconut shell which is the waste derived from production of coconut milk is produced around 280 ktonnes per year (Srisovanna, P., 2004; Office of Agricultural Economics, 2009). It is generally used as solid fuel, a good source for activated carbon production or in the manufacture of various crafts products. The shell is relatively similar to hard woods in chemical compositions, though lignin content is higher and cellulose content is lower (Reade Advanced Materials, 1997). Typical compositions of coconut shell are 20-36% of cellulose, 25-49% of hemicellulose and 29-30% of lignin (Kirubakarana, 2009; Wan Daud and Wan Ali, 2004).

2.1.2.4 Longan Fruit Seed

The annual production of longan fruit is about 480 ktonnes per year. It is processed in the form of fresh-, frozen-, canned-, and dried products and is one of the major exported fruit products of Thailand (Office of Agricultural Economics, 2009). 80% of longan production is from the northern area of Thailand and the rest of 16% and 4% are distributed in the central and northeast areas, respectively (Office of Agricultural Economics, 2009). Longan seed is an inner most part of a longan fruit which is round, jet-black and shining. The seed itself consists of two parts, brown kernel of inner seed and the outer thin black hull. It is discharged as solid waste of about 10 ktonnes annually from fruit canneries and is generally disposed by incineration or crushing for use as mulch (Office of Agricultural Economics, 2006).

2.2 Thermal Conversion Processes

Thermal conversion process is a simple route to convert biomass for energy production. It gives significant advantages over a biological conversion process because it gives a faster conversion rate and all components of biomass (cellulose, hemicellulose and lignin) can be used. Moreover, thermal processes encompass various applications; combustion process for producing hot gases used for heat supply and electricity generation, syngas produced from gasification process can be used with the advance gas turbines or fuel cells and pyrolysis liquid from biomass pyrolysis can be utilized as liquid fuels or valuable chemical feedstocks. (Boateng *et al.*, 2008; Pyne IEA Bioenergy, 2005). Applications of products combustion, gasification and pyrolysis are summarized in Figure 2.4 (Bridgwater and Peacocke, 2003).

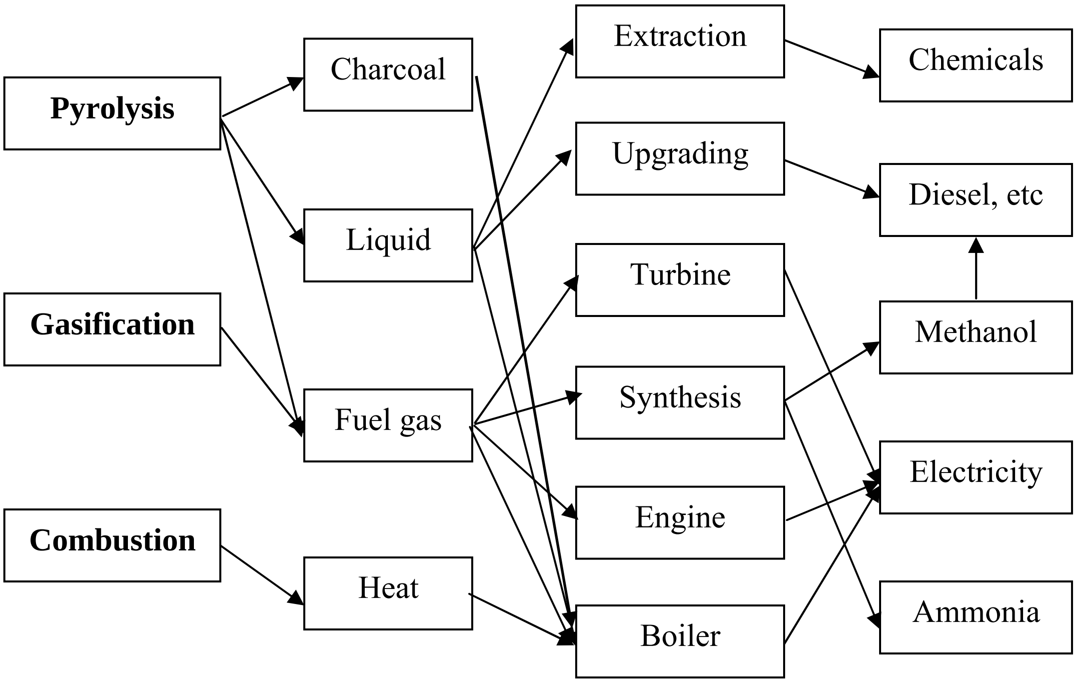

Figure 2.4 Applications of products derived from thermal conversion of biomasses (Bridgwater and Peacocke, 2003).

2.2.1 Combustion

Combustion is a process used to convert the chemical energy stored in biomass by burning biomass in air to provide heat, mechanical power, or electricity, etc (Bridgwater, 2003; Mckendry, 2002). Combustion temperature of biomass to provide hot gases is around 800-1000°C (Mckendry, 2002). Any type of biomass with moisture content less than 50 wt% can be combusted via various items of process equipment such as stoves, furnaces, boilers, steam turbines, turbo-generators, etc (Mckendry, 2002). The scale of biomass combustion process varies from very small scale (e.g. for domestic heating) up to large-scale industrial plants in the range of 100-3000 MW. Overall combustion efficiencies for generating electrical power are relatively low at typically 15% for small plants. Higher efficiency of up to 30% can be achievable for larger plants by applying new technology or co-combustion of coal and biomass (Bridgwater, 2003; Mckendry, 2002). However, the use of combustion process for one heat engine cycle or the stirling cycle has limitation to produce shaft power directly for small power outputs (Mckendry, 2002). In addition, there remains some technical problems of emissions and ash handling for the combustion process to cause high process expenditures (Bridgwater, 2003).

2.2.2 Gasification

Gasification is the conversion of biomass into combustible gas mixture by partial oxidation at high temperatures in the range of 800-900°C (Mckendry, 2002). Main product from the process is gases consisting of CO, CO_2, H_2O, CH_4 and other hydrocarbon gases. The derived gases can be used directly as fuel for power generation or as a starting feedstock for chemical manufacture. The applications of produced gas depend on its qualities which in turn depend on various factors including gasifier configurations, gasification conditions and feedstock compositions (Demirbas, 2009). The gas qualities can be classified by heating value and gas product compositions; gas with low heating value (LHV gas, 3.8-7.6 MJ/m^3) can be utilized for in a gas turbine as integrated gasification combined cycle (IGCC), medium heating value gas (MHV gas, 10.5-16 MJ/m^3) is suitable for synthesis of transport fuels and chemicals such as methanol and ammonia or for fuel cell, and high heating value gas (>21 MJ/m^3) can substitute for natural gas (Rezaiyan and Cheremisinoff, 2005). For generation of electricity, direct combustion and gasification have been known as the most competitive technologies but gasification shows better advantages of higher electrical efficiency and greater potential reduction in CO_2 (Office of Technology Assessment at the German Parliament (TAB), 1997). However, the gasification process is still costly for handling and transportation, thus the fuel gas produced should be used immediately. For power generation, integration of gasification and electricity generation such as integrated gasification combined cycles (IGCC) and integrated gasification fuel cell power system are recommended to offer more economical process (Mckendry, 2002; Rezaiyan and Cheremisinoff, 2005). The details of gasification process and applications of product gas are further elaborated in section of 2.3.

2.2.3 Pyrolysis

This process is defined as the thermal degradation of carbonaceous materials between 400 and 800°C in the complete absence of an oxidizing agent or with such a limited supply that gasification does not occur to an appreciable extent (Bridgwater and Cottam, 1992). Pyrolysis is always the first step in combustion and gasification process where it is followed by total or partial oxidation of the primary products (Bridgwater, 2003). There are five steps taken place during pyrolysis process; (1) temperature increase of solid particle by heat transfer from a heat source, (2) primary pyrolysis reaction with releasing volatiles and forming char at higher temperature, (3) heat transfer between hot volatiles and cooler solid fuel due to the flow of volatile toward cooler solids, (4) condensation of some volatiles in the condenser to produce pyrolysis liquid and (5) autocatalytic secondary pyrolysis reactions of pyrolysis products proceed simultaneously with primary pyrolyis reactions (Babu, 2008). Pyrolysis process has a variety of potentially useful products including solid (char), liquid (tar and an aqueous solution of organic materials) and gaseous products. In addition, it shows superiority to other thermal conversion processes by providing liquid product or bio-oil which has characters of ease of handling and transportation and ready utilization in many heat and power applications. More details of pyrolysis process are given in sections of 2.4-2.6.

2.3 Gasification Process

2.3.1 Gasifier Configurations

As mentioned earlier in section of 2.2.2, gas qualities from the gasification process vary based on a number of factors. Reactor configuration is not only a significant factor affecting gas qualities but also dictates the energy investment of gasification process. Description and operation characteristics of commercial gasifiers are listed in Table 2.2 (Bridgwater, 2003; Rezaiyan and Cheremisinoff, 2005). The survey of gasifier manufacturers in year 2000 has indicated that 75% of gasifiers are occupied commercially by downdraft fixed-bed reactors, 20% is offered by fluidized bed reactors (circulating fluid beds included), 2.5% is updraft fixed-bed reactors and other types are 2.5% (Bridgwater, 2003). Atmospheric downdraft reactor is an attractive gasifier due to its simple, reliable and proven process. This system is suitable for a small plant scaling up to about 1.5 MW_{th}. It is, however, limited by feed flow rate of up to 500 kg/hr and maximum moisture content of feedstock of 35 wt% (Bridgwater, 2003). Updraft gasifier finds less application for power applications. The disadvantages of this process are high tar content in the fuel gas and the maximum scale for a single reactor being around 2.5 MW_e (Bridgwater, 2003). Pressurized reactor is less attractive due to complex installation and operation but it provides the advantage in IGCC because fuel gas compression is not required before supplying into the combustion chamber of a gas turbine. For large scale applications, circulating fluidized-bed gasifier is the most reliable system proven for various feedstocks. It is easy to scale up and still the reliable process even for capacity above 100 MW_{th} but this system is not economical for small-scale plants. Finally, atmospheric entrained bed gasifier is still at a very early stage of development aimed at a much larger capacity (>100 MW_e) (Basu, 2006). The requirement of a very small particle size of feedstock for entrained bed gasifier have caused very low market attractiveness.

Table 2.2 Summary of characteristics of biomass gasifiers (Bridgwater, 2003; Rezaiyan and Cheremisinoff, 2005).

Configuration	Description	Operational characteristics
Downdraft-fixed bed reactor	- Air or oxidizing agent passes downward through the gasifier. - Solid and product gas move downward in co-current mode. - Gasification occurs near bottom of gasifier in a shallow hot reaction zone	- Simple, reliable and proven process for fuels that are relatively uniform in size and have a low content of fines (below 5 mm) - Low tar and high carbon conversion - Scaling-up limited about 500 kg/h feed rate - A maximum feed moisture content of around 35% wet basis
Updraft-fixed bed reactor	- Air or oxidizing agent passes upward through a hot reactive zone near bottom of gasifier. - Solid moves down a vertical shaft and contacts a counter-current upward moving product gas stream.	- Simple, reliable and proven process for fuels that are relatively uniform in size and have a low content of fines (below 5 mm) - Very dirty with high levels of tars - Scaling up limited to around 4 dry t/h feed rate - Good turn-down capability
Bubbling fluid bed	- Fuel is mixed with a hot bed material and they are agitated by fluidizing gas. - Biomass can be fed into the top, bottom or middle of gasifier. - Heat is supplied from preheated bed material and partially oxidation of oxidizing agent and fuel.	- Good temperature control and high reaction rates - High particulates in product gas and moderate tar levels in product gas - Good scaling-up potential to 10-15 dry t/h with high specific capacity and easily started and stopped - Greater tolerance to particle size range - Limited turn-down capability - Applicability of tar cracking catalyst
Circulating fluid bed	- Bed material circulates between gasifier and secondary vessel - Biomass can be fed into the top, bottom or middle of moving bed. - Heat is supplied from preheated bed material and partially oxidation of oxidizing agent and fuel.	- Large minimum size for viability, above around 15 t/h dry feed rate - High cost at low capacity - Difficulty for in-bed catalytic processing
Entrained flow	- Fuel and blast move in co-current flow. - Short residence time, high temperature and fine particles of feedstock are required.	- Simple reactor design - Only potentially viable above around 20 dry t/h feed rate - Costly feed preparation needed for woody biomass - Carbon loss with ash

2.3.2 Gas Cleaning Processes

Besides the desired product gas derived from a gasification process, particulates, tars, entrained soot, sulfur and ash are also contained in the produced gas stream. Figure 2.5 shows the ranges of particulate and tar levels for different gasifier types (Rezaiyan and Cheremisinoff, 2005). The product gas containing undesired components needs to be cleaned. However, the removal requirement of contaminants varies depending on the application, gasifier type and chemical contaminant in the fuel. Gas cleaning processes required for general gasification processes are briefly outlined next.

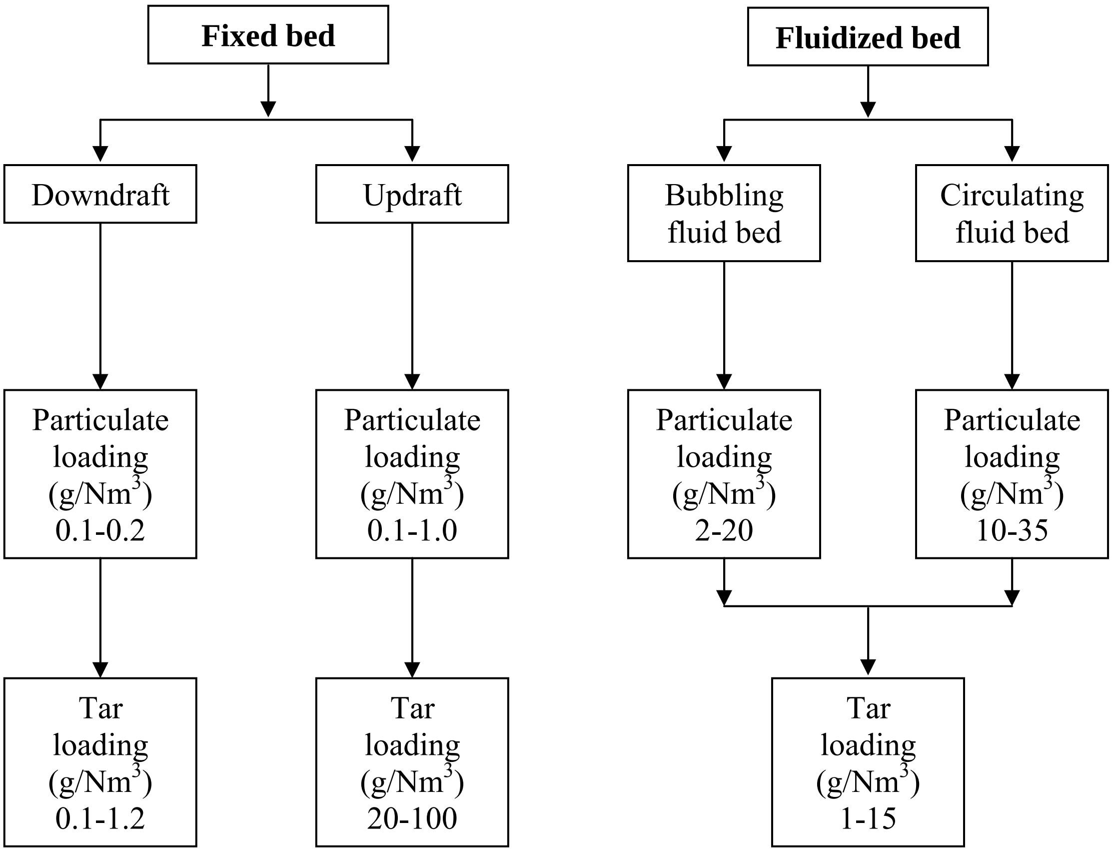

Figure 2.5 Ranges of particulate and tar levels for different biomass gasifiers (Rezaiyan and Cheremisinoff, 2005).

2.3.2.1 Sulfur Removal

Most biomass feedstocks contain low content of sulfur. However, it can damage catalyst in a gas synthetic process or fuel cell system even at a low level. Generally, all sulfur in a gasifier is converted to H_2S in the gasifier. It can be removed employing zinc-based regenerative sorbents operated at temperature up to 650°C (Higman and Burgt, 2008). Moreover, addition of calcined limestone inside the gasifier can capture H_2S to form calcium sulfide (CaS) as Equation (2.1) (Basu, 2006). More than 90% of sulfur is typically removed for an air blown gasifier (Higman and Burgt, 2008).

$$CaO + H_2S \longrightarrow CaS + H_2O \qquad (2.1)$$

2.3.2.2 Tar Removal

Tar is defined as hydrocarbons having higher molecular weight than that of benzene (Basu, 2006). Primary tar is derived from breaking molecular bonds of biomass, further reactions can produce secondary tar at the same temperature and tertiary tar at higher temperature. The pathway of tar formation is described as follows.

$$\underset{400^{\circ}C}{\text{Mixed oxygenates}} \longrightarrow \underset{500^{\circ}C}{\text{Phenolic ethers}} \longrightarrow \underset{600^{\circ}C}{\text{Alkyl phenolics}} \longrightarrow$$

$$\underset{700^{\circ}C}{\text{Heterocyclic ethers}} \longrightarrow \underset{800^{\circ}C}{\text{PAH}} \longrightarrow \underset{900^{\circ}C}{\text{Larger PAH}} \qquad (2.2)$$

Tar remains an important problem for fuel gas quality, in particular for a turbine system and for chemical synthesis. Two basic routes consisting of chemical and physical methods have been suggested to solve this problem (Basu, 2006). For physical methods, tar yield is reduced using various devices such as cyclone, filters, electrostatic precipitators and scrubbers. Catalytic cracking, thermal cracking, plasma reactor and the use of catalytic bed material are attractive options for chemical methods. Calcined dolomite and nickel-based catalysts are applied downstream of gasifier for tar cracking, while olivine, activated clay, bentonite and housebrick are used as bed materials and play the roles of catalyst and adsorbent for tar reduction.

2.3.2.3 Particulate Removal

Particulate matter is mostly removed by cyclones and it is further eliminated by hot or dry filtration or water scrubbing located downstream of the cyclone. For IGCC system, hot gas cleaning techniques that removes particulate matter from the product gas without cooling can improve efficiency of electricity generation, approximately 2% or more (Basu, 2006). There are a number of techniques for the removal of particulate matter at high temperature such as filtration by fabric filter, granular-bed filter and ceramic-barrier filter (Basu, 2006). Of these, ceramic filter in form of candles is the most promising filter that is ready for commercial cleaning process at temperature up to 500°C.

2.3.3 Applications

Applications of product gas derived from gasification processes are listed in Figure 2.6 (Bridgwater, 2003). They can be divided into three different routes including chemicals, synfuels and power (Higman and Burgt, 2008). The use of derived gas as chemical feedstock requires a very specific gas composition. Medium heating value gases derived from steam gasification or oxygen gasification are suitable for synthesis of chemicals due to the absence of diluent nitrogen (Bridgwater, 2003). However, gas product from air gasification containing high amount of nitrogen gas can be utilized in ammonia synthesis process. Generally, 1:3 mole ratio of N_2/H_2 is required for ammonia synthesis. Moreover, urea production using one mole of CO_2 and two moles of ammonia is normally in conjunction with this process (Higman and Burgt, 2008). To synthesize methanol, stoichiometric ratio of $\frac{H_2 - CO_2}{CO + CO_2}$ equal to 2.03 is an optimized synthesis gas composition, while the equivalent mole ratio of H_2 and CO is typical specification to produce oxo-alcohols (Higman and Burgt, 2008).

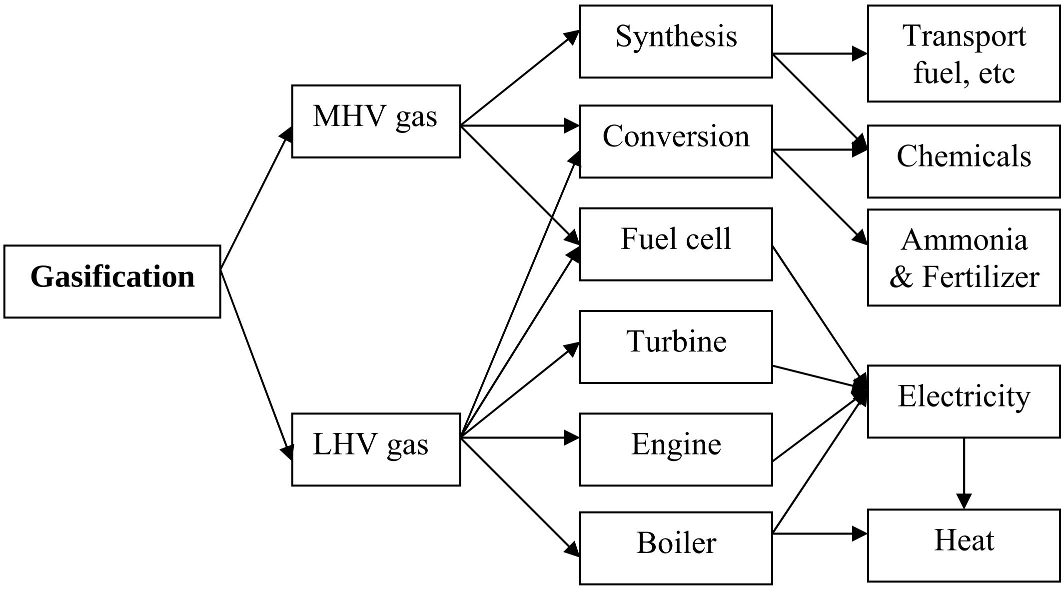

Figure 2.6 Applications for gas from biomass gasification (Bridgwater, 2003).

An attractive application of product gas is the production of ultra-clean designer fuels from Fischer-Tropsch process. A very high gas quality with low impurities such as NH_3, HCN and H_2S is required for this process. There are two different types of Fischer-Tropsch processes including ARGE and Synthol processes (Higman and Burgt, 2008). On ARGE process, synthesis gas with about 1.7 mole ratio of H_2/CO is converted to straight chain olefins and paraffins over cobalt catalyst at temperature of 200°C and pressure of 30-40 bar. The synthetic crude oil can be refined to produce excellent diesel fuel, lube oils, and naphtha (Boerrigter and Rauch, 2005). For direct production of gasoline and aromatic-rich product, 2.54 of H_2O/CO ratio is needed for Synthol process operating at higher temperature of 330-350°C, pressure of 30-40 bar over iron catalyst.

Currently, main application of product gas from biomass gasification is direct or indirect combustion to generate power with co-production of heat (Bridgwater, 2003). Low heating value gas with complex gas composition can be utilized for this application. The most effective application of fuel gas for heat and power generation is co-firing with fossil fuel in a large-scale boiler. Up to 10% of fuel gas co-firing with coal can be used in coal boiler without modifications (Boerrigter and Rauch, 2005). Moreover, the product gas can be fired on a gas engine for applying in combined heat and power (CHP) plants. It was found that product gas from air-blown gasification having calorific values of approximately 5-6 MJ/m^3 showed a satisfactory operation in a modified gas engine (Boerrigter and Rauch, 2005). For electricity production on larger scale, integrated gasification combined cycles (IGCC) is more suitable. This process incorporates gasification process to convert biomass into fuel gas that is used as fuel in a gas turbine for electricity generation. Fuel gas from biomass gasification needs to be carried out at typical pressure of 5-20 bars and temperature of 400-500°C for firing in a gas turbine (Boerrigter and Rauch, 2005). Pressurized gasifier is preferred for IGCC process. However, fuel gas generated from atmospheric gasifier can be applied but it must be pressurized before supplying to the gas turbine. IGCC process provides higher energy efficiency and much lower emission of NO_x, SO_x and particulates compared to conventional combustion processes. The net efficiencies are about 40-50% for a plant of 30-60 MW_e (Mckendry, 2002). Another approach for electricity production is converting pure hydrogen directly into electricity via fuel cells. This process can achieve higher electrical efficiencies compared to simple combustion systems but requires extremely pure gas. Some fuel types such as solid oxide fuel cell (SOFC) can convert other fuel gases such as CO and CH_4, it is thus considered as a suitable fuel cell for converting product gases from biomass gasification (Boerrigter and Rauch, 2005).

2.4 Pyrolysis Process

2.4.1 Classification of Pyrolysis

Pyrolysis process is usually divided according to the mode of heating (temperature and heating rate) and residence time. The pyrolysis processes can be classified into three types as shown in Table 2.3 (Demirbas, 2009), they are conventional pyrolysis or slow pyrolysis, flash pyrolysis and fast pyrolysis. Each individual type permits a production of gas, liquid and solid in significant different proportions (Demirbas, 2009). Conventional slow pyrolysis has been traditionally used to produce charcoal for thousand of years. It is defined as the pyrolysis that occurs under a slow heating rate. The carbonaceous material is slowly heated or held at a constant temperature and vapors produced is continuously removed as they are formed (Demirbas, 2009). Normally, this process is performed in a fixed bed reactor (Goyal *et al.*, 2008). Fast pyrolysis is a process that terminates the secondary conversion of products by high heating rates and rapid quenching of the liquid products with the purpose to produce mainly liquid and/or gas products (Yaman, 2004). For this pyrolysis mode, maximum liquid yield is produced from the conditions of low temperature, high heating rate and short gas residence time, while the main product of gases results from higher temperature, lower heating rate and longer residence time (Goyal *et al.*, 2008). Various reactor types have been applied in the field of fast pyrolysis such as entrained flow reactors, wire mesh reactors, vortex reactors, rotating reactors, etc (Goyal *et al.*, 2008). The commercial pyrolysis processes are currently only operated by circulating fluid-bed system. Furthermore, this process gives relatively low investment cost and high energy efficiency compared with other processes. Flash pyrolysis with the conditions of very high heating rate, short residence time and high temperature is generally used to provide high yield of liquid product. It requires the special reactor configuration to minimize residence time and thus the fairly small particle size of solid fuel should be used for achieving a high heating rate condition. The examples of flash pyrolysis process are solar flash pyrolysis, vacuum flash pyrolysis, rapid thermal process and flash hydro-pyrolysis (Goyal *et al.*, 2008). Comparisons of product distribution and bio-oil properties obtained from flash and slow pyrolysis processes are shown in Table 2.4 (Bridgwater and Cottam, 1992).

Table 2.3 Classification of pyrolysis process (Demirbas, 2009).

Process type	**Heating rate (°C/s)**	**Temperature (°C)**	**Particle size (mm)**	**Time (s)**
Conventional pyrolysis (Slow pyrolysis)	0.01-1	277-627	5-50	300-3600
Fast pyrolysis	10-200	577-977	<1	0.5-10
Flash pyrolysis	>1000	777-1,027	<0.2	<0.5

Table 2.4 Comparison of liquid product characteristics derived from flash and slow pyrolysis (Bridgwater and Cottam, 1992).

Properties	**Ensyn process Flash pyrolysis**	**Alten process Slow pyrolysis**
Products, approximate yields		
Liquid yield, wet, wt% on dry feed	75	64
Liquid yield, dry, wt% on dry feed	65	22
Gas yield, wt% on dry feed	15	18
Char yield, wt% on dry feed	10	18
pH	2.5	2.0
Specific gravity	1.210	1.195
Elemental analysis (moisture free), %		
C	56.4	61.9
H	6.2	6.0
N	0.2	1.05
S	<0.01	0.03
Ash	0.1	1.5
O (by difference)	37.1	29.5
C/H ratio	9.1	10.3
HHV (moisture-free basis), MJ/kg	23	26.3
HHV as produced, MJ/kg	19.3	-
Viscosity (40°C), cP	51	300
Pour point, °C	-23	27
Chemical analysis	not published	not done

2.4.2 Technological Requirements for the Pyrolysis Process

As mentioned in section 2.3.1, pyrolysis processes that are characterized by the modes of heating (temperature and heating rate) and residence time play an important role on distribution of pyrolysis products (solid, liquid and gases). In addition, there are several pyrolysis parameters that can affect the product yields and properties such as reactor configuration, type of feedstock, biomass particle size and sweep gas flow rate. Bridgewater (1999b) has summarized the technological aspects that can influence the products of pyrolysis process as follows.

2.4.2.1 Pyrolysis Reactors

The heart of pyrolysis process is the type of reactors since reactor configuration is not only an important factor in determining the product quantity and quality but it also dictates the process expenditure. Almost all research and development have focused on the type of operation reactors, especially, fast pyrolysis process (Bridgwater, 2003). The most common types of reactor for pyrolysis of lignocellulosic materials are fixed-bed and fluidized-bed reactors. Examples of currently applied pyrolysis reactors and heating method are listed in Table 2.5 (Bridgwater, 1999b). Summaries of characteristics, advantages and disadvantages of commonly used reactors are presented in Table 2.6 (Mohan *et al.*, 2006).

Table 2.5 Pyrolysis reactors and heating methods (Bridgwater, 1999b).

Reactor type	**Method of heating**	**Organization**
Ablative coil	Wall heating	BBC + Castle Capitalc now Enervision
Ablative mill	Wall (disc) heating	Colorado School Mines
Ablative plate	Wall heating	U. Aston, CNRS-Nancy
Ablative vortex	Wall heating	Interchem, NREL
Auger kiln	Wall heating	U. Tubingen, WTC
Circulating fluid bed	In-bed gasification of char to heat sand	CRES + Agric. U. Athens
Cyclone or vortex	Wall heating	CNRS-Nancy
Entrained flow	Combustion products	Egemin, GTRI
	Hot sand	U.Western Ontario
Fixed bed	Combustion products	Bio-Alternative, Chemviron
	Partial gasification	Alten, KTI+Italenergie
	Overfired gas	U. Cardiff
Fluid bed	Heated recycle gas	Dynamotive, INETI, IWC RTI, Union Fenosa, U. Hamburg U. Waterloo, Wellman, Worthing
	Hot inert gas	CPERI, NREL, U. Aston U. Leeds, U. Sassari, U. Stuttgart
	Partial gasification	Alten, Italenergie
	Fire tubes	MTCI
Horizontal bed	Fire tubes	AEIb, Pyrosolb, Wastech
Multiple hearth	Hearth heating	U. Laval
Rotary kiln	Wall heating	Deutsche Babcockb, PKA, Stenaub, Siemens+KWU, Waste Gasb
Rotating cone	Wall and sand heating	U. Twente+BTG+KARA
Stirred bed	Partial gasification	Alten
Transported bed	Recirculated hot sand	Ensyn & at ENEL, VTT, Red Arrow
Vacuum moving bed	Direct contact with hot surface	U.Laval+Pyrovac

Table 2.6 Characteristics, advantages and disadvantages of various commercial pyrolysis reactors (Mohan *et al.*, 2006).

Reactor type	**Method of heating**	**Suggested mode of transfer**	**Operational pyrolysis unit**	**Bio-oil yield (%)**	**Advantages**	**disadvantages**
Fluidized bed reactor	Heated recycle gas/hot inert gas	95% conduction 4% conventional 1% radiation	400 kg/hr at Dynamotive, 250 kg/hr at Welman (U.K.), 20 kg/hr at RTI	75	- Good temperature control - Easy scalability - Well-understood technology	- Requiring of small particle size - Heat transfer to bed proven at large scale
Circulating fluidized bed reactor	Particle gasification/ fire tubes	80% conduction 19% conventional 1% radiation	1000 kg/hr at Red Arrow (Ensyn), 20 kg/hr at VTT (Ensyn)	75	- Good temperature control - Large particle size applicability - Large throughputs - Well-understood technology	- More complexity of hydrodynamics - Finer char derived due to attrition at high velocities - Heat transfer to bed proven at large scale
Rotating cone reactor	Gasification of char to heat sand	95% conduction 9% conventional 1% radiation	120 kg/h at BTG (Netherlands)	65	- Sand and biomass moved by centrifugal force	- Heat transfer to bed proven at large scale - Requiring of small particle size
Vacuum reactor	Wall and sand heating	4% conduction 95% conventional 1% radiation	350 kg/hr at Pyrovac	35-50	- Lower temperature required - Large particle size applicability - No requirement of carrier gas	- Very high residence time - Low liquid yields (35-50% , dry feed basis)
Ablative reactor	Direct contract with hot surface	95% conduction 4% conventional 1% radiation	350 kg/hr at Fortum, Finland	75	- Large particle size applicability - No requirement of carrier gas - More intensive system - Low temperature (<600°C)	- Limitation of reaction rates by heat transfer of the reactor - High cost of scaling due to process controlled by surface area - High investment cost of reactor

2.4.2.2 Heat Supply and Heat Transfer

There are two steps required for heating solid fuel in a pyrolysis reactor namely, heat transfer from reactor to medium and heat transfer from medium to solid fuel. There are two important modes of heat transfer including heat conduction and heat convection which can be controlled by the reactor configuration and operating conditions. The heat transfer modes of various types of reactors are summarized in Table 2.6 (Mohan *et al.*, 2006). The high heat transfer rate is required to heat particles sufficiently quickly and the equipments are designed to achieve the high heat fluxes for matching the high heating rates and endothermic pyrolysis reaction. To approach true fast pyrolysis, heat fluxes of 50 W/cm^2 has been suggested but it is not practicable for a commercial process. Because of poor thermal conductivity of the biomass (0.1 W/mK along the grain, 0.05 W/mK across the grain), the biomass particles have to be very small to fulfill rapid heating rate for producing high liquid yield.

2.4.2.3 Reaction Temperature and Vapor Residence Time

Typical temperatures to provide a maximum liquid yield for fast pyrolysis of wood biomass are 500-520°C. The temperature effect on product yields has been well understood but that on product fuel quality is rather less well understood. The secondary gas/vapor phase history has an important influence on the bio-oil quality. Long residence time (>1 s) of lignin derived fraction may increase depolymerizations to produce a more homogeneous liquid as occurred in an ablative pyrolysis reactor. Secondary reaction of primary product cracking may cause lowering yield of specific products and organic liquids for temperatures higher than 500°C and long vapor residence time. These critical conditions are recommended for the design of commercial reactors in that the vapor residence time should be down to 30 ms to maximize the liquid product yield.

2.4.2.4 Feed Properties

Feedstock is an important parameter affecting quality and quantity of the pyrolysis products. Particle size of solid is limited by heat transfer in a reactor. For example, the maximum particle sizes for fluidized bed and circulating systems should be less than 2 mm and 6 mm, respectively (Bridgwater, 1999b). It has been known that the reduction of particle size has a qualitative influence on the costs in terms of economic and energy efficiency but the available data are not enough to define a penalty for optimizing the proper particle size of these systems. Moreover, moisture content of feedstocks is usually required to be less than 10 wt% to reduce water content in bio-oil since water could provide detrimental effects on stability, viscosity, pH, corrosiveness, and other properties.

2.4.2.5 Liquid Collection System

Commercial liquid recovery system is normally proprietary and its design is specified by individual feedstocks, reactor configuration and desired products. The vapor derived from a pyrolysis process is not the true vapor but it is a mist or fume presenting in an inert gas carrier and this can cause the problems of cooling and condensation. An electrostatic precipitator may be employed to obtain higher liquid yield but it has a problem of arcing during the flow of polar liquid product leading to shorting out of the system. A large-scale process usually applies some type of quick quenching to avoid slow cooling which may lead to the blockage of heavy products in the heat exchanger equipments.

2.4.2.6 Char and Ash Separations

Char separation is a required step for the pyrolysis process. This is because the produced char containing high concentration of alkali metals could be catalytically active to crack organic vapors, producing secondary char and water or to increase ageing rate of tar particle agglomeration during bio-oil storage. There is an upper limit both for amount and particle size of the derived char in bio-oil for certain bio-oil application. Generally, the char product can be separated by cyclones and hot gas filtration but the alkali metal associated with ash in the feedstocks can only be removed by hot gas filtration. The hot gas filtration gives a high quality char free product but the liquid yield is also reduced due to the accumulation of high molecule weight of bio-oil on the filter surface. For liquid filtration, it has proven difficult due to the interaction of char and lignin-derived fraction leading to a gel-like material.

2.5 Pyrolysis Products

2.5.1 Liquid Product

Pyrolysis derived liquid is referred to by many names including pyrolysis oil, bio-oil, bio-crude-oil, bio-fuel-oil, wood liquids, wood oil, liquid smoke, wood distillates, pyroligneous tar, pyroligneous acid, and liquid wood (Bridgwater, 2003). Physicochemical properties of typical crude bio-oils are summarized in Table 2.7 (Oasmaa and Czernik, 1994).

Table 2.7 Physicochemical properties of typical crude bio-oils (Oasmaa and Czernik, 1994).

Physicochemical properties	**Typical value**
Water content (wt%)	15-30
pH	2.0-3.7
Specific gravity	110-1250
Elemental analysis (wt%)	
C	32-49
H	6.9-8.6
O	44-60
N	0-0.2
Ash	0.004-0.3
Lower heating value (LHV) (MJ/kg)	13-18
Viscosity (at 50°C, cP)	13-80
Molecular weight (g/mol)	370-1000
Flash point (°C)	50-100
Pour point (°C)	-36--9
Conradson carbon residue (CCR) (wt%)	14-23

2.5.1.1 Characterization of Bio-oil

(1) Appearance - Typically, the crude pyrolysis oil is a liquid with almost black through dark red-brown, depending on its elemental chemical composition and the presence of micro-carbon which in turn depend on initial feedstock and pyrolysis mode. High nitrogen contents in the liquid can give a dark green tinge bio-oil. The absence of char particles in bio-oil provides a more translucent red-brown color (Bridgwater, 2003).

(2) Odor - The pyrolytic oil has a characteristic odor of acrid and burnt smell. For long exposure time, it can irritate the eyes and nose. Because of low molecular weight of aldehydes and acid, it also results in bad smell.

(3) Chemical Components - Bio-oils comprise more than 300 known compounds which are derived from depolymerization and fragmentation reactions of three basic biomass components; lignin produces generally phenols, eugenols and guaiacols, while cellulose and hemi-cellulose derivatives offer sugars, acetaldehyde and formic acids (Biomass Technology Group, 2003). The distribution of these compounds mostly depends on the type of biomass used and on the process conditions (temperature, residence time, and heating rate profiles). Bio-oil contains a large amount of oxygen, usually 45-50%. The single most abundant bio-oil component is water. The other major groups of compounds being identified are hydroxyaldehydes, hydroxyketones, sugars, carboxylic acids, and phenols (Oasmaa and Czernik, 1994). A large fraction of bio-oil is the phenolic fraction (up to 50 wt%). It consists of relatively small amounts of phenol, eugenol, cresols, and xylenols, and much larger quantities of alkylated (poly-) phenols (so-called water insoluble pyrolytic lignin) (Biomass Technology Group, 2003). Levoglucosan is a sugar anhydride derived from decompositions of cellulose and starch. It can be obtained about 18-33 wt% for pyrolysis of waste newsprint and cotton (Li and Zhang, 2004). Moreover, hydroxy-acetaldehyde, a sugar derivative can present in relatively large amounts in the bio-oil. Components that can also be derived from bio-oil are carboxylic acids; they are the significant chemicals which can cause high corrosiveness to common construction materials. Finally, furfural and furfural alcohol are presented in small amounts. The typical chemical compositions of fast pyrolysis liquids are given in Table 2.8 (Balat *et al.*, 2009).

Table 2.8 Chemical compositions of typical fast pyrolysis liquids (Balat *et al.*, 2009).

Main components	**Weight%**
Water	20-30
Lignin fragments: insoluble pyrolytic lignin	15-30
Aldehydes: formaldehyde, acetaldehyde, hydroxacetaldehyde, glyoxal, methylglyoxal	10-20
Carboxylic acids: formic acid, propionic, butyric, pentanoic, Hexanoic, glycolic (hydroxyacetic)	10-15
Carbohydrates: cellobiosan, α-D-levogosan, oligosaccharides, 1-6-anhydroglucofuranose	5-10
Phenols: phenol, cresols, guaiacols, syringols	2-5
Furfurals	1-4
Alcohols: methanol, ethanol	2-5
Ketones: acetol (1-hydroxy-2-propanone), cyclo-pentanone	1-5

(4) Miscibility - Bio-oil consists of a very complex mixture of oxygenated hydrocarbons with an appreciable proportion of water derived from both original moisture and reaction product (Lu *et al.*, 2009). Water in bio-oil can form a stable single-phase mixture in the range from 15 wt% to the upper limit of 30-50 wt% water, depending on miscible chemicals in the pyrolytic liquid. In addition, bio-oil from pyrolysis can dissolve well in polar solvents such as methanol and acetone.

(5) Ageing of Pyrolysis Liquid - The properties of bio-oil are not stable but tend to change with time, for example, increasing of viscosity, decreasing of volatility, phase separation and deposition of gums. The causes of ageing process are mainly attributed to the complexity and nature of bio-oil; the presence of a large number of oxygenated organic compounds is inherently reactive. The ageing rate depends on the oil composition which in turn depends on the feedstock, pyrolysis conditions, and the efficiency of solid removal and product collection. During bio-oil storage or handling, the chemical components in the bio-oil can react with each other to form secondary products via a number of reactions, for example, polymerizations of aldehydes causing the formation of larger molecules, etherification and esterification reactions between hydroxyl, carbonyl and carboxyl group components which can produce water molecules leading to oil-aqueous phase separation. However, the formation of additional aldehyde hydrates can contain water molecules by shifting the equilibrium reaction from acetals to hemiacetals (Diebold, 2000).

2.5.1.2 Applications of Bio-oil

The uses of bio-oil in many different applications have been developed, as illustrated in Figure 2.7 (Bridgwater, 2003).

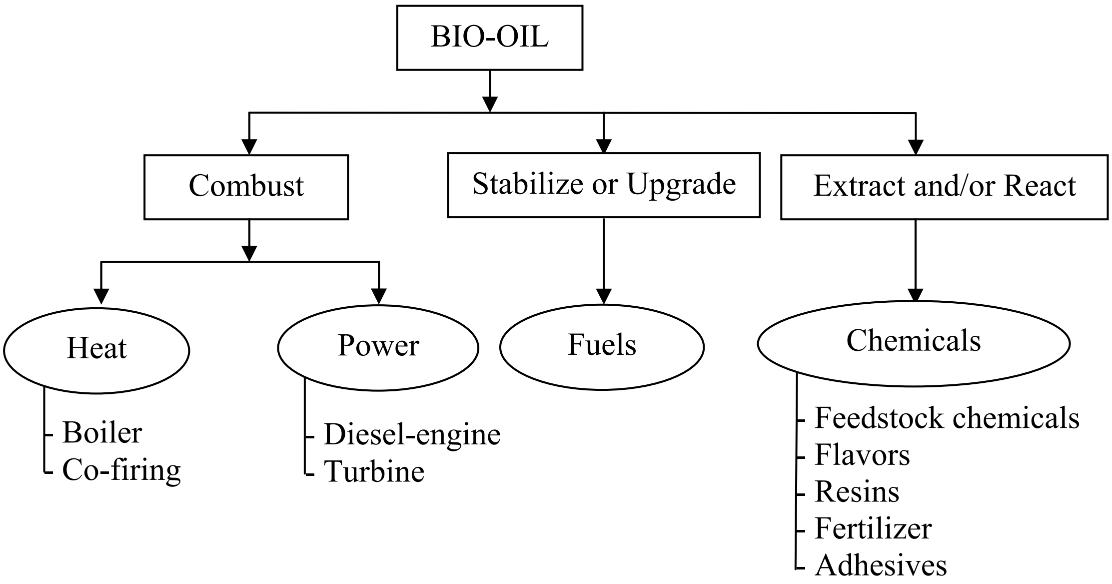

Figure 2.7 Applications of bio-oil (Bridgwater, 2003).

(1) Applications of Bio-Oil for Heat and Power - Bio-oil can be combusted in a boiler, furnace and engine to provide heat or in a turbine to generate power for electricity generation. It has been used commercially by co-firing with coal in a utility boiler for power generation (Mckendry, 2002). Large-scale tests of co-firing bio-oil with fossil fuels have been carried out at the Maintiwac power station to provide 5% of the thermal input to 20 MW_e boiler for electricity production (Czernilk and Bridgwater, 2004). The heating value of bio-oil is lower than that of fossil fuel, and a significant portion of the bio-oil consists of high amount of water (Biomass Technology Group, 2003). For flame combustion tests, fast pyrolysis oil can replace heavy oil and light fuel oil in industrial boilers. However, its combustion characteristics are more similar to light fuel oil. The first test on a gas turbine (J69-T-29 gas turbine combustor rig) using slow-pyrolysis liquid provided 95% efficiency of combustion at optimum operating conditions. Emissions of CO were higher, but hydrocarbon gases and NO_x were within the limits observed for petroleum fuels (Kasper *et al.*, 1983). In 1995, a 2.5 MW_e class GT2500 engine designed as the most suitable for low grade fuels including bio-oil was tested throughout the whole operational range. It indicated that bio-oil combustion gave less content of NO_x and SO_2 emissions but with higher amount of particulates than that of diesel fuel (Czernilk and Bridgwater, 2004). Moreover, combined heat and power (CHP) production have been developed using bio-oil as the main fuel. The tests proved that bio-oil could be efficiently burned with emissions below German standards. However, electrical and thermal efficiencies of the CHP were only 50-60% overall (Czernilk and Bridgwater, 2004).

(2) Applications of Bio-Oil for Engine Fuels - Bio-oil has been used as fuels in several tests on various diesel engines from laboratory units to large size modified dual fuel engines; the results indicated positive performance in terms of smooth running. However, some problems still need to be resolved especially the acidic nature of the oil (pH 3) and its tendency toward soot formation and re-polymerization. Modifications of diesel engine can render a quite acceptable substitute of bio-oil for diesel fuel in stationary engines. On combustion in diesel engines, pure pyrolysis oils should be limited to low-speed diesel engines with relatively high compression ratios, but blends of bio-oil and methanol could be used in high-speed engines, especially with cetane-improving additives (Suppes *et al.*, 1996). Micro-emulsions process of 5-95% bio-oil in diesel gives a significant positive effect on the oil stability. However, when testing bio-oil-diesel emulsions in four different engines, significant damage of injectors and fuel pumps was greater than that reported for pure bio-oil (Chiaramonti *et al.*, 2003a; 2003b).

(3) Applications of Bio-Oil for Producing Chemicals - Production of chemicals is a major commercial application of bio-oil. The chemicals from bio-oil can be extracted or reacted to produce food flavorings, specialties, resins, agri-chemicals, fertilizer, and emissions control agents. All chemicals are attractive possibilities due to their much higher added value. The commercial chemicals from bio-oil can be produced from many methods. Examples of using bio-oil as chemical sources are given as follows (Czernik and Bridgwater, 2004; Oasmaa and Czernik, 1994).

Whole bio-oil

- Carboxylic acids and phenols in bio-oil can react with lime to form calcium salts and phenates. This product is called bio-lime and was developed by Dynamotive Corporation. It consists of 50% water and 7-14% calcium and was proved successful in capturing SO_x emissions from coal combustors. Bio-lime is four times more efficient in capturing acid gases than the use of pure lime.
- High content of carbonyl groups of bio-oil can react with ammonia, urea or other NH_2 containing materials, giving various imide and amide compounds. Incorporating around 10% nitrogen with organic groups of bio-oil can provide an efficient biodegradable slow-release nitrogen fertilizer, with lower leachability comparing to mineral fertilizers.
- Being used as alternative wood preservative that could replace creosote. Especially, terpeniod and phenolic compounds in bio-oil are used as insecticides and fungicides. However, efficiency of bio-oil action is not long-lasting.

Bio-oil fractionation

- The water-soluble fraction extracted from the bio-oil is mostly carbohydrate compounds forming at the top layer. These aqueous extracts are effective meat browning agents. The red-color product can be used as such to brown and flavor sausages, bacon, fish, etc (Biomass Technology Group, 2003).
- The water-soluble fraction of bio-oil can be produced as a potential application of calcium salts of carboxylic acids. It is used as environmentally friendly road de-icers.

- Using pyrolytic lignin as phenol replaces phenol-formaldehyde resins. Those resins were successfully applied as adhesives in plywood and particleboard manufacturing.

Specific chemicals from bio-oil

- Levoglucosan (1, 6-anhydro-â-D-glucopyranose) has potential for the manufacturing of pharmaceuticals, surfactants, biodegradable polymers, and others. However, it has high production price due to high cost of recovery and purification processes.
- Levoglucosenone (6, 8-dioxabicyclo [3.2.1.]oct-2-en-4-one) is produced by fluidized bed pyrolysis of phosphoric acid-impregnated cellulose with the yield of 24%. It can be easily recovered by distillation. As with levoglucosan, it has potential in the synthesis of antibiotics and flavor compounds. However, it has not yet found a large-scale application.

2.5.2 Char Product

Char is a solid product, which is one of the major pyrolysis products. To obtain high yield of char, slow pyrolysis conditions or low temperature and low heating rate are normally applied during pyrolysis (Yaman, 2004) and a fixed bed reactor is usually employed. Char yield and physicochemical properties of char depend on biomass compositions and pyrolysis conditions. The volatile content left in the char depends on the extent of pyrolysis reaction. Heating value of the char obtained from pyrolysis is comparable to those of lignite and coke (about 32 MJ/kg) (Jorjani *et al.*, 2008). The char derived from pyrolysis can be used as solid fuel to supply the pyrolysis process or burned for drying or used as slurry by mixing with oil.

Moreover, solid char product obtained from thermochemical processes of gasification and pyrolysis can be further activated to produce activated carbon. It was reported that carbon adsorbents produced from the char from steam gasification of biomass have a hydrophilic surface and are effective for removing metal ions and other pollutants from water (Savova *et al.*, 2001).

2.5.3 Gas Product

To obtain high yield of gas, high temperature, low heating rate and long gas residence time should be applied (Yaman, 2004). Derived pyrolysis gases, having low to medium heating value, consist mainly of carbon dioxide (CO_2), carbon monoxide (CO), hydrogen (H_2), methane (CH_4) and minor amounts of higher molecular weight hydrocarbon gases. The gases produced can be burned for power generation or used as a heating medium for drying processes (Yaman, 2004).

2.6 Improvement of Fuel Quality of Biomass Pyrolysis Oils

The properties of bio-oil have important effects on fuel quality, including a high level of oxygen giving low heating value, high viscosity, corrosive nature and being relatively unstable. The effects of unusual characteristics of bio-oil and the possible solutions to the problems are shown in Table 2.9 (Bridgewater, 1999b). Details of different methods to improve bio-oil properties are summarized as follows (Bridgwater, 2003; Oasmaa, and Czernik, 1994).

Table 2.9 Characteristics of bio-oil and methods for improvements (Bridgewater, 1999b).

Characteristic	Effect	Solution
Suspended char	- Erosion - Equipment blockage - Combustion problems from slower rates of combustion - "Sparklers" can occur in combustion leading to potential deposits and high CO emissions	- Hot vapor filtration - Liquid filtration - Modification of the char for example by size reduction so that its effect is reduced - Modification of the application
Alkali metals	- Deposition of solids in combustion applications including boilers, engines and turbines - In turbines the damage potential is considerable particularly in high performance machines with, for example, coated blades	- Hot vapor filtration - Processing or upgrading of oil - Modification of application - Pretreatment of feedstock to remove ash
Low pH	- Corrosion of vessels and pipework	- Careful materials selection - Stainless steel and some olefin polymers are acceptable
Incompatibility with polymers	- Swelling or destruction of sealing rings and gaskets	- Careful materials selection
Heat temperature sensitivity	- Liquid decomposition on hot surfaces leading to decomposition and blockage - Adhesion of droplets on surfaces below 400°C	- Recognition of problem and appropriate cooling facilities - Avoidance of contact with hot surfaces above 500°C
High viscosity	- High pressure drops in pipelines leading to higher cost equipment and/or possibilities of leakage or even pipe rupture	- Careful low temperature heating, and/or addition of water, and/or addition of co-solvents such as methanol or ethanol
Water content	- Complex effect on viscosity, heating value, density, stability, pH, homogeneity etc.	- Recognition of problem - Optimization with respect to application
In-homogeneity	- Layering or partial separation of phases - Filtration problems	- Modify or change process - Modify pyrolysis parameters - Change feedstock to low lignin - Additives - Control water content

2.6.1 Hot-Vapor Filtration

Hot-vapor filtration is the filtering of bio-oil vapor through a filter made of sintered metal, porous ceramic or flexible ceramic fabric elements at a high temperature about 400-420°C prior to condensation. This method can reduce ash content in bio-oil to less than 0.01 wt% and alkali content to less than 10 ppm. The hot-vapor filtration is more effective than the application of conventional cyclone technology, especially with char particle size below 10 µm, and gives significantly higher efficiency of char removal. This method also causes thermal cracking of pyrolysis vapors that can reduce the size of oligomeric chains, giving bio-oil with lower viscosity, longer duration of storage and higher burning rate and shorter ignition time. However, difficulties associated with bio-oil filtration are the agglomeration of bio-oil particles and formation of sludge, resulting in high pressure drop across the filter surface and losses of bio-oil mass (<10% of bio-oil yield obtained after the process). Moreover, it is also difficult to remove effectively the char cake using a traditional back-flushing method.

2.6.2 Solvent Addition

To homogenize and reduce the viscosity of bio-oils, polar solvents should is generally added. General polar solvents suggested are water, methanol, and furfural. Methanol solvent shows a significant positive effect on oil stabilization. A significant reduction in the rate of viscosity increase can be achieved by the addition of polar solvents into bio-oil; almost 20 times of rate decreasing are obtained from the addition of 10 wt% methanol in bio-oil. There are three effects of solvent addition in bio-oil; physical dilution with no chemical reactions, reducing the reaction rate by molecular dilution or by changing the oil microstructure and chemical reactions between the solvent and the oil components to prevent further chain growth. This will upgrade bio-oil properties, for example, reducing acidity, improving volatility, giving higher heating value and better miscibility with diesel fuels.

2.6.3 Emulsion

It is a process for producing stable micro-emulsions with 5-30% of bio-oil content in diesel. CANMET Energy Technology Centre and University of Florence have developed bio-oil-diesel emulsions with 5-30% of bio-oil in diesel and 5-95% bio-oil in diesel, respectively (Bridgwater, 2003). One or more additives (surfactants and co-surfactants) are used to lower surface energy of interface of existing droplets. The droplet size and size distribution of the emulsions affect most of the properties of emulsion systems such as stability, viscosity, etc. Those emulsions show promising ignition characteristics and less corrosion problems.

2.6.4 Esterification

Esterification is a chemical upgrading method used to convert carboxylic acids in bio-oil to esters. Generally, excess alcohol is employed to affect reaction equilibrium coupled with the use of acid catalyst such as H_2SO_4, SO_4^{2-}/ZrO_2, $40SiO_2/TiO_2\text{-}SO_4^{2-}$ or Nafion SAC13 (Doshi *et al.*, 2005; Junming *et al.*, 2008; Mahfud *et al.*, 2007; Zhang *et al.*, 2006). The optimal reaction temperature varies from 50 to 80°C, depending to a large extent on alcohol type and chemical compositions in bio-oil (Doshi *et al.*, 2005; Junming *et al.*, 2008; Mahfud *et al.*, 2007). This method can give improved properties of bio-oil including lower acidity, higher heating value, and reduced viscosity. It was also reported that the odor of the oil was improved from an extremely annoying level to a not annoying level (Doshi *et al.*, 2005).

2.6.5 Chemical/Catalytic Upgrading Processes

It is a process to produce hydrocarbon fuels with properties ranging from moderate to high quality fuel products but is more complicated and costly than the physical upgrading methods. There are generally two main routes; hydrotreating and catalytic vapor cracking over zeolites (Oasmaa, and Czernik, 1994). These upgrading methods can remove completely the oxygen content and produce a conventional hydrocarbon fuel, and reform the components to stabilize the bio-oil.

2.6.5.1 Catalytic Hydrotreating Technique

Hydrotreating technology is one of the most commonly used refinery processes in petroleum industries since 1950s, designed to remove contaminants such as sulfur, nitrogen, condensed ring aromatics, or metals (UOP LLC, 2004). This process can be used in order to upgrade liquid products from biomass pyrolysis with the aid of catalyst and hydrogen supply. Typical conditions are 350°C to 450°C, 6.9 to 20.8 MPa and liquid hourly space velocity (LHSV) of 0.1 to 1.0 hr^{-1}, which are lower than typical petroleum processing. The traditional catalysts used are NiMo or CoMo on alumina supports. The reactions involved are hydrogenation of double bonds, elimination of oxygen as water and hydrogenation-hydrocracking of large molecules. The chemical reaction of the catalytic hydrotreating is shown as in the following (Bridgwater and Cottam, 1992);

$$C_6H_8O_4 + 6H_2 \rightarrow 6CH_2 + 4H_2O \tag{2.3}$$

Preliminary results from many workers indicate that conventional hydrotreating processes may be readily adapted to pyrolysis liquids. The product is a low-grade gasoline that would require orthodox refining and blending to give a marketable product (Nugranad, N., 1997). Hydrotreating may be performed in a plant that is close-coupled to the pyrolysis plant, either as a central operation followed by various small pyrolyzers or a central operation followed by a large pyrolyzer (Bridgwater and Cottam, 1992).

2.6.5.2 Catalytic Cracking Technique

Catalytic cracking technique is the process that involves deoxygenation without using reducing gases through simultaneous dehydration-decarboxylation of the pyrolysis vapors over catalyst. The oxygen is eliminated as carbon monoxide, carbon dioxide and water. Usually, catalytic cracking catalyst used is zeolite catalysts, especially ZSM-5. This process is the commercial Mobil MTG (methanol to gasoline) and MTO (methanol to olefines) process. The chemical reaction of catalytic cracking process for synthesizing gasoline from methanol is (Bridgwater and Cottam, 1992);

$$C_6H_8O_4 \rightarrow 4.6CH_{1.2} + 1.4CO_2 + 1.2H_2O \tag{2.4}$$

Other catalysts that have been selected to upgrade bio-oil are fluidized catalytic cracking (FCC) catalyst, alumina, Fe/Cr transition metal catalyst, MCM-41, Criterion-534 (Co-Mo), Na_2CO_3, K_2CO_3, ZnO, etc. Distinct structural characteristics and active site of each catalyst are the most important parameter which influence the products obtained. Because of a strong acidity, high activities and shape selectivity, ZSM-5 was used to convert the oxygenated oil to a hydrocarbon mixture in the C_1 to C_{10} range and mostly aromatic hydrocarbon product is obtained (Williams, P. T., and Nugranad, N., 2000). The catalytic cracking upgrading resulted in an increase of hydrocarbon gas yield including alkane and alkene gases and a decrease of oil yields because of a result of oxygen removal to water, CO_2 and CO and formation of coke on the catalyst. The molecular weight distribution of the oils after catalytic upgrading was shifted to lower molecular weights products having a molecular weight distribution from 60 to over 2000 Da. (Williams, P. T., and Nugranad, N., 2000). In addition, while the technology appears to be very attractive to give high yields of valuable hydrocarbons, there are several problems arising from the coking behavior of the catalyst.

2.7 Commercial Development of Gasification and Pyrolysis Technologies

Over the past 10-15 years, thermal conversion processes including gasification and pyrolysis of biomass have been developed as an emerging technology for commercial production of green energy. The continued increase in petroleum price and concerns over long term greenhouse effect have stimulated the rapid development of these processes (Higman and Burgt, 2008). Gasification of biomass is in various stages of development and has achieved some degrees of commercialization. The general trend of biomass conversion by gasification process has been the use of fluid-bed reactors operating at atmospheric pressure, although several other systems have been also chosen on a commercial scale (Higman and Burgt, 2008). For example, Lurgi circulating fluid-bed process with capacity of 400 t/d of waste wood in the Netherlands can produce hot gases to be co-fired in a 600 MW_e coal boiler. Foster Wheeler has developed a pressurized reactor operating at 20 bar with a capacity of 18 MW_{th} that forms the basis for the 6 MW_e biomass IGCC at Värnamo in Sweden (Higman and Burgt, 2008). The Choren company has operated a

1 MW_{th} pilot plant with air-blown entrained-flow gasifier coupled with a Fischer-Tropsch unit for manufacturing transport fuels at the proof-of-concept level. In addition, it has been found that a maximum capacity of 30-40 MW_{th} for a biomass gasification plant is limited by the logistics of biomass collection. To overcome this problem from economic point of view, bio-oils produced from several pyrolysis plants could be supplied to a central gasifier (Higman and Burgt, 2008).

It is known that pyrolysis process is capable of producing various useful products. The liquid product derived from this process can be directly used as a fuel with ease of handling and transportation and finds applications in various heat and power generation processes. Even though this process is still at an infancy stage but there are a number of small-scale commercial and demonstration plants that have been built such as those of Dynamotive, Canada; Wellman, UK; ENSYN, Canada; ENEL, Italy; VTT, Finland; BTG, Netherlands; Pyrovac, Canada, etc (Higman and Burgt, 2008). These companies are still working on several developing projects. BTG not only offers the improving BTG's fast pyrolysis technology but also provide technical services and technical assistance for end-use application of the pyrolysis oil. BTG is one of the initiators to establish a large European project to produce bio-oils suitable for co-refining in existing refineries (EU project - BIOCOUP) and various small high-pressure units were set-up in which the pyrolysis oil can be hydrotreated and deoxygenated. BTG owns several projects including bio-oil production at BTG’s Malaysian plant. The projects cover the investigation of using bio-oil to replace diesel and natural gas in a 150 kW boiler and bio-oil tests in two modified diesel engine and in large scale of entrained flow gasifiers, etc (Biomass Technology Group, 2009). Ensyn is an incorporate that commercializes its proprietary biomass-to-liquid technology. The main Ensyn's products are the manufacture of more than 30 commercial chemical and fuel products based on Ensyn's unique RTP™ technology. Rapid Thermal Process (RTP)™ or rapid pyrolysis process has been operated on a long-term commercial basis. Seven commercial RTP™ plants are running in the United States and Canada. The largest plant located in Renfrew, Ontario has the process capacity of 100 tonnes of dry residual wood per day and new plants with capacity of 5-10 times of Renfrew plant is now underway (Ensyn Corporation, 2009). Moreover, Ensyn and UOP bring together two experiences to provide a proven practical route of biomass pyrolysis for heat, power and green transport fuels. Dynamotive Energy Systems Corporation is a provider for energy solutions and leader in viable technologies for conversion of biomass residues into fuels which is environmentally, economically and competitive to fossil fuels. Dynamotive focuses on developing commercial bench-scale plants, a 15TPD Pilot Plant, a 130TPD Plant in West Lorne, and a 200TPD Plant in Guelph, Canada to produce bio-oil for using in a turbine for electricity generation. A commercial 100TPD plant which was constructed in 2003 can generate 2.5 MW_e electricity and at a capacity of 200TPD it is expected to produce bio-oil for electricity generation of 6-10 MW_e. Recently, Dynamotive has succeeded in refining bio-oil to create synthetic automobile fuels at a cost less than $2 per gallon through two stages upgrading (UBA-UBB); hydroreforming of raw bio-oil (UBA) and a conventional hydrotreatment over a commercial catalyst to convert UBA into a product designated as UBB (Dynamotive Energy Systems Corporation, 2009). Dynamotive intends to produce its main source of revenue from license fees and royalties via technical services and biofuel project investments. In addition, Dynamotive proposes to replace fossil fuel with the use of

BioOil Plus (a mixture of 80% bio-oil and 20% bio-char) in order to generate green house gas emissions reduction credits through established international mechanisms set out under the Kyoto Protocol.

Considering economic aspect, the costs of bio-oil production depend on several factors such as feedstock preparation, production scale, technology type, etc. Study by Biomass Technology Group (BTG) has shown that bio-oil can be produced at a cost between 75-300 € per tonne oil (4-18 €/GJ) and at capacity >5 tonne/hr the costs are 70-230 € per tonne oil (Bridgwater, 1999a). At this estimation, the cost of bio-oil is competitive with that of industrial light fuel oil (6.64 €/GJ excluding taxes) in the European markets. Due to the high oil price and high fossil fuel taxes in Europe, bio-oil is expected to be the most promising energy that can be used in an engine or turbine for electricity generation. In addition, the impetus from international agreements on environmental benefits has caused significant fiscal incentives being given for renewable electricity in many European countries. On exploitation of bio-oil as a source of renewable energy, European Commission (EC) intends to increase the share market of combined heat and power (CHP) for the European energy supply from less than 10% in the year 2000 to 18% in 2010 (Bridgwater, 1999a). The increased awareness on environmental problems will also make the investment of biomass pyrolysis process become more attractive (Bridgwater, 1999b). Furthermore, in order to sustain a continued development in the pyrolysis process, it is necessary to improve bio-oil quality as well as to make the users familiar with its benefits (Bridgwater, 2003).

2.8 References

American Bioenergy Association. (2005). What is biomass [On-line]. Available: **www. biomass.org/index_files/page0001.htm**.

Babu, B. V. (2008). Biomass pyrolysis: a state-of the-art review. **Biofuels, Bioproducts and Biorefining** 2: 393-414.

Basu, P., (2006). **Combustion and gasification in fluidized beds**. United State of America: CPC Press.

Balat, M., Balat, M., Kırtay, E., and Balat, H. (2009). Main routes for the thermo-conversion of biomass into fuels and chemicals. Part 1: pyrolysis systems. **Energy Conversion and Management** 50 (12): 3147-3157.

Biomass Technology Group (2003). Bio-oil Applications [On-line]. Available: **http://www.btgworld.com/technologies/bio-oil-applications.html**.

Biomass Technology Group (2009). Process, product & technology development [On-line]. Available: **http://www.btgworld.com/**.

Boateng, A. A., Weimer, P. J., Jung, H. G., and Lamb, J. F. S. (2008). Response of thermochemical and biochemical conversion processes to lignin concentration in alfalfa stems. **Energy&Fuels** 22 (4): 2810-2815.

Boerrigter, H. and Rauch, R. (2005). Syngas production and utilisation. In Knoef, H. A. M. (ed.). **Handbook biomass gasification**. Netherlands: Biomass Technology Group (BTG).

Bridgwater, A. V., and Cottam, M. L. (1992). Opportunities for biomass pyrolysis liquids production and upgrading**. Energy & Fuels**. 6(2): 113-120.

Bridgwater, A. V. (1999a). An introduction to fast pyrolysis of biomass for fuels and chemicals. In Bridgwater, A. V. (ed.). **Fast Pyrolysis of Biomass: a Handbook** (pp.1-13). United Kingdom: CPL Press.

Bridgwater, A. V. (1999b). Principles and practice of biomass fast pyrolysis processes for liquids. **Journal of Analytical and Applied Pyrolysis** 51(1-2): 3-22.

Bridgwater, A. V. (2003). Renewable fuels and chemicals by thermal processing of biomass. **Chemical Engineering Journal** 91 (2-3): 87-102.

Bridgwater, A. V., and Peacocke, G. V. C. (2000). Fast pyrolysis processes for biomass. **Renewable and Sustainable Energy Reviews** 4 (1): 1-73.

Chiaramonti, D., Bonini, M., Fratini, E., Tondi, G., Gartner, K., Bridgwater, A. V., Grimm, H. P., Soldaini, I., Webster, A., and Baglioni, P. (2003a). Development of emulsions from biomass pyrolysis liquid and diesel and their use in engines-Part 1: emulsion production. **Biomass and Bioenergy** 25 (1): 85-99.

Chiaramonti, D., Bonini, M., Fratini, E., Tondi, G., Gartner, K., Bridgwater, A. V., Grimm, H. P., Soldaini, I., Webster, A., and Baglioni, P. (2003b). Development of emulsions from biomass pyrolysis liquid and diesel and their use in engines-Part 2: tests in diesel engines. **Biomass and Bioenergy** 25 (1): 101-111.

Czernilk, S., and Bridgwater, A. V. (2004). Overview of applications of biomass fast pyrolysis oil. **Energy & Fuels**. 18 (2): 590-598.

Demirbas, A. (2009). Biorefineries: current activities and future developments. **Energy Conversion and Management** 50 (11): 2782-2801.

Department of Alternative Energy Development and Efficiency (2009). Biodiesel [On-line]. Available: **http://www.dede.go.th/dede/index.php?id=351**.

Diebold, J. P. (2000). A review of the chemical and physical mechanisms of the storage stability of fast pyrolysis bio-oils. **National Renewable Energy Laboratory** NREL/SR-570-27613.

Doshi, V. A., Vuthaluru, H. B., and Bastow, T. (2005). Investigations into the control of odour and viscosity of biomass oil derived from pyrolysis of sewage sludge. **Fuel Processing Technology** 86 (8): 885-897.

Dynamotive Energy Systems Corporation (2009).Technology [On-line]. Available: **http://www.dynamotive.com/**.

Ensyn Corporation (2009). Products [On-line]. Available: **http://www.ensyn.com/products.htm**.

Goyal, H. B., Seal, D., and Saxena, R. C. (2008). Bio-fuels from thermochemical conversion of renewable resources: a review. **Renewable and Sustainable Energy Reviews** 12 (2): 504-517.

Higman, C., and Burgt, M. (2008). **Gasification** (2nd ed.). United State of America: Elsevier Science.

Iluyemi, F. B., Hanafi, M. M., Radziah, O., and Kamarudin, M. S. (2006). Fungal solid state culture of palm kernel cake. **Bioresource Technology** 97 (3): 477-482.

Index Mundi (2009). Oil; palm-production, consumption, exports, and imports **statistics [On-line]. Available: http://www.indexmundi.com/en/commodities/agricultural/oil-palm/**.

Jeffries, T. (1995). Definitions [Online]. Available: **http://calvin.biotech.wisc.edu/ jeffries/definitions.html**.

Jorjani, E. J., Hower, C., Chehreh Chelgani, S. C., Shirazi, M. A., and Mesroghli, S. (2008). Studies of relationship between petrography and elemental analysis with grindability for Kentucky coals. **Fuel** 87: 707-713.

Junming, X., Jianchun, J., Yunjuan, S., and Yanju, L. (2008). Bio-oil upgrading by means of ethyl ester production in reactive distillation to remove water and to improve storage and fuel characteristics. **Biomass and Bioenergy** 32 (11): 1056-1061.

Kasper, J. M., Jasas, G. B., and Trauth, R. L. (1983). Use of pyrolysis-derived fuel in a gas turbine engine. **American Society of Mechanical Engineers** No. 83-GT-96.

Kirubakarana, V., Sivaramakrishnanb, V., Nalinic, R., Sekard, T., Premalathae, M., and Subramaniane, P. (2009). A review on gasification of biomass. **Renewable and Sustainable Energy Reviews** 13 (1): 179-186.

Lemeune, S. (2005). Le bios [On-line]. Available: **http://www.geocities.com/ Paris/LeftBank/5810/bois.html**.

Li, L., and Zhang, H. (2004). Preparing levoglucosan derived from waste material by pyrolysis. **Energy Sources** 26 (11): 1053-1059.

Lu, Q., Li, W., and Zhu, X. (2009). Overview of fuel properties of biomass fast pyrolysis oils. **Energy Conversion and Management** 50 (5): 1376-1383.

Mahfud, F. H., Melian-Cabrera, I., Manurung, R., and Heeres, H. J. (2007). Biomass to fuels upgrading of flash pyrolysis oil by reactive distillation using a high boiling alcohol and acid catalysts. **Process Safety and Environmental Protection** 85 (5): 466-472.

Mckendry, P. (2002). Energy production from biomass (part 2): conversion technologies. **Bioresource Technology** 83 (1): 47-54.

Mohan, D., Pittman, C. U., Jr., and Steele, P. H. (2006). Pyrolysis of wood/biomass for bio-oil: A critical review**. Energy & Fuels** 20 (3): 848-889.

Nagatomi, Y., Yamamoto, H., Yamaji, K., Iwasaki, H. and Yamada, K. (2006). A systems analysis of ethanol production using cassava pulp in Thailand. Paper presented at **Renewable Energy 2006** (pp. 1210-1213).

Nanda, S. K., Jyothi, A. N. and Balagopalan, C. (2005). Cassava waste treatment and residue management in India [On-line]. Available: **http://webapp.ciat.cgiar.org/asia_cassava/workshop_pdf/Paper73_S_K_Nanda_Cassava_waste_treatment_and_residue_manage.pdf**.

Nugranad, N. (1997). **Pyrolysis of Biomass**. Ph.D. Dissertation, University of Leeds, United Kingdom.

Office of Agricultural Economics (2006). Production of the important agricultural products in Thailand [On-line]. Available: **http://www.oae.go.th/Prcai/Longan.xls**.

Office of Agricltura Economics (2009). Agricaltural statistics [On-line]. Available: **http://www.oae.go.th/**.

Office of Technology Assessment at the German Parliament (TAB) (1997). Gasification and pyrolysis of biomass [On-line]. Available: **http://www.tab.fzk.de/ en/projekt/zusammenfassung/AB49.htm**.

Oasmaa, A., and Czernik, S. (1994). Fuel oil quality of biomass pyrolysis oils state of the art for the end users. **Energy & Fuels** 13 (4): 914-921.

Pansamut, V., Pongrit, V., and Intarangsi, C. (2003). **The oil palm**. Thailand: Department of Alternative Energy Development and Efficiency: Ministry of Energy.

Pyne IEA Bioenergy (2005). Applications [On-line]. Available: **http://www.pyne.co.uk/**

Reade Advanced Materials. (1997). Coconut shell powder [On-line]. Available: **http://www. reade.com/Products/Organic/coconut.html**.

Rezaiyan, J., and Cheremisinoff, N. P. (2005). **Gasification technologies: A primer for engineers and scientists**. United State of America: Taylor & Francis Group.

Savova, D., Apak, E., Ekinci, E., Yardim, F., Petrov, N., Budinova, T., Razvigorova, M., and Minkova, V. (2001). Biomass conversion to carbon adsorbents and gas. **Biomass and Bioenergy** 21 (2): 133-142

Scranton Green Chemistry (2005). A green chemistry module [Online]. Available: **http://academic.scranton.edu/faculty/CANNM1/inorganic/inorganicmodule.html**.

Sjostrom, E. (1993). **Wood chemistry fundamentals and applications** (2nd ed.). New York: Academic Press.

Srinorakutara, T. Kaewvimol, L., and Saengow, L. (2006). Approach of cassava waste pretreatments for fuel ethanol production in Thailand. **Journal of Scientific Research Chulalongkorn Universit**y 31(1):77-84.

Srisovanna, P. (2004). Thailand's Biomass Energy [On-line]. Available: **http://www.cogen3.net/doc/countryinfo/thailand/ThailandBiomassEnergy_report.pdf.**

Suppes, G. J., Natarajan, V. P., and Chen, Z. (1996). Autoignition of select Oxygenate fuels in a simulated diesel engine environment. Paper presented at **AIChE National Meeting** (Paper 74 e), New Orleans, LA.

UOP LLC (2004). Hydrotreating [On-line]. Available: **http://www.uop.com/ refining/ 1060.html.**

Wan Daud, W., and Wan Ali, W. (2004). Comparison on pore development of activated carbon produced from palm shell and coconut shell. **Bioresource Technology** 93 (1): 63-69.

Wattanachaisaereekul, S. (2001). **Animal feed from fermented cassava waste**. M.S. Thesis, Kasetsart University, Thailand.

Williams, P. T., and Nugranad, N. (2000). Comparison of products from the pyrolysis and catalytic pyrolysis of rice husks. **Energy** 25 (6): 493-513.

Yaman, S. (2004). Pyrolysis of biomass to produce fuels and chemical feedstock. **Energy Conversion and Management** 45 (5): 651-671.

Zhang, Q., Chang, J., Wang T., and Xu, Y. (2006). Upgrading Bio-oil over Different Solid Catalysts. **Energy & Fuels** 20 (6): 2717-2720.

CHAPTER III

THERMOGRAVIMETRIC ANALYSIS OF BIOMASSES

3.1 Abstract

Pyrolysis kinetics of biomasses were studied in a thermogravimetric analyzer. Effects of biomass type (cassava pulp residue, palm kernel cake, palm shell, coconut shell and longan fruit seed), particle size (106-1,325 µm) and heating rate (5-40°C/min) on thermal decomposition behavior were investigated and the pyrolysis kinetic data were tested with five pyrolysis models to confirm their validities. The major decomposition of all biomasses occurred in the range of 250-400°C and their first derivative curves (DTG) showed different characteristics of one or two major peaks depending on type of biomass. Different particle sizes gave almost no effect on the fractional weight remaining and its 1^{st} derivative but heating rate influenced strongly on the range of decomposition temperature and decomposition rate. On model fitting, the best fitting was obtained with the two parallel reactions model. The one-step global model assuming n^{th} order reaction and the two-step consecutive reaction model with provision of stoichiometric coefficient gave satisfactory prediction. However, the one-step global model assuming 1^{st} order reaction and the two-step consecutive reaction model of Guo and Lua showed relatively large deviation between predicted and experimental results.

3.2 Introduction

As mentioned earlier in Chapter II, Topic 2.2.3, pyrolysis process is defined as a thermal degradation process of carbonaceous materials in the absence of oxygen. It is an important thermal conversion process being the first step of combustion and gasification processes (Bridgwater, 2003). In addition, it is widely applied in chemical industries, for example, the preparation of char as a precursor for the production of activated carbon, cracking medium weight hydrocarbons of petroleum oil to produce lighter fractions of gasoline, etc (Answers Corporation, 2009). Thus, fundamental knowledge on thermal behavior of pyrolysis is a prerequisite for the design and optimization of various thermal conversion processes. In this work, the study of pyrolysis kinetics of test biomass was first carried out to characterize and understand the pyrolysis behavior for successful design and operation of the small scale fixed-bed reactor, which will be reported in the next chapter of this thesis. Thermogravimetric analysis (TGA) which is a common method to study thermal behavior was adopted for this purpose in this work. The thermal behavior of biomass was monitored as fractional weight change regarding temperature and time. The effects of biomass type including cassava pulp residue, palm kernel cake, palm shell, coconut shell and longan fruit seed, particle size and heating rate on the non-isothermal pyrolysis characteristics were investigated. Furthermore, to enable the prediction of non-isothermal pyrolysis behaviors of cassava pulp residue, five pyrolysis models were tested, namely the one-step global model with 1st order reaction, the one-step global model with nth order reaction, the two-step consecutive reaction model of Guo and Lua, the two-step consecutive reaction model with consideration of reaction stoichiometry and the two parallel reactions model.

3.3 Literature Reviews

3.3.1 Previous Studies

Pyrolysis kinetics of lignocellulosic materials can be studied under dynamic and static conditions. During the dynamic condition, pyrolysis temperature is increased with increasing time according to an assigned heating rate, while static condition maintains a selected constant temperature in a pyrolyzing chamber (Babu, 2008). Generally, studying thermal behavior of biomass can be carried out in various systems such as a tube furnace, an entrained-flow reactor, and a drop tube reactor but the most popular and simplest system is thermogravimetric analyzer (Di Blasi, 2008; Haines, 1995). Because of a large number of complicating reactions involving the complexity and variation of lignocellulosic compositions and the influences of heat and mass transfers during thermal decomposition, it is thus difficult to obtain the exact reaction mechanism to describe the pyrolysis reaction. The main problem of kinetic analysis is the combined effects of chemical reactions and transport phenomena. The important effects of heat and mass transfers could result from several factors. For example, the large size of sample particle results in temperature gradient in the particle or the thermal lag between the sample and the controlling thermocouple is due to the application of a high heating rate. To avoid these problems, most studies have employed small particle size and slow heating rate for pure kinetic control (Di Blasi, 2008). A number of pyrolysis models have been proposed and they can be classified into three types i.e., one-step global models, one-stage multireaction models and two-stage semi-global models (Di Blasi, 2008).

The one-step global model has been applied to many pyrolyis processes under dynamic and isothermal conditions and with different reaction zones.

The kinetic mechanism is assumed to be a one-step reaction and raw material is assumed as one component decomposing under fast heating and very high temperature conditions (Di Blasi, 2008). Generally, the values of activation energy derived from the global reaction model could vary widely between 56 and 174 kJ/mol (Di Blasi, 2008). This depends on the heating conditions occurring from using different reactor configurations. Moreover, it should be noted that the one global model cannot be applied for the case of non-negligible heat and mass transfers as it often offers much lower predicted activation energy (Antal and Varhegyi, 1995).

For the one-stage multireaction model, the pyrolysis mechanism consists of parallel reactions of different components of a feedstock or simultaneous and competing decomposition of a lignocellulosic material into different pyrolysis products such as tar, char, and gases. For the models of parallel reactions of multicomponents, the model assumes that raw material comprises three pseudo-components following the main cellulosic composition of biomass, namely cellulose, hemicellulose and lignin. It was found that this model can explain well for the biomass showing a peak of decomposition rate with a shoulder (Di Blasi, 2008). The simulated results indicated that thermal degradation of pseudocomponents of hemicellulose and cellulose occurred independently over the main decomposition temperature but the pseudo-component of lignin was pyrolyzed slowly over a wide range of temperature. The predicted values of activation energy derived from parallel reactions model were about 80-116 kJ/mol for hemicellulose, 195-286 kJ/mol for cellulose and 18-65 kJ/mol for lignin (Gronli *et al.*, 2002). For the case of simultaneous reactions of decomposing one component into several products, several investigators have applied this scheme including Thurner and Mann (1981) for studying oak wood pyrolysis, Di Blasi and Branca (2001) for studying beech wood pyrolysis, Wagenaar *et al.* (1994) for studying pine wood pyrolysis, etc. It was found that different values of activation energy (E) for productions of char (C), liquid (L) and gas (G) were derived as follows: 73-125 kJ/mol for E_C, 119-148 kJ/mol for E_L and 139-153 kJ/mol for E_G (Di Blasi, 2008).

Finally, the two-stage semi-global models are applied to describe the two stage reactions of pyrolysis in which the first products are further decomposed into secondary products. This hypothesis have been adopted by a number of researchers including Koufopanos *et al.* (1989), Radlein (1995), Miller and Bellan (1996), Guo and Lao (2001). One of the commonly used model is that by Koufopanos (1989) who proposed that the virgin biomass is broken up into the first two component groups including volatiles of gases and char and both groups are decomposed further to the second volatiles of gases and char. This model can give good prediction for pyrolysis of several biomasses such as beech wood, olive husk, hazelnut shell and corn cob (Babu, 2008). Moreover, the model proposed by Babu and Chaurasia (2003) which adopted the reaction scheme of Koufopanos and incorporated the effects of heat and mass transport phenomena was also validated.

On simulation of the pyrolysis process, the reaction schemes must be represented by mathematic equations. The common kinetics equations to describe a pyrolysis process under various assumptions are summarized in Table 3.1 (Guo and Lua, 2003; Haines, 1995). In this required, the rate equation can be written as

$$\frac{d\alpha}{dt} = k \cdot f(\alpha) \tag{3.1}$$

where k is the rate constant at absolute temperature *T*, and $f(\alpha)$ is a mathematical expression of α which is defined in terms of the mass change of sample at time *t*, where $\alpha = \frac{W_0 - W}{W_0 - W_f}$ and W_0, W_f and *W* are initial, final and actual weight of sample, respectively. The integrating solution is expressed as a function of $g(\alpha)$ as follows:

$$g(\alpha) = \int \frac{d\alpha}{f(\alpha)} = kt \tag{3.2}$$

Table 3.1 Common functions for solid state thermal decomposition reactions (Guo and Lua, 2003; Haines, 1995).

Type	**f(α)= rate/k**	**g(α)=kt**
Sigmoid curves		
An Avrami-Erofe’ev (n=2, 3 or 4)	$n(1-\alpha)\left(-\ln(1-\alpha)\right)^{\frac{n-1}{n}}$	$\left(-\ln(1-\alpha)\right)^{\frac{1}{n}}$
Prout-Tompkins	$\alpha(1-\alpha)$	$\ln\left(\frac{\alpha}{1-\alpha}\right)+C$
Geometric		
Contracting area	$2(1-\alpha)^{\frac{1}{2}}$	$1-(1-\alpha)^{\frac{1}{2}}$
Contracting volume	$3(1-\alpha)^{\frac{1}{3}}$	$1-(1-\alpha)^{\frac{1}{3}}$
Acceleratory		
Power law (m>1)	$m(\alpha)^{\frac{m-1}{m}}$	$\alpha^{\frac{1}{m}}$
Diffusion		
One-dimension	$\frac{1}{2\alpha}$	α^2
Two-dimension	$\left(-\ln(1-\alpha)\right)^{-1}$	$(1-\alpha)\ln(1-\alpha)+\alpha$
Three- dimension	$\frac{3}{2}(1-\alpha)^{\frac{2}{3}}\left(1-(1-\alpha)^{\frac{1}{3}}\right)^{-1}$	$\left(1-(1-\alpha)^{\frac{1}{3}}\right)^2$
Ginstling-Brounshtein	$\frac{3}{2}\left((1-\alpha)^{\frac{1}{3}}-1\right)^{-1}$	$1-\frac{2\alpha}{3}(1-\alpha)^{\frac{2}{3}}$
Equation orders		
First order	$1-\alpha$	$-\ln(1-\alpha)$
Second order	$(1-\alpha)^2$	$\frac{1}{(1-\alpha)}$
Third order	$(1-\alpha)^3$	$\left(\frac{1}{(1-\alpha)}\right)^2$

3.3.2 Kinetic Model Description

It is possible that the pyrolysis of a lignocellulosic material at different conditions may be described by different pyrolysis mechanism. To check for the appropriate model for describing pyrolysis behaviors of cassava pulp residue for different particle sizes and heating rates, five models based on three pyrolysis schemes consisting of one-step global reaction, two-step consecutive reaction, two parallel reactions were tested in this work. The model descriptions are presented as follows.

3.3.2.1 One-Step Global Model

The one-step global model is the simplest kinetic model which assumes that the decomposition rate of the pyrolysis process depends on an arbitrary reaction order. The reaction scheme can be represented as

$$\text{Raw material} \xrightarrow{k} \text{Char + Volatiles} \tag{3.3}$$

where k is the rate constant of the reaction following the Arrhenius law. The rate of pyrolysis decomposition is defined in the following manner

$$\frac{d\alpha}{dt} = k(1-\alpha)^n = A\exp(-\frac{E}{RT})(1-\alpha)^n \tag{3.4}$$

where α is defined in terms of the fractional mass change of sample, $\alpha = \frac{W_0 - W}{W_0 - W_f}$, where W_0, W_f and W are initial, final and weight of sample at any time t, respectively. A is frequency or pre-exponential factor, E is the activation energy of pyrolysis process, R is the universal gas constant, T is absolute temperature and n is the order of reaction. The study of pyrolysis kinetic is usually performed at a constant heating rate, β, therefore

$$\beta = \frac{dT}{dt} \tag{3.5}$$

Thus, the decomposition rate as a function of temperature can be expressed as

$$\frac{d\alpha}{dT} = \frac{A}{\beta}\exp(-\frac{E}{RT})(1-\alpha)^n \tag{3.6}$$

In this study, the weight remaining data (TG data) was tested by the one-step global model assuming both first-order and nth order reactions. The analytical solutions of 1st order reaction model and nth order reaction model are respectively,

$$\alpha = 1 - \exp\{-\frac{ART^2}{\beta E}(1-\frac{2RT}{E})\exp(-\frac{E}{RT})\} \tag{3.7}$$

$$\alpha = 1 - \{1-(1-n)(-\frac{ART^2}{\beta E})(1-\frac{2RT}{E})\exp(-\frac{E}{RT})\}^{\frac{1}{1-n}} \tag{3.8}$$

3.3.2.2 Two-Step Consecutive Reaction Model

Guo and Lua (2001) have proposed the two-step consecutive reaction model taken into account the softening effect in pyrolysis reaction of solid waste palm shell. The two reaction steps consist of decomposition of a starting material to produce the first volatile matters and an intermediate substance followed by decomposition of the intermediate to generate solid char and the second volatiles, that is

$$\text{Raw material} \xrightarrow{k_1} \text{Intermediate + Volatile (I)} \tag{3.9}$$

$$\text{Intermediate} \xrightarrow{k_2} \text{Char + Volatile (II)} \tag{3.10}$$

where k_1 and k_2 are reaction rate constants of the first and second steps of reaction, respectively. The model is simplified by assuming pure kinetic reaction control, no secondary reactions of the gaseous products and the pyrolytic reactions for low and high-temperature regimes following first order reaction and contracting volume mechanism, respectively. The kinetic equations describing the pyrolysis process are presented as the following set of equations,

$$\frac{dU}{dT} = -\frac{2A_1}{\beta}\exp(-\frac{E_1}{RT})U \tag{3.11}$$

$$\frac{dZ}{dT} = \frac{A_1}{\beta}\exp(-\frac{E_1}{RT})U - \frac{6A_2}{\beta}\exp(-\frac{E_2}{RT})Z^{\frac{2}{3}} \tag{3.12}$$

$$\frac{dW}{dT} = \frac{3A_2}{\beta}\exp(-\frac{E_2}{RT})Z^{\frac{2}{3}} \tag{3.13}$$

where, U, Z and W are weight fractions of raw material, intermediate and solid char, respectively. The initial conditions for these three ordinary differential equations are U=1, Z=W=0 and T=T_0. The residual weight fraction of sample at any temperature and time should be equal to the summation of raw material, intermediate and char.

The above set of ordinary differential equations can be solved, for example, using ODE solver of MATLAB program.

In addition, the data fitting by applying the modified two-step consecutive reaction was further studied in the present work. This model was proposed by Luangkiattikhun P. (2007) by adding the stoichiometric coefficients of the reactions, x and y, in the reaction schemes of the original two-step consecutive model. That is,

$$\text{Raw material} \xrightarrow{k_1} x \cdot \text{Intermediate} + \text{Volatile (I)} \tag{3.14}$$

$$\text{Intermediate} \xrightarrow{k_2} y \cdot \text{Char} + \text{Volatile (II)} \tag{3.15}$$

The assumptions are a pure kinetic controlled process, no secondary reactions among the gaseous products and the pyrolysis reactions following first order reaction for the first step and n^{th} order for the second step, respectively. The decomposition rate of raw material and generation rates of intermediate and char are expressed as

$$\frac{dU}{dT} = -\frac{A_1}{\beta}\exp(-\frac{E_1}{RT})U \tag{3.16}$$

$$\frac{dZ}{dT} = x\frac{A_1}{\beta}\exp(-\frac{E_1}{RT})U - \frac{A_2}{\beta}\exp(-\frac{E_2}{RT})Z^n \tag{3.17}$$

$$\frac{dW}{dT} = y\frac{A_2}{\beta}\exp(-\frac{E_2}{RT})Z^n \tag{3.18}$$

where n is the order of the second step of pyrolysis reaction and the relationship between x and y is correlated with the final char yield, m_f, written as

$$x = \frac{m_f}{y} \tag{3.19}$$

The residual weight fraction of sample at any time or temperature is the sum of weight fractions of raw material, intermediate and char. The differential equations are solved using ODE solver in MATLAB program with the initial values of U=1, Z=W=0 and T=T_0.

3.3.2.3 Two Parallel Reactions Model

The two parallel reactions model which has been proposed by Luangkiattikhun, P. (2007) was also tested for describing the reaction of biomass pyrolysis in the present study. It is assumed that raw material consists of two components, M_1 and M_2, which decompose simultaneously according to Equations (3.20) and (3.21), respectively. The reaction is controlled by kinetic process only and there are no secondary reactions among the gaseous products and char.

$$\mathrm{M_1} \xrightarrow{k_1} \text{Volatile + char} \tag{3.20}$$

$$\mathrm{M_2} \xrightarrow{k_2} \text{Volatile + char} \tag{3.21}$$

where k_1 and k_2 represent the rate constant of reaction occurring from the first and the second fractions, respectively. The first fraction is assumed to decompose via first order reaction and the second fraction obeys n^{th} order reaction. The decomposition rates of the two parallel reactions are presented as the following,

$$\frac{d\alpha_1}{dT} = -\frac{A_1}{\beta}\exp(-\frac{E}{RT})\alpha_1 \tag{3.22}$$

$$\frac{d\alpha_2}{dT} = -\frac{A_2}{\beta}\exp(-\frac{E}{RT})\alpha_2{}^n \tag{3.23}$$

The residual weight fractions of solid product are defined as follows

$$\alpha = \frac{M - m_f}{1 - m_f}; \quad \alpha_1 = \frac{M_1 - m_{f1}}{1 - m_f}; \quad \alpha_2 = \frac{M_1 - m_{f2}}{1 - m_f} \tag{3.24}$$

where m_f is the final yield of char and m_{f1} and m_{f2} are the final mass fractions of the first and second components, respectively. M, M_1 and M_2 are mass fractions of total residual weight, residual weight of the first and second components present at time t, respectively. Their relationships are

$$m_f = m_1 + m_2 \tag{3.25}$$

$$M = M_1 + M_2 \tag{3.26}$$

By integrating Equations (3.22) and (3.23), the solutions of the remaining mass of the first and second components at any temperature, α_1 and α_2, can be obtained as the following equations

$$\alpha_1 = \exp\left[-\frac{A_1RT^2}{\beta E_1}\left(1 - \frac{2RT}{E_1}\right)\exp\left(-\frac{E_1}{RT}\right) + \ln(a)\right] \tag{3.27}$$

$$\alpha_2 = \left[\frac{(n-1)A_2RT^2}{\beta E_2}\left(1-\frac{2RT}{E_2}\right)\exp\left(-\frac{E_2}{RT}\right) + b^{(1-n)} \right]^{\frac{1}{1-n}} \tag{3.28}$$

where *a* and *b* are the initial weight fractions of the first and second components. The total remaining mass at any temperature is the sum of each residual fraction, that is

$$\alpha = \exp\left[-\frac{ART^2}{\beta E_1}(1-\frac{2RT}{E_1})\exp(-\frac{E_1}{RT}) + \ln(a) \right] + \left[\frac{(n-1)A_2RT^2}{\beta E_2}(1-\frac{2RT}{E_2})\exp(-\frac{E_2}{RT}) + b^{(1-n)} \right]^{\frac{1}{1-n}} \tag{3.29}$$

All models were fitted with the experimental data (TG data) to determine their kinetic parameters. The derived kinetic parameters were estimated by minimizing the sum of square of relative error (*SSRE)*, defined as

$$SSRE = \sum_{i=1}^{N}\left[\frac{(\alpha_{\exp})_i - (\alpha_{cal})_i}{(\alpha_{\exp})_i} \right]^2 \tag{3.30}$$

where $(\alpha_{\exp})_i$ and $(\alpha_{cal})_i$ are the experimental and calculated values, respectively, and *N* is the total number of data points.

3.4 Materials and Methods

3.4.1 Feedstock Characterization

Biomass feedstocks including cassava pulp residue, palm kernel cake, palm shell, coconut shell and longan fruit seed were milled and sieved to obtain an average particle size of 106 μm for biomass characterization and pyrolysis kinetic studies. In addition, four particle sizes of cassava pulp residue including 106, 431, 750 and 1,325 µm were also used for studying particle size effect on the pyrolysis kinetic. The sieved biomasses were dried at 120°C for 24 hours in an oven. The dried biomass samples were characterized for bulk density, true density (Helium pycnometer, AccuPyc 1330 Micromeritics), proximate analysis (moisture content (ASTM D2867-95), volatile content (ASTM D5832-95), ash content (ASTM D2866-94) and fixed carbon content (by difference)), elemental analysis (CHNS/O analyzer, Perkin Elmer PE2400 series II) and heating values (ASTM D3286-96).

3.4.2 Kinetic Studies

Thermal decomposition behavior of various biomasses was studied using a thermogravimetric analyzer (SDT 2960 simultaneous DSC-TGA model, TA instruments). For this analysis, a sample of 10-15 mg was heated from room temperature to 650°C with a heating rate varying from 5 to 40ºC/min under a nitrogen flow rate of 100 cm^3/min. All test conditions are summarized in Table 3.2. The fractional weight remaining (TG data) and its first derivative (DTG data) as a function of increasing temperature were recorded continuously. The weight remaining TG data derived under varying heating rates (5-40°C/min) and particle sizes (106-1,325 µm) of cassava pulp residue were fitted with the previous proposed five models (detailed in section 3.3.2) to simulate the kinetic of pyrolysis process using optimization function of MATLAB program based on Equation (3.30).

Table 3.2 Pyrolysis conditions for pyrolysis kinetic studies.

Parameters affecting pyrolysis kinetic	**Fixed conditions**	**Studied parameters**
Biomass type	Particle size of 106 µm, Heating rate of 20°C/min	Cassava pulp residue
		Palm kernel cake
		Palm shell
		Coconut shell
		Longan fruit seed
Particle size (µm)	Cassava pulp residue, Heating rate of 20°C/min	106
		431
		750
		1,325
Heating rate (°C/min)	Cassava pulp residue, Particle size of 106 µm	5
		10
		20
		40

3.5 Results and Discussions

3.5.1 Feedstock Properties

Table 3.3 shows basic physical properties and compositions of the biomasses studied. Bulk densities of the various biomasses at average particle size of 106 µm are in the range of 0.36-0.79 g/cm^3. The bulk density of cassava pulp residue is lowest being about half of the other biomasses. For cassava pulp residue, increasing particle size from 106 to 1,325 µm gives slightly decrease of solid bed density. The true densities of all biomasses are not so greatly different varying in the range from 1.385-1.507 g/cm^3. Proximate and elemental analyses show that the main composition of biomasses is volatile contents and carbon and oxygen are the major elements. The gross heating values of all biomasses are approximately the same with the value of about 22 MJ/kg.

Table 3.3 Biomass properties and chemical compositions.

Properties	**Biomass type**				
	Cassava pulp residue	**Palm kernel cake**	**Palm shell**	**Coconut shell**	**Longan fruit seed**
Bulk density (g/cm^3)					
particle size of 106 µm	0.362	0.711*	0.786*	0.797*	0.789*
particle size of 431 µm	0.341				
particle size of 750 µm	0.332				
particle size of 1,325 µm	0.320				
True density (g/cm^3)	1.507	1.385	1.416	1.421	1.470
Proximate analysis (Dry basis) (wt%)					
Volatiles	81.98	79.57	75.69	82.38	84.51
Fixed carbon	11.83	16.74	19.20	16.33	14.80
Ash	6.19	3.69	5.11	1.29	0.70
Elemental analysis (wt%)					
C	35.89	47.19	48.74	49.76	43.75
H	5.47	6.38	4.99	5.60	6.30
O	58.27	43.28	45.63	44.30	48.81
N	0.36	3.15	0.64	0.35	1.14
H/C (mole ratio)	1.829	1.622	1.229	1.727	1.350
O/C (mole ratio)	1.218	0.688	0.702	0.837	0.668
Gross heating value (MJ/kg)	22.41	21.91	22.29	21.28	21.16

Note: * = Bulk density at particle size of 106 µm

3.5.2 Non Isothermal Pyrolysis of Biomasses

Non-isothermal thermogravimetric analysis of various biomasses were investigated as a function of particle size and heating rate and the thermal analysis results are presented in Figures 3.1-3.3 as weight percent remaining (TG curves) and its first derivative (DTG curves). Generally, the TG curves showed sigmoid shape and DTG curves exhibited one or two major peaks depending on the type of biomass.

For the effect of biomass type, Figure 3.1 (a) shows that the TG curves almost superimposed on one another, except the cassava pulp residue, where its curve shifted downward at temperatures higher than 350°C. From DTG curves in Figure 3.1 (b), it was noted that the main pyrolysis decomposition of all biomasses occurred roughly in the range of 250-400°C. Obviously, the thermal decomposition of these biomasses will result from contributions of their lignocellulosic components (hemicellulose, cellulose and lignin), which generally decompose over the temperature range of 200-400°C (Antal, 1983). Lignin usually decomposes first at the lowest temperature and continues up to the temperature around 900°C. Hemicellulose and cellulose decompose over the temperature range of 160-360°C and 240-390°C, respectively (Vamvuka *et al.*, 2003). At pyrolysis temperature of 350°C cassava pulp residue gave the lowest weight remaining with its final weight at 650°C being 19.9 wt%, whereas that of the other biomasses was about 26.2 wt% at the same pyrolysis conditions (Figure 3.1(a) and Table 3.4). This may imply that cassava pulp residue may contain larger fractions of cellulose and hemicellulose, thus contributing to the releasing of more volatile components, while other biomasses could contain higher lignin content that is responsible for the production of higher char yield (Koufopanos *et al.*, 1989; Shafizadeh and McGinnis, 1971; Williams and Besler, 1994). It can be also noted that there are three distinct characteristics of DTG curves as displayed in Figure 3.1 (b). Cassava pulp residue and longan fruit seed had only one distinct peak of DTG curve, while palm shell and coconut shell gave two peaks of decomposition and the palm kernel cake showed one major peak with a small shoulder. In addition, the temperature that gives the maximum decomposition rate depends on the biomass type. Two maximum of decomposition rates of palm shell and coconut shell occurred at approximately the same temperatures of 295 and 350°C, while the maximum decomposition rate of palm kernel cake, cassava pulp residue and longan fruit seed occurred at the temperature of 290, 310 and 320°C, respectively.

Cassava pulp residue was also used to study the effects of particle size and heating rate on the pyrolysis characteristics. Figures 3.2 (a) and (b) indicate that cassava pulp residue pyrolysis at particle size in the range of 106-1,325 µm gave almost no effect on the weight remaining and its 1st derivative. The main decomposition occurred between 210 and 380°C and the final weight remaining was about 19.6 wt% (Table 3.4). The insensitivity of the thermograms with respect to changes in particle size tends to indicate that the particle size studied is small enough to cause no effects of heat and mass transfer resistances inside the particle. This agrees with the work of Guo and Lua (2001) that pyrolysis is controlled by pure reaction kinetics for the sample particle sizes of smaller than 2 mm. On the effect of heating rate, Figure 3.3 (a) shows that pyrolysis at the heating rate of 5-40°C/min exhibited almost no effect on the TG curves at temperatures less than 350°C. However, at higher temperatures, pyrolyzing at higher heating rate gave lower value of weight remaining. It is probable that rapid heating could impose faster rate of decomposition; the plot of DTG curve indicated that the pyrolysis at higher heating rate provided higher rate of decomposition and wider temperature ranges of decomposition (Figure 3.3 (b)). However, the temperature giving maximum rate of decomposition was shifted to a higher temperature when higher heating rate was applied (Figure 3.3 (b) and Table 3.4). This may be explained that the increase of heating rate could cause larger temperature gradient between the surface and inside the particles which would cause a lower average temperature inside the particle for the same pyrolysis temperature and thus shifting the maximum decomposition rate to a higher temperature. Furthermore, a small shoulder was observed at heating rates greater than 20°C/min and this may result from the effect of heat transfer lag that could prolong the decomposition of some biomass components.

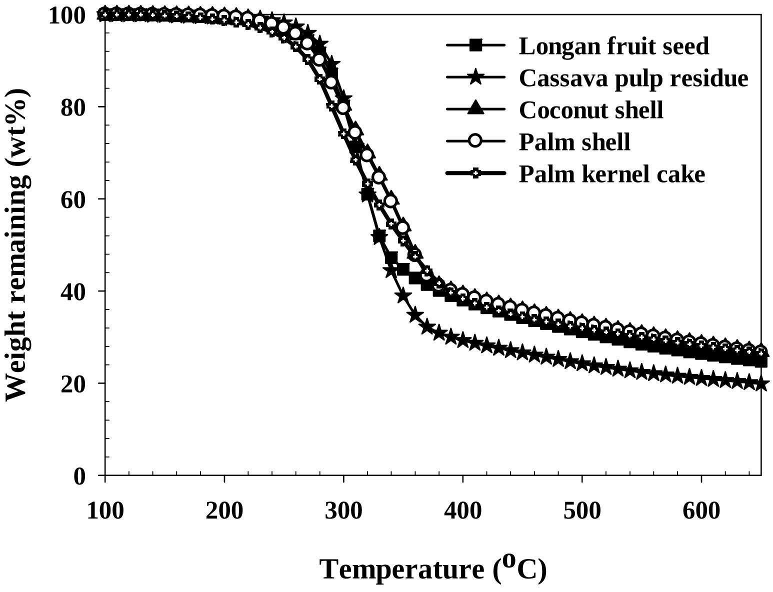

(a)

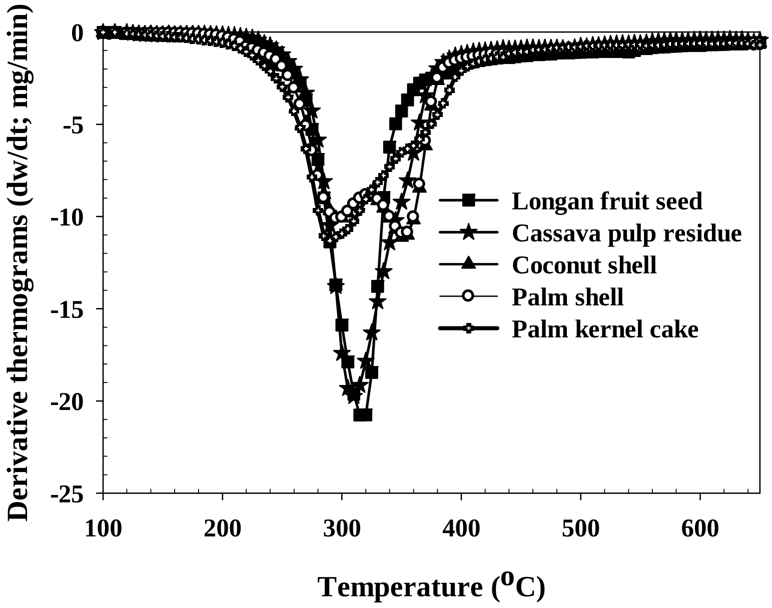

(b)

Figure 3.1 Thermal analysis of various biomasses: (a) TG and (b) DTG (average particle size of 106 µm, heating rate of 20°C/min and nitrogen flow rate of 100 cm^3/min).

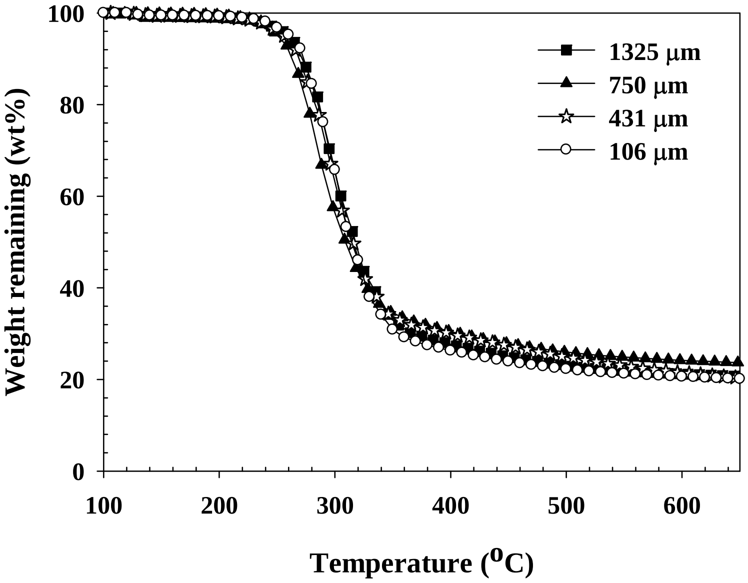

(a)

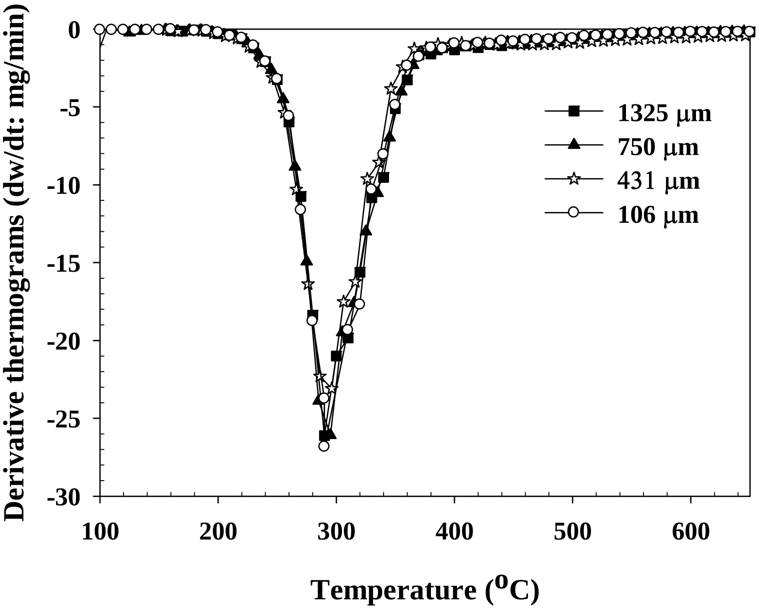

(b)

Figure 3.2 Thermal analysis of cassava pulp residue at various particle sizes: (a) TG and (b) DTG (heating rate of 20°C/min and nitrogen flow rate of 100 cm^3/min).

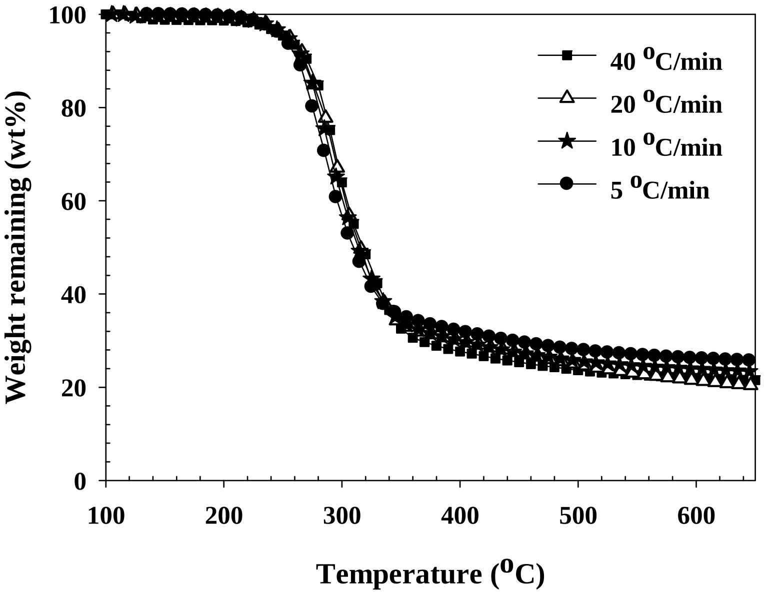

(a)

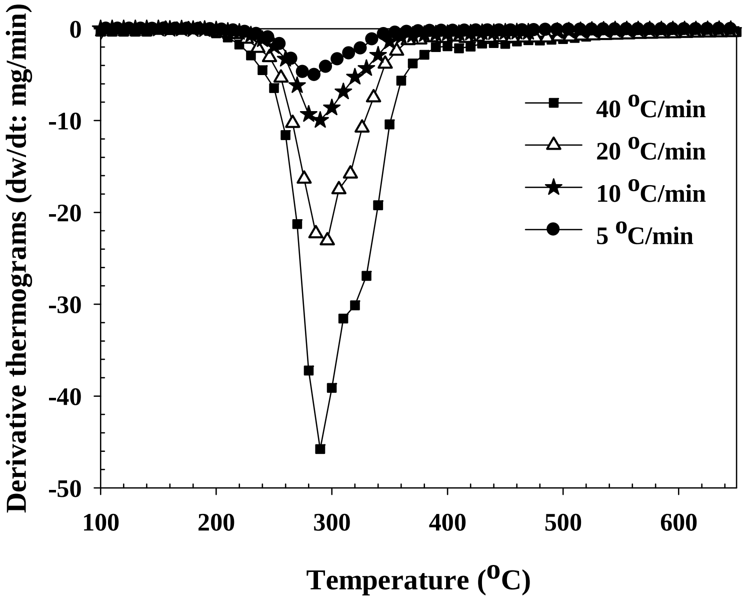

(b)

Figure 3.3 Thermal analysis of cassava pulp residue at various heating rates: (a) TG and (b) DTG (particle sizes of 431 μm and nitrogen flow rate of 100 cm^3/min).

Table 3.4 First and second maximum decomposition rates ($(\frac{dw}{dt})_{1,\max}$ and $(\frac{dw}{dt})_{2,\max}$) at corresponding temperatures ($T_{1,\max}$ and $T_{2,\max}$) and final residual weights (m_f) of various studied biomasses.

Biomass type	**Heating rate (°C/min)**	**Particle size (µm)**	**$T_{1,max}$ (°C)**	**$(\frac{dw}{dt})_{1,max}$ (wt%/min)**	**$T_{2,max}$ (°C)**	**$(\frac{dw}{dt})_{2,max}$ (wt%/min)**	**m_f (wt%)**
Cassava pulp residue	20	106	310	-19.78	-	-	19.89
Palm kernel cake			290	-11.98	-	-	26.42
Palm shell			295	-10.30	350	-11.09	26.81
Coconut shell			295	-10.80	350	-11.13	26.65
Longan fruit seed			320	-21.05	-	-	24.73
Cassava pulp residue	20	106	290	-27.00	-	-	19.11
		231	290	-24.18	-	-	19.35
		725	290	-26.59	-	-	20.90
		1,325	290	-27.11	-	-	19.16
Cassava pulp residue	5		283	-5.06	-	-	23.84
	10		288	-9.97	-	-	20.77
	20		290	-24.18	-	-	19.35
	40		290	-45.77	-	-	19.09

3.5.3 Model Fitting and Estimation of Kinetic Parameters

In this section, the TG data of cassava pulp residue pyrolysis at different particle sizes and heating rates were further tested with the five kinetic models and pyrolysis kinetic parameters determined from the model fitting.

3.5.3.1 One-Step Global Model

The simplest model of one-step global model was expected to give reasonable fitting for single peak of DTG curves derived from cassava pulp residue decomposition. However, as Figure 3.4 shows the one-step global model assuming first-order reaction underpredicted the experimental value at the upper and lower inflection points. Maximum errors resulting from the mismatch were in the range of 22.51-28.43% (Table 3.5). The fitting parameters including frequency factor, *A* and activation energy, *E* were in the range of $1.05\text{x}10^3$-$1.04\text{x}10^6$ s^{-1} and $6.84\text{x}10^1$-$8.92\text{x}10^1$ kJ/mol, respectively, with no definite trend for the effect of heating rate and particle size (Table 3.5). On the other hand, the fitting by one-step global model assuming n^{th} order reaction provided improved fitting but relatively large error in the range of 7.96-13.98% was still observed (Figure 3.5 and Table 3.6). The estimated reaction order for cassava pulp residue pyrolysis was not remarkably different for the influence of particle size but tended to decrease with increased heating rate. The activation energy, *E*, was considered relatively constant being about $1.99\text{x}10^2$-$2.53\text{x}10^2$ kJ/mol, while the frequency factor, *A* appeared to decrease with increasing in particle size and heating rate (Table 3.6). Concerning the fitted results, using one-step global model, great deviations were still obtained especially at the inflection points of the TG curves. Next, the two-step consecutive reaction model and the two parallel reactions model were further applied to test their validities in describing the actual pyrolysis kinetic of the test biomasses.

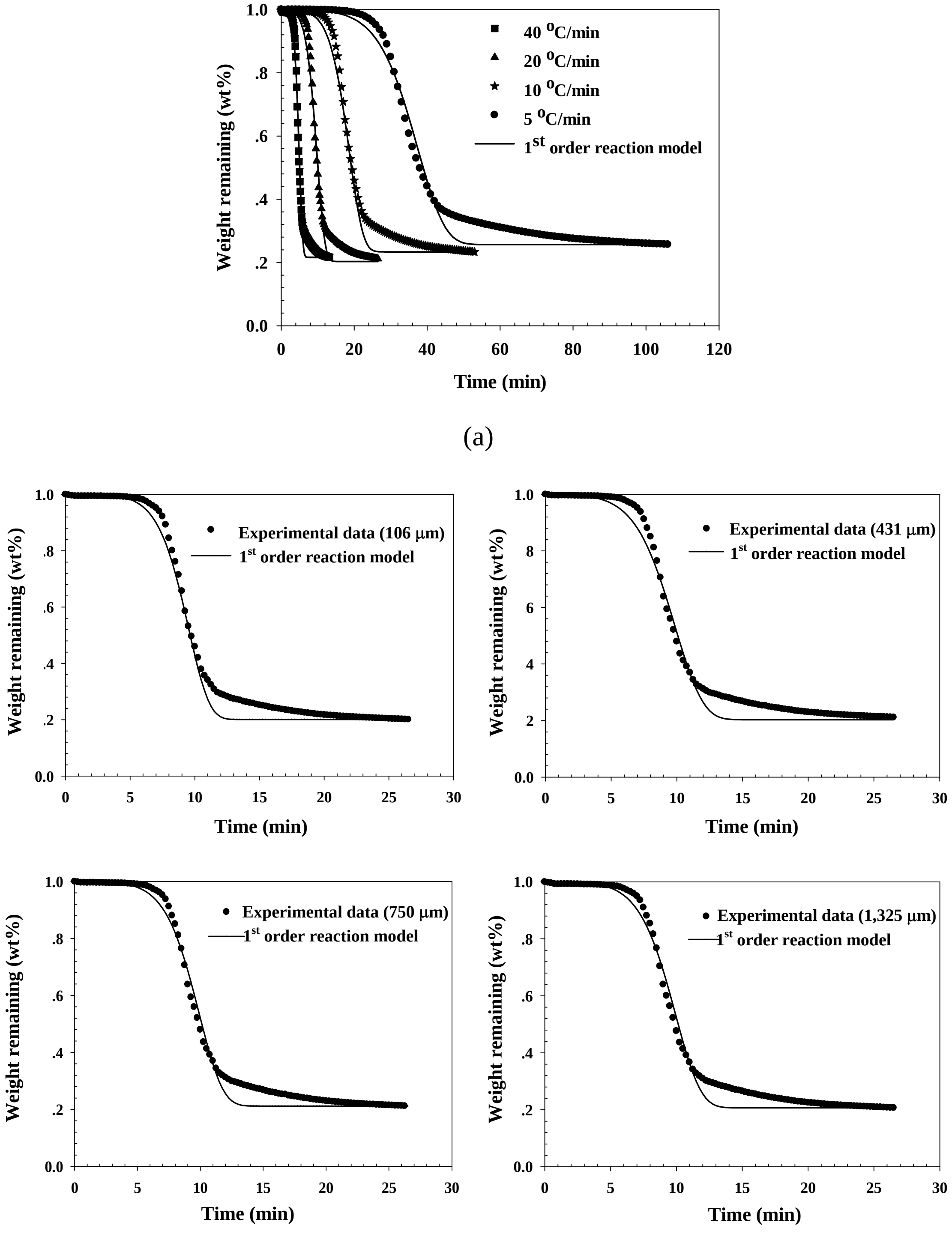

(a)

(b)

Figure 3.4 Comparison of the fitting results of one-step global model with assuming first-order reaction and experimental data for effects of (a) heating rate and (b) particle size.

Table 3.5 Kinetic parameters of one-step global model assuming 1st order reaction for cassava pulp residue pyrolysis.

Particle size (µm)	**Heating rate (°C/min)**	***A*** **(s^{-1})**	***E*** **(kJ/mol)**	**Maximum error (%)**
106	20	1.04×10^{6}	8.92×10^{1}	28.43
431		9.06×10^{5}	6.84×10^{1}	27.01
725		7.77×10^{4}	7.84×10^{1}	25.63
1,325		5.77×10^{4}	7.71×10^{1}	26.16
431	5	1.42×10^{4}	7.54×10^{1}	22.51
	10	2.28×10^{4}	7.53×10^{1}	25.17
	20	9.06×10^{3}	6.84×10^{1}	27.01
	40	1.05×10^{3}	7.65×10^{1}	23.14

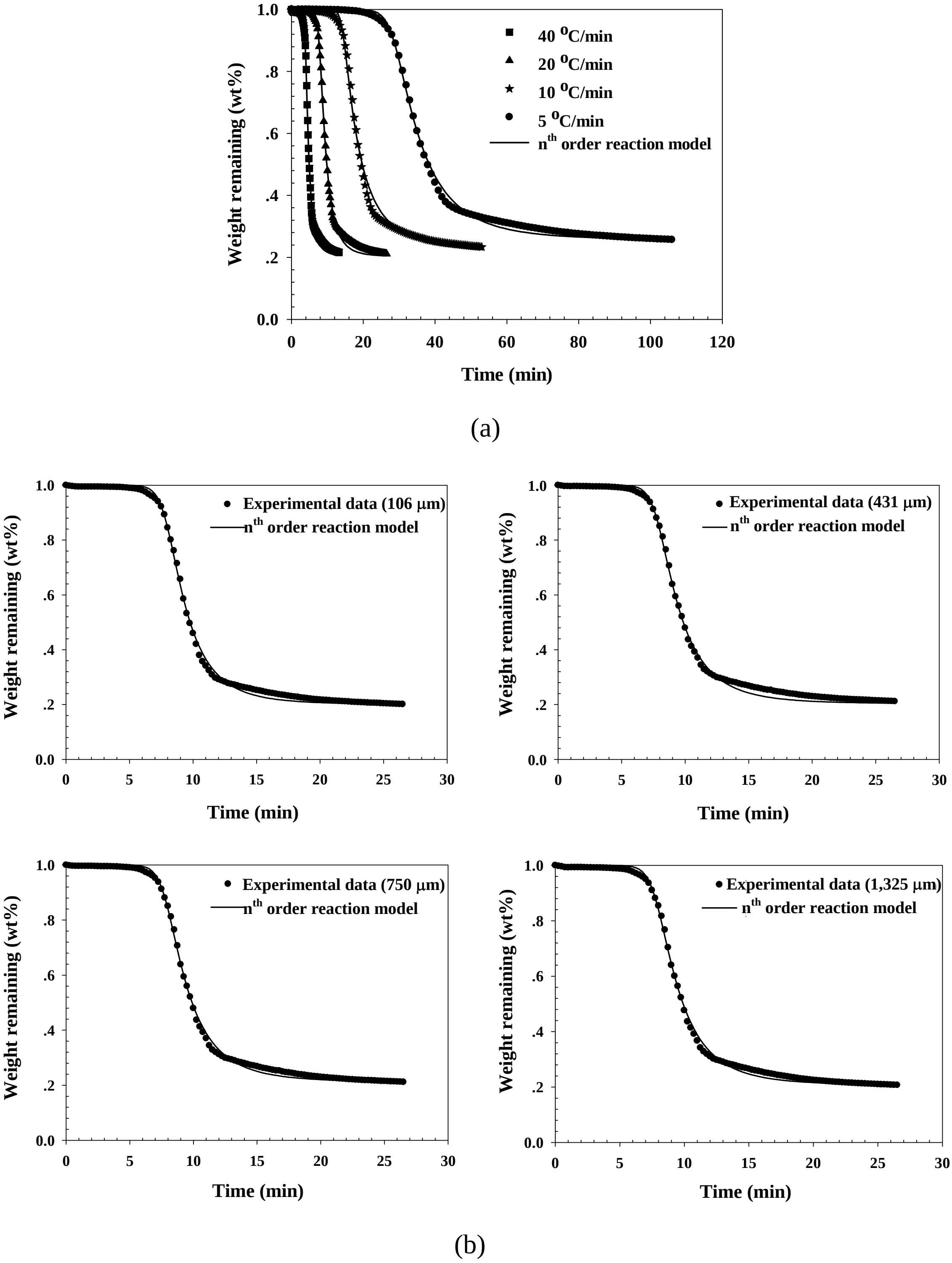

Figure 3.5 Comparison of the fitting results of one-step global model with assuming n^{th} order reaction and experimental data for effects of (a) heating rate and (b) particle size.

Table 3.6 Kinetic parameters of one-step global model with assuming nth order reaction for cassava pulp residue pyrolysis.

Particle size (μm)	**Heating rate (°C/min)**	***A*** **(s^{-1})**	***E*** **(kJ/mol)**	**n**	**Maximum error (%)**
106	20	1.53×10^{20}	2.35×10^{2}	4.34	8.42
431		9.15×10^{19}	2.32×10^{2}	4.62	10.82
725		6.46×10^{19}	2.33×10^{2}	4.59	8.32
1,325		2.32×10^{19}	2.26×10^{2}	4.55	8.38
431	5	8.72×10^{21}	2.53×10^{2}	5.34	7.96
	10	5.65×10^{19}	2.31×10^{2}	5.60	13.98
	20	9.15×10^{19}	2.32×10^{2}	4.62	10.82
	40	1.13×10^{19}	1.99×10^{2}	3.97	8.32

3.5.3.2 Two-Step Consecutive Reaction Model

The fitting of experimental TG data by using the two-step consecutive reaction model of Guo and Lua (Guo and Lua, 2001) indicated that the agreement between the experimental and the predicted values was satisfactory up to the weight remaining of about 30% at which the main decomposition period had been passed (Figure 3.6). Afterwards, the weight remaining of cassava pulp residue pyrolysis decreased slowly but the predicted value from the model approached a constant value. This results in the maximum error lying between 3.53-24.83% (Table 3.7). The maximum errors tended to increase with increased heating rate but there was no definite trend as to the effect of particle size on the maximum error, with particle size of 106 μm giving the maximum error of 25%. The frequency factor and activation energy of the first reaction (A_1 and E_1) remained relatively constant independent of particle size and heating rate, with the average values being about 2.12×10^{8} s^{-1} and 1.12×10^{2} kJ/mol, respectively (Table 3.7). For the frequency factor and activation energy of the secondary reaction (A_2 and E_2), they did not give a definite trend with respect to changes in particle size and heating rate, varying in the range of 1.52x10^2-3.90x10^2 s^{-1} and 1.23x10^1-4.45x10^1 kJ/mol, respectively.

The limitation of applying Guo and Lua model is that it cannot describe the pyrolysis kinetic of cassava pulp residue after the main decomposition period. The modified Guo and Lua model, the two-step consecutive reaction with the allowance for reaction stoichiometry, was then attempted to overcome this shortcoming. Figure 3.7 showed that using the modified Guo and Lua model can improve the fitting results considerably for all conditions. The maximum errors were in the range of 3.06-8.34%. The stoichiometric coefficients for the primary and secondary reactions derived from the model fitting were 0.44 and 0.49, respectively. The kinetic parameters including frequency factor (A), activation energy (E) and reaction order (n) seems to be insensitive to the changes in heating rate and particle size (Table 3.8). The A_1 and E_1 of the primary reaction assuming first-order reaction were approximately constant of about 1.34x10^{10} s^{-1} and 1.30x10^2 kJ/mol, respectively, while the average values of A_2 and E_2 of the secondary reaction were 1.24x10^{24} s^{-1} and 2.69x10^2 kJ/mol, respectively, and the orders of reaction varied widely in the range 6.55 to 8.76 (Table 3.8). The higher values of the fitting parameters, A_2 and E_2 compared to A_1 and E_1 indicates that the decomposition rate of the secondary reaction is greater than that of the primary reaction but the decomposition of the secondary reaction is more difficult to proceed.

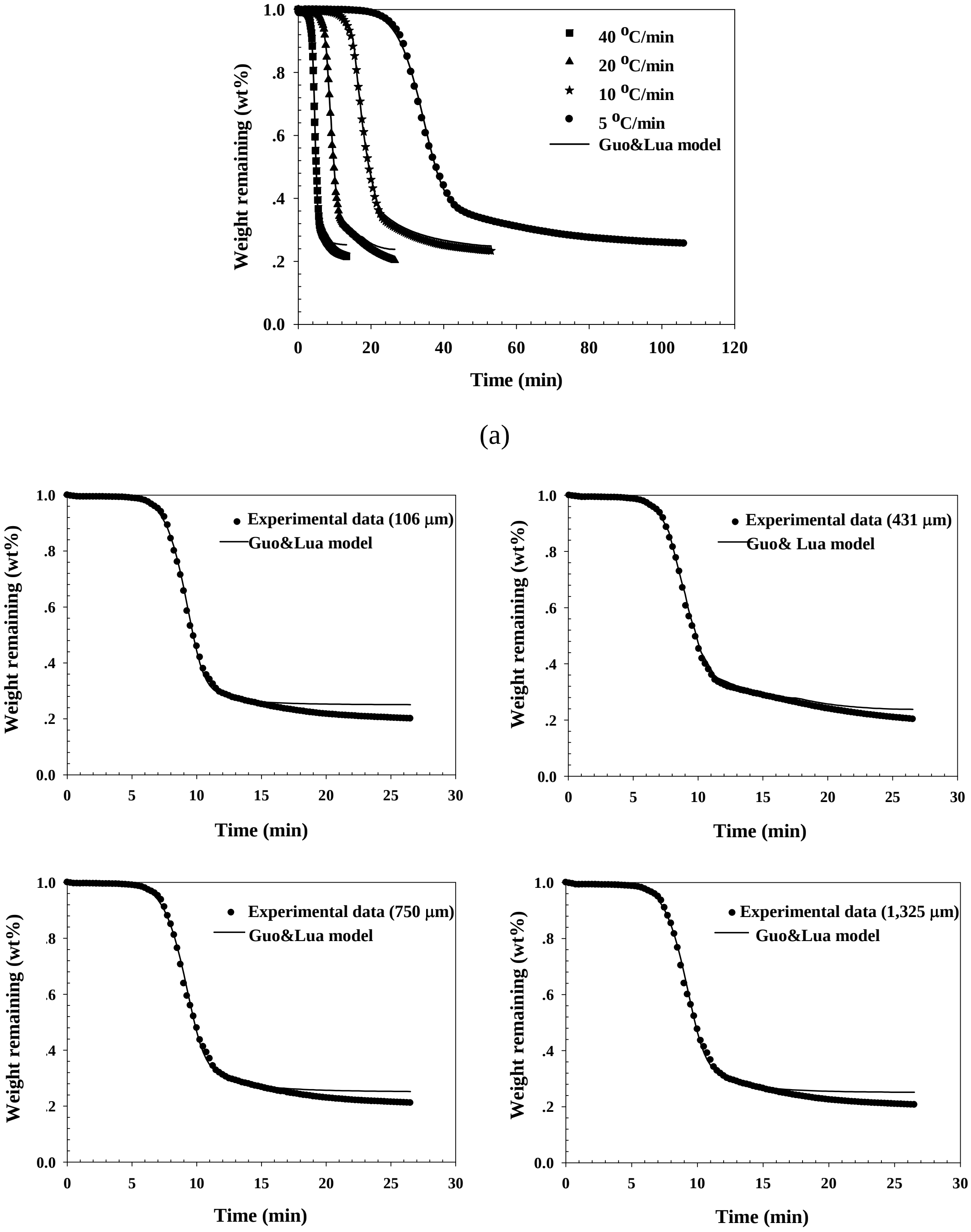

(a)

(b)

Figure 3.6 Comparison of the fitting results of two-step consecutive reaction model based on Guo and Lua concept and experimental data for effects of (a) heating rate and (b) particle size.

Table 3.7 Kinetic parameters of two-step consecutive reaction model based on Guo and Lua concept for cassava pulp residue pyrolysis.

Particle size (μm)	**Heating rate (°C/min)**	A_1 (s^{-1})	E_1 (kJ/mol)	A_2 (s^{-1})	E_2 (kJ/mol)	**Maximum error (%)**
106	20	$2.11\text{x}10^8$	$1.15\text{x}10^2$	$1.69\text{x}10^2$	$4.18\text{x}10^1$	24.83
431		$2.14\text{x}10^8$	$1.10\text{x}10^2$	$2.11\text{x}10^2$	$3.73\text{x}10^1$	17.31
725		$1.18\text{x}10^8$	$1.13\text{x}10^2$	$2.72\text{x}10^2$	$3.59\text{x}10^1$	19.21
1,325		$2.02\text{x}10^8$	$1.15\text{x}10^2$	$1.52\text{x}10^2$	$4.45\text{x}10^1$	21.52
431	5	$2.76\text{x}10^8$	$1.10\text{x}10^2$	$2.54\text{x}10^2$	$1.23\text{x}10^1$	3.53
	10	$2.07\text{x}10^8$	$1.09\text{x}10^2$	$2.78\text{x}10^2$	$1.28\text{x}10^1$	6.43
	20	$2.14\text{x}10^8$	$1.10\text{x}10^2$	$2.11\text{x}10^2$	$3.73\text{x}10^1$	17.31
	40	$2.52\text{x}10^8$	$1.13\text{x}10^2$	$3.90\text{x}10^2$	$3.42\text{x}10^1$	16.96

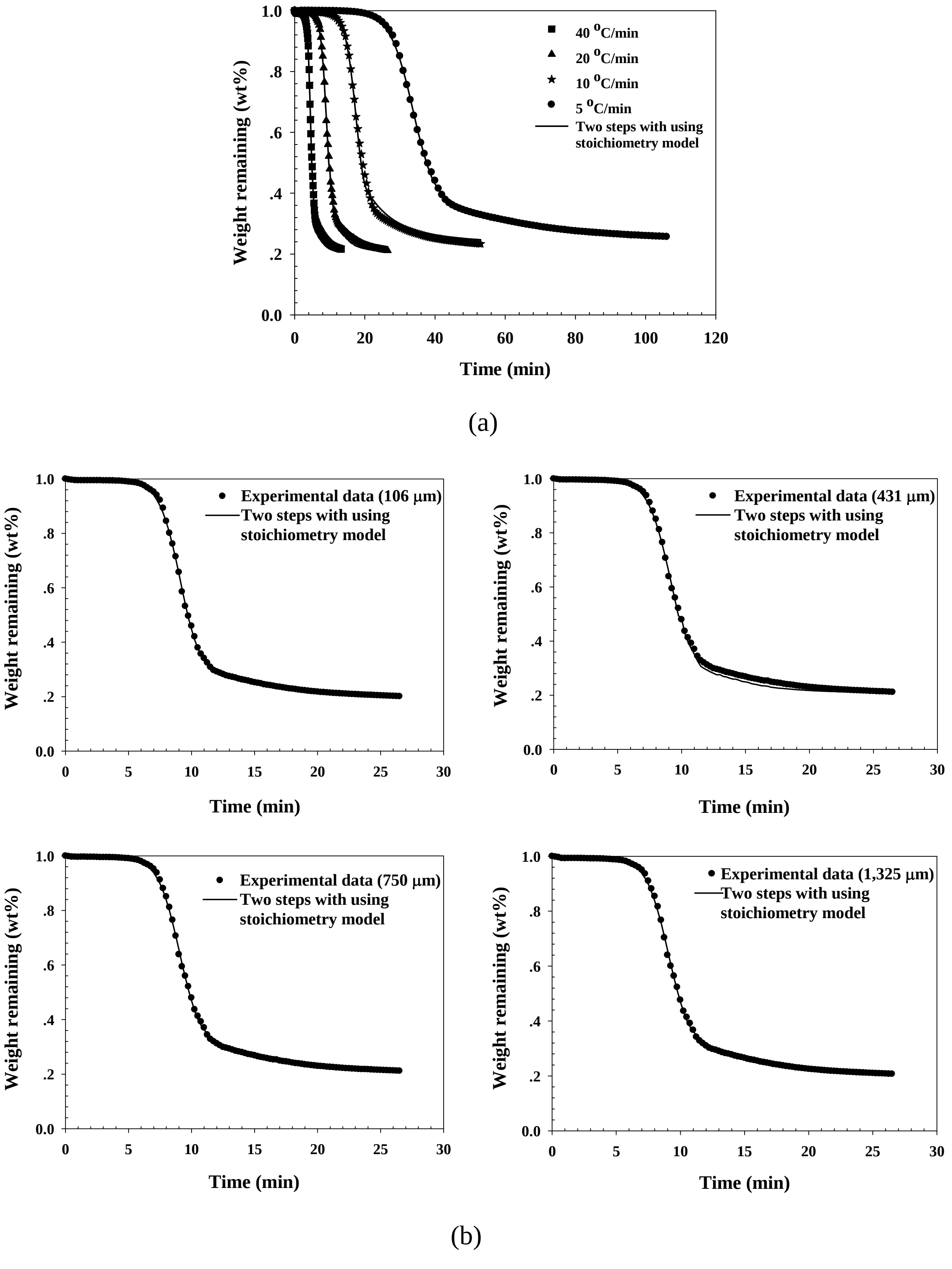

Figure 3.7 Comparison of the fitting results of two-step consecutive reaction model with provision of stoichiometric coefficient and experimental data for effects of (a) heating rate and (b) particle size.

Table 3.8 Kinetic parameters of modified two-step consecutive reaction model with provision of stoichiometric coefficient for cassava pulp residue pyrolysis.

Particle size (μm)	**Heating rate (°C/min)**	A_1 **(s^{-1})**	E_1 **(kJ/mol)**	A_2 **(s^{-1})**	E_2 **(kJ/mol)**	**n**	**Maximum error (%)**
106	20	1.35x10^{10}	1.31x10^{2}	8.27x10^{23}	2.67x10^{2}	7.05	3.48
231		1.10x10^{10}	1.30x10^{2}	1.02x10^{24}	2.70x10^{2}	6.98	7.87
725		1.10x10^{10}	1.30x10^{2}	1.03x10^{23}	2.70x10^{2}	6.97	3.32
1,325		1.26x10^{10}	1.30x10^{2}	8.67x10^{23}	2.69x10^{2}	6.94	3.28
231	5	1.76x10^{10}	1.29x10^{2}	4.34x10^{24}	2.71x10^{2}	7.72	3.06
	10	1.89x10^{10}	1.31x10^{2}	6.78x10^{23}	2.63x10^{2}	8.76	8.34
	20	1.10x10^{10}	1.30x10^{2}	1.02x10^{24}	2.70x10^{2}	6.98	7.87
	40	1.19x10^{10}	1.27x10^{2}	1.05x10^{24}	2.69x10^{2}	6.55	5.15

3.5.3.3 Two Parallel Reactions Model

The fitting by the two parallel reactions model gave excellent agreement between experimental data and predicted results for all pyrolysis conditions (Figure 3.8) with maximum errors lying between 3.1-3.6%. The model fitting gave the fractions of the first and second fractions to be 0.51 and 0.49, respectively. The reaction order of the second component varied in the range of 4.91-8.24. The frequency factor of the first component (A_1) tended to decrease with increasing particle size, while A_2 tended to decrease with increasing heating rate. A_1 and A_2 varied in the range of 1.03x10^{8}-4.14x10^{9} s^{-1} and 2.05x10^{16}-9.31x10^{20} s^{-1}, respectively (Table 3.9). The activation energy of the first and second components were almost constant varying in the narrow range of 1.06x10^{2}-1.27x10^{2} kJ/mol and 1.80x10^{2}-2.47x10^{2} kJ/mol, respectively (Table 3.9). It is noted that A_1 and E_1 are lower than A_2 and E_2 which implies that the first component of cassava pulp residue could decompose at a slower rate than the second component as well as easier to decompose than the second component. Since *E_1* and *E_2* fall in the range of activation energy for the pyrolysis of hemicellulose (80-116 kJ/mol) and cellulose (195-286 kJ/mol) (Gronli, *et al.*, 2002), it may be inferred that the first component is decomposed at a lower temperature than the second component. In addition, the first and the second components should represent the lighter compound of hemicellulose and heavier compound of cellulose, respectively.

Since there are many model parameters to be searched for, it is suggested that a sensitivity analysis on each optimized parameter should be performed to assess its significance on the model predictive capability.

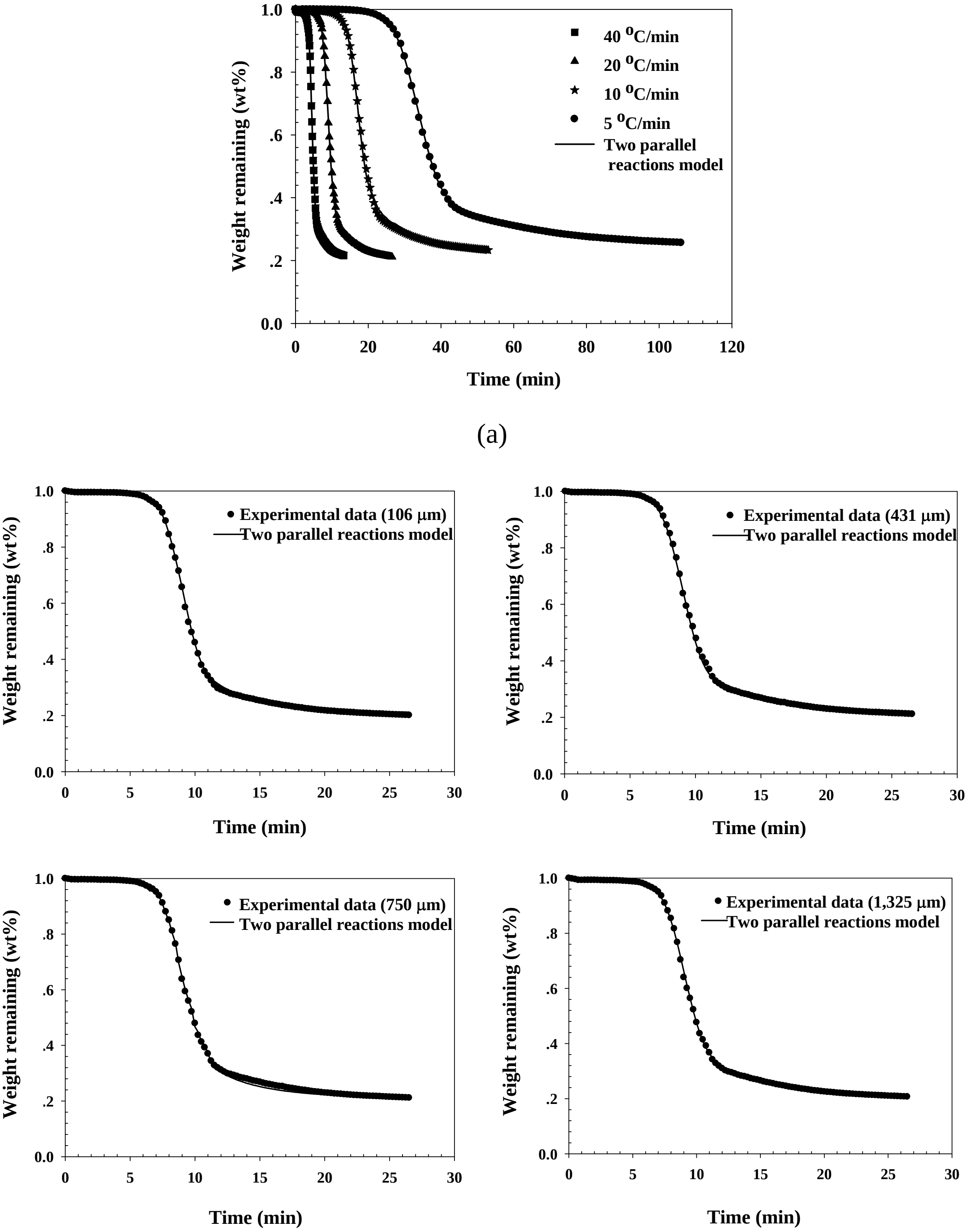

(a)

(b)

Figure 3.8 Comparison of the fitting results of two parallel reactions model and experimental data for effects of (a) heating rate and (b) particle size.

Table 3.9 Kinetic parameters of two parallel reactions model for cassava pulp residue pyrolysis.

Particle size (μm)	**Heating rate (°C/min)**	**A_1 (s^{-1})**	**E_1 (kJ/mol)**	**A_2 (s^{-1})**	**E_2 (kJ/mol)**	**n**	**Maximum error (%)**
106	20	4.14×10^{9}	1.27×10^{2}	2.26×10^{19}	2.12×10^{2}	5.67	3.20
431		2.90×10^{8}	1.14×10^{2}	8.02×10^{17}	1.99×10^{2}	5.47	3.43
725		2.39×10^{8}	1.13×10^{2}	1.43×10^{20}	2.21×10^{2}	6.00	3.55
1,325		1.35×10^{8}	1.10×10^{2}	5.98×10^{19}	2.18×10^{2}	5.89	3.47
431	5	1.08×10^{8}	1.13×10^{2}	9.31×10^{20}	2.27×10^{2}	6.78	3.09
	10	3.54×10^{8}	1.26×10^{2}	2.06×10^{20}	2.47×10^{2}	8.24	3.15
	20	2.90×10^{8}	1.14×10^{2}	8.02×10^{17}	1.99×10^{2}	5.47	3.43
	40	1.03×10^{8}	1.06×10^{2}	2.05×10^{16}	1.80×10^{2}	4.91	3.09

3.6 Conclusions

Non-isothermal pyrolysis characteristics of various biomass were studied as a function of particle size and heating rate in a thermogravimetric analyzer and different kinetic models, namely one-step global model, two-step consecutive reaction model and two parallel reactions model were tested and validated and the obtained results can be concluded as follows.

- Thermograms of various biomass decompositions presented as weight remaining with respect to temperature were sigmoid shape, with main decomposition occurring in the range of 250-400°C.
- Biomass type and heating rate (5-40°C/min) had significant effects on TG and DTG curves but thermograms derived from pyrolysis of cassava pulp residue at different particle sizes (106-1,325μm) were not greatly different.

- DTG curves of different biomasses showed the following characteristic curves, cassava pulp residue and longan fruit seed had only one distinct peak at 310 and 320°C, respectively, palm shell and coconut shell gave two peaks of decomposition at 295 and 350°C and palm kernel cake showed one major peak at 290°C with a small shoulder.

- Cassava pulp residue pyrolysis at different heating rates caused different char yield, decomposition rate and decomposition temperature range; pyrolysis at higher heating rate contributed lower char yield, higher decomposition rate and wider temperature range of decomposition.

- Fitting of thermal decomposition data of cassava pulp residue gave unsatisfactory results when one-step global model assuming first order reaction and two-step consecutive reaction model based on Guo and Lua concept were applied. The fitting results using one-step global model assuming nth order reaction and the two-step consecutive reaction plus incorporation of reaction stoichiometry were satisfactory. The use of two parallel reactions model showed the best fitting between predicted results and experimental data under all pyrolysis conditions.

- Optimized parameters derived from model fitting by the two parallel reactions model at different conditions were relatively constant or did not give a definite trend, varying in range of 1.03×10^8-4.14×10^9 s^{-1} for A_1, 1.06×10^2-1.27×10^2 kJ/mol for E_1, 2.05×10^{16}-9.31×10^{20} s^{-1} for A_2, 1.80×10^2-2.47×10^2 kJ/mol for E_2 and 4.91-8.24 for reaction order of the second component (n). Weight fraction of the first and second fractions which could represent lighter component of hemicellulose and heavier component of cellulose were found to be 0.51 and 0.49, respectively.

3.7 References

Answers Corporation (2009). Pyrolysis [On-line]. Available: **http://www.answers.com/topic/pyrolysis**.

Antal, M. J. (1983). Biomass pyrolysis: a review of the literature: part 1 carbohydrate pyrolysis. In Boer, K. W., and Duffie, J. A. (eds.), **Advances in Solar Energy. American Solar Energy Society** (pp. 61-111). Boulder, CO.

Antal, M. J., and Varhegyi, G. (1995). Cellulose pyrolysis kinetics: the current state of knowledge. **Industrial & Engineering Chemistry Resear**ch 34 (3): 703-717.

Babu, B. V. (2008). Biomass pyrolysis: a state-of the-art review. **Biofuels, Bioproducts and Biorefining** 2: 393-414.

Babu, B. V., and Chaurasia, A. S. (2003). Modeling, simulation, and estimation of optimum parameters in pyrolysis of biomass. **Energy Conversion and Management** 44 (13): 2135-2155.

Bridgwater, A. V. (2003). Renewable fuels and chemicals by thermal processing of biomass. **Chemical Engineering Journal** 91 (2-3): 87-102.

Di Blasi, C. (2008). Modeling chemical and physical processes of wood and biomass pyrolysis. **Progress in Energy and Combustion Science** 34 (1): 47-90.

Di Blasi, C., and Branca, C. (2001). Kinetics of primary product formation from wood pyrolysis. **Industrial & Engineering Chemistry Research** 40 (23): 5547-5556.

Gronli, M. G., Varhegyi, G., and Di Blasi C. (2002). Thermogravimetric analysis and devolatilization kinetics of wood. **Industrial & Engineering Chemistry Research** 41 (17): 4201-4208.

Guo, J., and Lua, A.C. (2001). Kinetic study on pyrolytic process of oil-palm solid waste using two-step consecutive reaction model. **Biomass and Bioenergy** 20 (3): 223-233.

Haines, P. J (1995). **Thermal methods of analysis principles, applications and problems**. Great Britain: The alden press.

Koufopanos, C. A., Maschio, G., and Lucchesi, A. (1989). Kinetic modeling of the pyrolysis of biomass components. **The Canadian Journal of Chemical Engineering** 67 (1): 75-84.

Luangkiattikhun, P. (2007). **Activated carbon from oil-palm solid wastes: preparation and CFD simulation of spouted bed activator**. Ph.D. Dissertation, Suranaree University of Technology, Thailand.

Miller, R. S., and Bellan, J. A. (1996). A generalized biomass pyrolysis model based on superimposed cellulose, hemicellulose and lignin kinetics. **Combustion Science and Technology** 126 (1):97-137.

Radlein, D. (1995). The chemistry of fast pyrolysis of biomass. Paper presented at **PYNE Pyrolysis Network for Europe, Minutes of First Meeting**, Solihull, UK.

Shafizadeh, F., and McGinnis, G. D. (1971). Chemical composition and thermal analysis of cotton wood. **Carbohydrate Research** 16 (2): 273-277.

Thurner, F., and Mann, U. (1981). Kinetic investigation of wood pyrolysis. **Industrial and Engineering Chemistry Process Design and Development** 20 (3): 482-488.

Vamvuka, D., Kakaras, E., Kastanaki, E., and Grammelis, P. (2003). Pyrolysis characteristics of biomass residuals mixture with lignite. **Fuel** 82 (15-17): 1949-1960.

Wagenaar, B. M., Prins, W., and Van Swaaij, W. P. M. (1994). Flash pyrolysis kinetics of pine wood. **Fuel Processing Technology** 36 (1-3): 291-302.

Williams, P. T., and Besler, S. (1994). Thermogravimetric analysis of the components of biomass. In Bridgwater A.V. (ed.). **Advances in thermochemical biomass conversion** (pp.771-783). London: Blackie Academic & Professional.

CHAPTER IV

SLOW PYROLYSIS OF BIOMASS

4.1 Abstract

Slow pyrolysis studies of five biomasses including cassava pulp residue (CPR), palm kernel cake (PKC), palm shell (PS), coconut shell (CS) and longan fruit seed (LFS) were conducted in a fixed bed reactor. Maximum liquid yield derived from the five biomasses varied in the range of 42.4-54.3 wt% at pyrolysis temperature 600-800°C, heating rate of 20°C/min, N_2 gas flow rate of 200 cm^3/min and particle size of 2.03 mm. For all biomass tested, fuel properties of pyrolysis liquids were in the following ranges: density, 1.01-1.18 g/cm^3; pH, 2.1-5.6; flash point, 74-110°C and pour point, -21-1°C. Dewatered PKC oil had boiling range distribution closest to that of diesel oil and its heating value was approximately equal to that of fuel oil (40 MJ/kg), while heating values of other bio-oils are lower varying in the range of 14-28 MJ/kg and all bio-oils possesses serious problem of high acidity. The composition of dewatered bio-oils from PKC and PS consisted mainly of n-C_8-C_{18} acids, phenols and esters, whereas CPR oil had the highest amount of methanol fraction consisting of polar and non-volatile compounds. Low amounts of n-paraffins, olefins and aromatics were also identified in these bio-oils. Increasing pyrolysis temperature led to higher contents of high molecular weights of n-alkanes and polycyclic aromatic hydrocarbon (PAH) and lower contents of esters and phenol. On gas compositions, CPR, PS and CS pyrolysis gave the highest concentration of syngas production, while PKC

pyrolysis offered the highest CO_2 composition and the highest CH_4 content was obtained from LFS pyrolysis. Solid char products from biomass pyrolysis offered calorific values varying from 29-35 MJ/kg, with PKC and PS chars showing a characteristic of reasonably high porosity material.

4.2 Introduction

Biomass pyrolysis has been known as one of the most promising process for energy recovery along with the production of valuable products. Nevertheless, the pyrolysis process requires several operational units and reliable process technologies to achieve the desired pyrolysis conditions. This could cause complication of process construction and operation. The mode of pyrolysis is a significant factor that can decide the complexity of pyrolysis system. For example, flash pyrolysis with the conditions of very high heating rate, short residence time and high temperature requires complicated feed preparation to obtain fairly small size particles, a special reactor and heat supply systems, large supply of sweeping gas, and recovery of fine char particles contaminated in bio-oil (Bridgwater, 1999; Goyal *et al.*, 2008). On the other hand, slow pyrolysis process, which has been known as the primary thermochemical process to convert biomass into energy source, offers much simpler construction and relatively low operating cost. These factors plus the flexibility of regulating pyrolysis conditions to produce the desired proportions of liquid, solid and gas products could make the slow pyrolysis process more attractive from the economic point of view.

In this work, the study of biomass pyrolysis was performed in a fixed-bed tubular reactor. The biomass feedstocks used in this work, including cassava pulp residue, palm kernel cake, palm shell, coconut shell and longan fruit seed are solid wastes of economically important crops in Thailand. High annual production of these biomasses should warrant their uses as low cost raw materials for converting them into a variety of valuable products by the simple process of pyrolysis. This work focused on studying the effect of biomass type and pyrolysis conditions (temperature, particle size, N_2 sweeping gas flow rate and heating rate) on product yields of solid char, pyrolysis liquids and gases. The derived pyrolysis products were characterized for their chemical and fuel properties to assess their potential uses as a source of renewable fuel and/or chemical feedstocks.

4.3 Literature Reviews

Biomass pyrolysis has been studied extensively in several pyrolysis systems (Bridgwater, 1999). The effects of pyrolysis conditions on yields and chemical compositions of pyrolysis products derived from different biomasses have been the subject of numerous investigations (Demirbaş, 2007). The pyrolysis conditions that affect the product yields and compositions include biomass type, reactor type, pyrolysis temperature, heating rate, sweep gas flow rate and biomass particle size.

4.3.1 Effects of Pyrolysis Conditions on Product yields

4.3.1.1 Effect of Biomass Type

Many different kinds of biomass have been studied, for example, linseed, cottonseed cake, legume straw, apricot stone, straw and stalk of rapeseed, sweet sorghum bagasse, soy-bean cake, etc. (Karaosmanoğlu *et al.*, 1999; Özbay *et al.*, 2001; Pütün *et al.*, 2002). It was found that the type of raw material had a strong effect on product yields. For instance, pyrolysis of sunflower pressed bagasse gave a maximum oil yield of 45.7 wt% at pyrolysis temperature of 550°C, while the pyrolysis of Euphorbia rigida and hazel nut shell at 500°C provided the maximum oil yields of 31.5 and 23.1 wt%, respectively (Pütün *et al*., 2001).

4.3.1.2 Effect of Pyrolysis Temperature

Generally, the increase of oil yield is observed as the pyrolysis temperature is increased from 400°C to a level of 500-550°C at which the oil yield is maximum, followed by a decrease in the oil yield at pyrolysis temperatures higher than 550°C. The increasing of pyrolysis temperature tended to decrease char yield and increase gas yield. (Onay and Koçkar, 2004; Özbay *et al.*, 2001). Moreover, the pyrolysis temperature has been reported to have an effect on water content in liquid product for the pyrolysis of biomasses such as linseed, cottonseed cake and Euphorbia rigida; maximum values of water content (18-27 wt%) were obtained at 500-700(C (Acıkgoz *et al.*, 2004; Özbay *et al.*, 2001; Pütün *et al.*, 2001). However, some biomasses such as sunflower oil cake, sunflower pressed bagasse and hazelnut shell showed no significant effect of temperature on the water yield (Pütün *et al.*, 2001; Yorgun *et al.*, 2001).

4.3.1.3 Effect of Heating Rate

Generally, rapid heating tends to produce high bio-oil yield (Karaosmanoğlu *et al.*, 1999; Onay and Koçkar, 2004). However, slow pyrolysis of safflower seed at the heating rate of 5°C/min gave surprisingly higher oil yield than that obtained at 40 and 80°C/min heating rates (Beis *et al.*, 2002). The work of Acıkgoz *et al.* (2004) on fast pyrolysis of linseed at heating rates of 100, 300 and 800°C/min showed also that there was no effect of heating rate on the oil yield. In addition, work of Karaosmanoğlu *et al.* (1999) indicated that no effect of heating rate on liquid yield was observed for pyrolysis at high pyrolysis temperature of 650°C for two different heating rates of 10 and 30°C/min.

4.3.1.4 Effect of Sweep Gas Flow Rate

Usually, maximum oil yield for fixed bed pyrolysis was obtained at 100-200 cm^3/min of nitrogen sweep gas flow rate and the nitrogen flow rate was found to have no significant effect on the gas and char yields (Onay and Koçkar, 2004; Pütün *et al.*, 2002). Work of Onay and Koçkar (2004) also indicated that the increase of sweep gas flow rate gave the same trend of oil yield for rapeseed pyrolysis at two different heating rates of 30 and 300°C/min. However, the effect of carrier gas flow rate on product yields showed different results for different particle sizes of the feedstock (Yorgun *et al.*, 2001). It was noted that the highest yield of bio-oil occurred at 300 cm^3/min of nitrogen gas flow rate for particle size in the range of 0.224-0.850 mm, with larger particle size giving higher oil and gas yield. On the other hand, pyrolysis of biomass with particles smaller than 0.224 mm showed less dependence of liquid yield on N_2 flow rate in the range of 25-600 cm^3/min.

4.3.2 Effects of Pyrolysis Conditions on Chemical Compositions of Pyrolysis Products

Apart from product yields, cellulosic composition of biomass and other process variables can have a profound influence on the chemical compositions of both gas and liquid products (Branca *et al.*, 2003; Yaman, 2004; Yang *et al.*, 2007). The effects of biomass type and pyrolysis temperature on product compositions are present next.

Cellulose and hemicellulose consisting of a polysaccharide and hetero-polysaccharide, respectively, can be decomposed to produce major components of carbohydrates, sugars, furans, acetaldehydes and high contents of formic acids, acetic acid, and acetol (Biomass Technology Group, 2003; Demirbas, 2007; Mohan *et al.*, 2006). Decomposition of lignin which is the polymer of complex cross-linked phenolic compounds leads to the formation of phenolics guaiacols, eugenols and syringols vanillins (Demirbaş, 2007; Yaman, 2004). In addition, it was reported that softwood lignins was degraded typically to guaiacyl products, while both guaiacyl and syringyl products were derived from hardwood lignin (Branca *et al.*, 2003). Considering the effect of biomass type on gas compositions, cellulose with high carbonyl and carboxyl contents gave higher CO content, hemicellulose generated higher CO_2, mainly attributed to the cracking of carboxyl compounds and lignin with a high proportion of aromatic ring and methoxyl components yielded higher H_2 and CH_4 contents (Yang *et al.*, 2007). Also, these gases are produced at temperatures corresponding with decomposition temperature of the three main compositions of biomass. CO and CO_2 were released at low temperature range of 200-450°C, while CH_4 mainly was generated at 400-600°C and H_2 was evolved out at the temperature higher than 400°C. For the effect of pyrolysis temperature on liquid composition, it was found that furan derivatives were derived from primary degradation at the low temperature of 650 K (377°C) and then their concentration slightly decreased at higher temperatures resulting from secondary reactions (Mohan *et al.*, 2006). Both hydroxyacetaldehyde and levoglucosan (contributed from pyrolysis of carbohydrates) increased with increasing in the pyrolysis temperature. The methoxy phenol groups such as syringols, guaiacols, and eugenols tended to decrease with an increase in pyrolysis temperature (their maximum yields were found at 750-800 K (477-527°C)), while the amounts of phenols and alkylated phenol increased continuously (Branca *et al.*, 2003; Lemeune, 2005). Moreover, the influence of heating rate and particle size was reported to cause the changes in chemical compositions of bio-oil. For example, the higher heating rates rendered the formation of levoglucosan and hydroxyacetaldehyde with a decrease in the carboxylic acids (Branca *et al.*, 2003). On the particle size effect, it was found that larger size particles (> 90 μm) containing higher cell wall materials (cellulose, hemicellulose and lignin, >80 wt%) led to higher amounts of acetaldehyde, acetic acid, furfural, eugenol, vanillin and levoglucosan as compared to those of smaller size particles (<90 μm) (Bridgeman *et al.*, 2007)

4.4 Materials and Methods

4.4.1 Feedstock Preparation and Characterization

Biomass feedstocks including cassava pulp residue, palm kernel cake, palm shell, coconut shell and longan fruit seed were milled and sieved to obtain an average particle size of 0.11 mm for biomass characterization and the particle sizes of 0.71, 1.35, 2.03, 3.56 mm for pyrolysis experiments. The sieved biomasses were dried at 120°C for 24 hours in an oven to speed up the removal of excess moisture and then left at room condition until no weight change was noticed. The drying was carried out in order to study the pyrolysis products produced solely from thermal decomposition of the biomass feed without the occurrence of secondary products from reactions involving the excess moisture (water-gas reaction, steam reforming, etc.) and to prevent the possible increase of water content in the bio-oil from vapor condensation. The dried biomass samples were characterized for bulk density, true density (Helium pycnometer, AccuPyc 1330 Micromeritics), proximate analysis (moisture content (ASTM D2867-95), volatile content (ASTM D5832-95), ash content (ASTM D2866-94) and fixed carbon content (by difference)), elemental analysis (CHNS/O analyzer, Perkin Elmer PE2400 series II) and heating values (ASTM D3286-96).

4.4.2 Pyrolysis Experiments

The pyrolysis of biomasses was performed in a stainless steel fixed-bed reactor (4.5 cm i.d. and 46 cm long) inserted in a vertical tube furnace (PTF 12/50/450, Protherm Electrical Furnaces). Figure 4.1 shows the schematic diagram of the experimental set up used in this work. About 100 g of palm kernel cake, palm shell, coconut shell and longan fruit seed or 50 g of cassava pulp residue was packed into the reactor. The biomass sample was heated from room temperature to the final desired pyrolysis temperature at the specified heating rate and held at this temperature for the required period of time. During this heating-up period, ultra high purity grade of nitrogen gas (99.9995% of N_2 supplied by TIG, Thailand) was continuously supplied in the downward direction through the fixed bed of biomass particles at a constant selected flow rate. Nitrogen gas of high purity was used to avoid the concomitant reactions that may occur by the contaminant gases such as O_2, H_2O and CO_2. The pyrolysis vapor produced flowed through two condensers connected in series into which the entrained char and liquid product were collected. The first condenser utilized a mixture of salt-ice in a bath maintaining at -6 to -8°C. The second condenser operated at -20°C using a temperature-controlled water bath filled with a glycerin-water mixture. The pyrolysis was run until no liquid was collected (by visual observation) and no major gases (excluding N_2) were produced as checked by GC analysis, usually taking about 60 min after the final temperature was reached. During the course of experimental run, non-condensable gas was periodically sampled for its gas composition analysis. The final products of char left in the reactor and the liquid oil from the two condensers were collected and weighed and the corresponding product yields were calculated based on mass of biomass feed. Gas yield was calculated by mass balance, knowing the yields of collected solid char and liquid oil. Table 4.1 summarizes the experimental conditions used for the pyrolysis study.

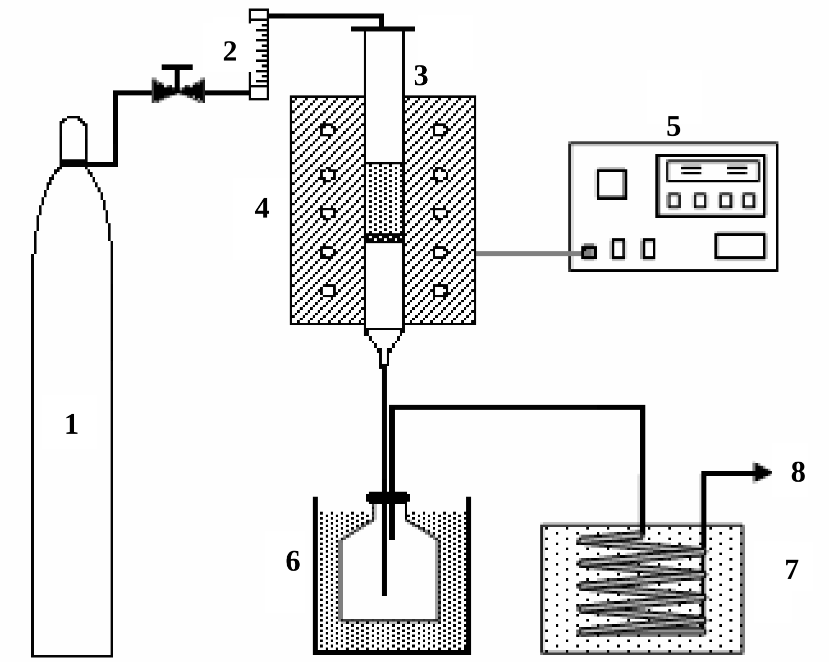

1. N_2 tank	5. Furnace controller
2. Gas flow meter	6. Condenser 1 (mixture of salt-ice)
3. Fixed bed reactor	7. Condenser 2 (mixture of glycerin-water)
4. Vertical tube furnace	8. Non-condensable gases to exhaust

Figure 4.1 Schematic diagram of the fixed-bed pyrolysis apparatus.

Table 4.1 Pyrolysis conditions used in the present study.

Conditions	**Varying parameters**
Effect of pyrolysis temperature Biomasses: cassava pulp residue, palm kernel cake, palm shell, coconut shell and longan fruit seed Particle size: 2.03 mm N_2 flow rate: 200 cm^3/min Heating rate: 20°C/min	300, 400, 500, 600, 700 and 800°C
Effect of average particle size Biomasses: cassava pulp residue, palm kernel Temperature: 700°C N_2 flow rate: 200 cm^3/min Heating rate: 20°C/min	0.71, 1.35, 2.03 and 3.56 mm
Effect of N_2 purge rate Biomasses: cassava pulp residue, palm kernel Temperature: 700°C Particle size: 2.03 mm Heating rate: 20°C/min	50, 100, 200, 400 and 600 cm^3/min
Effect of heating rate Biomasses: cassava pulp residue, palm kernel Temperature: 700°C Particle size: 2.03 mm N_2 flow rate: 200 cm^3/min	5, 10, 20°C/min

4.4.3 Analysis of Pyrolysis Products

4.4.3.1 Liquid Product

Bio-oils collected from the pyrolysis process were analyzed for their physicochemical properties. It was noted that the bio-oil obtained from palm kernel cake consisted of two immiscible layers of oil and aqueous phase, with the latter being separated directly by decanting. However, bio-oil derived from pyrolysis of cassava pulp residue gave a homogeneous liquid phase, while palm shell oil, coconut shell oil and longan fruit seed oil showed a dispersion of oil phase in aqueous phase. Water remaining in these derived crude oils was later removed and its content was determined by refluxing the oil with toluene solution using the Dean-Stark method (ASTM D95-83).

Bio-oils derived from pyrolysis of various biomasses were characterized for elemental analysis (CHNS/O Analyzer, Perkin-Elmer 2400 Series II), chemical functional groups using Fourier transform infrared spectroscopy (FT-IR) and chemical compositions using gas chromatography technique. Crude bio-oils and dewatered bio-oils derived from pyrolysis at 700°C were analyzed for chemical functional groups by a FT-IR spectrometer (PerkinElmer: Spectrum GX). A spectrum for FT-IR analysis was prepared by spreading a thin uniform layer of bio-oil sample on KBr disc. The FT-IR spectra were recorded in the transmission between 4000 and 400 cm^{-1} and the functional groups types of bio-oils were identified by comparing with IR spectra libraries (Skoog and Leary, 1992). For chemical compositions analysis, the dewatered bio-oils of cassava pulp residue, palm kernel cake pyrolysis at temperature of 500 and 700°C and dewatered palm shell oil derived from pyrolysis at 700°C were analyzed by GC-MS technique. Due to the presence of a large number of chemicals in bio-oil, it was necessary to fractionate the oil sample into different fractions prior to analysis of chemical composition. Dewatered bio-oil was first fractionated by employing the technique of liquid chromatography as follows. Silica gel of 70-230 mesh (63-300 μm) size fraction was packed in a glass column of 2 cm inside diameter and 10 cm high. Next, 0.25 g of dewatered bio-oil sample was poured into the column and eluted successively with pentane (10-20 cm^3), toluene (20-30 cm^3), diethyl ether (30-40 cm^3) and methanol (80 cm^3) to obtain aliphatic, aromatic, oxygenated and polar fractions, respectively. The fractions extracted with pentane, toluene and diethyl ether were further analyzed by gas chromatography/mass spectrometry (GC-MS). The amount of each solvent used was determined by trial and error based on the criterion that the solvent quantity should be low enough to extract all affinitive chemicals and yet give sufficiently high concentration of eluted species for accurate interpretation of GC-MS results. Methanol was the last solvent used to extract all remaining components, including non-volatile compounds and the heaviest hydrocarbon fraction of asphaltenes. The relatively high quantity of methanol was employed to ensure a complete leaching out of chemical species, as traced by the change in the color of column effluent from dark to a clear liquid solvent. The collected methanol fraction could not be directly analyzed and quantified by GC-MS and thus it was dried in a rotary evaporator and weighed.

The GC-MS system used is Varian Cp-3800 gas chromatography with a mass selective detector and the column used is VF-5MS capillary column (30 m x 0.39 mm, 0.25 μm film thickness). The flow rate of helium carrier gas was 0.5 cm^3/min and injector temperature of 260°C. The temperature program used was as follows:

- 40°C for 6 min followed by heating to 270°C at 5°C/min
- 270°C for 8 min followed by heating to 300°C at 15°C/min
- 300°C for 10 min followed by heating to 320°C at 20°C/min
- 30 min dwell time at 320°C

The types and concentrations of chemical constituents in the oil fractions were obtained from the spectra library of NIST MS Search 2.0 and the known concentrations of standard chemicals.

In addition, the crude bio-oil and water-free bio-oil obtained under the pyrolysis temperature of 700°C were also measured for their basic fuel properties, including boiling range distribution (ASTM D86-96), calorific value (ASTM D240-92), flash point (ASTM D93-97), pour point (ASTM D97-96a), density (Gay-Lussac bottle), viscosity (ASTM D445-96), carbon residue (ASTM D524-97) and ash content (ASTM D482-95).

4.4.3.2 Char Product

Chars derived from pyrolysis of five biomasses at pyrolysis temperatures of 700°C and the chars of cassava pulp residue and palm kernel cake pyrolysis at 500°C were characterized for bulk density, true density (He pycnometer, Accupyc 1330 Micromeritics), proximate analysis (moisture content (ASTM D2867-95), volatile content (ASTM D5832-95), ash content (ASTM D2866-94) and fixed carbon content (by mass balance)), elemental analysis (CHNS/O analyzer, Perkin Elmer PE2400 series II), heating value (ASTM D3286-96) and porous properties (surface area analyzer; Micromeritics ASAP 2010).

4.4.3.3 Gas Product

Gas products were identified and quantified by a gas chromatography (GC-14B, Shimadzu) with a thermal conductivity detector. Porapak Q column (1m. long and 4 mm i.d.) was used for CO_2 analysis, whereas molecular sieves 5A column (1m. long and 4 mm. i.d.) was used for the analysis of H_2, O_2, N_2, CO and CH_4. Operational conditions for GC were argon carrier gas flow rate of 25 cm^3/min, injector temperature of 80°C, column temperature of 50°C for Porapak Q column and 100°C for molecular sieves 5A column, and detector temperature of 100°C.

4.5 Results and Discussions

4.5.1 Feedstock Properties

Table 4.2 shows the basic physical properties and compositions of the five biomasses studied. The average particle sizes of the feed in the range 0.71-3.56 mm of cassava pulp residue and palm kernel cake exert a slight effect on the bulk density with smaller sizes particle giving higher bulk density. Bulk density of cassava pulp residue is about half that of other biomasses but the true densities of all biomasses are not greatly different being in the range of 1.385-1.507 g/cm^3. Proximate and ultimate analyses show that the main composition of biomasses is volatile contents with carbon and oxygen being the major elements. Palm shell has the highest fixed carbon content and the lowest volatile content, while cassava pulp residue has the lowest fixed carbon and gives also the lowest content of carbon element and the highest content of oxygen element. The five biomasses have approximately the same heating value of about 22 MJ/kg.

Table 4.2 Biomass properties and chemical compositions.

Properties	**Biomass**				
	Cassava pulp residue	**Palm kernel cake**	**Palm shell**	**Coconut shell**	**Longan fruit seed**
Bulk density (g/cm^3)					
particle size of 0.71 mm	0.348	0.600			
particle size of 1.35 mm	0.326	0.573			
particle size of 2.03 mm	0.294	0.568	0.610*	0.626*	0.614*
particle size of 3.56 mm	0.284	0.501			
True density (g/cm^3)	1.507	1.385	1.416	1.421	1.470
Proximate analysis (Dry basis, wt%)					
Volatiles	81.98	79.57	75.69	82.38	84.51
Fixed carbon	11.83	16.74	19.20	16.33	14.80
Ash	6.19	3.69	5.11	1.29	0.70
Elemental analysis (wt%)					
C	35.89	47.19	48.74	49.76	43.75
H	5.47	6.38	4.99	5.60	6.30
O	58.27	43.28	45.63	44.30	48.81
N	0.36	3.15	0.64	0.35	1.14
H/C (mole ratio)	1.829	1.622	1.229	1.350	1.727
O/C (mole ratio)	1.218	0.688	0.702	0.668	0.837
Gross heating value (MJ/kg)	22.41	21.91	22.29	21.28	21.16

Note: * = Bulk density of particle size 2.03 mm.

4.5.2 Effect of Pyrolysis Conditions on Product Yield

4.5.2.1 Pyrolysis Temperature

Figure 4.2 shows the effect of pyrolysis temperature on the product yields of various biomasses including cassava pulp residue, palm kernel cake, palm shell, coconut shell and longan fruit seed (pyrolysis conditions: average particle size 2.03 mm, N_2 flow rate 200 cm^3/min and heating rate 20°C/min). Pyrolysis of cassava pulp residue, palm kernel cake and palm shell gave maximum yields of liquid at 700°C but those of coconut shell and longan fruit seed pyrolysis were derived at 600 and 800°C, respectively (Figure 4.2 (a)). The maximum liquid yield of various biomass pyrolysis were in the range of 42.4-54.3 wt% and palm kernel cake pyrolysis provided the highest liquid yield among other biomasses. Previous studies have demonstrated that optimum pyrolysis temperature that produces a maximum in liquid yield depends mainly on biomass type varying in the range of 500-800°C for slow pyrolysis (Demirbaş, 2006; Pütün *et al*., 1999). It may be hypothesized that different biomasses differ in their main compositions, whereby decomposing at varying temperatures. This agrees with the results from thermogravimetric analysis in Chapter III, which showed that five biomasses provided different maximum decomposition rate at different temperatures (Figure 3.1 (b)). Over the temperature range from 300-800°C, char yields of various biomass pyrolysis tended to decrease and gas yields increased with increasing pyrolysis temperature, with a rapid change occurring at temperatures below 500°C. Figure 4.2 (b) indicates that there was a rapid decrease of char yield from 300 to 500°C, followed by a slow decrease at higher temperatures and approaching a constant value at 800°C. This coincided with the increased generation of liquid and gas products which was pronounced up to 500°C and became relatively constant at higher pyrolysis temperatures (Figures 4.2 (a) and (c)). In addition, it was observed that there was a marked increase of gas yield with a corresponding decrease of liquid yield at the temperature higher than 700°C for palm kernel cake pyrolysis. The increase in the gas yield could result from the increased rate of char decomposition at the high pyrolysis temperature (Pütün *et al.*, 2001; Yorgun *et al.*, 2001). At the same time, pyrolysis at this high temperature could also produce more gaseous product from decomposition of liquid product, hence giving the decreasing of observed liquid yield. Similar observation was also reported in previous investigations (Onay and Koçkar, 2004; Özbay *et al.*, 2001) that the liquid yields derived from pyrolysis of rapeseed and cotton cake tended to decrease at pyrolysis temperatures higher than 500°C. However, longan fruit seed pyrolysis showed the increase of liquid product and decreasing char yield at 800°C. This may be due to further decomposition of longan seed or secondary reaction of its char at high temperature to generate higher amount of pyrolysis liquid.

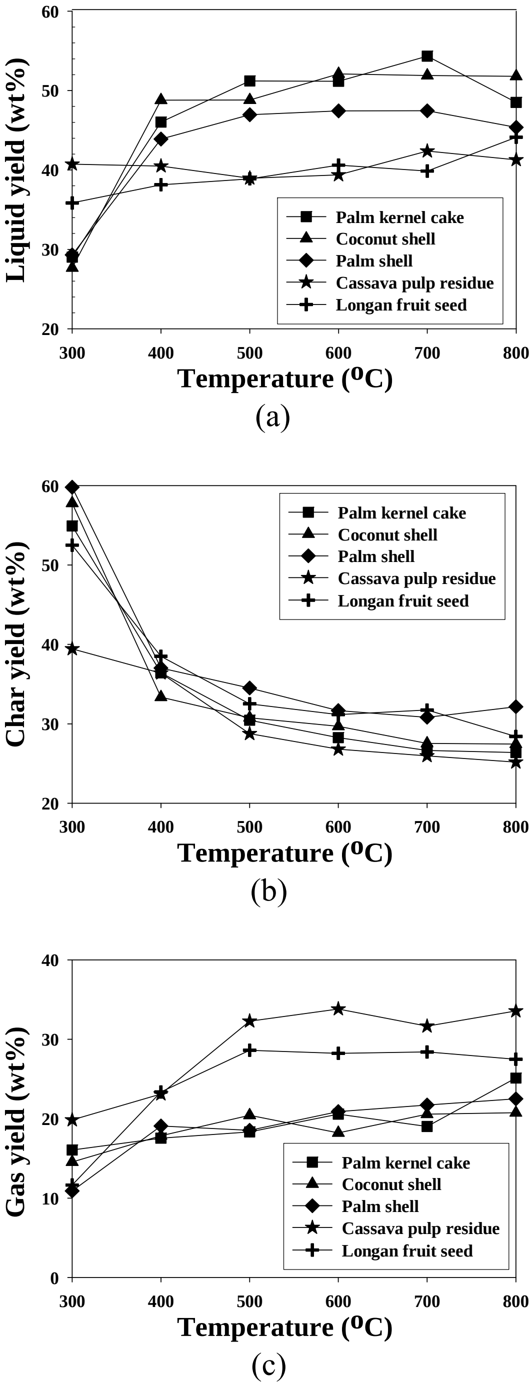

(a)

(b)

(c)

Figure 4.2 Effect of pyrolysis temperature on product yields; (a) liquid, (b) char and (c) gas derived from pyrolysis of various biomasses (pyrolysis conditions: particle size 2.03 mm, heating rate of 20°C/min and N_2 flow rate 200 cm^3/min).

4.5.2.2 Particle Size

The effect of particle size in the range of 0.71-3.56 mm on product yields was studied at the temperature of 700°C with the heating rate of 20 °C/min and N_2 flow rate 200 cm^3/min. Figure 4.3 shows that the pyrolysis of the two biomasses with the average size of 2.03 mm gave the maximum in liquid yield of 54.3 wt% and 42.4 wt% for palm kernel cake and cassava pulp residue, respectively. For particle sizes smaller than 2.03 mm, they produced higher gas and char yields but a lowering in liquid yields as the particle size was decreased. This is probable that the denser packing of smaller size particles (see Table 4.2 for bulk density property) could impede the flow of N_2 purge gas. This would prolong the pyrolysis products to stay in the reaction zone, thus allowing secondary reactions via thermal cracking, repolymerization, and recondensation to occur, whereby giving additional decomposition of higher molecular weight volatiles to gas product with lowering in the amount of liquid product and more formation of solid char (Onay and Koçkar, 2004).

For particle sizes larger than 2.03 mm, the variation in product yields was not so sensitive to the changes in particle size, with slight decreasing of liquid product and small increasing of gas and char products being observed for increasing particle size. This effect may be hypothesized to result from heat and mass transfer resistances in larger size particles. This may cause a temperature gradient and an increase in the diffusion path of volatile matters inside the particle, thus leading to less thermal decomposition and hence increased char yield and decreasing of liquid product. These effects were also observed in the work of Guo and Lua (2001), from which they found that pyrolysis of particles larger than 2 mm was controlled by heat and mass transfer resistances, resulting in slower rate of pyrolysis and lower conversion.

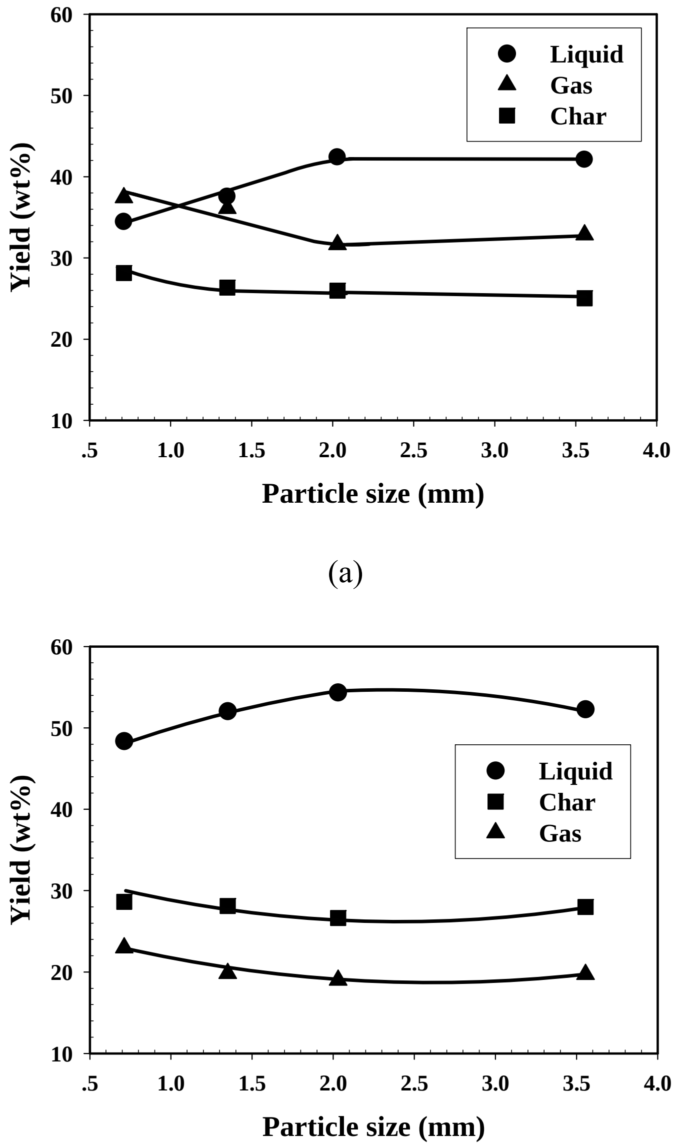

(a)

(b)

Figure 4.3 Effect of particle size on product yields derived from pyrolysis of (a) cassava pulp residue and (b) palm kernel cake (pyrolysis conditions: temperature of 700°C, heating rate of 20°C/min and N_2 flow rate 200 cm^3/min).

4.5.2.3 N_2 Purge Rate

Pyrolysis of cassava pulp residue and palm kernel cake at different N_2 gas flow rates were studied under the following conditions: pyrolysis temperature of 700°C, heating rate of 20°C/min, and average particle size of 2.03 mm. Results shown in Figure 4.4 indicates that the application of N_2 flow rate in the range of 50-600 cm^3/min exerted a definite influence on the product yields for kernel cake pyrolysis, whereas the effect was much less for the pyrolysis of cassava pulp residue. Maximum in liquid yields of 54.3 wt% and 42.4 wt% were obtained at N_2 flow rate of 200 cm^3/min for palm kernel cake and cassava pulp residue, respectively. This result agrees with various previous works (Onay and Koçkar, 2004; Pütün *et al.*, 2002) that maximum oil yield was usually obtained at 100-200 cm^3/min of nitrogen sweep gas flow rate for fixed bed reactors. At N_2 flow rates lower than 200 cm^3/min, lower N_2 flow rate gave lower liquid yields with correspondingly higher contents of gas and char. Again this may be reasoned that lower gas flow rate would lead to longer residence time for the purge gas, which would allow secondary reactions of pyrolysis products such as thermal cracking of higher molecular weight components to produce more gaseous products and reactions of repolymerization and condensation to form additional char and coke (Onay and Koçkar, 2004). On the other hand, N_2 gas flow rate higher than 200 cm^3/min would provide the opposite trend for the product yields. This could be explained by the decreasing of pyrolysis temperature of biomass particles and shorter residence time for the pyrolysis products to stay in the reaction zone when higher N_2 gas flow rate is applied. The overall effect would lead to less decomposition of feedstock and the derived products, thus giving lower liquid yield and higher yield of char.

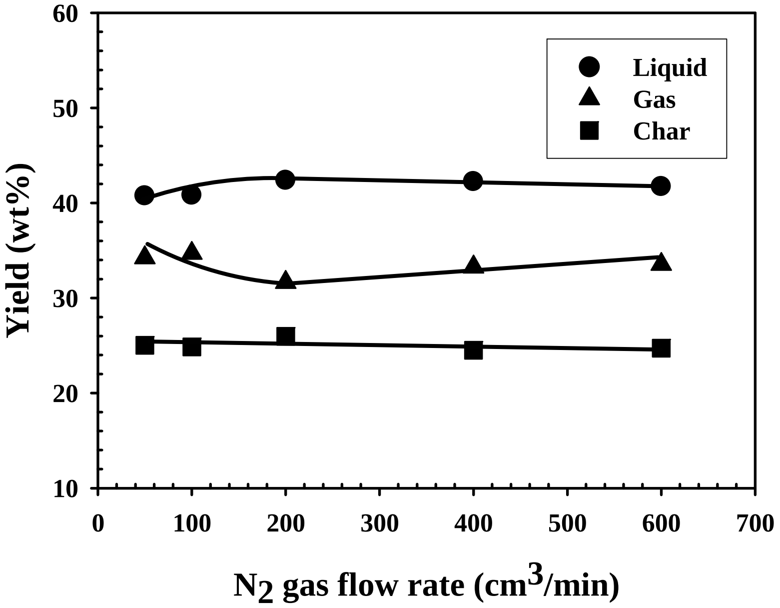

(a)

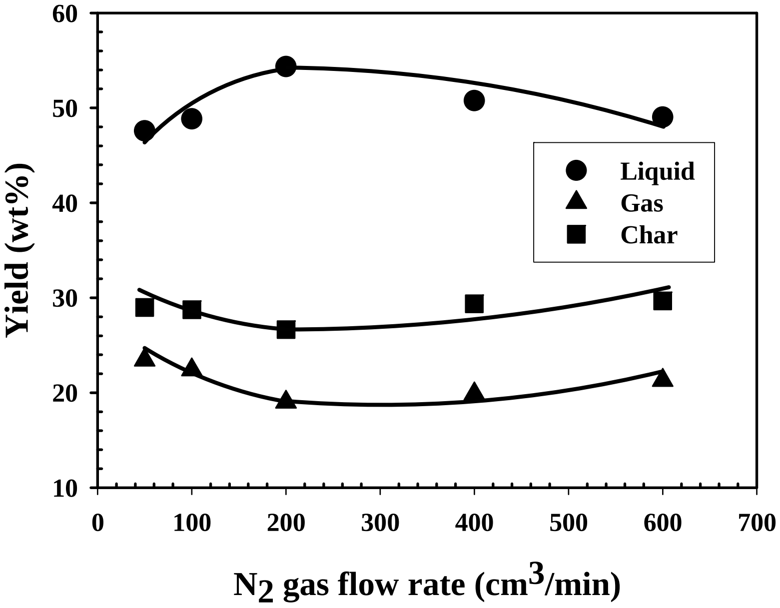

(b)

Figure 4.4 Effect of N_2 gas flow rate on product yields derived from pyrolysis of (a) cassava pulp residue and (b) palm kernel cake (pyrolysis conditions: temperature of 700°C, heating rate of 20°C/min, and particle size of 2.03 mm).

4.5.2.4 Heating Rate

In studying the effect of heating rate, the pyrolysis was performed under the following conditions: heating rate in the range of 5-20°C/min, pyrolysis temperature of 700°C, N_2 flow rate of 200 cm^3/min and particle size of 2.03 mm. The obtained results are shown in Figure 4.5. It is noted that the product yields including liquid, char and gas were not greatly dependent on the applied heating rate over the range of 5-20°C/min. The largest variation was only 3.2% which was observed for the liquid yield derived from pyrolysis of palm kernel cake. This result agreed with the work of Pütün *et al.* (1996) and Tsai *et al.* (2006), which showed that pyrolysis study at temperature from 500-700°C had no important effect of heating rate on product yields in the range of 7-40°C/min and 100-500°C/min, respectively. However, the work of Karaosmanoğlu *et al.* (1999) indicated that heating rate higher than 30°C/min provided higher yields of liquid and gas products and lower char yields than those derived from pyrolysis at 10°C/min. This observation on the effect of heating rate, however, did not significantly affect the amount of liquid product when the pyrolysis was undertaken at the higher temperature of 650°C. Thus, based on the results from these limited investigations, it is hypothesized that heating rate should have less effect on the product yields at a relatively high pyrolysis temperature (e.g. 700°C in this work) since the heating-up period to this high temperature using any applied heating rate must in effect pass the main devolatilization temperature range (e.g. 250-400°C in this work) where major weight loss has already occurred.

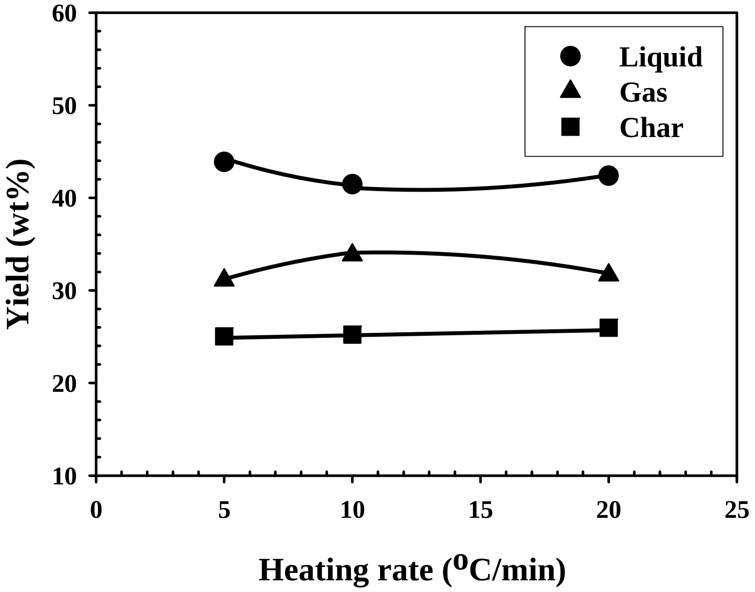

(a)

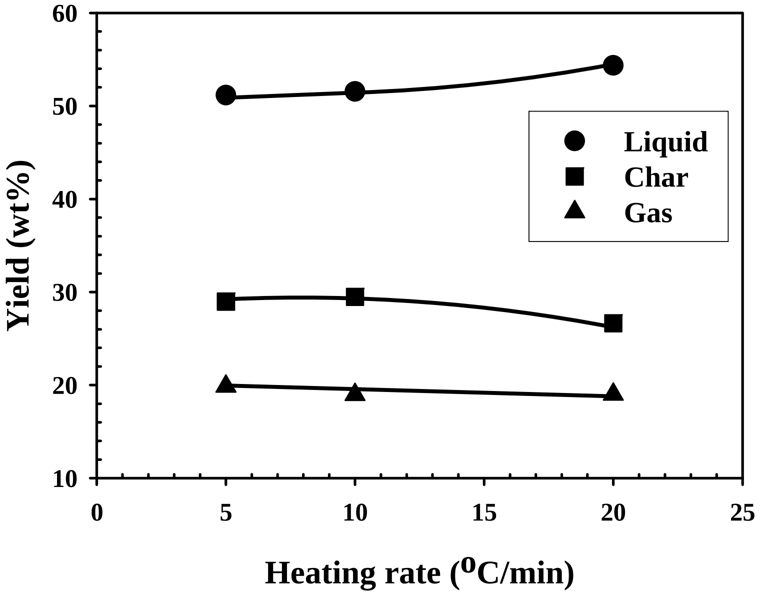

(b)

Figure 4.5 Effect of heating rate on product yields derived from pyrolysis of (a) cassava pulp residue and (b) palm kernel cake (pyrolysis conditions: temperature of 700°C, particle size of 2.03 mm and N_2 flow rate of 200 cm^3/min).

4.5.3 Bio-oil Properties

4.5.3.1 Physical and Fuel Properties

The pyrolysis liquids derived from the various types of biomass studied differed in both color and odor. Cassava pulp residue oil showed a single transparent phase with dark red-brown color. Palm kernel cake oil had opaque dark color and gave the separation of oil-aqueous phase, from which the aqueous solution could be easily separated from the oil phase by decanting. In addition, a state of dispersion of opaque dark oil drops in dark red-brown aqueous solution was derived for pyrolysis liquids from palm shell, coconut shell and longan fruit seed. Generally, bio-oil and water can mix to form a single phase chemical solution but the phase separation can occur when the water content exceeds about 30 to 45 wt%. (Yaman, 2004). Moreover, there was evidence that the separation of oil-aqueous phase may result from the immiscible chemicals presenting in the pyrolysis liquid (Bridgwater, 2003).

Table 4.3 shows the fuel properties of bio-oils derived from pyrolysis of the five biomasses at 700°C and those of high-speed diesel oil (Islam *et al.*, 1999) and heavy fuel oil (Zhang *et al.*, 2007). Ranges of some important fuel properties of the derived bio-oil are as follows: density, 1.01-1.18 g/cm^3; pH, 2.1-5.6; flash point, 74-110°C and pour point, -21-1°C. According to these results, bio-oils possess some advantageous properties of higher flash point and lower pour point in comparison with diesel. However, it was observed that crude bio-oils contained relatively high water contents being in the range 48.8-65.4 wt%. Viscosity of crude oils at 40°C was relatively low, about 1.3-3.8 cSt. However, after water removal, viscosities of the bio-oils increased substantially varying in the range of 20.4-58.7

cSt. In addition, removing of water from the oils caused about twice an increase in the values of ramsbottom carbon residue and ash content. It should be noted that the calorific value could only be determined when water was removed from the raw oils and the measured values varied widely in the range of 13.8-40.0 MJ/kg. It was further noticed that the heating value of water-free oil derived from kernel cake pyrolysis had the same value as that of fuel oil. Distillation curves of the bio-oils derived from pyrolysis of the five biomasses are displayed and compared with that of diesel fuel as shown in Figure 4.6. Crude bio-oils gave the constant boiling range distribution at about 100°C for the first 55-75 vol% of the collected liquid depending on the type of biomass, showing that water and/or light oxygenated compounds such as alcohols and acid are major components in the bio-oil. The dewatered bio-oils showed similar pattern of distillation curves to that of diesel fuel, with kernel cake derived oil giving the closest boiling range distribution to that of diesel fuel. By comparing the important fuel properties between bio-oils and petroleum-based fuels, it is seen that based on its heat content, we can use bio-oil from palm kernel cake pyrolysis directly without pretreatment as a substitute for heavy fuel oil. When compared with bio-oil from commercial fast pyrolysis of wood and bagasse (DynaMotive Energy Systems Corporation, 2009), kernel cake oil from this simple slow pyrolysis offers about twice higher in heating value (40 versus 15-20 MJ/kg oil) but a 17% less in terms of total heating value (10 versus 12 kJ/kg biomass). In order to use bio-oil from palm kernel cake in diesel engines, however, steps must be taken to lower the oil viscosity to an acceptable level, for example, by applying hot-vapor filtration or addition of viscosity-reducing solvents such as methanol or mixture of methanol and water to effectively lower the oil viscosity (Bridgwater, 2003; Oasmaa and Czernik, 1994). Another difficulty associated with the use of bio-oils in any combustion systems is its low pH value which could cause a serious corrosion problem. This problem may be alleviated by blending the bio-oil in appropriate proportion with diesel oil in the form of emulsions with the aid of a surfactant or by converting some acid chemicals through esterification reaction or chemical/catalytic upgrading (Bridgwater, 2003; Junming *et al.*, 2008). Apart from its high viscosity and acidic property, bio-oils from cassava pulp residue and longan fruit seed are less attractive to be used as a liquid fuel because of its relatively low heating value. Conversion of oxygenated compounds in the oil to obtain higher contents of hydrocarbons via chemical upgrading such as hydrotreating, and catalytic cracking is recommended to mitigate this shortcoming (Oasmaa and Czernik, 1994; Zhang *et al.*, 2007). In addition, blending the raw bio-oil with its char to produce a slurry fuel could be an alternative approach for the application of bio-oils possessing high water contents and low heating value. Concerning these problems, the improvement of bio-oil properties by different promising methods have been carried out, the details of which are presented in Chapter V.

Table 4.3 Fuel properties of various bio-oils derived from the pyrolysis temperature at 700°C.

Properties	Diesel oil	Heavy fuel oil	Bio-oil									
			Cassava pulp residue		Palm kernel cake		Palm shell		Coconut shell		Longan fruit seed	
			Crude oil [a]	Water removed	Crude oil [b]	Water removed	Crude oil [c]	Water removed	Crude oil [c]	Water removed	Crude oil [c]	Water removed
Calorific value (MJ/kg)	45.0-46.0	40.0	*	14.90	-	40.00	*	26.93	*	28.39	*	13.77
Flash point (°C)	75.0	-	98.0	110.0	-	74.0	99.0	108.0	98.0	110.0	95.0	108.0
Pour point (°C)	-2.0	-	-6.0	-17.0	-	1.0	-10.0	-14.0	-10.0	-21.0	-5.0	-8.0
pH	-	-	2.95	2.82	-	5.62	2.98	2.77	2.37	2.11	4.47	4.06
Density at 30°C (g/cm^3)	0.78 [d]	0.94 [d]	1.10	1.16	-	1.01	1.11	1.18	1.11	1.17	1.08	1.11
Viscosity at 40°C (cSt (mm^2/s))	1.8-4.1	180 [e]	1.46	28.30	-	58.72	1.75	20.38	3.79	22.70	1.34	24.09
Ramsbottom carbon residue (wt%)	-	-	2.57	4.43	-	5.39	2.93	6.98	2.3	5.36	0.90	2.21
Ash content (wt%)	0.01	0.1	0.081	0.167	-	0.041	0.071	0.171	0.049	0.089	0.042	0.08
Water content (wt%)	-	0.1	56.41	-	57.00	< 0.6	48.78	-	52.56	-	65.41	-

Note: a = homogeneous phase of oil-water, b = phase separation between oil and water and c = a dispersion of oil phase in aqueous phase

d = density at 15°C (g/cm^3), e = viscosity (cSt (mm^2/s)) at 50°C, * = not measurable

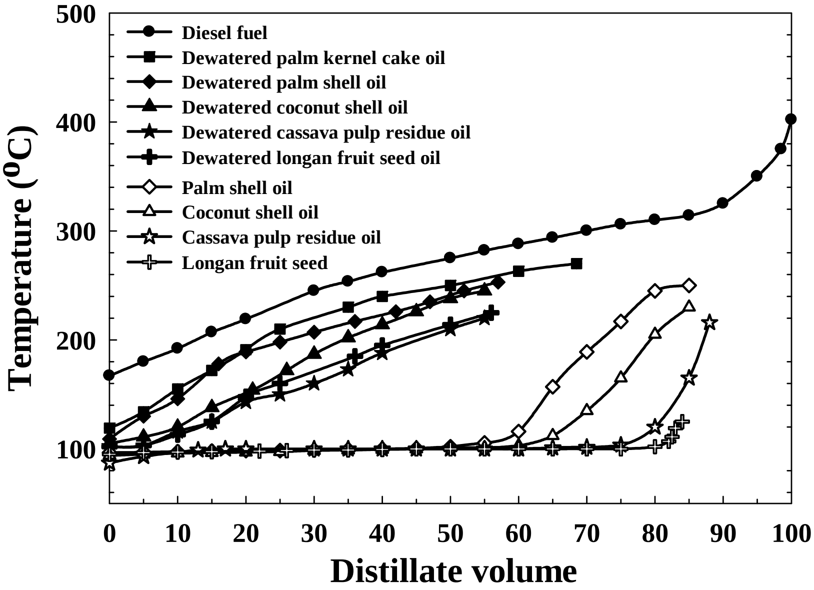

Figure 4.6 Distillation curves of diesel and bio-oils derived from pyrolysis of biomasses at 700°C.

4.5.3.2 Chemical Analysis

Five bio-oils derived from pyrolysis of different biomasses at 700°C were characterized for functional groups by FTIR and elemental analysis and the dewatered bio-oils derived from pyrolysis of cassava pulp residue, palm kernel cake and palm shell were analyzed for their chemical compositions using GC-MS analysis.

Figures 4.7 and 4.8 present the Fourier transform infrared (FTIR) spectra, representing functional group analysis of crude bio-oils and dewatered bio-oils derived from pyrolysis at 700°C. A broad absorbance peak of the O-H stretching vibrations between 3000 and 3600 cm^{-1} indicates the presence of water, alcohols and/or phenols in bio-oils (Skoog and Leary, 1992). The C=O stretching vibrations between 1650 and 1850 cm^{-1} represent esters, ketones and aldehydes and the presence of O-H and C=O stretching vibrations show the groups of carboxylic acids and their derivatives (Nugranad, N., 1997). The absorption due to C-O stretching vibrations of ethers occurs between 850 and 950 cm^{-1} and the primary, secondary and tertiary alcohols are also identified by the peaks of C-O stretching and O-H deformation vibrations between 950 and 1325 cm^{-1} (Nugranad, N., 1997). The hydrocarbon compounds in the bio-oil include the functional groups of alkanes, alkenes and aromatics. The strong absorbance peak of C-H stretching vibrations between 2850 and 2970 cm^{-1} and the C-H deformation vibrations between 1340 and 1470 cm^{-1} display the groups of alkanes (Skoog and Leary, 1992). The peaks of C=C stretching vibrations between 1575 and 1625 cm^{-1} represent alkenes or aromatics and the evidence of absorbance peaks at 675-900 cm^{-1} and 1420-1610 cm^{-1} indicate the detection of single ring aromatic, alkylated aromatic compounds and polycyclic aromatic compounds (Pütün *et al.* 1999). Moreover, it was also observed that the presence of hydrocarbon functional groups were more dominant for dewatered bio-oils. This was also proved by the results of elemental analysis; the high oxygen content of cassava pulp residue oil was decreased by about 27 wt% when water in bio-oil was removed (Table 4.4). However, the oxygen contents of dewatered oil derived from cassava pulp residue and longan fruit seed pyrolysis were still high being ~50 wt% of bio-oils. Water removal of palm kernel cake oil and coconut shell oil contributed much higher contents of carbon and hydrogen and much lower amount of oxygen element than that of cassava pulp residue oil and longan fruit seed oil (19 and 23 wt%, respectively). For dewatered palm shell oil, it gave intermediate values for elemental analysis and was comparable to typical values derived from flash pyrolysis of hardwood (Trebbi *et al.*, 1997).

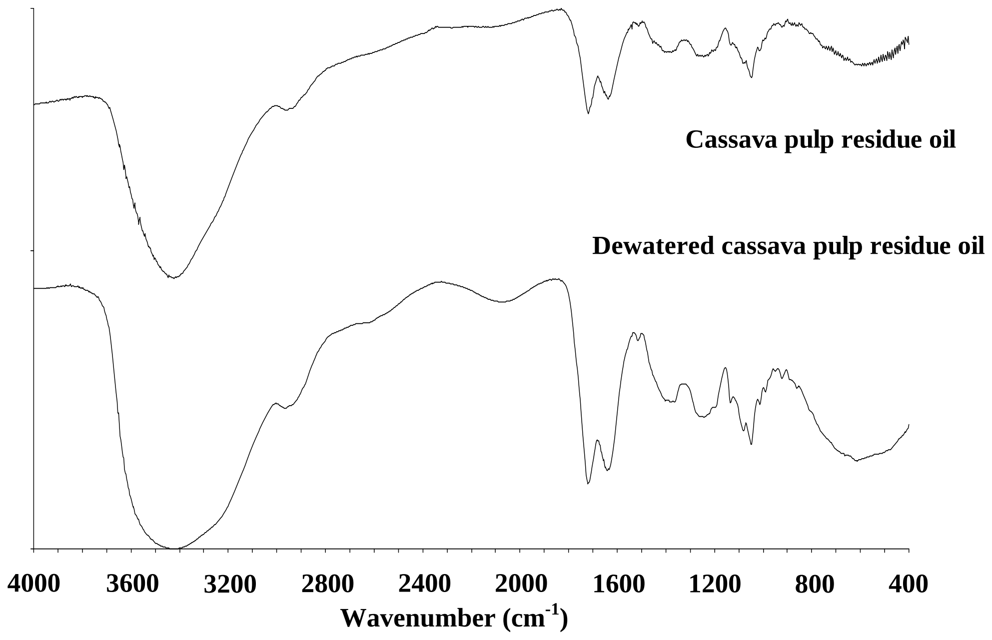

(a)

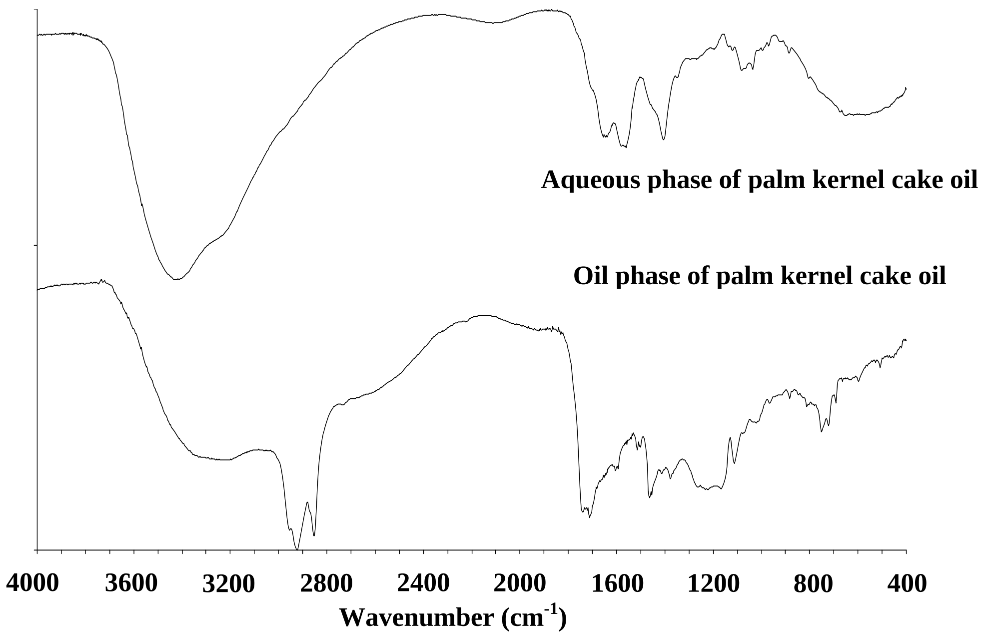

(b)

Figure 4.7 FTIR spectra of crude oils and dewatered bio-oils derived from pyrolysis (a) cassava pulp residue and (b) palm kernel cake at 700°C.

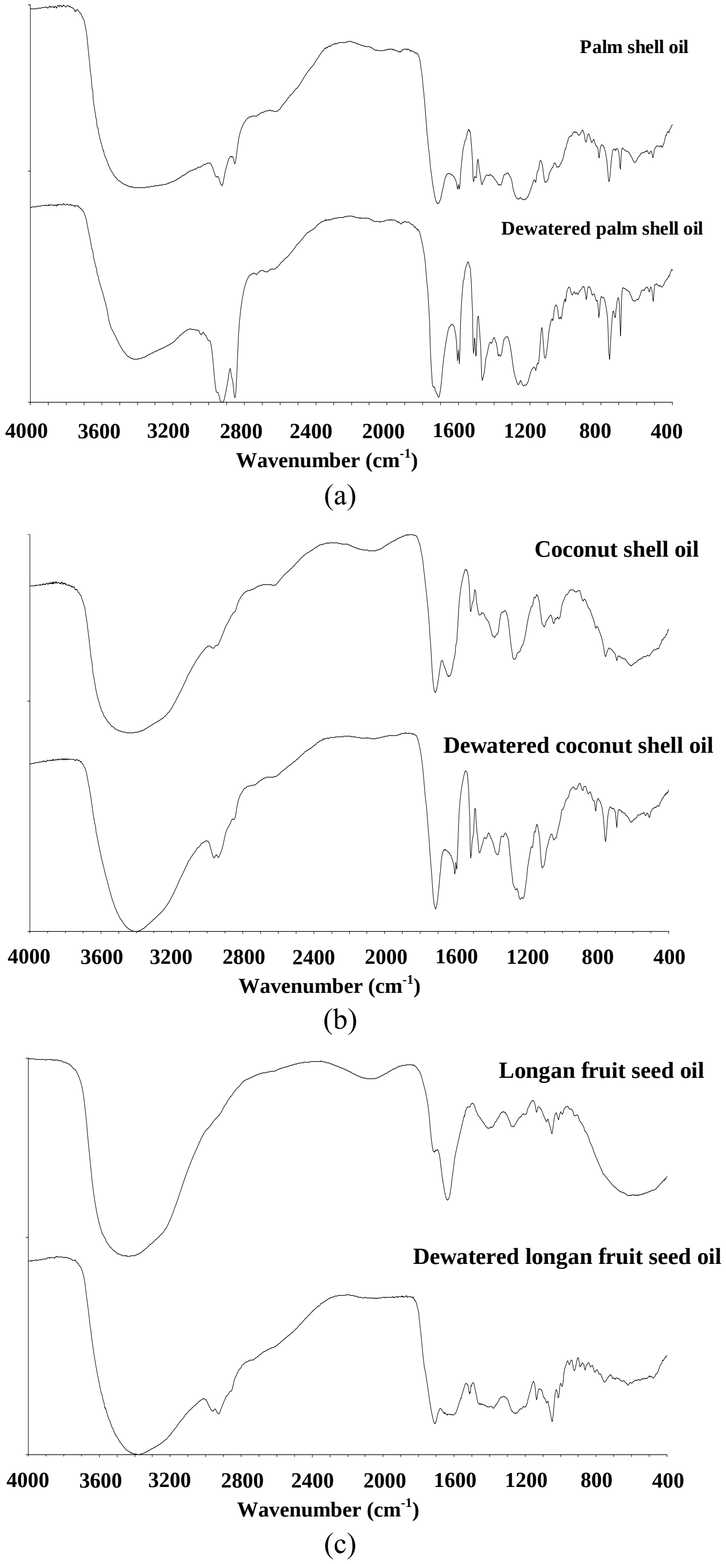

Figure 4.8 FTIR spectra of crude oils and dewatered bio-oils derived from pyrolysis

(a) palm shell, (b) coconut shell and (c) longan fruit seed at 700°

Table 4.4 Elemental analysis of various bio-oils derived from pyrolysis at 700°C.

Elemental analysis (wt%)	**C**	**H**	**O**	**N**	**H/C (mole ratio)**	**O/C (mole ratio)**
Cassava pulp residue oil	15.26	8.95	75.22	0.57	7.036	3.697
Dewatered cassava pulp residue oil	44.38	5.59	48.68	1.36	1.510	0.823
Dewatered palm kernel cake oil	67.51	8.88	19.03	4.58	1.579	0.211
Dewatered palm shell oil	56.59	6.48	36.92	0.01	1.374	0.489
Dewatered coconut shell oil	66.2	10.05	23.39	0.37	1.821	0.265
Dewatered longan fruit seed oil	45.23	6.99	45.26	2.52	1.854	0.750

For chemical composition analysis, the dewatered bio-oils were fractionated prior to identification and quantification by GC-MS analysis. Eluted fractions of the dewatered cassava pulp residue oil and dewatered palm kernel cake oil derived at the pyrolysis temperatures of 500 and 700°C and dewatered palm shell oil derived at the pyrolysis temperatures of 700°C are shown in Table 4.5. Major components of palm kernel cake oil and palm shell oil were fractions eluted by diethyl ether, consisting of oxygenated compounds such as phenols, acids, esters, etc. On the other hand, the main fraction of cassava pulp residue oil was that eluted by methanol, representing polar and/or non-volatile compounds. The amount of bio-oil fraction eluted by pentane was lowest which consisted mainly of alkanes and light aromatic compounds. The fraction eluted by toluene varied in the range of 2.9-11.7 wt% comprising the aromatic compounds and high molecular weight alkanes. Kernel cake oil gave the highest contents of pentane and toluene fractions as compared to the oils derived from cassava pulp residue and palm shell. On the effect of pyrolysis temperature, at higher pyrolysis temperature of 700°C cassava pulp residue oil and palm kernel oil gave higher contents of toluene fraction but lower contents of diethyl ether fraction and approximately the same amounts of methanol fraction compared to the condition at the lower temperature of 500°C. Increasing pyrolysis temperature from 500 to 700°C tended to decrease the pentane fraction of the oil derived from cassava pulp residue, whereas pyrolysis temperature exerted almost no effect for the case of kernel cake derived oil.

Table 4.5 Chemical fractionations of bio-oils.

Bio-oil fraction	**Weight (%)**				
	Cassava pulp residue		**Palm kernel cake**		**Palm shell**
	500°C	**700°C**	**500°C**	**700°C**	**700°C**
Pentane	3.11	1.97	3.69	3.97	2.90
Toluene	2.88	4.32	8.67	11.70	4.10
Diethyl ether	15.40	13.84	58.37	48.40	56.56
Methanol	56.79	58.86	29.23	30.06	39.06
Total	78.18	78.99	99.96	94.13	102.62

Table 4.6 shows the hydrocarbon compounds present in the bio-oils obtained from pyrolysis of three biomasses at pyrolysis temperatures of 500 and 700°C. The analysis results show that the hydrocarbons in bio-oils consisted of n-paraffins, aromatics and small amount of olefins. Alkanes were distributed in the range of C_8-C_{34} with the highest concentrations of n-C_8 being detected. This agrees with the previous works for slow pyrolysis of various biomasses (Acıkgoz *et al.*, 2004; Pütün *et al.*, 1999; Pütün *et al.*, 2001) which reported that pentane fraction consisted of normal alkanes in the range of C_7-C_{33}. The content of normal octane (n-C_8) in the palm kernel cake oil remained practically unchanged at the two pyrolysis temperatures studied but lower concentration of n-C_8 was observed at the higher temperature of 700°C for liquid product of cassava pulp residue. At the lower pyrolysis temperature of 500°C, C_8-C_{28} alkanes were observed for kernel cake derived oil, while cassava pulp residue oil yielded C_8-C_{32} alkane fraction. However, increasing of C_{14}-C_{34} contents was detected in both bio-oils at the higher pyrolysis temperature of 700°C. This could result from polymerization of low molecular weight alkanes, giving high molecular weight products at this high temperature condition (Onay and Koçkar, 2004). Moreover, loss of hydrogen radicals in the long chain alkane could further produce alkenes at higher cracking temperature (Kossiakoff and Rice, 1943). In this study, a definite increasing of alkene yield was observed for cassava pulp residue oil with increased pyrolysis temperature, whereas palm kernel cake oil showed a slight increasing of alkenes but a much higher alkene content than that derived from cassava pulp residue oil. For aromatic group, the major aromatic compounds identified were benzene, toluene, ethylbenzene and xylene. Polycyclic aromatic hydrocarbons (PAH), which are a group of two or more fused aromatic rings, were also detected in the bio-oil products. Several PAHs are carcinogens such as benz[a]anthracene, benzo[a]pyrene and dibenz[a,h]anthracene (Tsai *et al.*, 2007). However, some PAHs such as naphthalene and its derivatives can be used in leather tanning to solve the problem of harmful insects, while indene is used to produce indene/cumarone thermoplastic resins (Pütün *et al.*, 2008). In this study, some PAHs including indene, naphthalene, 1,2,3,4-tetrahydro-1,4 dimethyl and phenanthracene were detected and the amounts were increased at higher temperature of 700°C. This agrees with the work of Williams, P. T., and Nugranad, N. (2000) who reported the significant increase of single aromatics and PAH concentrations with increasing in temperature from 450 to 600°C. They hypothesized that the presence of aromatics and PAH at the higher temperature of 600°C could result from the polymerization and aromatization of alkenes and/or decomposition of lignin to give mono and polycyclic aromatics at this high temperature. However, the opposite trend of decreasing contents of single aromatics with increasing of pyrolysis temperature was observed for cassava pulp residue oil in this study. In addition, the high molecular weight of PAHs or some carcinogen chemicals of cassava pulp residue oil and palm shell oil were not detected by GC-MS in this study; it is likely that they could present in the form of non-volatile compounds in the methanol fraction that could not be directly analyzed.

Table 4.6 Hydrocarbon compounds of three bio-oils at different pyrolysis temperatures.

Chemical	**Chemical concentration in bio-oil (wt%)**				
	Cassava pulp residue		**Palm kernel cake**		**Palm shell**
	500°C	**700°C**	**500°C**	**700°C**	**700°C**
n-Octane, C_8	2.312	1.134	2.786	2.415	2.108
1,4-dimethyl-cyclohexane	0.810	0.075	0.195	0.112	0.101
Methyl cycloheptene	ND	0.062	0.058	0.218	0.099
1,3-dimethyl-cyclohexane	ND	0.021	ND	0.008	0.015
Ethyl cyclohexane	ND	0.014	ND	0.004	ND
n-Nonane, C_9	0.005	0.015	0.011	0.041	ND
n-Decane, C_{10}	0.002	ND	0.017	0.014	ND
n-Undecane, C_{11}	0.012	0.005	0.220	0.073	ND
n-Dodecane, C_{12}	ND	ND	0.025	0.028	ND
n-Tridecane, C_{13}	0.008	ND	0.085	0.070	0.005
n-Tetradecane, C_{14}	0.004	0.007	0.068	0.061	ND
n-Pentadecane, C_{15}	0.023	0.029	0.052	0.149	0.026
n-Hexadecane, C_{16}	0.012	0.057	0.055	0.038	0.121
n-Heptadecane, C_{17}	0.072	0.114	0.026	0.190	0.181
n-Octadecane, C_{18}	0.026	0.043	0.012	0.007	0.059
n-Nonadecane, C_{19}	0.011	0.221	0.043	0.017	0.008
n-Eicosane, C_{20}	0.006	0.011	0.023	0.020	0.009
n-Docosane, C_{22}	0.005	0.083	0.026	0.017	0.017
n-Tricosane, C_{23}	0.005	0.169	0.121	0.022	0.153
n-Tetracosane, C_{24}	0.011	0.203	0.026	0.028	0.083
n-Pentacosane, C_{25}	0.011	0.279	0.078	0.116	0.149
n-Hexacosane, C_{26}	0.047	0.241	0.097	0.055	0.318
n-Heptacosane, C_{27}	0.041	0.053	0.189	0.137	0.302
n-Octacosane, C_{28}	0.017	0.207	0.190	0.102	0.483
n-Nonacosane, C_{29}	0.013	0.232	ND	0.123	0.456
n-Triacontane, C_{30}	0.018	0.222	ND	0.048	0.470
n-Hentriacontane, C_{31}	0.013	0.109	ND	0.179	0.695
n-Dotriacontrane, C_{32}	0.019	0.119	ND	0.718	0.056
n-Tritriacontane, C_{33}	ND	0.073	ND	0.134	0.858

Note: ND = Non detectable

Table 4.6 Hydrocarbon compounds of three bio-oils at different pyrolysis temperatures (Continued).

Chemical	**Chemical concentration in bio-oil (wt%)**				
	Cassava pulp residue		**Palm kernel**		**Palm shell**
	500°C	**700°C**	**500°C**	**700°C**	**700°C**
n-Tetratriacontane, C_{34}	ND	ND	ND	0.022	ND
Alkanes (Unknown)	0.061	0.312	ND	0.006	ND
Total of alkanes	3.564	4.11	4.403	5.172	6.771
Total of alkenes (Unknown)	0.005	0.010	0.133	0.143	0.027
Benzene	0.430	0.341	0.658	0.710	0.520
Toluene	1.933	0.432	0.568	0.342	0.566
Ethylbenzene	0.582	0.066	0.187	0.154	0.037
Xylene	0.169	0.014	0.122	0.540	0.083
Styrene	ND	ND	0.094	0.076	0.008
1-methylethyl-benzene	ND	0.022	0.044	0.033	0.009
n-propylbenzene	ND	ND	0.025	0.019	ND
1,2,3-trimethylbenzene	ND	ND	ND	0.021	ND
Isopropylbenzene	ND	0.005	ND	0.004	ND
2-propenyl-benzene	ND	ND	0.080	0.032	ND
3-phynyl-1-propyne	ND	0.016	0.080	0.070	ND
Indene	ND	ND	0.008	0.022	ND
Butyl benzene	ND	ND	0.006	ND	ND
Pentyl benzene	ND	ND	0.009	ND	ND
Cyclohexyl benzene	0.216	0.054	0.011	0.377	ND
3-methylpentyl benzene	ND	ND	0.024	ND	ND
1,2,3,4-tetrahydro-1,4-dimethyl naphthalene	ND	0.030	0.024	0.080	ND
Octyl benzene	ND	ND	0.019	ND	ND
Bibenzyl	0.004	0.004	ND	0.007	ND
Phenanthracene	ND	0.032	ND	0.030	ND
Total of aromatics	3.334	1.026	1.959	2.517	1.223
Total of hydrocarbons	6.902	5.146	6.495	7.832	8.021

Note: ND = Non detectable

Chemical compositions of oxygenated compounds were illustrated in Table 4.7. There are about 50 different types of chemical species that could be identified, including phenolic compounds, ethers, esters, acids, some species of furans, etc. Oil from cassava pulp residue showed much lower concentration of acids (0.03-2.25 wt%) and esters (0.17-2.11 wt%) but with dominant contents of ethers, ketones and aldehydes (7.29-7.97 wt%). For kernel cake derived oil, acids (n-C_8-C_{18}) and esters were the major oxygenated compound amounting to 14.79-18.09 wt% and 14.93-19.68 wt%, respectively. It may be possible that the high content of free fatty acids derived from palm kernel oil could come from the remaining extracted oil present in the original biomass feedstock, which contains high contents of lauric acid, myristic acid, palmitic acid and oleic acid. The dewatered palm shell oil contains high contents of alcohols and phenols (20.75 wt%), esters (15.31 wt%) and acids (12.63 wt%) but only 2.67 wt% of ethers, ketones and aldehydes. In addition, palm shell oil and palm kernel cake oil had obviously higher concentration of phenolics and alcohols (20.75 wt% and 9.26-14.17 wt%, respectively) such as cresol, guaiacol, eugenol, and syringol than those obtained with cassava pulp residue oil (3.06-3.88 wt%). It is probable that higher lignin content in palm shell and palm kernel cake could be responsible for the increase of these compounds, as they were produced by the cracking of phenyl-propane unit of lignin structure (Branca *et al.*, 2003; Demirbaş, 2000). It is also interesting to note that cassava pulp residue, which contains higher polysaccharides (starch content of 64-70 wt% (Srinorakutara, T., *et al.*, 2006)) should provide much high contents of sugars, furans, acetaldehydes and acids (Biomass Technology Group, 2003). However, these chemical compounds probably exist in too low concentrations to be detected in dewatered cassava pulp residue oil.

It may be reasoned that some of these chemicals presenting in the crude bio-oils may have lost with water during the water removing step, since it has been reported that water soluble fraction of bio-oils contained products derived from hydrolysis and oxidation of glucose such as acetic acid, acetone, alcohols, aldehydes and sugars (Thomas and Wornat, 2008). On the temperature effect, it has been reported in some literatures that phenol contents increased continuously with increasing pyrolysis temperature (Branca *et al.*, 2003). However, in this work, a decrease in phenol content of palm kernel oil and cassava pulp residue oil was observed at the high pyrolysis temperature (700°C), and this could result from further reactions of phenol to give higher concentrations of furans, aldehydes and ketones (Demirbaş, 2000). Furthermore, pyrolysis at the temperature of 700°C gave rise to a decrease in ester group. This could arise from the hydrolysis of esters to alcohols and acids, followed by their decomposition to CO_2 and H_2 (Wang *et al.*, 1997).

The bio-oils derived from pyrolysis of biomasses in the present study provide a source of potential chemical feedstocks such as octane, toluene, benzene, naphthalene, lauric acid, oleic acid, phenol, etc. However, due to their presence in low concentrations, the complete separation of individual specific component is too costly and it is more logical and practical to utilize them by separating into different fractions having similar chemical properties or by converting the whole bio-oil into useful chemicals, making use of its abundant functional groups (Mohan *et al.*, 2006). For example, dewatered bio-oils from palm shell and palm kernel cake contain reasonable amounts of carboxylic acids and phenols which can readily react with lime to form calcium salts and used for efficient capture of acid gases from coal-fired power plants (Czernik and Bridgwater, 2004). In addition, phenolic compounds in palm shell oil and kernel cake oil may be used as partial or total replacement for pure phenol in making phenol-formaldehyde resins after separation via the process of solvent extraction with pH adjustment (Chum and Kreibich, 1993). The dominant contents of ketone and aldehyde groups in bio-oil from cassava pulp residue could be separated by dissolution into an added water phase which can be used, for example, as a meat browning agents for providing smoky flavors (Czernik and Bridgwater, 2004).

Table 4.7 Oxygenated compounds of three bio-oils at different pyrolysis temperatures.

Chemical	**Chemical concentration in bio-oil (wt%)**				
	Cassava pulp residue		**Palm kernel cake**		**Palm shell**
	500°C	**700°C**	**500°C**	**700°C**	**700°C**
1,4-doxane-2,3-diol	5.646	3.415	0.898	2.077	0.762
Furfural	ND	0.432	0.143	0.466	0.227
3-furanmethanol	0.482	0.436	0.792	1.610	0.038
2-methyl-2-cyclopenten-1-one	0.040	0.048	0.082	0.134	0.092
1-(2-furanyl) ethanone	0.068	0.028	0.080	0.243	ND
Cyclohexanone	0.076	0.023	ND	ND	0.083
Benzaldehyde	0.667	0.689	0.308	0.822	0.083
2-furanmethanol acetate	0.026	ND	0.015	0.094	ND
2,5,dihydro-3,5-dimethyl-2-furanone	0.082	0.031	0.257	0.356	0.037
2-hydroxy-3-methyl-1-cyclopentene-1-one	ND	0.391	0.180	0.326	0.204
3-ethyl-2-hydroxy-2-cyclopenten-1-one	0.203	0.068	0.099	0.076	0.054
2-methyl-benzofuran	ND	ND	0.026	0.024	ND
1,2,4-trimethoxybenzene	ND	ND	0.830	0.998	0.939
Verapamil	ND	2.405	ND	ND	0.151
Total of ethers, ketones and aldehydes	7.290	7.966	3.710	7.226	2.670
Benzoic acid	ND	ND	ND	0.650	0.719
Octanoic acid (Caprylic acid)	ND	ND	0.714	0.688	ND
Decanoic acid (Capric acid)	ND	ND	0.999	1.094	0.549
Dodecanoic acid (Lauric acid)	0.028	0.876	9.446	6.933	3.429
Tetradecanoic acid (Myristic acid)	ND	0.491	3.271	2.093	1.348
Hexadecanoic acid (Palmitic acid)	ND	0.499	1.394	1.410	4.127
(9Z)-Octadecenoic acid (Oleic acid)	ND	0.246	2.106	1.456	1.947
Octadecanoic acid (Stearic acid)	ND	0.140	0.168	0.473	0.514
Total of acids	0.028	2.252	18.098	14.797	12.633
Benzyl alcohol	ND	0.109	0.281	0.233	0.089
Phenol	1.643	0.291	2.747	2.010	9.045
2-methyl-phenol, (o-Cresol)	0.113	0.042	ND	ND	0.372
4-methyl-phenol, (p-Cresol)	0.235	0.066	0.498	0.600	0.711
2-methoxy-phenol, (Guaiacol)	0.229	0.156	ND	0.482	1.380

Note: ND = Non detectable

Table 4.7 Oxygenated compounds of three bio-oils at different pyrolysis temperatures (Continued).

Chemical	**Chemical concentration in bio-oil (wt%)**				
	Cassava pulp residue		**Palm kernel cake**		**Palm shell**
	500°C	**700°C**	**500°C**	**700°C**	**700°C**
2,3-dimethyl-phenol	ND	ND	0.086	ND	ND
3,4-dimethyl phenol	0.051	ND	1.136	0.247	0.169
2-methoxy-4-methyl-phenol	0.144	ND	0.624	0.451	1.451
1,2-benzenediol	0.307	0.170	0.657	0.722	0.606
4-ethyl-4-methoxy-phenol	0.142	0.832	0.950	1.181	1.355
Benzenepentanol	0.007	ND	ND	ND	ND
4-methyl-1,2-benzenediol	ND	ND	0.562	0.467	0.279
2-methoxy-4-vinylphenol (Eugenol)	ND	0.468	0.531	0.664	ND
2,6 dimethoxy-phenol (Syringol)	0.081	0.033	0.961	1.360	1.770
4-methyl-1,3-benzenediol	ND	ND	ND	0.531	ND
2-methoxy-4-(1-propenyl)-phenol	0.035	ND	ND	0.298	0.363
2-methoxy-6-(2-propenyl)-phenol	ND	ND	ND	0.258	0.316
Methylparaben	ND	ND	ND	0.200	0.309
2,5-bis(1,-dimethylethyl)-phenol	ND	0.075	ND	0.243	0.058
2,6-dimethoxy-4-(2-propenyl)-phenol	ND	ND	0.230	0.117	ND
2,6-dimethoxy-4-(2-propenyl)-phenol	ND	ND	ND	1.307	0.363
2,4,6-tris(1,1 dimethyl ethyl)-phenol	ND	0.040	ND	1.632	0.061
2-(1,1-dimethylethyl)-4(1-methyl-1-phenylethyl) phenol	ND	0.108	ND	ND	ND
2,6-bis(1,1-dimethylethyl)-4-(1-1-methyl)-1-phenylethyl)-phenol	ND	0.201	ND	ND	ND
2,2'-methylene bis(6-1,1-dimethyl ethyl)-4-methyl-phenol	ND	0.067	ND	1.090	0.349
2,4-bis(dimethylbenzyl)-6-t-butyphenol	0.077	1.224	ND	0.081	1.704
Total of alcohols and phenols	3.064	3.882	9.263	14.174	20.752
Total of esters	2.108	0.172	19.688	14.938	15.314
Total of Unknown	1.998	0.711	13.476	5.103	4.270
Total oxygenated compounds	14.488	14.983	64.235	56.238	55.539

Note: ND = Non detectable

4.5.4 Char Properties

Characteristics of the chars derived from pyrolysis of the various biomasses at 500 and 700°C were listed in Table 4.8. Bulk densities of the chars derived from pyrolysis depended on biomass type and they were lower than that of the corresponding raw materials (about 40-50% for cassava pulp residue and longan fruit seed and 3-13% for palm kernel cake, palm shell and coconut shell). A slight increase of bulk and true densities of chars were observed when the pyrolysis temperature was increased from 500 to 700°C for the chars from cassava pulp residue and palm kernel cake, resulting mainly from additional char devolatilization causing particle shrinkage. As expected, higher pyrolysis temperature caused the increases of fixed carbon and a consequent decrease in the volatile contents. The main component of chars was fixed carbon being in the range 52.9-82.1 wt%. Comparing the results of elemental analysis in Tables 4.2 and 4.8 indicates that the carbon content increased and the amounts of the other elements decreased after pyrolysis. It may be explained that during pyrolysis, hydrogen and oxygen were consumed via reactions of dehydrogenation and/or deoxygenation to produce CO_2, CO, H_2, H_2O, etc (Uzun *et al.*, 2007). This should cause the decrease of molar ratio of H/C and O/C in chars. Calorific values of the derived chars varied in the range of 29-35 MJ/kg which is comparable to that of coal (~35 MJ/kg) (Jorjani *et al.*, 2008). The increase of pyrolysis temperature from 500 to 700°C caused higher calorific values of the chars.

Porous characteristics of the produced chars after pyrolysis at 700°C are shown in Table 4.8. The porous properties of chars derived at pyrolysis temperature of 500°C were not reported here because their N_2 adsorption isotherms could not be measured due to the inaccessibility of N_2 molecule into a not well developed pore structure of this char at low measuring temperature of -196°C. The results, at pyrolysis temperature of 700°C, show that palm shell based char gives the highest surface area and total pore volume among other chars. The chars of palm shell and kernel cake have much higher total pore volume and surface area and consist mainly of microporosity (83.2 and 87.1%, respectively), while the cassava pulp residue based char possesses lesser proportion of micropores (59.1%) and larger average pore size. The lower micropore volume of cassava pulp residue char, which results in much lower BET surface area (34 m^2/g) compared to that derived from kernel cake char and palm shell char (209 and 367 m^2/g, respectively), is hypothesized to result from the differences in their chemical compositions and physical structure. The higher volatile content of cassava pulp residue and its softer and looser structure may facilitate the more rapid and intense release of volatiles, thus creating char structure with relatively larger pore sizes and hence lower surface area and microporosity (Bansal *et al.*, 1988). The reasonably high microporosity and surface area of kernel cake char and palm shell char indicate that they should have a potential to be further activated to produce highly porous activated carbons.

Table 4.8 Properties of chars derived from pyrolysis of various biomasses.

Properties	**Char product**						
	Cassava pulp residue		**Palm kernel cake**		**Palm shell**	**Coconut shell**	**Longan fruit seed**
	500°C	**700°C**	**500°C**	**700°C**	**700°C**	**700°C**	**700°C**
Bulk density (g/cm^3) (particle size of 2.03 mm)	0.168	0.176	0.496	0.523	0.568	0.610	0.321
True density (g/cm^3)	1.651	1.754	1.549	1.784	1.689	1.512	1.911
Proximate analysis (Dry basis) (wt%)							
Volatile	36.78	29.23	28.00	14.61	12.66	17.33	19.91
Fixed carbon	52.94	56.36	60.72	69.08	82.11	80.72	76.18
Ash	10.28	14.41	11.28	16.32	5.23	1.95	3.90
Elemental analysis (wt%)							
C	58.69	55.30	64.28	60.88	72.45	72.30	65.57
H	2.84	1.65	3.33	1.52	1.789	2.201	1.444
O	38.34	42.48	31.21	35.06	25.24	25.05	31.89
N	0.13	0.57	1.18	2.54	0.513	0.453	1.096
H/C	0.58	0.36	0.62	0.30	0.30	0.37	0.26
O/C	0.49	0.58	0.36	0.43	0.26	0.26	0.36
Calorific value (MJ/kg)	28.60	29.28	30.57	34.65	33.36	34.97	29.88
Porous characteristics							
BET surface area (m^2/g)	NA	33.6	NA	209.3	367.2	NA	NA
Micropore area (m^2/g)		26.9		185.6	322.8		
Average pore size (nm)		2.58		2.04	2.14		
Total pore volume (cm^3/g)		0.022		0.107	0.178		
Micropore volume (cm^3/g)		0.013		0.089	0.155		

Note: NA = Not analyzed

4.5.5 Gas Compositions

Table 4.9 shows gas yields and compositions obtained from the pyrolysis of various biomasses at pyrolysis temperatures of 500 and 700°C. There is almost no difference in total gas yields at 500 and 700°C for the pyrolysis of cassava pulp residue and palm kernel cake. However, pyrolysis of five different biomasses at 700°C showed relatively large variation in total gas yield. Gas yields obtained from cassava pulp residue and longan fruit seed were higher than those derived from other biomasses; that from cassava pulp residue and longan fruit seed varied in the range of 28.0-32.4 wt% (0.21-0.27 m^3/kg-biomass) and 19.4-22.3 wt% (0.13-0.20 m^3/kg-biomass) was derived from palm kernel cake, palm shell and coconut shell. Li *et al.* (2004) found that biomass components had a direct effect on the product yields; cellulose and hemicellulose can generate higher gas product than that of lignin at the same pyrolysis temperature. Thus, it is possible that cassava pulp residue and longan fruit seed could contain higher cellulose and hemicellulose contents but have lower lignin than those of the others. The gas product produced from longan fruit seed pyrolysis 700°C gave the highest HHV (4.42 MJ/kg biomass) followed by that derived from pyrolysis of cassava pulp residue (3.47 MJ/kg biomass), while pyrolysis of palm shell, coconut shell and longan fruit seed at the same temperature gave lower HHV of gases being about 2.19-2.85 MJ/kg biomass. The increase of pyrolysis temperature from 500 to 700°C caused twofold higher HHV of gas products for pyrolysis of cassava pulp residue and palm kernel pyrolysis. The gas products consists of H_2, CO, CO_2 and CH_4 with CO_2 being the dominant component among the others (11.2-21.1 wt%). Figure 4.9 shows gas compositions for the pyrolysis of five biomasses at 500 and 700°C. On the effect of pyrolysis temperature, it was observed that increasing pyrolysis temperature caused a decrease in CO and CO_2 contents and an increase in H_2 and CH_4 compositions. It is also noted that pyrolysis temperature had a strong influence on H_2 content. It increased from 1.13 to 16.5 vol% for palm kernel cake and 2.03 to 20.36 vol% for cassava pulp residue when the pyrolysis temperature was increased from 500°C to 700°C. There existed a difference in the compositions of gas product derived from the pyrolysis of each feedstock. Cassava pulp residue, palm shell and coconut shell gave the highest syngas content (H_2 and CO, ~51.2 vol%) and had about the same H_2/CO ratio of about 0.63 (Table 4.9). Pyrolysis of palm kernel cake provided dominant gas component of CO_2 with the highest contents of 39.3 vol%. Longan fruit seed gave the largest amount of CH_4 (27.6 vol%) and the highest molar ratio of H_2/CO (0.81).

Table 4.9 Gas yields, mole ratio of H_2/CO, gas volumes and high heating value derived from pyrolysis of various biomasses.

Gas component	**Gas yield (wt%) (N_2 and H_2O free)**						
	Cassava pulp residue		**Palm kernel cake**		**Palm shell**	**Coconut shell**	**Longan fruit seed**
	500°C	**700°C**	**500°C**	**700°C**	**700°C**	**700°C**	**700°C**
H_2	0.04	0.50	0.01	0.25	0.34	0.31	0.49
CO	9.69	11.06	4.31	4.92	7.98	6.58	8.53
CO_2	21.14	17.12	13.97	13.19	11.20	12.18	13.49
CH_4	1.57	3.04	1.13	2.58	2.79	1.95	5.45
Total yield (wt%)	32.44	31.72	19.42	20.94	22.31	21.01	27.96
H_2/CO (mole ratio)	0.06	0.63	0.04	0.72	0.60	0.66	0.81
Gas volume (m^3/kg-biomass)	0.21	0.27	0.13	0.17	0.20	0.18	0.26
High heating value (HHV, MJ/kg-biomass)	1.90	3.47	1.14	2.28	2.85	2.19	4.42

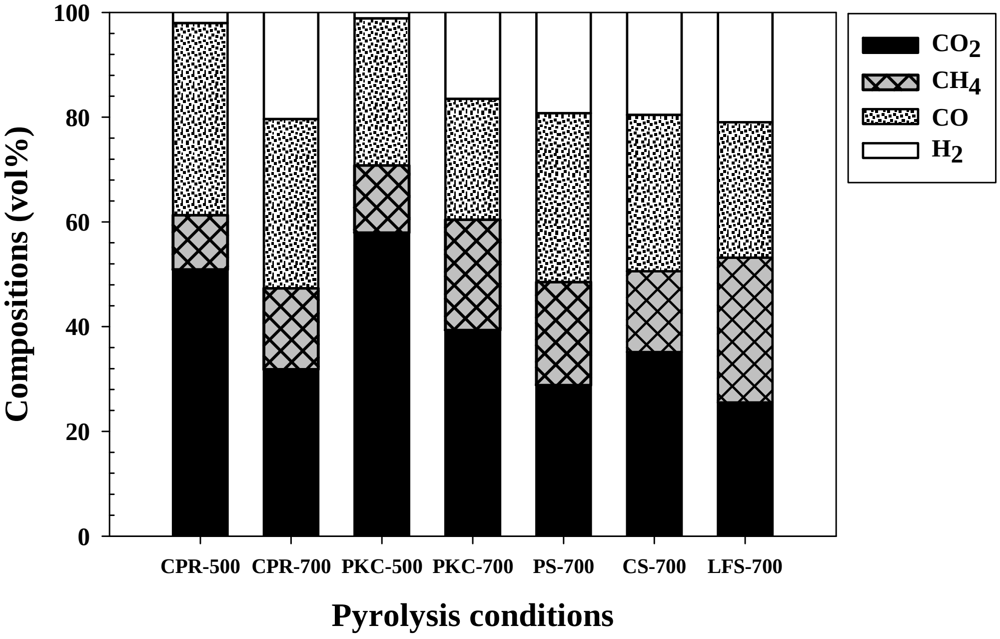

Figure 4.9 Gas compositions from pyrolysis of various biomasses at pyrolysis temperatures of 500 and 700°C (CPR: cassava pulp residue, PKC: palm kernel cake, PS: palm shell, CS: coconut shell and LFS: longan fruit seed).

Figure 4.10 shows gas product distribution as a function of pyrolysis time for the batch pyrolysis of five biomasses at the temperature of 700°C. It shows that the production of gases derived from the five biomasses occurred over the same pyrolysis time but differed in the amounts of produced gases, depending on biomass type. Trace amounts of CO_2 and CO were first produced at 350°C, then they rapidly reached the maximum concentration at 550°C, and afterward its concentration started to decline. This is in accord with the results from pyrolysis of various biomasses from which organic compounds such as C=O, C-O-C, etc from hemicellulose and cellulose mainly released out in the form of CO_2 and CO at low temperatures of 200-400°C and 300-450°C, respectively (Li *et al.*, 2004; Yang *et al.*, 2007; Zanzi *et al.*, 2002). The components of CH_4 and H_2 were evolved out at a higher temperature and the maximum contents of CH_4 and H_2 were produced around 700°C during the hold time period. Previous works (Panigrahi *et al.*, 2002; Xianwen *et al.*, 2000; Yang *et al.*, 2006) have indicated that the production of H_2 at higher temperatures could result from secondary reactions, possibly due to tar and char cracking and water gas shift reaction. In addition, these reactions might also cause the increase or decrease in the content of the other gases (CO, CH_4 and hydrocarbon gases). Furthermore, it is also noted from Figure 4.10 that the existence of maximum heating values of gas products for the five biomasses coincides roughly with the maximum generation of combustible gases of H_2 and CH_4 (Table 4.10 and Figure 4.10). At this pyrolysis time, the maximum heating values of the biomasses varied in the range 13.5-15.9 MJ/m^3 which are comparable with that of medium heating value gases derived from biomass gasification (Mahishi and Goswami, 2007).

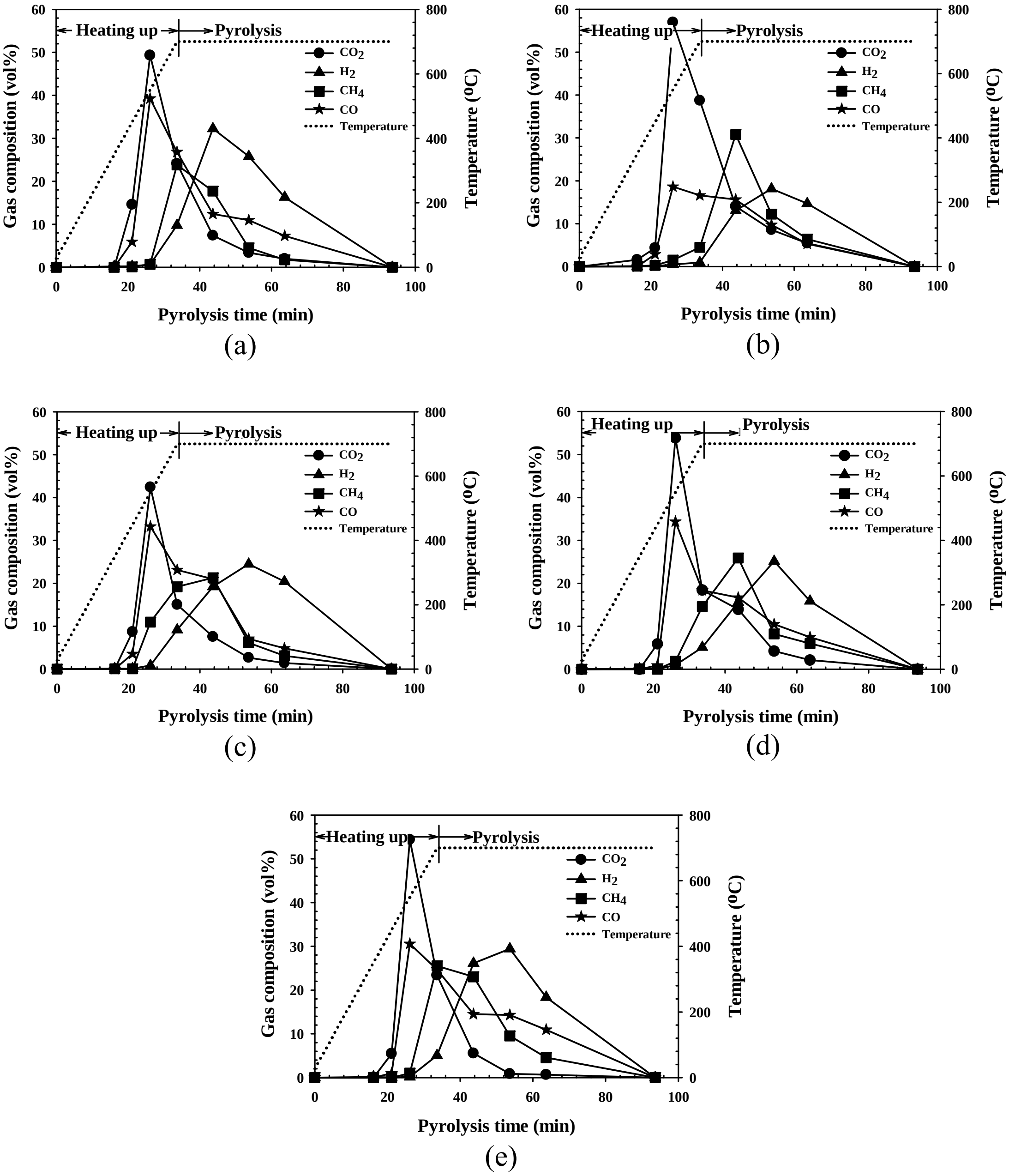

(a) (b) (c) (d) (e)

Figure 4.10 Gas product distribution versus pyrolysis time derived from pyrolysis of various biomasses (a) cassava pulp residue, (b) palm kernel cake, (c) palm shell, (d) coconut shell and (e) longan fruit seed at final temperature of 700°C.

Table 4.10 Heating values of gas products derived from pyrolysis of various biomasses as a function of time for the final temperature of 700°C.

Time (min)	Pyrolysis temperature (°C)	Heating values of gas products (MJ/m^3)				
		Cassava pulp residue	Palm kernel cake	Palm shell	Coconut shell	Longan fruit seed
0	27	-	-	-	-	-
16	350	0.02	0.04	0.04	0.05	0.02
21	450	0.82	0.49	0.49	0.12	0.13
26	550	5.31	3.01	8.66	5.20	4.28
34	700	14.09	4.00	11.71	8.77	13.91
44	700	12.74	15.89	13.57	14.40	14.32
54	700	6.47	8.40	6.46	7.80	9.35
64	700	3.69	5.09	4.45	5.34	5.54
94	700	-	-	-	-	-

4.6 Conclusions

Study of batch pyrolysis in a fixed-bed reactor for various types of biomasses including cassava pulp residue, palm kernel cake, palm shell, coconut shell and longan fruit seed, has led to the following conclusions.

- Maximum liquid yields of various biomasses were obtained from the following pyrolysis conditions; heating rate of 20°C/min, N_2 gas flow rate of 200 cm^3/min, and particle size of 2.03 mm but at different pyrolysis temperature (600°C for coconut shell; 700°C for cassava pulp residue, palm kernel cake and palm shell; and 800°C for longan fruit seed).
- Maximum liquid product varied in range of 42.4-54.3 wt% and pyrolysis of palm kernel cake gave the highest liquid yield of 54.3 wt% among other biomasses.

- Pyrolysis temperature (300-700°C) and average particle size in range of 0.71-2.03 mm exerted a great influence on product yields (liquid, gas and char), while N_2 purge rate (200-600 cm^3/min) and heating rate (5-20°C/min) gave almost no effect.

- Considering physical appearances of bio-oils, palm kernel cake derived oil contained two phases (aqueous-oil phase) with opaque dark color, while cassava pulp residue liquid oil showed a homogeneous single phase of dark red-brown transparent liquid. Liquid products from palm shell, coconut shell and longan fruit seed gave a dispersion of opaque dark oil drops in dark red-brown aqueous solution.

- Typical fuel properties of bio-oils are as follows: density, 1.01-1.18 g/cm^3; pH, 2.1-5.6; flash point, 74-110°C and pour point, -21-1°C. After water removing, an increase in values of viscosity, ramsbottom carbon residue and ash content was observed. Oil heating value could be measured only when water was removed. The value depended on type of biomass, giving for palm kernel cake oil, 40 MJ/kg, oils from palm shell and coconut shell, ~28 MJ/kg and cassava pulp residue oil and longan fruit seed oil, ~14 MJ/kg.

- It was possible to use dewatered bio-oil from kernel cake pyrolysis as a substitute for petroleum-based fuel because of its high heating value, and giving similar boiling range distribution to that of diesel fuel. Until the problems of their high viscosity and carbon residue and low pH value are resolved, other bio-oils are less attractive for using as a liquid fuel.

- Crude bio-oils had dominant functional groups of alcohols, ketones, ethers, esters, aldehydes and carboxylic acids and groups of alkanes, alkenes and aromatics were obviously detected after water in the bio-oil was removed.

- Major compounds in dewatered oils from palm kernel cake and palm shell were acid group of n-C_8-C_{18} (12.6-18.1 wt%), ester group (14.9-19.7 wt%) and phenolics (9.3-20.8 wt%), while dewatered cassava pulp residue oil showed main contents of polar fraction and non-volatile compounds of methanol fraction (56.8-58.9 wt%). Moreover, pyrolysis temperature had a strong effect on presence of some oxygenated compounds in bio-oils, with higher pyrolysis temperature of 700°C giving lower amounts of esters and phenol.

- Hydrocarbon components presenting mainly in pentane and toluene fractions consisted of n-paraffins of C_8-C_{34} (3.56-6.77 wt%), aromatics (1.03-3.33 wt%) and small amount of olefins (0.01-0.14 wt%). In addition, higher molecular weights of n-alkanes and a polycyclic aromatic hydrocarbon (PAH) were derived at higher pyrolysis temperature of 700°C.

- Derived char had high calorific value of 29-35 MJ/kg comparable to that of coal (~35 MJ/kg). Considering porous characteristics, the derived chars from palm kernel cake and palm shell showed good promise as a precursor for further production of activated carbon due to its relatively high BET surface area of about 209 and 367 m^2/g, respectively.

- Compositions of gas product depended on type of biomass feedstock. Pyrolysis of cassava pulp residue, palm shell and coconut shell at 700°C gave the highest syngas composition (H_2 and CO), ~51.2 vol%, while the highest content of CO_2 (39.3 vol%) was obtained from pyrolysis of palm kernel cake and longan fruit seed pyrolysis contributed the highest amount of CH_4 (27.6 vol%). The heating values of gases produced from pyrolysis of biomasses at 500 and 700°C were in range of 1.14-4.42 MJ/kg-biomass.

4.7 References

Acıkgoz, C., Onay, O., and Kockar, O. M. (2004). Fast pyrolysis of linseed: product yields and compositions. **Journal of Analytical and Applied Pyrolysis** 71 (2): 417-429.

Bansal, R. C., Donnet, J. B., and Stoeckli, F. (1988). **Active carbon**. New York: Marcel Dekker.

Beis, S. H., Onay, Ö., and Koçkar, Ö. M. (2002). Fixed-bed pyrolysis of safflower seed: influence of pyrolysis parameters on product yields and compositions. **Renewable Energy** 26 (1): 21-32.

Biomass Technology Group (2003). Bio-oil Applications [On-line]. Available: **http://www.btgworld.com/technologies/bio-oil-applications.html**.

Branca, C., Giudicianni, P., and Blasi, C.D. (2003). GC/MS characterization of liquids generated from low-temperature pyrolysis of wood. **Industrial & Engineering Chemistry Research** 42 (14): 3190-3202.

Bridgeman, T. G., Darvell, L. I., Jones, J. M., Williams, P. T., Fahmi, R., Bridgwater, A. V., Barraclough, T., Shield, I., Yates, N., Thain, S. C., and Donnison, I. S. (2007). Influence of particle size on the analytical and chemical properties of two energy crops. **Fuel** 86 (1-2): 60-72.

Bridgwater, A. V. (1999). Principles and practice of biomass fast pyrolysis processes for liquids. **Journal of Analytical and Applied Pyrolysis** 51(1-2) 3-22.

Bridgwater, A V. (2003). Renewable fuels and chemicals by thermal processing of biomass. **Chemical Engineering Journal** 91 (2-3): 87-102.

Chum, H. L., and Kreibich, R. E. (1993). **Process for preparing phenolic formaldehyde resin products derived from fractionated fast pyrolysis oils**. U.S. Patent 5,091,499.

Czernik, S., and Bridgwater, A V. (2004). Overview of applications of biomass fast pyrolysis oil. **Energy & Fuels** 18 (2): 590-598.

Demirbaş, A. (2000). Mechanisms of liquefaction and pyrolysis reactions of biomass. **Energy Conversion and Management** 41 (6): 633-646.

Demirbaş, A. (2006). Effect of temperature on pyrolysis products from four nut shells. **Journal of Analytical and Applied Pyrolysis** 76: 285-289.

Demirbaş, A. (2007). The influence of temperature on the yields of compounds existing in bio-oils obtained from biomass samples via pyrolysis. **Fuel Processing Technology** 88 (6): 591-597.

Dynamotive Energy Systems Corporation (2009). The evaluation of energy: alternative fuels from cellulose for a better world [On-line]. Available: **www.dynamotive.com**.

Goyal, H. B., Seal, D., and Saxena, R.C. (2008). Bio-fuels from thermochemical conversion of renewable resources: a review. **Renewable and Sustainable Energy Reviews** 12 (2): 504-517.

Guo, J., and Lua, A. C. (2001). Kinetic study on pyrolytic process of oil-palm solid waste using two-step consecutive reaction model. **Biomass & Bioenergy** 20 (3): 223-233.

Islam, M. N., Zailani, R., and Ani, F. N. (1999). Pyrolytic oil from fluidized bed pyrolysis of oil palm shell and its characterization. **Renewable Energy** 17: 73-84.

Jorjani, E., Hower, J. C., Chelgani, S. C., Shirazi, M., and Mesroghli, A. S. (2008). Studies of relationship between petrography and elemental analysis with grindability for Kentucky coals. **Fuel** 87 (6): 707-713.

Junming, X., Jianchun, J., Yunjuan, S., and Yanju, L. (2008). Bio-oil upgrading by means of ethyl ester production in reactive distillation to remove water and to improve storage and fuel characteristics. **Biomass&Bioenergy** 32 (11): 1056-1061.

Karaosmanoğlu, F., Tetik, E., and Göllü, E. (1999). Biofuel production using slow pyrolysis of the straw and stalk of the rapeseed plant. **Fuel Processing Technology** 59 (1): 1-12.

Kossiakoff, A., and Rice, F. O. (1943). Thermal decomposition of hydrocarbons, resonance stabilization and isomerization of free radicals. **Journal of the American Chemical Society** 65 (4): 590-601.

Lemeune, S. (2005). Le bios [On-line]. Available: **http://www.geocities.com/Paris/LeftBank/5810/bois.html**.

Li, S., Xu, S., Liu, S., Yang, C., and Lu, Q. (2004). Fast pyrolysis of biomass in free-fall reactor for hydrogen-rich gas. **Fuel Processing Technology** 85 (8-10): 1201-1211.

Mahishi, M., and Goswami, D. (2007). An experimental study of hydrogen production by gasification of biomass in the presence of a CO_2 sorbent. **International Journal of Hydrogen Energy** 32 (14): 2803-2808.

Mohan, D., Pittman, C. U., Jr., and Steele, P. H. (2006). Pyrolysis of wood/biomass for bio-oil: a critical review. **Energy & Fuels** 20 (3): 848-889.

Nugranad, N. (1997). **Pyrolysis of Biomass**. Ph.D. Dissertation, University of Leeds, United Kingdom.

Oasmaa, A., and Czernik, S. (1999). Fuel oil quality of biomass pyrolysis oils-state of the art for the end users. **Energy & Fuels**. 13 (4): 914-921.

Onay, O., and Koçkar, O. M. (2004). Fixed-bed pyrolysis of rapeseed (Brassica napus L.). **Biomass & Bioenergy** 26 (3): 289-299.

Özbay, N., Pütün, A. E., Uzun, B. B., and Pütün, E. (2001). Biocrude from biomass: pyrolysis of cottonseed cake. **Renewable Energy** 24 (3-4): 615-625.

Panigrahi, S., Chaudhari, S. T., Bakhshi, N. N., and A K. Dalai (2002). Production of synthesis gas/high-Btu gaseous fuel from pyrolysis of biomass-derived oil. **Energy & Fuels** 16 (6): 1392-1397.

Pütün, A. E., Apaydin, E., and Pütün, E. (2002). Bio-oil production from pyrolysis and steam pyrolysis of soybean-cake: product yields and composition. **Energy** 27 (7): 703-713.

Pütün, A. E., Gerçel, H. F., Koçkar, Ö. M., Ege, Ö., Snape, C. E., and Pütün, E. (1996). Oil production from an arid-land plant: fixed-bed pyrolysis and hydropyrolysis of Euphorbia rigida. **Fuel** 75 (11): 1307-1312.

Pütün, A. E., Özcan, A., Gerçel, H. F., and Pütün, E. (2001). Production of biocrudes from biomass in a fixed-bed tubular reactor: product yields and compositions. **Fuel** 80 (10): 1371-1378.

Pütün, A. E., Özcan, A., and Pütün, E. (1999). Pyrolysis of hazelnut shells in a fixed-bed tubular reactor: yields and structural analysis of bio-oil. **Journal of Analytical and Applied Pyrolysis** 52 (1): 33-49.

Pütün, E., Ateş, F. and Pütün, A. E. (2008). Catalytic pyrolysis of biomass in inert and steam atmospheres. **Fuel** 87 (6): 815-824.

Skoog, D. A., and Leary, J. J. (1992). **Principles of instrument analysis.** United States of America: A Harcourt Brace Jovanovich College.

Srinorakutara, T., Kaewvimol, L., and Saengow, L. (2006). Approach of cassava waste pretreatments for fuel ethanol production in Thailand. **Journal of Scientific Research Chulalongkorn University** 31(1) 77-84.

Thomas, S., and Wornat, M. J. (2008). The effects of oxygen on the yields of polycyclic aromatic hydrocarbons formed during the pyrolysis and fuel-rich oxidation of catechol. **Fuel** 87 (6): 768-781.

Trebbi, G., Rossi, C., and Pedrelli, G. (1997). Plans for the production and utilization of bio-oil from biomass fast pyrolysis. In Bridgwater, A. V., and Boocock D. G. B. (Eds), **Developments in Thermochemical Biomass Conversion** (Vol. 1, pp.378-387). London: Blackie Academic & Professional.

Tsai, W. T., Lee, M. K., and Chang, Y. M. (2006). Fast pyrolysis of rice straw, sugarcane bagasse and coconut shell in an induction-heating reactor. **Journal of Analytical and Applied Pyrolysis** 76 (1-2): 230-237.

Tsai, W. T., Mi, H. H., Chang, Y. M., Yang, S. Y., and Chang, J. H. (2007). Polycyclic aromatic hydrocarbons (PAHs) in bio-crudes from induction-heating pyrolysis of biomass wastes. **Bioresource Technology** 98 (5): 1133-1137.

Uzun, B. B., Pütün, A. E., and Pütün, E. (2007). Composition of products obtained via fast pyrolysis of olive-oil residue: effect of pyrolysis temperature. **Journal of Analytical and Applied Pyrolysis** 79 (1-2): 147-153.

Wang, D., Czernik, S., Montané, D., Mann, M., and Chornet, E. (1997). Biomass to hydrogen via fast pyrolysis and catalytic steam reforming of the pyrolysis oil or its fractions. **Industrial & Engineering Chemistry Research** 36 (5): 1507-1518.

Williams, P. T., and Nugranad, N. (2000). Comparison of products from the pyrolysis and catalytic pyrolysis of rice husks. **Energy** 25 (6): 493-513.

Xianwen, D., Chuangzhi, W., Haibin, L., and Yong, C. (2000). The fast pyrolysis of biomass in CFB reactor. **Energy & Fuels** 14 (3): 552-557.

Yaman, S. (2004). Pyrolysis of biomass to produce fuels and chemical feedstock. **Energy Conversion and Management** 45 (5): 651-671.

Yang, H., Yan, R., Chen, H., Lee, D. H., Liang, D. T., and Zheng, C. (2006). Pyrolysis of palm oil waste for enhanced production of hydrogen rich gases. **Fuel Processing Technology** 87 (10): 935-942.

Yang, H., Yan, R., Chen, H., Lee, D. H., and Zheng, C. (2007). Characteristics of hemicellulose, cellulose and lignin pyrolysis. **Fuel** 86 (12-13): 1781-1788.

Yorgun, S., Şensoz, S., and Koçkar, Ö. M. (2001). Flash pyrolysis of sunflower oil cake for production of liquid fuels. **Journal of Analytical and Applied Pyrolysis** 60 (1): 1-12.

Zanzi, R., Sjöström, K., and Björnbom, E. (2002). Rapid pyrolysis of agricultural residues at high temperature. **Biomass&Bioenergy** 23 (5): 357-366.

Zhang, Q., Chang, J., Wang, T., and Xu, Y. (2007). Review of biomass pyrolysis oil properties and upgrading research. **Energy Conversion and Management** 48 (1): 87-92.

CHAPTER V

BIO-OIL UPGRADING AND UTILIZATION

5.1 Abstract

Attempt was made to improve certain characteristics of bio-oils derived from pyrolysis of potential biomasses. Three different methods were applied for upgrading three raw bio-oils from three different biomasses. Bio-oil from cassava pulp residue showing a single transparent phase of aqueous solution was upgraded by blending with its char to form a slurry fuel of increased heat content. For this study, effects of slurry type, solid concentration, particle size, temperature and shearing time on rheological characteristics and fuel properties of char-bio-oil slurries were investigated. The rheological data measured were found to be well fitted by power law model with yield stress and the model parameters were determined. Results indicated that slurries of cassava residue char and raw oil displayed pseudoplastic behavior for all preparation conditions. The flow characteristics of other slurry systems can be summarized as follows. Cassava pulp residue char-water slurry showed the flow curve approaching Newtonian fluids, slurry of palm shell char-aqueous solution gave pseudoplastic behavior exhibiting almost same flow characteristics as that of cassava residue char-raw oil slurry and palm shell char-oil slurry showed a flow transition from pseudoplastic to dilatant behavior at a definite shear rate. Fuel properties of char-bio-oil slurries indicated that their pH and calorific values (3.54-3.98 and 18.0-31.7 MJ/kg, respectively, for 30 wt% solid) were

improved compared with those of the original bio-oils and the combustion of these slurries showed no ignition delay compared with their solid chars.

Dewatered palm kernel bio-oil possessing the highest heating value (40.0 MJ/kg) but with high viscosity and carbon residue content was used to study the oil upgrading by blending with diesel fuel and alcohol. Studies of phase behavior and fuel properties indicated that the blended fuel gave satisfactory fuel properties in spite of high amounts of alcohol being required for phase stability and the use of butanol as a cosolvent showed better characteristics of phase behavior and fuel properties than using ethanol. In estimating fuel properties of fuel mixtures, it was found that heating value, density, ash content and pH can be well estimated by the Kay's mixing rule, whereas modified Grunberg-Nissan equation and Andrade equation gave good fitting of viscosities of blended fuels at different temperatures.

Finally, to solve acidity of bio-oil, dewatered palm shell oil having low pH value was selected for studying bio-oil upgrading via esterification using solid acid catalyst of Amberlyst15 and liquid H_2SO_4. This method can convert carboxylic acids to esters and reduce also amount of active aldehydes in the bio-oil. However, using Amberlyst15 as catalyst gave lower esterification conversion than the use of liquid H_2SO_4 catalyst. Moreover, the effects of important parameters including reaction temperature and time, amounts of Amberlyst15 catalyst, alcohol type and alcohol amount on esterification conversion were also examined. The upgraded oils without alcohol recovery gave calorific value of 23.1-25.4 MJ/kg, improved bio-oil properties by lowering values of viscosity, carbon residue content, ash content and pour point, a slight increase of pH value compared to that of raw bio-oil and with flash point being close to room temperature.

5.2 Introduction

It is known that bio-oil possesses certain disadvantages of corrosiveness, high viscosity and ageing characteristic because of its containing a complex mixture of oxygenated compounds (from short chain organic compounds to polymer) (Bridgwater, 2003). Therefore, upgrading or treatment of crude bio-oil to improve the desired properties of bio-oil is obviously required. There are several means to improve bio-oil properties as mentioned in Chapter II including reduction of oligomeric molecules and ash removal by hot-vapor filtration or converting some acid chemicals through chemical/catalytic upgrading, etc. (Bridgwater, 2003; Oasmaa and Czernik, 1994). However, the complexity of chemical components in bio-oil, low yield of upgraded oil and high costs of chemical recovery have caused the upgrading by the previously mentioned processes become less attractive (Demirbas and Balat, 2006). As a result of these limitations, more simple alternative processes to improve bio-oil properties for use as an alternative fuel were explored in this study.

As presented in Chapter IV, different bio-oils gave distinctive appearances, odor and physicochemical properties. Accordingly, different types of raw bio-oil need to be upgraded by different methods. Three potential bio-oils from pyrolysis of cassava pulp residue, palm kernel cake and palm shell were thus selected for the study of oil upgrading. Cassava pulp residue oil showed the characteristics of dark red-brown transparent oil with low pH (2.95) and relatively low density and viscosity of 1.1 g/cm^3 at 25°C and 1.46 cSt at 40°C, respectively. However, its heating value cannot be directly determined due to the high oxygenated contents which make this oil unsuitable for use as a liquid fuel. A simple solution to this problem was initiated in this work by blending the raw bio-oil with its co-product char to form a uniform homogenous slurry suspension. In studying the possibility of using a mixture of bio-oil and char as a slurry fuel, the measurements of rheological behavior and fuel properties of cassava pulp residue char-raw oil slurries were conducted and slurries prepared from palm shell oil and its char were also studied to examine the effect of slurry type. Considering dewatered bio-oil from palm kernel cake, its oil phase provides the advantageous properties of giving the highest pH value (5.62) and a comparable heating value to that of fuel oil (40.0 MJ/kg) with boiling range distribution approaching that of diesel fuel among other derived bio-oils. As a result, it is safe to infer that this bio-oil may be directly used as a fuel oil. However, it has certain drawbacks such as high viscosity (58.72 cSt at 40°C) and high carbon residue (5.39 wt%), thus its use could be prone to incomplete combustion. To solve this problem, we suggested the preparation of a blended fuel of bio-oil-diesel-alcohol. Studies of phase equilibrium and fuel properties of the bio-oil-diesel-alcohol blends were presented. Finally, bio-oil upgrading via esterification for dewatered bio-oil from palm shell was investigated. The improvement of bio-oil properties by esterificaiton reaction is to be expected both for increasing pH and heating value of bio-oil by way of converting carboxylic acids to esters. Moreover, the lowering of viscosity and ageing of bio-oil could also be anticipated from the addition of alcohol. In this respect, the effect of esterification conditions on the conversion and properties of the upgraded bio-oil were therefore studied.

5.3 Rheology and Fuel Properties of Char-Bio-Oil Slurries

5.3.1 Introduction

Slurry fuel has been suggested as an attractive application of pyrolysis products (Bridgwater, 2002; Czernik and Bridgwater, 2004). The slurry exhibits the advantages of relatively high energy density and fluid-like characteristics leading to ease of handling and transportation and capability of pressurized feeding (Bridgwater, 2002; Food and Agriculture Organization of the United Nations, 2009). It has been demonstrated that the use of bio-oil and char derived from a pyrolysis process in the form of a slurry can substitute light fuel oil, heavy fuel oil, or natural gas in industrial and commercial burners and boilers (Dynamotive Energy Systems Corporation, 2009). Here, it was proposed to study the preparation of char-bio-oil slurry to increase the low heating value characteristic of bio-oil and yet still maintaining the flow behavior of the liquid oil. A scarce research on studying rheological characteristics and fuel properties of char-bio-oil slurry is a motivation in the present work to explore the possibility of using it for industrial applications. Bio-oils and chars derived from slow pyrolysis of two biomasses of cassava pulp residue (CPR) and palm shell (PS) were used for slurry preparation. The reasonably high calorific value of derived chars being in range of 29.3-33.4 MJ/kg can help increase the calorific value of both bio-oils as in their original form that they cannot be used directly as liquid fuel due to relatively high content of water. Effects of slurry type, solid concentration, char particle size and slurry temperature on rheological behaviors of slurries were examined using a coaxial cylinder viscometer and the rheological data obtained were fitted with an appropriate flow model. In addition, fuel properties and combustion characteristics of char-bio-oil mixtures were also measured.

5.3.2 Literature Reviews

5.3.2.1 Previous Studies

Slurry fuel has been successfully used in many applications such as boilers, furnaces and kilns. It offers several benefits including no dust explosion during storage, capability of transportation in pipeline, combustion behavior resembling fuel oil and favorable economic commercialization (Cheng *et al.*, 2008; Shin and Shen, 2007). There are various types of slurry being used as slurry fuels such as coal-water slurry (Cheng *et al.*, 2008; Logos and Nguyen, 1996; Papachristodoulou and Trass, 1987), coal-oil mixture (Cui *et al.*, 2008; Guo *et al.*, 1998; Slagle *et al.* 1978), coal-water-oil slurry (Majumder *et al.*, 2006) and biomass-oil slurry (Benter *et al.*, 1997). The studying results indicated that slurry type showed a significant influence on the rheological behavior and combustion characteristics. Coal-water slurry offered a wide range of flow behavior from Newtonian at low solid concentrations to shear-thinning with a yield stress at higher concentrations (Logos and Nguyen, 1996), whereas coal-oil mixture exhibited the change from shear-thinning to shear-thickening with increasing of solid concentration from 50 to 55 wt% (Cui *et al.*, 2008). As to the combustion process, coal-oil mixtures gave better characteristics of ignition, flame stability and higher heating value per unit volume than those of coal-water slurries (Papachristodoulou and Trass, 1987; Shin and Shen, 2007).

Furthermore, parameters including solid concentration, particle size distribution, physicochemical properties of solid, chemical dispersants and slurry temperature can have a direct bearing on slurry flow characteristics. Obviously, the slurry fuel possessing high solid loading, low viscosity, and good stability against settling are required (Cui *et al.*, 2008). Cheng *et al.* (2008) reported that the good characteristics of coal-water slurry fuel used in a boiler or gasifier were obtained from the slurry containing solid concentration of 60-70 vol% solid with average particle size of 40-50 μm, giving an apparent viscosity of 800-1200 mPas. Controlling size distribution of particles of coal-water slurries can improve significantly the rheological behaviors to achieve optimum slurry of low viscosity and high solid concentration (Logos and Nguyen, 1996). Also, an average char particle size has an important effect on the operation of slurry flow; the slurry containing finer particle sizes results in higher viscosity but giving better stability. The slurry that contains larger size particles provides lower viscosity but having poorer flame stability during combustion, leading to the wear of piston ring and cylinder liner (Cui *et al.*, 2008; Gu *et al.*, 2008). Physicochemical properties of solid fuel such as chemical composition (moisture, volatile, ash, oxygen and carbon), type of functional groups on solid surface, particle shape and porous characteristics (surface area, wettability, adsorption, zeta potential, etc) are determining factors for proper slurry fuel preparation. It was noted that high specific surface area and pore volume with hydrophilic surface of low rank coal could adsorb more water molecules leading to increased viscosity, while slurries prepared from spherical shape particles of higher rank coals showed much higher solid loading, giving lower apparent viscosity at the same solid concentration. In addition, to maintain the highest possible coal concentration with a good slurry stability at a given optimum viscosity, a chemical additive such as naphthalene sulfonate formaldehyde condensate (NSF), carboxymethyl cellulose sodium salt (CMC-Na), polymethacrylate, polystyrene sulfonic acid and biopolymers such as xanthan gum were needed for some slurries

(Natarajan and Suppes, 1997; Xu *et al.*, 2008). It was also marked that increasing the amount of NSF dispersant from 0.6 to 1.0 wt% could increase solid loading from 52.2 to 53.6 wt% at a given viscosity of 1000 mPas. On the effect of temperature, the flow behavior of slurry was changed from shear thinning fluid to shear thickening behavior when the slurry temperature was higher than 50°C (He *et al.*, 2004). Furthermore, the decrease of slurry viscosity with increasing temperature depended on the type of suspending medium, for example, heavy oil based slurries gave much greater decrease of viscosity than water based slurries mainly because of larger reduction of heavy oil viscosity when the temperature was increased (Guo *et al.*, 1998).

5.3.2.2 Principles of Rheology

Rheology is the study of deformation of a body that can be solids, liquids or gases under the influence of stress. An ideal solid can be elastically deformed and the required energy for deformation is fully recovered when the stress is removed. On the other hand, deformation of ideal fluids including liquids and gases are irreversible and the strain energy is spent in the form of heat within the fluid and cannot be recovered after the stress is removed (Schramm, 2005). Therefore, the applied stress can force the fluid to flow which can be considered to be viscous and the resistance of a fluid to flow is a measure of viscosity. The flow behavior of an ideal fluid and solid can be best described by the models of Newtonian fluids and perfectly elastic solids, respectively (Schramm, 1994).

(1) Rheological Behavior of Fluids

The flow behavior of an ideal fluid in one dimensional laminar flow is represented as Figure 5.1. The behavior can be described by the well known Newton's law of viscosity (Bird *et al.*, 2002), expressed as Equation (5.1).

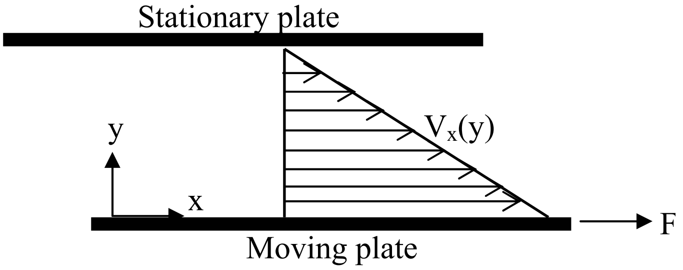

Figure 5.1 Flow behavior of an ideal fluid contained between two parallel plates (Bird *et al.*, 2002).

$$\tau = \mu \cdot \gamma \qquad (5.1)$$

where τ = shear stress defined as $\tau = \frac{F}{A}$ (Pa), F is shearing force (N) and A is the shear area parallel to the direction of applied force (m^2)

γ = shear rate or velocity gradient in y direction perpendicular to the flow (x-direction) defined as $\gamma = \frac{dV_x}{dy}$ (s^{-1})

μ = coefficient of viscosity (Pa·s)

It should be reminded that this rheological equation can describe only for laminar flow; a greater degree of fluid resistance and the mixing of moving layers occurring in turbulent flow cannot be applied. The fluid which gives shear stress proportionally to shear rate or exhibits a constant viscosity coefficient over the whole range of shearing is known as "*Newtonian fluids*", whereas the fluid whose flow behavior deviates from this criteria is called "*Non-Newtonian fluids*" (Anandha Rao, 1999). There are several different types of non-Newtonian fluids which lead to some interesting flow properties. The types of fluids can be classified from the flow behaviors which are observed from a plot of shear stress versus shear rate or viscosity versus shear rate. The typical flow curves and viscosity curves of various fluid types are shown in Figures 5.2 (a) and (b), respectively (Schramm, 2005). Viscosity of Non-Newtonian fluids is termed "*apparent viscosity* (μ_a)", defined as the ratio of shear stress and shear rate at the point of measurement on the rheogram (Dinger, 2002). The non-Newtonian fluid viscosity depends on shear rate, thus it is essential to specify the applied shear rate. Generally, the shear rates for industrial pumping and processing equipment in the range of 1 to 1000 s^{-1} are typically employed. Table 5.1 shows examples of approximate shear rates applied in various industrial processes (Schramm, 2005).

The description of different rheological behaviors of various fluids is summarized in Table 5.2 (Schramm, 2005). *Pseudoplastic* fluid or shear-thinning fluid is a non-Newtonian fluid that the shear stress-shear rate curve begins to be concave upward at the origin and the viscosity decreases with increasing shear rate (Figures 5.2 (a) and (b)). The pseudoplastic fluid may be thought of the fluid having characteristic of an interparticle or intermolecular network that can be broken down when the stress is applied. For *dilatant* fluid or shear-thickening fluid, the shear stress-shear rate plot begins to be concave downward at the origin and the viscosity increases with increasing shear rate (Figures 5.2 (a) and (b)). The dilatant fluid which has dense packing of particles in a very concentrated dispersion exhibits dilatancy of sample volume during shearing. At low shear rate, the particles can move past each other but at high shear rate, they wedge together such that the size of structural increases and the fluid cannot lubricate the increased void volume leading to the increase of viscosity. In case of some fluids, the flow cannot commence until a threshold value of stress is overcome and this exceeded stress is called the "yield stress". The fluid which can flow only when the applied stress exceeds the strength of the network and then behaves as Newtonian fluids is referred to as a *Bingham* plastic fluid. The fluids showing pseudoplastic and dilatant behaviors at stress exceeding the yield stress are entitled as pseudoplastic fluid with yield stress and dilatant fluid with yield stress, respectively. Moreover, the flow behaviors may depend on duration of shear (time dependent fluids). The fluid that exhibits time-dependent pseudoplastic behavior is called *thixotropic* fluid and the fluid that shows the opposite characteristic is called *antithixotropic* fluid or *rheopectic* fluid.

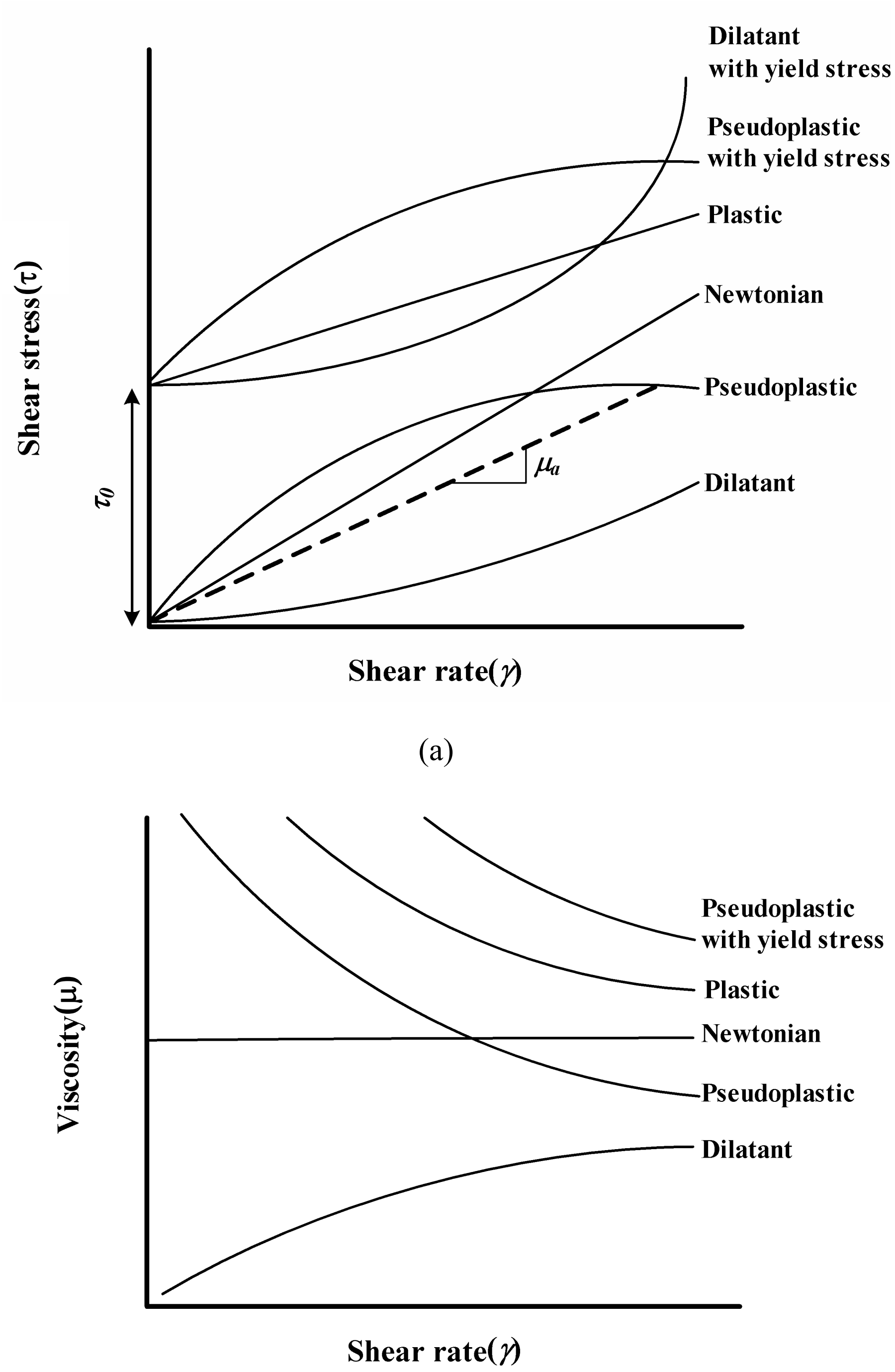

(a)

(b)

Figure 5.2 Typical flow curves (a) and viscosity curves (b) versus shear rate (Schramm, 2005).

Table 5.1 Some approximate values of shear rate appropriate to various processes (Schramm, 2005).

Process	**Approximate shear rate (s^{-1})**
Very slow stirring	0.01-0.1
Reservoir flow in oil recovery	1-5
Mixing	10-100
Pumping	100-1,000
Brushing, Coating	10,000
Spraying	100,000

(2) Rheological Models for Time-Independent Flow Behavior

A rheological flow model is a mathematical equation that can describe the rheological behavior of a particular fluid, for example, relationship of shear stress-shear rate, viscosity versus temperature data, effect of structure or composition on stress and viscosity, etc (Anandha Rao, 1999). The models do not only provide a convenient and concise manner of explaining the data but it can also quantify the effect of state variables (such as temperature, composition, solid concentration, etc) from the values of model parameters. A number of flow models have been proposed in terms of the relationship of shear stress and shear rate. The typical rheological models for describing the behavior of time-independent fluid are summarized in Table 5.3 (Anandha Rao, 1999). It is known that the simplest model applied for the Newtonian fluid is the Newtonian model, whereas power-law model with yield stress is the most commonly used model to describe non-Newtonian fluid behavior (Steffe, 1996).

Table 5.2 Rheological characteristics of various non-Newtonian fluids.

(Schramm, 2005).

Rheological classification	**Description**	**Examples**
Pseudoplastic (shear-thinning)	As shear rate increases, viscosity decreases	Paint, polymer solutions. In paint (a suspension of pigment particles in a liquid) irregular particles can align to match the induced flow, lowering the viscosity.
Dilatant (shear-thickening)	As shear rate increase, viscosity increases.	Wet beach sand, starch suspensions. PVC plastisols. In the "drying" of wet beach sand when walked on, a dense packing of particles can move past each other, whereas under high shear the particles wedge together such that the fluid can not fill the increased void volume
Pseudoplastic with yield stress	Pseudoplastic flow being only after a threshold shear stress, the yield stress, is exceeded.	Toothpaste, lipstick, grease, oil-well drilling mud. In oil-well drilling mud, the inter-particle network offers resistance to any positional changes. Flow only occurs when these forces are over-come.
Thixotropic	Time-dependent pseudoplastic flow. At constant applied shear rate, viscosity decreases. In a flow curve, hysteresis occurs.	Paint, quicksand. In bentonite clay "gels" which "liquefy" on shaking and "solidify" on standing to match the induced flow. After the shear rate is reduced it takes some time for the original alignment to be restored.
Rheopectic	Time-dependent dilatant flow. At constant applied shear rate, viscosity increase. In a flow curve, hysteresis occurs	Clay suspensions. A suspension which sets slowly on standing, but quickly when gently agitated due to time-dependent particle interference under flow.

Table 5.3 Some flow models for describing shear rate versus shear stress data (Anandha Rao, 1999).

$\tau - \tau_0 = \mu' \cdot \gamma$	Bingham model
$\tau = \kappa \cdot \gamma^n$	Power law model
$\tau - \tau_0 = \kappa \cdot \gamma^n$	Power law model with yield stress model
$\tau = \mu_\infty \cdot \gamma + \kappa \cdot \gamma^n$	Sisko model
$\tau^{n_1} = {\tau_0}^{n_1} + \kappa \cdot \gamma^{n_2}$	Generalized Herschel-Bulkley model
$\tau^{0.5} = {\tau_0}^{0.5} + \kappa \cdot \gamma^{0.5}$	Casson model
$\tau^{0.5} - \tau_0 = \kappa \cdot \gamma^n$	Mizrahi and Berk model, a modification of the Casson model
$\gamma = \kappa_1 \cdot \tau + \kappa_2 \cdot \tau^n$	Ellis model
$\mu = \mu_\infty + \dfrac{\mu_0 - \mu_\infty}{\left[1 + (\kappa \cdot \gamma)^2\right]^n}$	Carreau model
$\tau = \left[(\tau_0)^{\frac{1}{n}} + \kappa \cdot \gamma \right]^n$	Vocadlo model
$\gamma = \kappa_1 \cdot \tau + \kappa_2 \cdot \tau^3 + \kappa_3 \cdot \tau^5 + \ldots$ $\tau = \kappa_1 \cdot \gamma + \kappa_2 \cdot \gamma^3 + \kappa_3 \cdot \gamma^5 + \ldots$	Power series

Note: τ = shear stress

γ = shear rate

τ_o = yield stress

μ' = Bingham plastic viscosity

μ_0 = limiting viscosity at zero shear rate

μ_∞ = limiting viscosity at infinite shear rate

κ, κ_1, κ_2 and κ_3 = arbitrary constants

n, n_1 and n_2 = power law indices

The power law model with yield stress is also known as Herschel-Bulkley model. The model provides the relation between shear stress and shear rate, given by Equation (5.2), where τ is shear stress (Pa), τ_o is yield stress (Pa), κ is the consistency index and *n* is the flow index (Tanner, 2000).

$$\tau = \tau_o + \kappa \cdot \gamma^n \tag{5.2}$$

From Equation (5.2), the apparent viscosity (μ, Pa·s) can be calculated as in the following equation,

$$\mu = \frac{\tau}{\gamma} = \tau_o \gamma^{-1} + \kappa \gamma^{n-1} \tag{5.3}$$

This model has been widely used to describe various flow behaviors including Newtonian, Bigham plastic, pseudoplastic, dilatant, etc (Steffe, 1996). The limiting values of model parameters for different fluids are shown in Table 5.4 (Steffe, 1996).

Table 5.4 Limiting values of model parameters for different fluids (Steffe, 1996).

Fluid type	τ_o	κ	***n***
Newtonian fluid	0	>0	1
Bigham plastic fluid	>0	>0	1
Pseudoplastic fluid	0	>0	0<n<1
Pseudoplastic fluid with yield stress	>0	>0	0<n<1
Dilatant fluid	0	>0	0<n<∞
Dilatant fluid with yield stress	>0	>0	0<n<∞

5.3.3 Materials and Methods

5.3.3.1 Materials

The chars and bio-oils used in this study were obtained from slow pyrolysis of two biomasses, cassava pulp residue and palm shell. The biomass with an average particle size of 2.03 mm was heated from room temperature to the pyrolysis temperature of 700°C at heating rate of 20°C/min in a tubular fixed bed reactor under a constant flow of nitrogen at 200 cm^3/min.

Crude bio-oils collected from pyrolysis of the two biomasses showed distinctive differences in the physical appearances. Oil from cassava pulp residue gave a single transparent phase with dark red-brown color, while palm shell derived oil appeared as a dispersion of oil phase in aqueous solution phase. The two phases of palm shell oil were separated by centrifugation at the speed of 3000 rpm for 30 min. Finally, bio-oil samples were filtered by Whatman filter paper No.1 to remove the residual char and then stored in a refrigerator controlled at -20°C prior to rheological measurement. The solid char products left in the reactor were crushed and sieved to obtain particle size fraction of < 38 μm and kept in the desiccator. In addition, to study the effect of char particle size, char derived from cassava pulp residue was further classified by sieving to particle size fractions of < 75 μm, < 106 μm and 38-106 μm.

5.3.3.2 Material Characterization

(1) Bio-Oils

Four types of bio-oils to be used as suspending media for slurry preparation are crude oil from cassava pulp residue pyrolysis, crude oil from palm shell pyrolysis, separated aqueous solution and oil phase of palm shell crude bio-oil. They were analyzed for the following fuel properties: calorific value (ASTM D240-92), density (Gay-Lussac bottle), viscosity (ASTM D445-96), carbon residue (ASTM D524-97), ash content (ASTM D482-95) and pH (744 pH meter, Metrohm). Since the raw bio-oils of cassava pulp residue and palm shell contain large amount of water, their water contents were determined by refluxing the oil with toluene solution using the Dean-Stark method (ASTM D95-83).

(2) Solid Chars

Char products from pyrolysis of the two biomasses (cassava pulp residue and palm shell) were characterized for their physicochemical properties. The physical properties measured are bulk density, true density (He pycnometer, Accupyc 1330 Micromeritics), calorific value (ASTM D3286-96), particle size distribution (laser diffraction particle-size analyzer; Mastersizer S, Malvern), and porous properties (surface area analyzer; Micromeritics ASAP 2010). Proximate analysis (moisture content (ASTM D2867-95), volatile content (ASTM D5832-95), ash content (ASTM D2866-94) and fixed carbon content (by mass balance)), elemental analysis (CHNS/O analyzer, Perkin Elmer PE2400 series II), and pH of water extracted from char (ASTM D3838-80) were determined for the chemical properties. Size distributions of char particle are fitted with the following well-known Rosin-Rammler equation

$$P(x) = 1 - \exp\left[-(\frac{x}{k})^{m} \right] \tag{5.4}$$

where *P(x)* is the cumulative weight fraction less than a sieve size *x*, *k* is the size modulus and *m* is the distribution modulus. The average particle size of char was computed from size distribution data in terms of volume-surface mean diameter ($D_{3,2}$).

(3) Slurries

Basic fuel properties of the slurries including density, viscosity (ASTM D445-96), calorific value (ASTM D240-92), ash content (ASTM D482-95) and pH (744 pH Meter, Metrohm) were determined. Combustion behaviors of bio-oils, chars and char-bio-oil slurries were further investigated using a thermogravimetric analyzer (SDT 2960 simultaneous DSC-TGA model, TA instruments). 10-15 mg of the sample was heated from room temperature to 700°C at the heating rate of 5°C/min using air flow rate of 100 cm^3/min in order to follow the remaining weights as a function of increasing temperature.

5.3.3.3 Rheological Measurement

Rheological characteristics of the slurries were measured using a Haake VT550 concentric cylinder viscometer. Two sensors of NV and SV-I were used for low and high viscosity measurements, respectively. The cylindrical system of NV type has a cup-to-bob radius ratio of 1.02 mm and bob radius of 20.1 mm, while the radius ratio and bob radius of SV-I system are 1.14 and 10.1 mm, respectively.

The rheologies of the slurries prepared under different conditions (Table 5.5) were examined under steady-state shearing conditions. The measurements were performed in a laminar flow region covering shear rates from 0.712-690.2 s^{-1} (0.8-775.6 rpm). A critical bob (inner cylinder) speed for the onset of turbulent flow (N_{crit}) is inferred by employing the following equation (Tangsathitkulchai, C., 1987):

$$N_{crit} = \frac{6.6\mu_a}{\rho' R_b^{\,2}} \sqrt{\frac{S}{(S-1)^3}} \tag{5.5}$$

where μ_a is the apparent viscosity of slurry (Pa·s) at a given shear rate, S is the ratio of bob-to-cup radius, ρ' is the slurry density (kg/m^3) and R_b is the bob radius (m). In studying the time effect on shearing history, the stress responses as a function of time for cassava pulp residue char-raw oil slurries with 30 and 40 wt% of solid concentration and particle size < 38 µm were monitored at constant shear rates of 0.712, 344.7 and 690.2 s^{-1}.

Table 5.5 Conditions of slurries used for rheological measurements.

Parameters affecting rheology	**Fixed conditions**	**Varying conditions**
Slurry type	- 30 wt% solid concentration - Particle size <38 µm - Measuring temperature of 25°C	Cassava pulp residue char-raw oil, Palm shell char-aqueous solution, Palm shell char-oil, Cassava pulp residue char-water
Solid concentration	- Cassava pulp residue char-raw oil slurry or palm shell char-oil slurry - Particle size <38 µm - Measuring temperature of 25°C	- 10, 25, 30, 35 and 45 wt% for cassava pulp residue char-raw oil slurry - 30 and 40 wt% for palm shell char-oil slurry
Char particle size	- Cassava pulp residue char-raw oil slurry - 30 wt% solid concentration - Measuring temperature of 25°C	<38 µm, <75 µm, <106 µm and 38-106 µm.
Slurry temperature	- Cassava pulp residue char-raw oil slurry - 30 wt% solid concentration - Particle size <38 µm	15, 25 35 and 45°C.

5.3.4 Results and Discussions

5.3.4.1 Feedstock Properties

The fuel properties of suspending liquids used for slurry preparation are listed in Table 5.6. Among the test bio-oils, transparent bio-oil derived from cassava pulp residue gives the lowest density and viscosity of 1.09 g/cm^3 and 2.94 cSt at 25°C, respectively. For bio-oil from palm shell, the opaque dark oil phases having higher density (1.13 g/cm^3) gives much greater viscosity (23.39 cSt) than that of its aqueous phase (3.48 cSt) which also gives a lower density (1.10 g/cm^3). All bio-oils derived from biomass pyrolysis offer relatively low pH in the range 2.95-3.21, largely due to the presence of oxygenated compounds such as acids, phenols, etc (see Table 4.7 in Chapter IV). The crude bio-oils contain high content of water, 56.41 wt%, for cassava pulp residue oil and 48.78 wt% for palm shell crude oil. Calorific values of cassava pulp residue oil and aqueous phase of palm shell oil cannot be directly measured, whereas oil phase of palm shell oil gives moderate heating value of 25.55 MJ/kg. It is noted that the oil phase of bio-oil from palm shell provides the highest values of ramsbottom carbon residue (6.35 wt%) and ash content (0.089 wt%).

Physicochemical properties of the derived pyrolysis chars are presented in Table 5.7. Cassava pulp residue char and palm shell char give comparable true density values, while bulk density of palm shell char is significantly higher than that of cassava pulp residue char for the same particle size of < 38 μm. The pH values of extracting water derived from both chars are relatively high, 8.64 and 9.53 for palm shell and cassava pulp residue, respectively. From chemical composition analysis, cassava pulp residue char shows higher volatile and O/C. The char obtained from palm shell pyrolysis provides higher content of fixed carbon

(82.11 wt%) and H/C (0.402) and this may explain the higher calorific value of palm shell char (33.36 MJ/kg) than that of cassava pulp residue char (29.28 MJ/kg). For porous characteristics, palm shell char which has smaller average pore size gives much higher BET surface area and total pore volume as well as percentage of micropore volume compared to those of cassava pulp residue char. Figure 5.3 shows particle size distribution of the test chars. It was found that larger size fraction shows wider size distribution range. It is also noticed that palm shell char gives wider size distribution than that of char from cassava pulp residue with the same sieve size range (< 38 μm). Particle size distributions of all samples are well fitted with Rosin-Rammler size distribution function, with the average regression coefficient (R^2) being 0.9993 and the fitted parameters (*k* and *m*) are listed in Table 5.7.

Table 5.6 Properties of liquid carriers used for rheological study.

Properties	**Bio-oils**				**Water**
	Cassava pulp residue	**Palm shell**			
		Crude oil	**Oil phase**	**Aqueous phase**	
Density (g/cm^3) at 25°C	1.09	1.11	1.13	1.10	1.02
Viscosity (cSt) at 25°C	2.94	4.75	23.39	3.48	1.02
pH	2.95	2.98	3.21	2.95	6.88
Calorific value (MJ/kg)	*	*	25.55	*	*
Ramsbottom carbon residue (wt%)	2.57	2.93	6.35	2.88	-
Ash content (wt%)	0.081	0.071	0.089	0.063	-
Water content (wt%)	56.41	48.78	**	**	**

Note: * = Not measurable

** = Not analyzed

Table 5.7 Properties of solid chars produced from slow pyrolysis of two biomasses.

Properties	**Char products**				
	Cassava pulp residue				**Palm shell**
True density (g/cm^3)	1.754				1.689
Particle size (μm)	< 38	< 75	< 106	38-106	< 38
Bulk density (g/cm^3)	0.588	0.556	0.535	0.442	0.801
Volume-surface mean diameter, D$_{3,2}$ (μm)	8.19	11.10	12.50	13.00	2.39
Size modulus, *k	19	27	29	32	21
Distribution modulus, *m	1.26	1.22	1.26	1.29	0.9486
pH of water extracted from char	9.53				8.64
Calorific value (MJ/kg)	29.28				33.36
Proximate analysis (wt%) (Dry basis)					
Volatile	29.23				12.66
Fixed carbon	56.36				82.11
Ash	14.41				5.23
Elemental analysis (wt%)					
C	55.28				79.31
H	1.66				2.66
O	42.47				17.99
N	0.57				-
S	0.02				0.04
H/C	0.360				0.402
O/C	0.576				0.170
Porous characteristics					
BET surface area (m^2/g)	34				367
Micropore area (m^2/g)	26.9				322.8
Average pore size (nm)	2.58				2.14
Micropore volume (cm^3/g)	0.013				0.155
Total pore volume (cm^3/g)	0.022				0.178
%Micropore volume	59.09				87.08

Note: * = Parameter of Rosin-Rammler size distribution equation

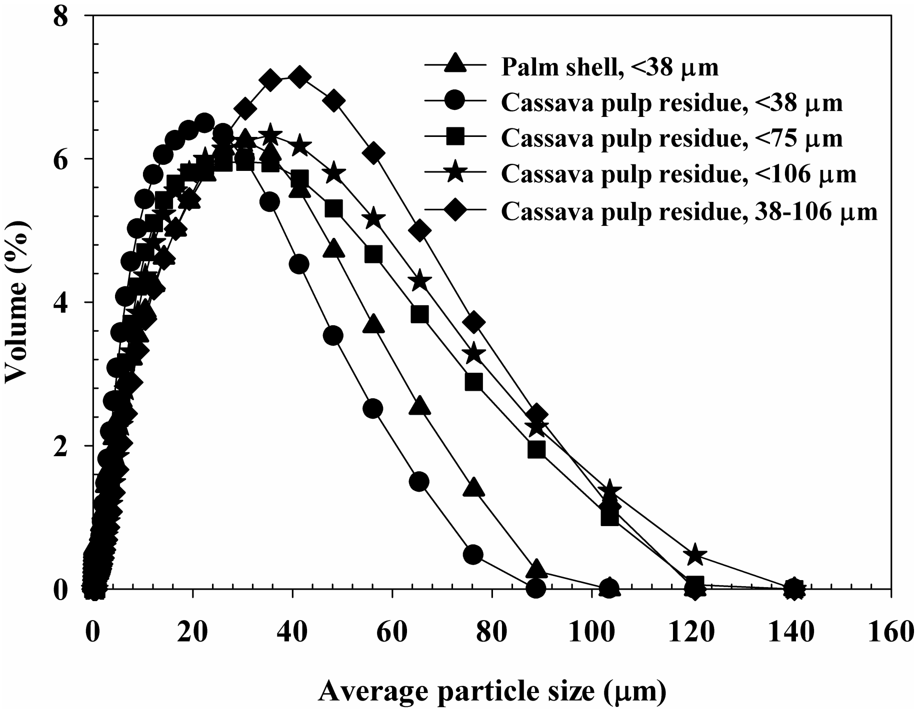

Figure 5.3 Particle size distributions of test chars for slurry preparation.

5.3.4.2 Time Effect during Shearing

Figure 5.4 shows typical variation of shear stress as a function of shearing time for char-bio-oil slurries of cassava pulp residue at two solid concentrations and various shear rates. The results indicate that at low solid concentration of 30 wt% and shear rates smaller than 345 s^{-1}, the shear stress remains substantially constant independent of shearing time. At higher shear rate of 690 s^{-1}, however, a slight decrease in the shear stress is observed for the first five minutes of shearing time before attaining a constant value at longer times. At higher solid concentration of 40 wt% where particles are getting closer, the drop in the shear stress occurs at a lower shear rate of 345 s^{-1} compared to the case of 30 wt% slurry and the time required to achieve a steady shear stress is longer as the shear rate is increased (30 and 50 min for shear rates of 345 and 690 s^{-1}, respectively). The observed variation of shear stress with time is believed to result from the breakdown and realignment of some agglomerates in the suspension due to cohesion of very fine particles (Schramm, 2005). High shearing rate on a slurry with high solid concentration requires longer time for the restructuring of solid particles in the direction of flow. It should be noted that all reported shear stress for rheological study in this work are the final steady values. No attempt was made to study the time-dependence behavior of these slurries.

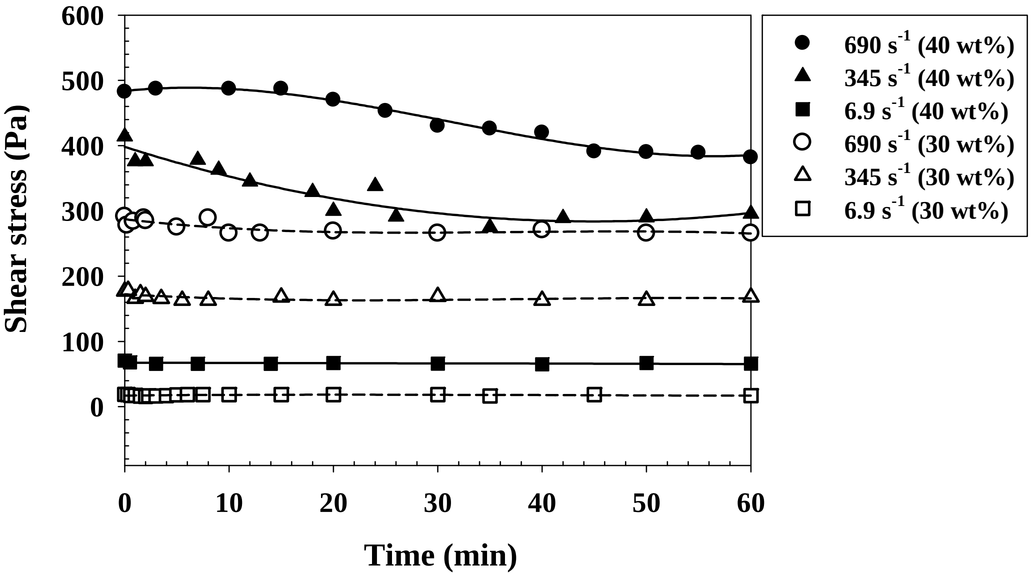

Figure 5.4 Effect of shearing time on shear stress at various shear rates for cassava pulp residue char-raw oil slurry, 30 wt% and 40 wt% solid concentration, char particle size of <38 μm and testing temperature of 25°C.

5.3.4.3 Rheological Characteristics and Modeling

The rheology of slurries of char and bio-oil under various testing conditions was studied in the laminar region. It was found that the relation between stress and shear rate of all slurries can be best described by a power law model with yield stress, as given by Equation (5.2). The typical rheological behavior of char-bio-oil slurry fitted by power law model with yield stress is shown in Figure 5.5. It indicates that the power law model with yield stress can describe well the experimental data of shear stress and viscosity. For this set of data, the slurry exhibits pseudoplastic characteristic, i.e., the stress increases and viscosity decreases continuously with increasing shear rate.

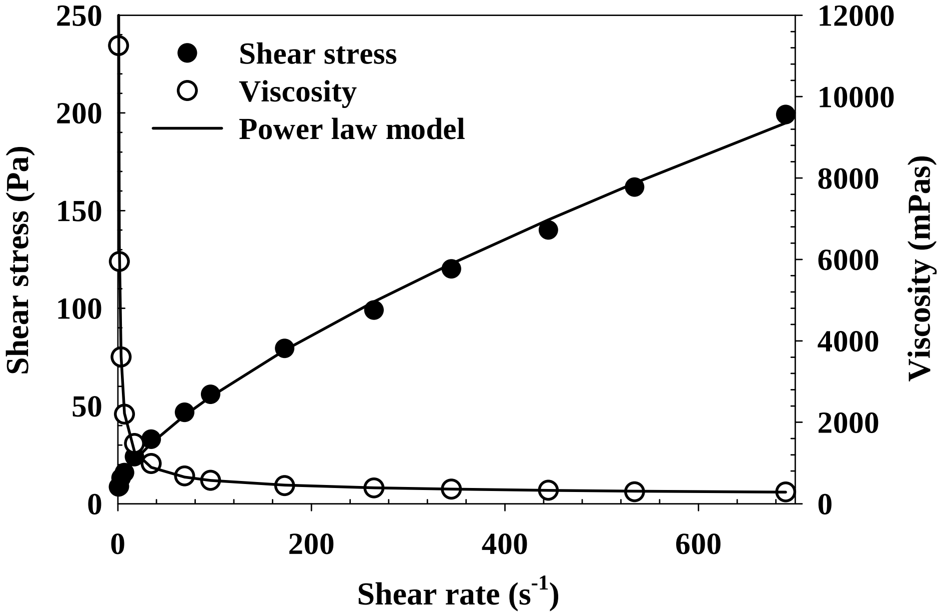

Figure 5.5 Typical flow behaviors of char-bio-oil slurry fitted by power law model with yield stress (cassava pulp residue char-raw oil slurry with 30 wt% solid, char particle size <38 μm and testing temperature of 25°C).

.

(1) Effect of Slurry Type

Preliminary rheological study of char-raw bio-oils slurries indicated that the char-oil slurry from cassava pulp residue formed a stable homogeneous slurry from which its rheology can be readily measured, while the slurry prepared from original two-phase palm shell oil and its char gave fluctuation of shear stress during shearing. In this work, four different slurry systems prepared by a combination of different chars and suspending media were employed for studying the nature of slurry type on the rheological behavior, using conditions of 30 wt% solid concentration, particle size <38 μm and at 25°C. Results shown in Figures 5.6 (a) and (b) indicate that the four types of slurries displayed non-Newtonian pseudoplastic behavior with different degrees of pseudoplasticity and the rheological parameters are listed in Table 5.8. Cassava pulp residue char-water slurry exhibited the rheological behavior resembling to Newtonian flow with flow index (*n*) of 0.91 and a low yield stress, while the rest of char-bio-oil slurries gave the value of *n* varying in the range 0.43-0.63. It is further observed from Figure 5.6 (b) that the apparent viscosity of char-water slurry was much lower than those of the other types of slurries. If the solid and suspending medium are both inert, the apparent viscosity of a slurry should be proportional to the medium viscosity. That is, the relative viscosity of slurry defined as the ratio of slurry viscosity (μ_s) and medium viscosity (μ_L) must remain substantially constant. However, as Figure 5.7 shows, large differences of relative viscosities of the test slurries still discernible. This result appears to indicate that, in comparison with water, several different chemical components in bio-oil should be responsible for the much higher viscosity of char-bio-oil slurries as compared to that of char-water slurry. This hypothesis is supported in part by the work of Shin and

Shen (2007) which indicated that slurries prepared from coal and organic solvents such as cyclohexanone and alcohols gave higher viscosities compared to coal-water slurry under the same measurement conditions. Although, using bio-oil as a suspending medium gave higher stress and viscosity than using water it has, however, certain advantage of providing better slurry stability. On standing, the char-water slurry which appeared as a less viscous suspension gave complete sedimentation within 5 hrs, while the char-bio-oil slurries offered longer time for complete sedimentation (>72 hrs for 30 wt% solid slurry).

Considering cassava residue char-raw oil slurry and palm shell char-aqueous solution slurry, both slurries showed similar flow curves but gave different values of rheological model parameters (Figures 5.6 (a) and (b) and Table 5.8). Cassava residue char-raw oil slurry gave much greater yield stress (τ_o) and higher flow index (*n*) than those of palm shell char-aqueous solution slurry (Table 5.8). The slightly higher values of shear stress and relative viscosity of cassava residue char-raw oil slurry (Figures 5.6 (a) and (b)) could arise from its higher affinity between bio-oil and char surface than that of palm shell char-aqueous solution slurry. Since cassava residue char has significantly higher O/C ratio than that of palm shell char (0.576 vs 0.170) which indicates that it has more polar functional groups on the surface that can form stronger attractive force between char particle surface and the surrounding polar liquid compared to the case of palm shell char slurry (Gu *et al.*, 2008).

As shown in Figure 5.6, palm shell char-oil slurry showed a difference of flow characteristics compared to other slurries. It displayed pseudoplastic behavior at shear rates less than 445 s^{-1} but changed to dilatant flow behavior at higher shear rates. The main reason could be attributed to much higher viscosity of palm shell oil than that of other suspending liquid media, thus giving much denser slurry that leads to dilatant behavior at high shear rates. In addition, it should be noted that palm shell char-oil slurry showed a much lower shear stress than that of palm shell char-aqueous solution slurry. Again, this could be hypothesized that the affinity of palm shell char and aqueous solution could be higher than that of palm shell char and oil and this is reflected by the increased resistance to flow.

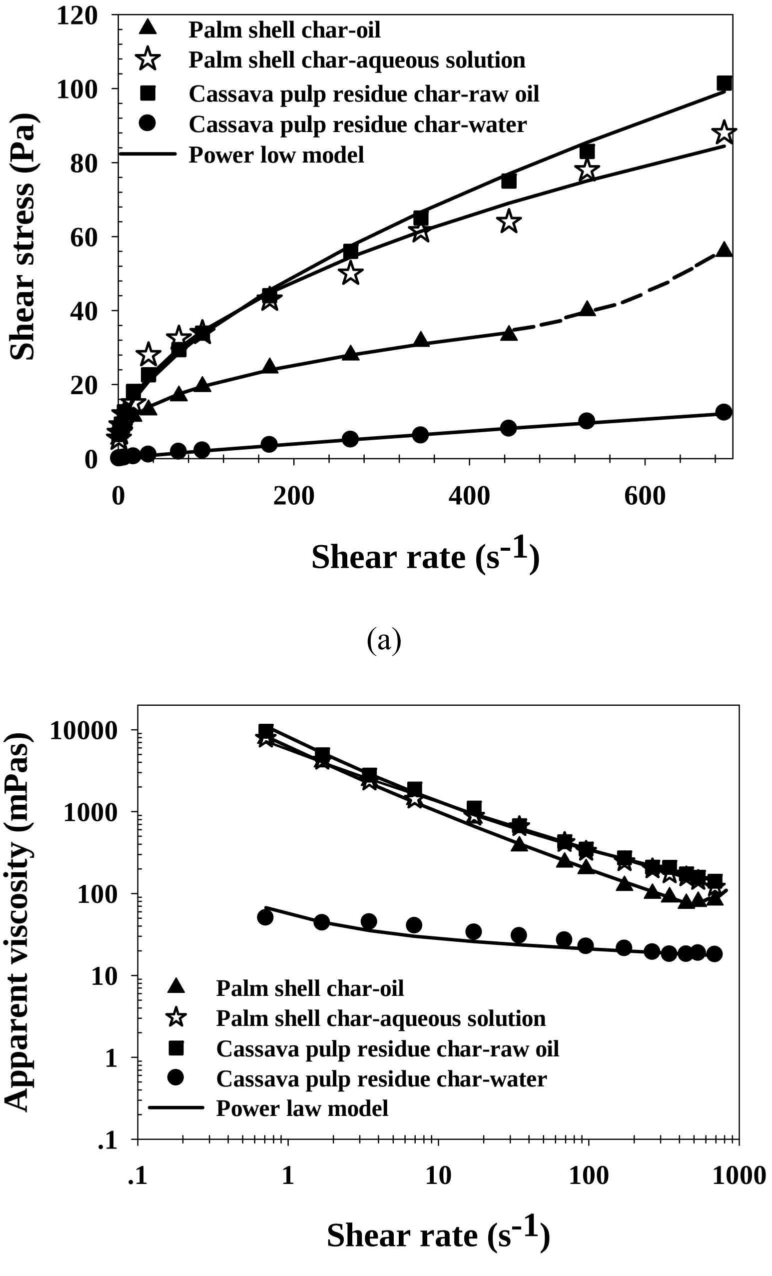

Figure 5.6 Effect of slurry types on (a) shear stress and (b) viscosity at testing temperature of 25°C with char particle size <38 μm and solid concentration of 30 wt%.

Table 5.8 Rheological model parameters

Conditions	**Rheological parameters**			**Regression coefficient (R^2)**
	τ_0 (Pa)	**κ**	**n**	
Slurry type (at 25°C, particle size <38 µm and 30 wt% solid)				
Cassava pulp residue char-water	0.025	0.032	0.910	0.9984
Cassava pulp residue char-raw oil	6.61	1.56	0.625	0.9967
Palm shell char-aqueous solution	1.92	3.78	0.472	0.9990
Palm shell char-oil	4.06*	2.14*	0.432*	0.9967
Solid concentration (wt%) (cassava pulp residue char-raw oil slurry at 25°C and particle size <38 µm)				
10	0.233	0.028	0.837	0.9989
25	2.88	0.15	0.740	0.9949
30	6.61	1.56	0.625	0.9967
35	8.01	1.90	0.702	0.9981
40	40.0	7.27	0.593	0.9968
Solid concentration (wt%) (palm shell-oil slurry at 25°C and particle size <38 µm)				
30	4.06*	2.14*	0.432*	0.9625
40	9.03	0.0004	2.39	0.9992
Particle size (µm) (cassava pulp residue char-raw oil slurry at 25°C and 30 wt% solid)				
< 38 µm ($D_{3,2}$, 8.19 µm)	6.61	1.56	0.625	0.9967
< 75 µm ($D_{3,2}$, 11.1 µm)	4.88	1.42	0.690	0.9994
< 106 µm ($D_{3,2}$, 12.5 µm)	4.83	1.20	0.747	0.9984
38-106 µm ($D_{3,2}$, 13.0 µm)	6.95	2.24	0.751	0.9997
Temperature (°C) (cassava pulp residue char-raw oil slurry particle size <38 µm and 30 wt% solid)				
15	7.97	1.36	0.668	0.9967
25	6.61	1.56	0.625	0.9967
35	5.15	1.24	0.614	0.9986
45	2.39	1.68	0.576	0.9979

Note: * = Rheological parameters derived from fitting data in the range of 0-445 s^{-1}.

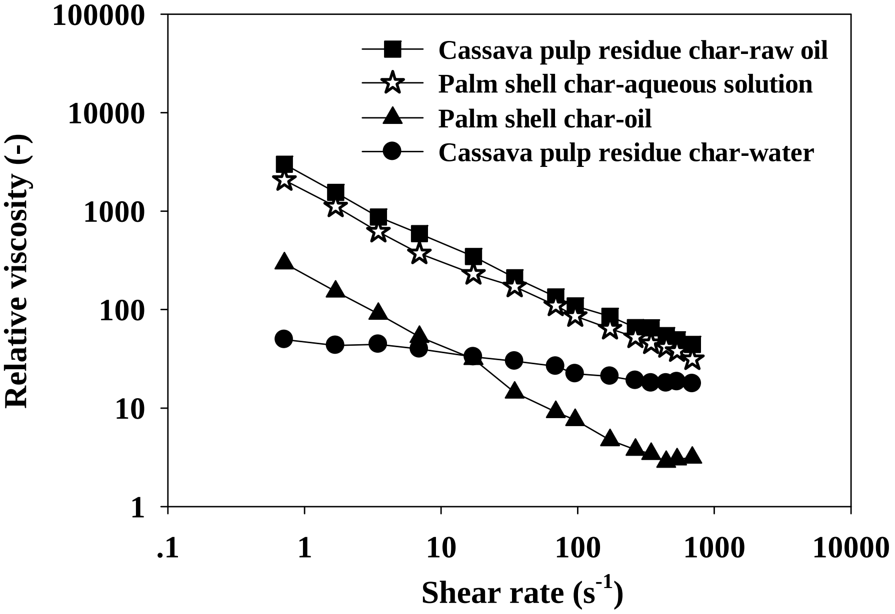

Figure 5.7 Relative viscosity ($\frac{\mu_S}{\mu_L}$) versus shear rate of different slurry types

(μ_S : viscosity of slurry and μ_L : viscosity of liquid suspending media).

(2) Effect of Solid Concentration

Obviously, the highest energy content of a slurry is determined by the maximum solid loading that still permits the slurry flow. In this work, the effect of solid concentration, in the range of 10 to 40 wt% for cassava pulp residue char-raw oil slurries and 30 and 40 wt% for palm shell char-oil slurries with char particle size of <38 μm and at testing temperature of 25°C, on the rheological behavior were investigated. For cassava pulp residue char-raw oil slurry, all slurries showed pseudoplastic characteristic with continued increasing of yield stress (τ_0) and decreasing of flow index (n) as the slurry concentration was increased (Figure 5.8 and Table 5.8). The flow curves indicate almost Newtonian behavior for slurries at low solid concentrations of 10 and 25 wt%. However, at concentrations higher than 25 wt% solid the pseudoplastic behavior became more pronounced. Figure 5.9 further shows the variation of these parameters with solid concentration in the slurry. It illustrates that there are a marked increase of yield stress and consistency index from 35 to 40 wt% solid. This indicates the dense packing of cassava pulp residue char in the vicinity of 40 wt% or 29.29 vol% solid concentration and this is reflected by a very high viscosity of the slurry (> 1000 mPas at 100 s^{-1}). Thus, it should be noted that the maximum solid concentration of cassava pulp residue char-raw oil slurry to be used as a slurry fuel should be around 40 wt% solid loading. Obviously, the selection of a suitable solid concentration should be based on a balance between an increase in energy content and an increase in the flow resistance of slurry which means the increased pumping cost for slurry transport.

In the case of palm shell char-oil slurry, Figure 5.10 (a) shows that different solid concentration of 30 and 40 wt% gave different characteristics of flow curves. The slurry of 40 wt% solid showed the dilatant behavior over the range of measuring shear rate and can be well fitted by power law model giving flow index (n) of 2.39. However, this model can describe the flow behavior of 30 wt% solid slurry only up to the shear rates of 445 s^{-1}, giving the flow index (n) of 0.432. Closer examination of slurry viscosity as a function of shear rate as shown in Figure 5.10 (b) reveals that the 40wt% slurry showed pseudoplasticity at shear rates less than about 50 s^{-1} and dilatancy at higher shear rates. This behavior was also true for the 30 wt% slurry but the shear rate at which pseudoplasticity changed to dilatant behavior occurred at a larger value of shear rate of 400 s^{-1}. This indicates that the use of palm shell char-oil slurry as fuel may create problems of pump and injector blockages and poor atomization in burners when operating at a very high shear rate. To solve this problem, some additives may be necessary to affect the rheology characteristics or lower the viscosity of slurry (Cui *et al.*, 2008).

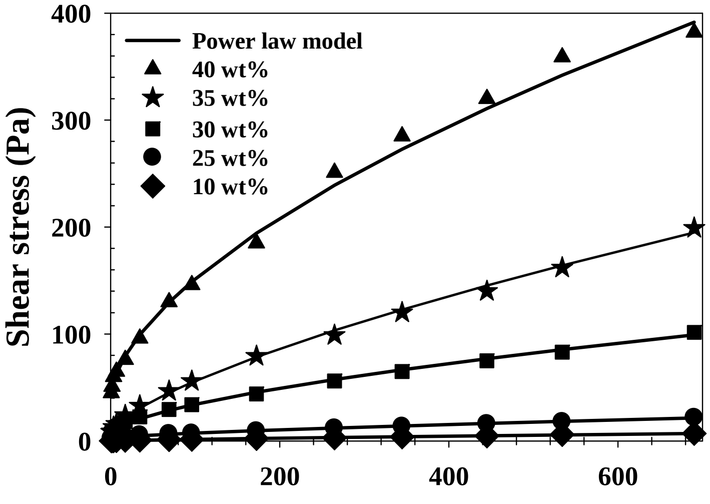

(a)

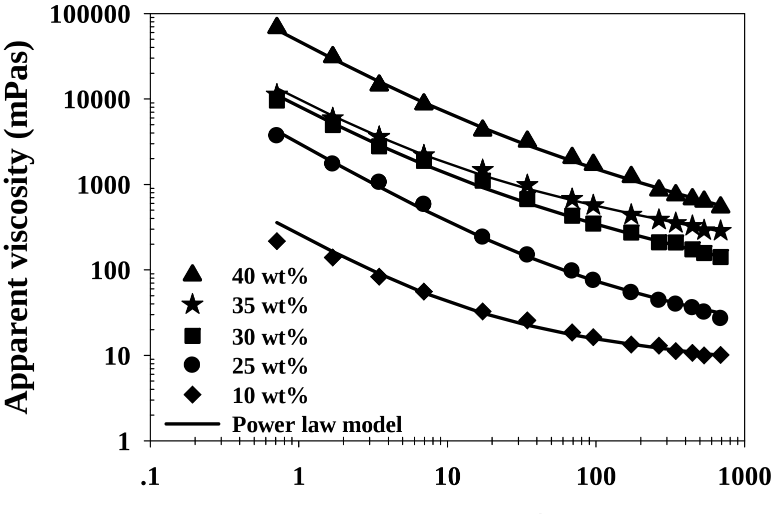

(b)

Figure 5.8 Effect of solid concentration on (a) shear stress and (b) viscosity of cassava pulp residue char-raw oil slurry with char particle size <38 μm at testing temperature of 25°C.

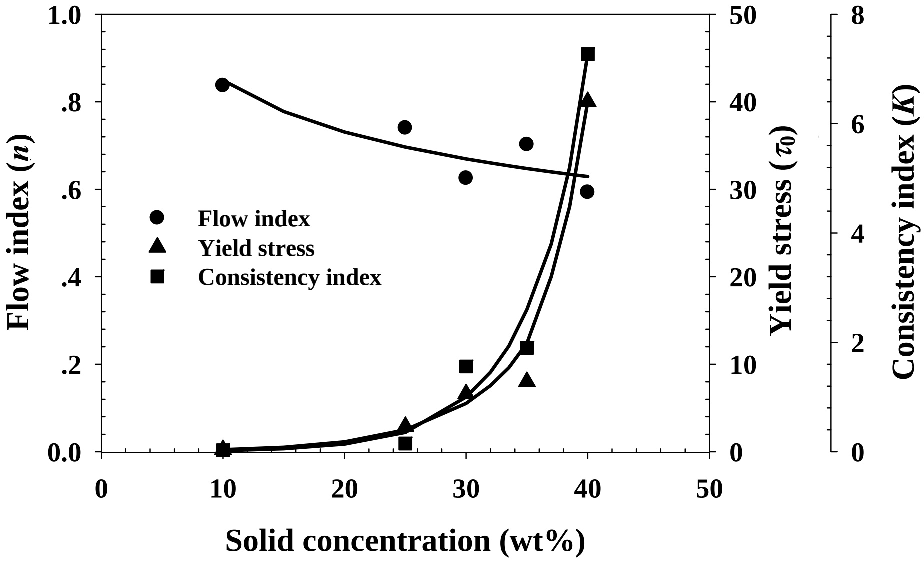

Figure 5.9 Rheological parameters of power law model versus solid concentration of cassava pulp residue char-raw oil slurry with char particle size <38 μm at testing temperature of 25°C.

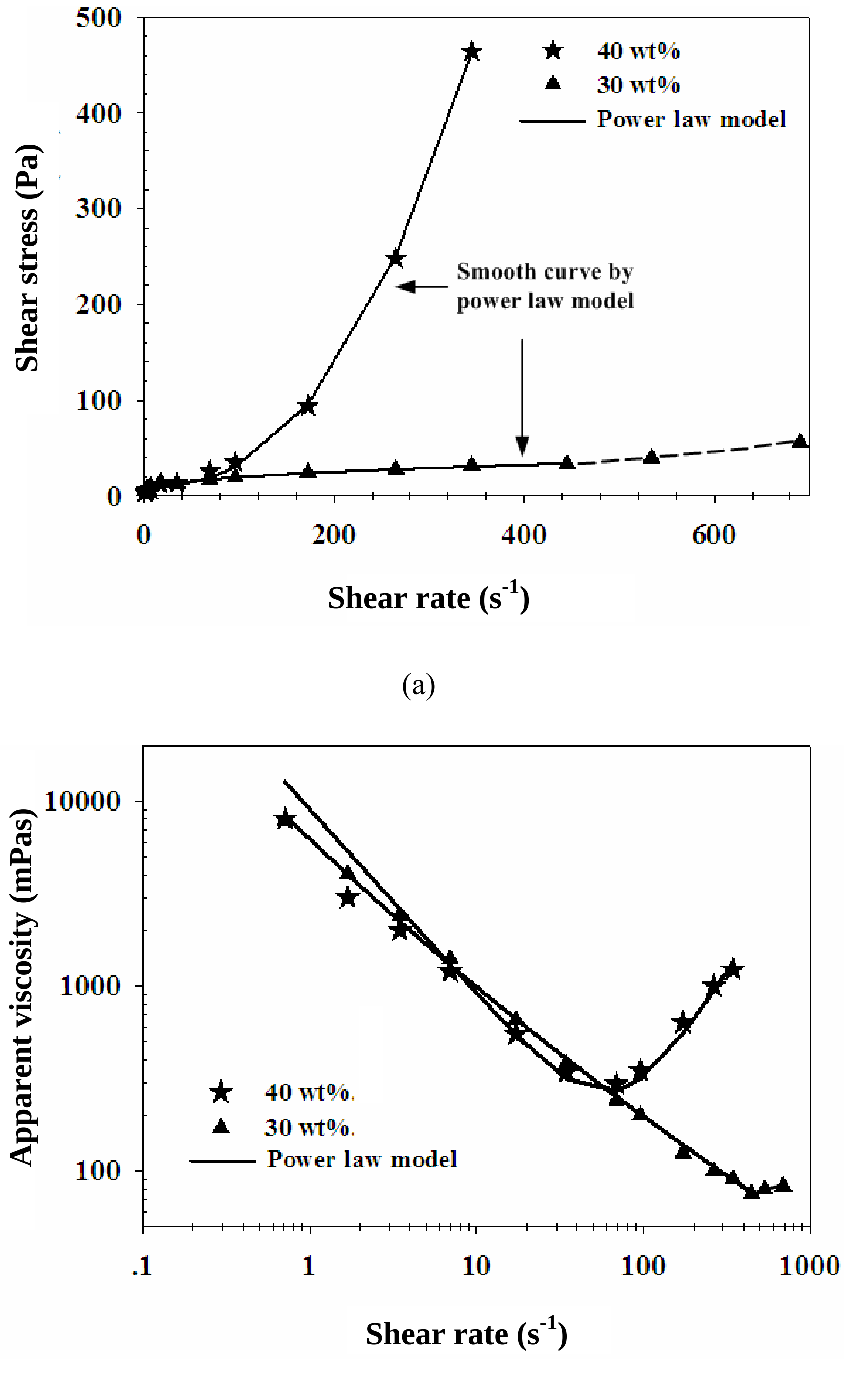

(a)

(b)

Figure 5.10 Effect of solid concentration on (a) shear stress and (b) viscosity of palm shell char-oil slurry with char particle size <38 µm at testing temperature of 25°C.

(3) Effect of Char Particle Size

In this study, cassava pulp residue char-raw oil slurries with four particle size ranges of < 38 μm, <75 μm, <106 μm and 38-106 μm (mean sizes of 8.19, 11.1, 12.5 and 13.0 μm, respectively) at 30 wt% solid and testing temperature of 25°C were used to study the effect of particle size on the slurry rheology. Figures 5.11 (a) and (b) shows that the four particle sieve sizes gave slurries with pseudoplastic characteristic and at a given shear rate the shear stress and viscosity increased with increasing in the mean particle size of char. On the rheological parameters as shown in Table 5.8, it indicates that the wider natural size fraction gave lower values of yield stress (τ_o) and consistency index (κ) and the rheological behavior was getting closer to Newtonian behavior (larger flow index (n)). However, it should be noted that the size fraction of 38-106 μm gave the highest values of these parameters as well as the highest shear stress and viscosity over the range of studied shear rates. These results may be related to the way particles with narrower size distribution could give poorer particle packing with less volume of interstitial liquid, thus giving increased slurry viscosity (Dinger, 2002).

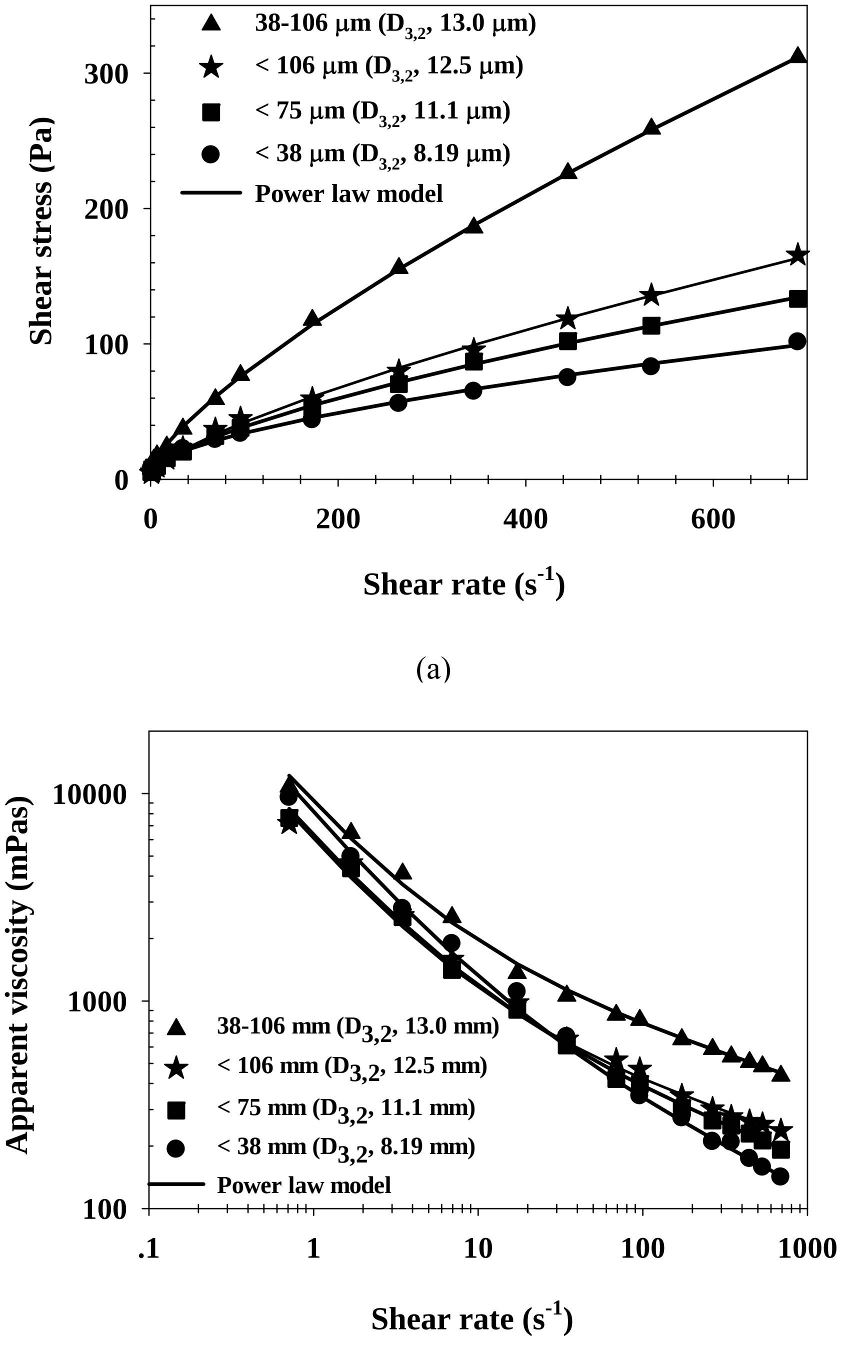

(a)

(b)

Figure 5.11 Effect of char particle size on (a) shear stress and (b) viscosity of cassava pulp residue char-raw oil slurry with solid concentration of 30 wt% at testing temperature of 25°C.

(4) Effect of Temperature

The effect of temperature in the range of 15-45°C on the rheological characteristics of slurries were studied using cassava pulp residue char-raw oil slurry at 30 wt% solid concentration and with char particle size of <38 µm. As Figure 5.12 (a) and Table 5.8 show, the slurry exhibited pseudoplastic characteristic with increasing degree of non-Newtonian behavior and lowering of yield stress as the temperature was increased. This should result mainly from the reduction of liquid medium viscosity. Therefore, it should be advantageous to operate a slurry at a higher temperature to impart more pseudoplastic character, giving decreased viscosity particularly at a high shear rate (Figure 5.12 (b)). However, only a slight decrease of viscosity was observed when the temperature was increased from 35 to 45°C (Figure 5.12 (b)). As well, the higher temperature gave the reduction of shear stress but increasing temperature from 35 to 45°C had almost no effect on the shear stress. It is likely that some bio-oil may have evaporated during the measurement giving more viscous slurry at the high testing temperature of 45°C. This reasoning was checked by running the measurement at 50°C and it was found that the stress increased markedly with the depletion of slurry volume as time progressed. Therefore, it should be noted that the appropriate temperature for operating this slurry should not exceed 45°C.

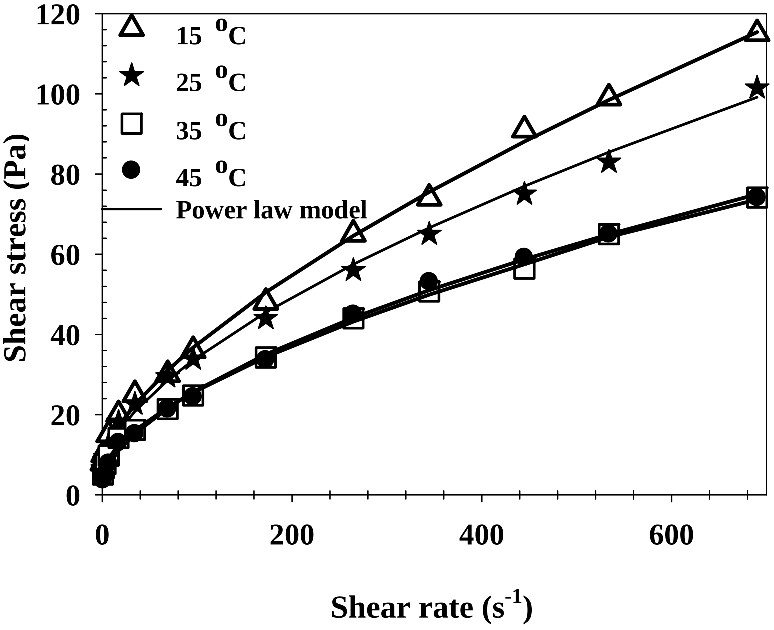

(a)

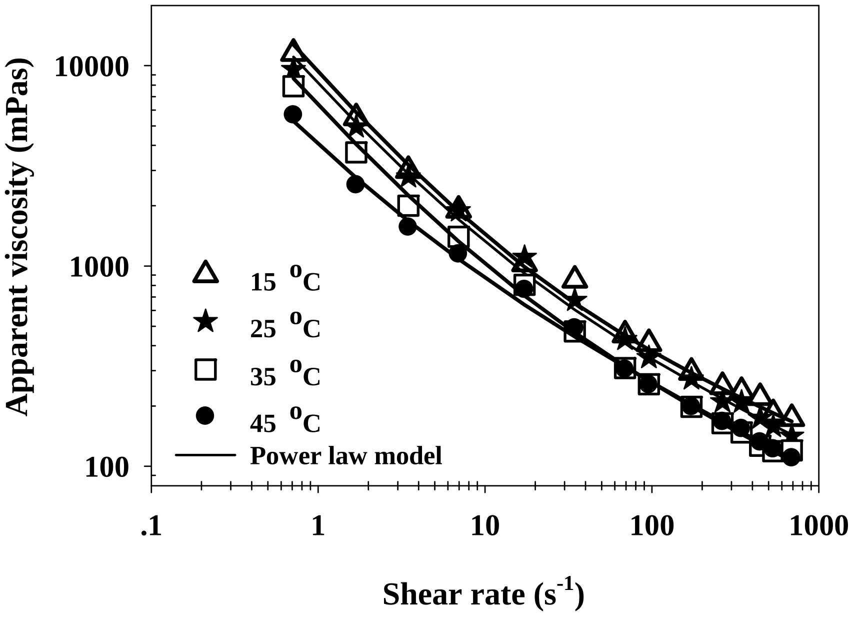

(b)

Figure 5.12 Effect of temperature on (a) shear stress and (b) viscosity of cassava pulp residue char-raw oil slurry with char particle size <38 μm and solid concentration of 30 wt%.

5.3.4.4 Fuel Properties of Slurries

Fuel properties of four types of slurries prepared from cassava pulp residue char and palm shell char using different suspending media are presented in Table 5.9. Fuel properties of all slurries and pH values were found to increase over those of liquid bio-oils. However, when increasing the density of slurries from 30 to 40 wt% solid, two to four fold increase in slurry viscosity were observed but only about 5-12% increases of heating value were achieved for palm shell char-oil slurry and cassava pulp residue char-raw oil slurry. It should be also noted that the heating value of cassava residue char-raw oil slurry was measurable only when solid concentration in the slurry was at least 30 wt% or greater. However, at the same slurry concentration of 30 wt% solid, it was not possible to measure the heating value of char-water slurry. At 30 wt% solid, palm shell char-oil slurry could be an attractive fuel because of its relatively higher calorific value and lower viscosity compared to that of cassava pulp residue-raw oil slurry and palm shell char-aqueous solution slurry. However, care must be taken in using palm shell char-oil slurry when operating at high shear rates due to its dilatant characteristic at shear rates higher than 445 s^{-1}.

Combustion characteristics of bio-oils and chars are shown in Figures 5.13 (a) and (b), respectively. Figure 5.13 (a) shows that approximately 80 wt% of the raw bio-oil from cassava pulp residue was devolatilized at temperatures lower than 120°C followed by a slow devolatilization at higher temperature. At temperatures lower than 120°C only 40 wt% of palm shell oil (oil phase fraction) was devolatilized and showed an exothermic decomposition at higher temperature range of 400-540°C. This implies that cassava pulp residue oil contains mainly water and light oxygenated compounds, while palm shell oil has light oxygenated compounds and heavy molecular weight compounds of hydrocarbons which can generate heat from bio-oil combustion. For char combustion (Figure 5.13 (b)), palm shell char provided wider temperature range of combustion than that of cassava pulp residue char; 320-500°C for palm shell char and 320-460°C for cassava pulp residue char. Moreover, maximum value of temperature difference of palm shell char was higher and was obtained at higher temperature (at 440°C) than that of cassava pulp residue char (at 400°C) (Figure 5.13 (b)). The higher maximum value of temperature difference of palm shell char than that of cassava pulp residue char may result from higher calorific value of palm shell char compared to cassava pulp residue char. The combustion behaviors of the two slurries are shown in Figure 5.14. Cassava pulp residue char-raw oil slurry presented two regions of decomposition including endothermic decomposition at 25-120°C and exothermic decomposition at 280-450°C, corresponding to the combustion of bio-oil and char, respectively. On the other hand, temperature difference derived from combustion of palm shell char-oil slurry showed a characteristic of two combined peaks derived from combustion of bio-oil and char varying in the range of 320-560°C. As a result, it may be mentioned that the two slurries exhibited a better combustion characteristic compared with that of coal-water slurry which shows a longer burnout time (Miller and Schobert, 1993).

Table 5.9 Some fuel properties of various prepared slurries.

Slurry types	Fuel properties				
	Density at 25°C (g/cm^3)	Viscosity at 25°C, 100 s^{-1} shear	Calorific value (MJ/kg)	Ash (wt%)	pH
Cassava pulp residue char-raw oil at different solid concentrations (char particle size <38 µm)					
0 wt%	1.09	2.94	-	0.081	2.95
10 wt%	1.15	15.5	-	2.55	2.95
25 wt%	1.20	74.1	-	5.58	3.04
30 wt%	1.26	344	18.19	6.64	3.86
35 wt%	1.37	562	18.88	8.21	4.05
40 wt%	1.52	1,520	20.32	9.22	4.27
Palm shell char-oil at different solid concentrations (char particle size <38 µm)					
0 wt%	1.13	23.39	25.55	0.089	3.21
30 wt%	1.30	179	31.68	4.15	3.98
40 wt%	1.61	327	33.17	4.53	4.12
Palm shell char-aqueous solution (30 wt% of solid, char particle size <38 µm)	1.29	351	17.95	3.85	3.54
Cassava pulp residue char-water (30 wt% of solid, char particle size <38 µm)	1.16	21.4	-	5.61	10.69

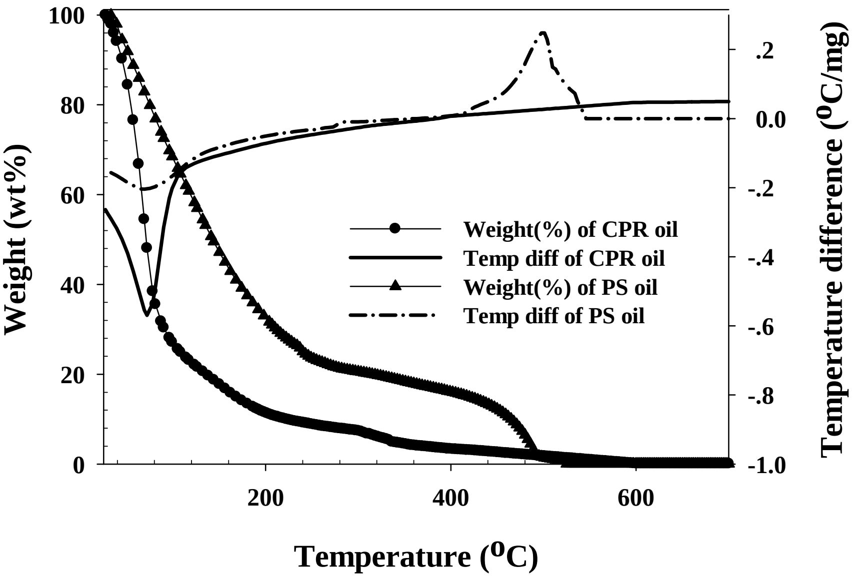

(a)

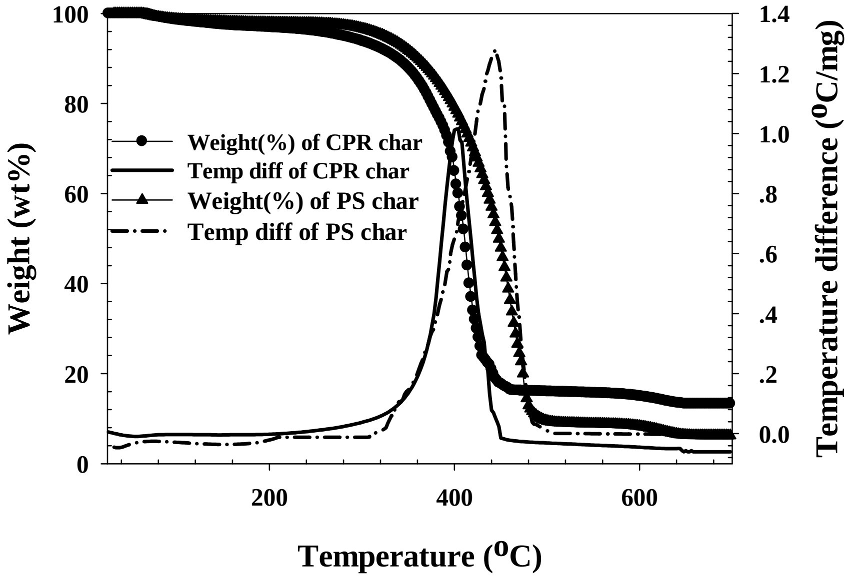

(b)

Figure 5.13 Residual weight and temperature differences during combustion of (a) bio-oils and (b) chars (CPR: cassava pulp residue PS: palm shell).

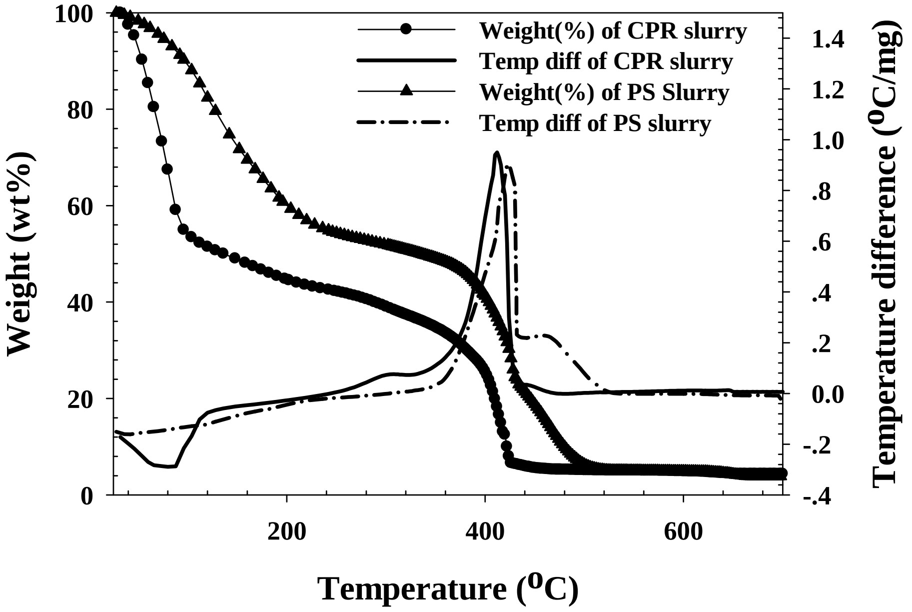

Figure 5.14 Residual weight and temperature differences during combustion of slurries at 30 wt% solid with char particle size of <38 μm (CPR: cassava pulp residue PS: palm shell).

5.4 Phase Behaviors and Fuel Properties of Bio-Oil-Diesel-Alcohol Blends

5.4.1 Introduction

Previous studies on bio-oil upgrading and the utilization of bio-oil in various combustion engines have been reviewed in Chapter II. It appears that the simplest route to solve the undesirable properties associated with the use of bio-oil in internal combustion engines is by blending bio-oil with diesel fuel (Zhang *et al.*, 2007). Since, bio-oil contains large amount of polar chemicals such as acids, phenols, ethers, ketones, aldehydes and ester, it is normally immiscible in non-polar phase of diesel. Thus, to obtain a stable homogeneous phase of bio-oil-diesel blend, a proper additive is obviously required.

In this study, alcohol was proposed as a potential additive to induce a single homogeneous solution of bio-oil and diesel. Detailed study of this three component system for use as a combustion fuel is relatively scarce. Thus, it is tempting to investigate the phase behavior and the basic fuel properties of this fuel blends in the present work. Dewatered palm kernel bio-oil was selected as a representative oil for this study because it showed the most promising properties. It gave the highest heating value of ~40 MJ/kg, lowest acidity (pH ~5.6) and the closest boiling range distribution to that of diesel. In the present study, two types of absolute alcohol namely ethanol and n-butanol were used to investigate the effect of additive type on the phase behavior. These alcohols were used as they can be readily produced from renewable sources through the fermentation of sugar and starch. The important fuel properties of the blended fuels covering both the binary and ternary systems (palm kernel bio-oil-alcohol and palm kernel bio-oil-diesel-alcohol) were also investigated. In addition, empirical correlations for estimating some physical properties of fuel blends were also proposed.

5.4.2 Literature Reviews

5.4.2.1 Previous Studies

The blending of diesel fuel with bio-oil in the form of an emulsion with the purpose to eliminate some undesirable properties of the bio-oil has been the subject of a certain number of investigations (Chiaramonti *et al.*, 2003a; 2003b; Ikura *et al.*, 2003). It was reported that up to 10 wt% of bio-oil in diesel in form of emulsion could give a reasonable cetane number of ~43 (Ikura *et al.*, 2003). Further, a 50% reduction of NO_x emission from combusting a mix of 30 wt% fast-pyrolysis oil was observed as compared to the burning of pure diesel (Bertoli *et al.*, 2000). The influence of such parameters as bio-oil concentration, type and concentration of surfactant, mixing time and speed, and emulsification temperature on the emulsion stability has been also investigated (Ikura *et al.*, 2003). It was discovered that the least stratification amounting to 0.2 vol% of separated phase was achievable under the following conditions: 30 wt% bio-oil blended with diesel, 1.5 wt% surfactant of Hypermer B246SF diluted in methanol with ratio of 5:2, 20 min of mixing time and at mixing speed of 1750 rpm. The most influential parameter on the emulsion stability is the type of surfactant which should be properly selected to suit individual emulsion, based on the bio-oil compositions and content of bio-oil in diesel (Chiaramonti *et al.*, 2003a). CANMET, a non-ionic surfactant of DETA EO/PO copolymers, is known as the most effective additive to stabilize bio-oil in diesel emulsion (Chiaramonti *et al.*, 2003a; Ikura *et al.*, 2003). It could provide the more stable homogenous phase of emulsion mixture of bio-oils derived from various types of wood pyrolysis among other surfactants. Nevertheless, bio-oils produced from different types of biomass and/or different process conditions have different characteristics and this complicates the selection of a suitable additive for a specific bio-oil-diesel emulsion. In this regard, a simpler approach such as the use of a cosolvent to create a more stable phase of the bio-oil-diesel mixture would be an interesting alternative.

Alcohol has been considered as an important renewable fuel. When mixed with diesel, alcohol is known to mitigate some drawbacks of diesel fuel such as reducing black smoke and emissions of CO and NO_x (Karabektas and Hosoz, 2009). Alcohol content of up to 20% in diesel can be used in IC engines without modification (Karabektas and Hosoz, 2009). However, alcohol type played a significant role on combustion characteristics of the engines. It was found that methanol and ethanol offered longer ignition delay period of combustion due to their higher latent heat of vaporization compared to that of diesel. In addition, isobutanol having similar latent heat of vaporization and with added advantages of full miscibility in diesel and higher calorific value provides greater combustion characteristic in diesel engines (Karabektas and Hosoz, 2009). Mixing alcohol with bio-oil has been reported to improve the undesirable characteristics of bio-oil involving low heating value, high viscosity and acidity (Nguyen and Honnery, 2008; Stamatov *et al.*, 2006). Also, it was noticed that solvent addition can prevent the bio-oil from ageing effects (Diebold, 2000; Nguyen and Honnery, 2008). On combustion tests, bio-oil blended with ethanol gave shorter, wider and brighter flame but poorer atomization than those of diesel fuel when they were performed in a circular jet spray at atmosphere pressure (Stamatov *et al.*, 2006).

From these previous works, it is interesting to explore the possibility of using bio-oil-diesel-alcohol blend as an alternative fuel. Thus, in the present work attempt was made to study the phase stability of binary and ternary mixtures as well as the measurement of fuel properties of these blended fuels.

5.4.2.2 Type of Liquid Mixture and Ternary Liquid System

Ordinarily, bio-oil derived from the pyrolysis process cannot dissolve in diesel fuel. As previously mentioned, two methods can be used to produce a stable bio-oil/diesel mixture, that is, the use of surfactant to obtain a microemulsion and the addition of alcohol which acts as a cosolvent to form a single-phase solution. Both types of liquid mixtures are homogeneously stable but have different characteristics. Emulsion is a mixture of two or more immiscible liquids in which one is dispersed in the other. The emulsion that has the dispersed drops being between 5 and 200 nm in size shows a characteristic of light scattering and gives a cloudy appearance (Gammon, 2002; Levine, 2001). On the other hand, solution is a mixture of two or more substances that are completely homogenized at a molecular or atomic level. Light can usually pass through the solution, thus it shows no effect of light scattering. However, sometime a solution and a microemulsion can have similar appearance, for example, the microemulsion which has small dispersed drop sizes typically about 10-100 nm will show only little light scattering (Schramm, 2005).

To better understand the phase stability of bio-oil-diesel-alcohol blends, ternary liquid-liquid equilibrium should be studied. Usually, the ternary liquid-liquid equilibrium can be represented on a triangular diagram. For example, typical types of different ternary systems are displayed in Figure 5.15. Type I is the system which has only one partially miscible binary pair, that is the pair of components '2' and '3', whereas the other pairs show complete miscibility. Type II refers to the system having two partially miscible binary pairs that are the pairs of components '1' and '3' and components '2' and '3', while full solubility is acquired from the components of '1' and '2'. The regions of single phase and two phases are divided by solubility curve (the thick solid line) and compositions of the two separated liquid phases which are in equilibrium are connected by a tie lie. Usually, this kind of information is derived from equilibrating a mixture at the desired temperature and withdrawing the sample of each phase for composition analysis, ignoring the sample in the vapor phase (Kyle, 1999).

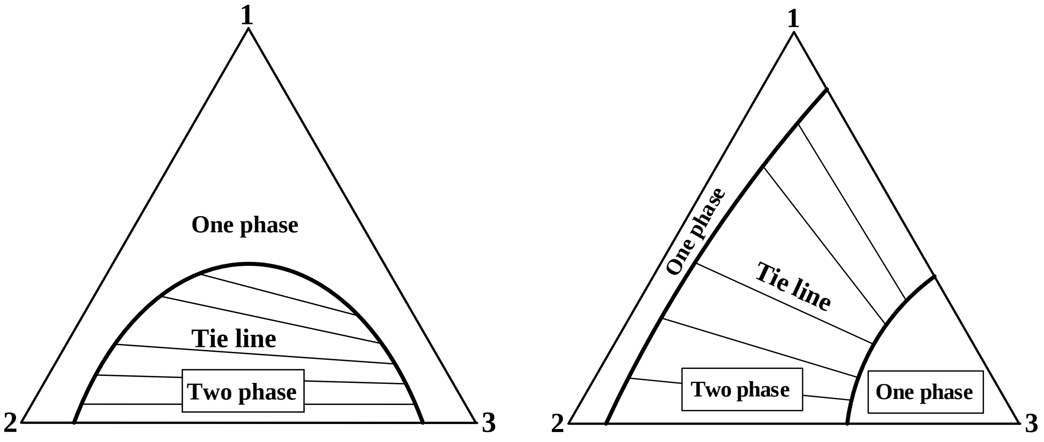

(a) (b)

Figure 5.15 Typical phase diagram of ternary liquid systems (a) Type I and (b) Type II (Kyle, 1999).

5.4.2.3 Estimation of Fuel Properties of Liquid Mixtures

Kay's mixing rule has been used as a simple approach for predicting the physical properties of liquid mixtures in hydrocarbon industries and it is capable of describing the fuel properties of biodiesel-diesel blends such as density, heating value, and cloud point (Benjumea *et al.*, 2008). The Kay's mixing rule is given as

$$\varphi_B = \sum_i^n x_i \varphi_i \tag{5.6}$$

where φ_B is a property of the blend, φ_i is the corresponding property of pure component *i* and x_i is its mole fraction.

For the viscosity of a liquid mixture, it can be estimated from various methods (Dominguez *et al.*, 2000; Poling *et al.*, 2001). However, the Grunberg-Nissan equation is most commonly used for liquids below or slightly above their normal boiling points (Poling *et al.*, 2001). The liquid viscosity for the mixture is estimated from the following equation,

$$\ln \mu_B = \sum_i^n x_i \ln \mu_i + \sum_i^n \sum_j^n x_i x_j G_{ij} \tag{5.7}$$

where μ_B is the dynamic viscosity of mixture (mPa·s), μ_i is the dynamic viscosity of pure *i* component (mPa·s), x_i is the mole fraction of component *i* and G_{ij} is the interaction parameter, $G_{ij}=0$ for $i=j$. G_{ij} can be estimated from the group contribution method which was proposed by Isdale (Poling *et al.*, 2001) as follows

$$G_{ij} = \sum \Delta_i - \sum \Delta_j + W \tag{5.8}$$

where $\sum \Delta_i$ and $\sum \Delta_j$ are derived from group contribution as listed in Table 5.10 and W is defined as shown in Equation (5.9) or it is set as zero if either i or j contains atoms other than carbon and hydrogen:

$$W = \frac{0.361(N_i - N_j)^2}{N_i + N_j} - 0.1188(N_i - N_j) \tag{5.9}$$

where N_i is the number of carbon atoms for component i and N_j is the number of carbon atoms for component j.

The selection of i component (first component) is decided by the priority rule as follows: (1) an alcohol, (2) an acid, (3) the component with the most carbon atoms, (4) the component with the most hydrogen atoms, (5) the component with the most-CH_3 groups, and if none of this rule is met, then G_{ij}=0. In addition, it should be noted that G_{ij} of some chemical compositions can be a function of temperature.

To predict liquid viscosity of a pure liquid (η, mm^2/s) as a function of temperature (T), it is often a good approximation to assume ln(η) to be a linear function of reciprocal of absolute temperature. This has been proposed by de Guzman (Benjumea *et al.*, 2008) and shown as Equation (5.10). To improve model accuracy, Equation (5.10) was extended to a three-parameter viscosity model known as Andrade equation (Benjumea *et al.*, 2008), represented by Equation (5.11).

$$\ln \eta = A + \frac{B}{T} \tag{5.10}$$

$$\ln \eta = A + \frac{B}{T} + \frac{C}{T^2} \tag{5.11}$$

Table 5.10 Group contributions for G_{ij} at 25°C (Poling *et al.*, 2001).

Group	**Notes**	**Value of Δ_i**
$-CH_3$		-0.100
$>CH_2$		0.096
>CH-		0.204
>C<		0.433
Benzene ring with substitution by		0.766
• Ortho		0.174
• Meta		-
• Para		0.154
Cyclohexane ring		0.887
-OH	• Methanol	0.887
	• Ethanol	-0.023
	• Higher aliphatic alcohols	-0.443
>C=O	• Ketones	1.046
-Cl		$0.653-0.161 \cdot N_{Cl}$
-Br		-0.116
-COOH	Acid with:	
	• Non-associated liquids	$-0.411+0.06074\, N_C$
	• Ketones	1.130
	• Formic acid with ketones	0.167

Note: N = number of atom

5.4.3 Materials and Methods

5.4.3.1 Characterization of Raw Materials

Palm kernel bio-oil was obtained from the slow pyrolysis of palm kernel cake in a tubular fixed bed reactor at 700°C with a heating rate of 20°C/min and N_2 flow rate of 200°C/min. The derived bio-oil showed two separated phases of organic aqueous phase and oil phase. The upper aqueous phase was removed by decanting and the oil phase was kept for further study. Commercial diesel fuel (Delta-X Euro III) was purchased from Petroleum Authority of Thailand Public Company Limited (PTT) and analytical grade of ethanol (99.8%) and n-butanol (98.0%) used were acquired from Carlo Erba, Co., Ltd and Sigma-Aldrich Co. Ltd, respectively

5.4.3.2 Phase Behaviors of Ternary Mixtures

Ternary phase behaviors were investigated by blending three components of bio-oil, diesel and alcohols (ethanol or butanol) at room temperature. Mutual solubilities of two component systems consisting of bio-oil-diesel, bio-oil-alcohol, diesel-alcohol were preliminarily examined. For the three component systems, the phase behavior studies were performed by blending various volume fractions of bio-oil and diesel with successive increasing amount of an alcohol until a homogeneous mixture was visually observed. Phase stabilities of the homogeneous mixed samples were further ascertained by centrifuging at the speed of 3000 rpm for 20 min and the homogeneity of the mixtures was again decided by visual observation. In the case of an opaque dark sample, a laser beam was allowed to pass through the sample to assist in this observation process. The blend compositions that gave a homogeneous phase characteristic after centrifugation were plotted on a solubility phase diagram.

5.4.3.3 Fuel Properties

Palm kernel bio-oil, diesel, alcohols and blended fuels were characterized for their basic fuel properties including boiling range distribution (ASTM D86-96), calorific value (ASTM D240-92), flash point (ASTM D93-97), pour point (ASTM D97-96a), density (Gay-Lussac bottle), viscosity (ASTM D445-96), carbon residue (ASTM D524-97), ash content (ASTM D482-95) and acidity (744 pH meter, Metrohm).

5.4.4 Results and Discussions

5.4.4.1 Phase Behaviors of Palm Kernel Bio-oil-Diesel-Alcohol Systems

Generally, a palm kernel bio-oil-diesel blend did not give a homogeneous phase at any blend composition. It was noted that diesel oil could temporarily dissolve in a continuous phase of bio-oil at concentrations less than 10 vol% but lasting for about an hour before the phase separation finally took place. Afterwards, it was observed that the color of diesel phase was changed from transparent yellow to dark red brown indicating the dissolution of some chemical components of bio-oil into the diesel phase. Moreover, darker color of diesel was observed with increasing proportion of bio-oil in the mixture.

On solubility of bio-oil in alcohols, it was observed that bio-oil can mix with ethanol and butanol at all proportions. The complete phase dissolution should result from polar characteristic of palm kernel bio-oil containing high amount of polar molecules, including 14.2 wt% of alcohols and phenols, 14.8 wt% of fatty acids, 7.2 wt% of ketones and aldehydes and 14.9 wt% esters (see Table 4.7). For alcohols-diesel system, it was found that ethanol showed partial miscibility in diesel, with either less than 10 vol% or greater than 88 vol% of diesel offering single phase solutions. However, due to longer chain of aliphatic hydrocarbon in butanol, a complete solubility of butanol-diesel mixture was observed at all concentrations.

Figure 5.16 shows phase behaviors of palm kernel bio-oil-diesel-alcohol system for two types of alcohol. It indicates that solubility characteristics of the two ternary systems are somewhat different. The soluble area of bio-oil-diesel-butanol system is much greater than that of bio-oil-diesel-ethanol system. This means that larger amount of ethanol is required to ensure a single phase system for the same amounts of bio-oil and diesel. Using butanol as a cosolvent gave better miscibility at high content of diesel (~70 vol%), while the single stable phase of bio-oil-diesel-ethanol mixture could be achieved only at diesel content of less than 12.8 vol%. In addition, requirement of larger amount of butanol at high bio-oil content than at high diesel content indicates that butanol is better miscible in diesel than in bio-oil. Therefore, it may be addressed that alcohol type is a determining factor on the phase behavior of a ternary system. It should be expected that if longer chains of aliphatic alcohol is employed to stabilize a ternary system, higher amount of alcohol is required for a fuel mixture containing high composition of bio-oil than with high content of diesel. However, it should be observed that complete construction of solubility phase diagram for the two ternary systems cannot be achievable because of limitation of determining phase stability by visual observation for the case of opaque dark sample containing high proportions of palm kernel bio-oil. Also, at high diesel content the minimum amount of alcohol to induce a homogenous phase cannot be determined either in this study.

To reduce the amount of alcohol required, the miscibility of the fuel blend was assisted by mild heating at 60°C for 5 hr. A composition of the mixtures which is close to the true solubility line (40 vol% bio-oil, 10 vol% diesel and 50 vol% ethanol or butanol) was selected for this purpose. However, it was found that it was not able to maintain a stable phase of the system by this thermal treatment.

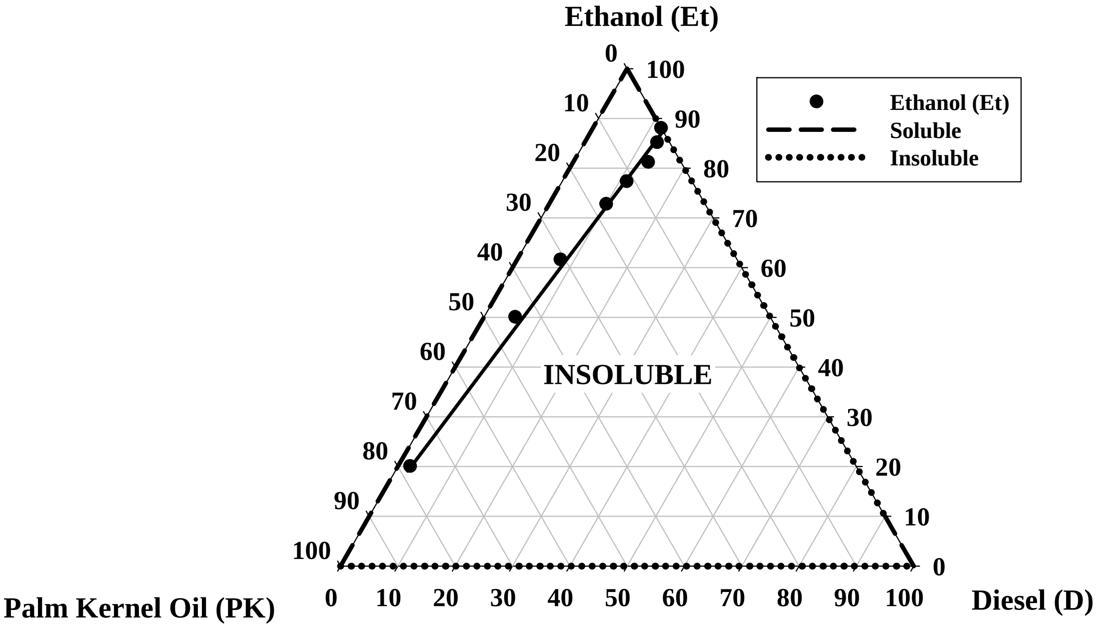

(a)

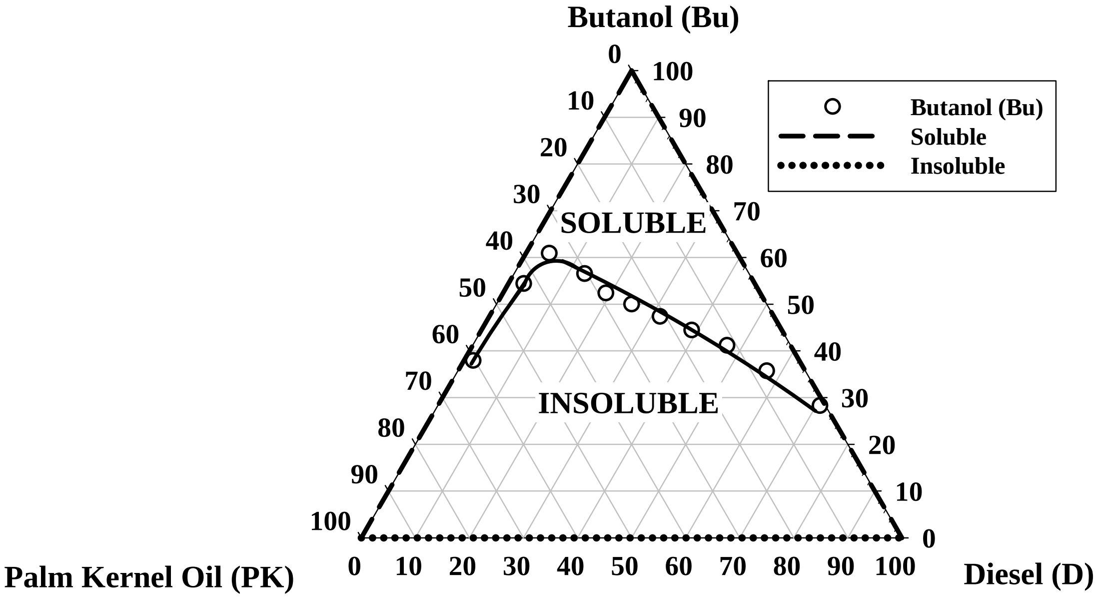

(b)

Figure 5.16 Phase behaviors of three component system; (a) palm kernel bio-oil-diesel-ethanol and (b) palm kernel bio-oil-diesel-butanol.

5.4.4.2 Fuel Properties of fuel Blends

Although palm kernel bio-oil possesses the properties of high calorific value (39.5 MJ/kg) and low acidity (pH ~5.9) among other bio-oils (see Table 4.3), it still has certain drawbacks such as high values of viscosity (58.7 mm^2/s), carbon residue (6.3 wt%.) and ash content (0.063 wt%.) and these characteristics may cause an adverse effect on the atomization quality, fuel droplet size and penetration in the combustion engines (Nguyen *et al.*, 2008; Stamatov *et al.*, 2006). To study the possibility of using the upgraded bio-oils derived by blending with diesel and alcohol as alternative fuels, their basic fuel properties were thus investigated. The blends of bio-oil-ethanol, bio-oil-butanol and four compositions of bio-oil-diesel-alcohol fuels (as shown in Figure 5.17) were selected for this purpose.

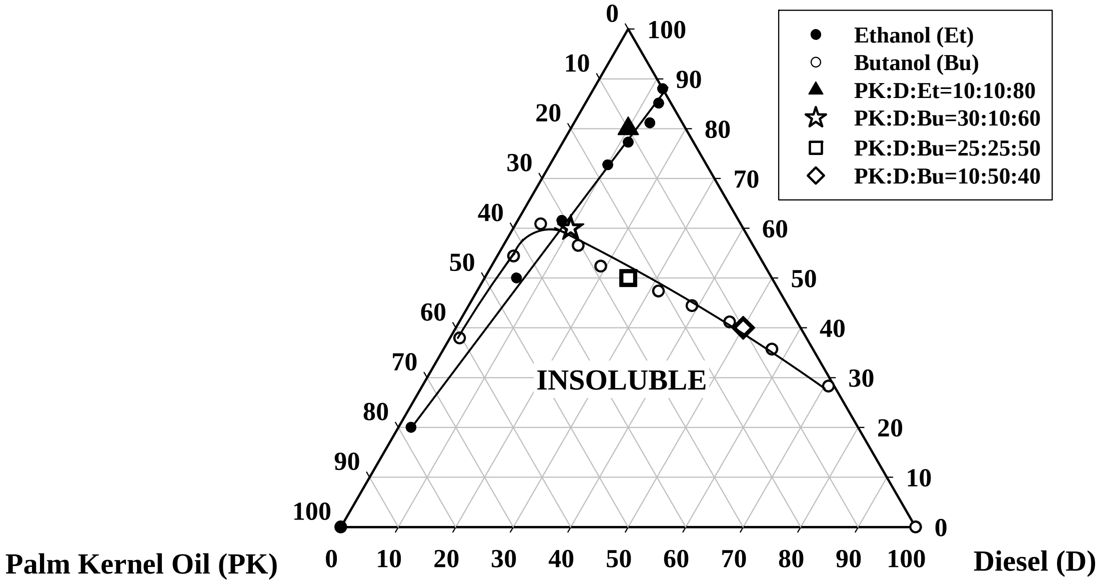

Figure 5.17 Comparison of phase behaviors derived from the mixtures of palm kernel bio-oil-diesel-ethanol and palm kernel bio-oil-diesel-butanol.

Fuel properties of the four primary fuels and various types of mixed fuels are summarized in Table 5.11. Blending of bio-oil (50 wt%) with ethanol or butanol (50 wt%) provided the advantageous properties of lowering the amounts of ash and carbon residue, reducing values of viscosity and pour point and giving slight increasing of pH. However, their heating value and flash point were lower compared to those of virgin bio-oil. For the effect of alcohol type on the fuel properties, both ethanol and butanol gave similar fuel properties for the binary system. However, blending of bio-oil with ethanol gave superior properties of lowering of viscosity and pour point. The viscosity of 50 vol% ethanol blended with bio-oil (~4.3 mm^2/s at 40°C) is comparable to that of commercial diesel fuel, whereas viscosity of butanol and bio-oil blend is higher with the value of about 9.2 mm^2/s. The flash point of blended fuel of bio-oil and ethanol is relatively low (21°C), thus increasing the likelihood of self ignition during storage. On the other hand, the blend of bio-oil-butanol offers better properties of flash point and heating value for the similar compositions. Therefore, using the blended fuels of bio-oil-alcohol gives a benefit to cold flow operability but the safety during storage should be of concern.

For ternary system of bio-oil-diesel-alcohol, alcohol composition had a significant influence on their heating values. Because of the requirement for high alcohol content to keep the phase stable, the heating value of bio-oil-diesel-ethanol at the ratio of 10:10:80 by vol% was therefore closer to that of ethanol. Using butanol as a cosolvent gave relatively high calorific value in the range of 37.2-41.2 MJ/kg at the butanol contents of 40-60 vol%. In addition, alcohol type had direct effect on flash point and pour point in the ternary blended fuels. The various compositions of blends using butanol as a cosolvent gave relatively fixed values of flash point and pour point at 40 °C and -7°C, respectively, whereas those properties were 19°C and less than -25°C when using ethanol at 80 vol% concentration. Increasing content of bio-oil affected directly the amounts of carbon residue, viscosity and ash content in the blended fuels. The viscosities of these blended fuels are comparable to that of diesel fuel, whereas the ash content and the amount of carbon residue are slightly higher than those of diesel. However, a slight effect of fuel composition on the acidity and density was noted; pH is in the range of 6.2-6.5 and density is around 0.86 g/cm^3 at 25°C.

Table 5.11 Fuel properties of blending fuels (palm kernel bio-oil (PK), diesel (D), ethanol (Et) and butanol (Bu)).

Chemical	**Calorific value (MJ/kg)**	**Density at 25°C (g/cm^3)**	**Viscosity at 40°C (mm^2/s)**	**pH**	**Ramsbottom carbon residue (wt%)**	**Ash (wt%)**	**Flash point (°C)**	**Pour point (°C)**
Palm kernel oil (PK)	39.5	1.120	58.7	5.87	6.32	0.063	82	1
Diesel (D)	44.5	0.844	3.69	-	0.060	0.018	78	-10
Ethanol (Et)	28.7	0.793	1.22	6.58	0.021	-	14*	-114.0**
Butanol (Bu)	33.4	0.810	2.43	6.70	0.027	-	34	-89.0**
PK:Et=50:50	35.2	0.960	4.31	6.11	4.66	0.034	21	-19
PK:Bu=50:50	37.1	0.946	9.21	6.18	4.20	0.039	42	-7
D:Et=10:90	30.9	0.793	1.35	6.63	-	-	17	<-25
D:Et=90:10	41.9	0.829	3.22	6.66	-	0.018	21	-11.5
D:Bu=50:50	39.8	0.820	2.58	6.65	-	0.013	42	-10
PK:D:Et=10:10:80	32.5	0.834	1.77	6.46	1.02	0.018	19	<-25
PK:D:Bu=10:50:40	41.2	0.838	3.53	6.54	1.12	0.016	40	-8.5
PK:D:Bu=25:25:50	39.3	0.876	5.30	6.21	2.16	0.034	40	-6
PK:D:Bu=30:10:60	37.2	0.891	5.86	6.24	2.53	0.031	41	-7

Note: * = Flash point (Oxford University, 2008)

** = Freezing point (Oxford University, 2005a; 2008)

Figure 5.18 shows the boiling point curves of various types of fuel blends. It is noticed that bio-oil gave the boiling distribution curve closest to that of diesel fuel but its high carbon residue content limited the maximum volume of distillate to 70 vol%. Blending of alcohol in bio-oil can reduce the carbon residue content in the fuel blends (Table 5.11) and the mixture of bio-oil-butanol (50:50 by vol%) provided wider distillation range up to 88% of distillate volume. For the three components system, the range of boiling distribution could be extended to more than 90 vol%. Bio-oil-diesel-ethanol fuel with composition 10:10:80 by vol% showed a complete distillation curve. However, its boiling curve was lowest and showed three steps of distillation range with the lowest initial and final boiling point being at 74°C and 268°C, respectively. For the mixtures of bio-oil-diesel-butanol, their initial boiling points were about 95°C but their final boiling points depended on the compositions of fuel. The highest final boiling point was attained for the fuel blends containing highest fraction of diesel (PK:D:Bu=10:50:40 by vol%). Nevertheless, its final boiling point was lower than that of diesel fuel (338°C for blended fuel versus 378°C for diesel). This may be an advantageous characteristic of the fuel blend because it can provide the lower smoke and exhaust emissions (Sittichaitaweekul, Y., 2003; Stamatov *et al.*, 2006). Moreover, lower initial boiling points derived from the presence of alcohol in the blends could give the better properties of cold-starting and warming-up than those of diesel fuel (Sittichaitaweekul, Y., 2003). As to the effect of fuel composition, the higher diesel content in the bio-oil-diesel-butanol mixture showed the marked rising of the distillation curve after the complete distillation of butanol. This is also noticed from the distillation curve of the blended fuel consisting only of diesel and butanol (50:50 by vol%). It should be noted that the large difference of distillation temperature between 10 vol% and 80 vol% (~190°C) derived from the blends of PK-10:D-50:Bu-40 and D-50:Bu-50 compared with that of conventional diesel fuel (125°C) could result in longer warming-up time for the engines (Sittichaitaweekul, Y., 2003). On the other hand, higher bio-oil content in the blends (PK:D:Bu=25:25:50 and 30:10:60 by vol%) showed a gradual increase of distillation temperature, thus giving smaller difference (140°C) of distillation temperature between 10 and 80 vol% distillate in comparison with the blends of PK-10:D-50:Bu-40 and D-50:Bu-50. However, complete distillation was not obtained (only 94 vol% distillate) with the mixtures containing high bio-oil content.

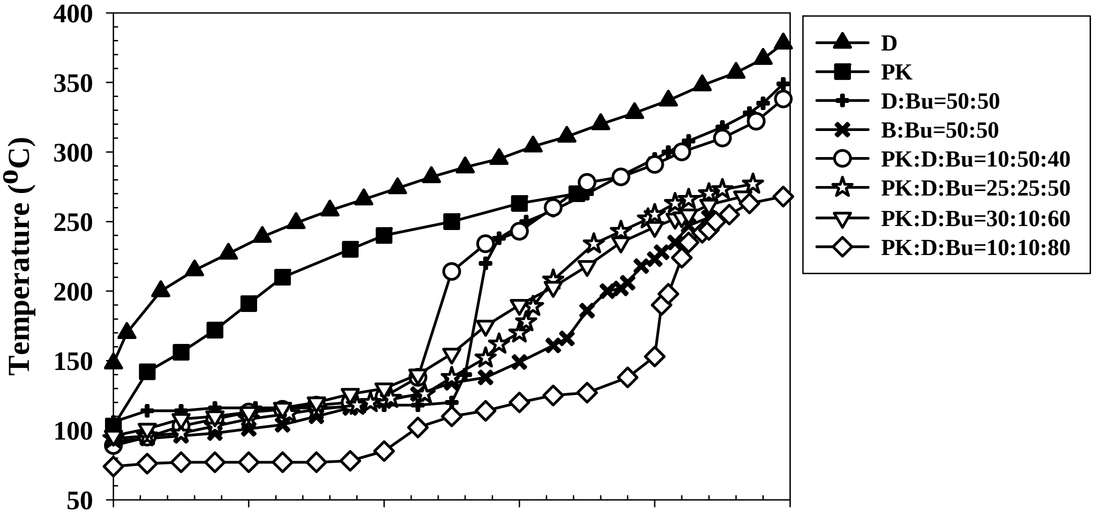

Figure 5.18 Distillation curves of fuel blends (palm kernel bio-oil (PK), diesel (D), ethanol (Et) and butanol (Bu)).

5.4.4.3 Prediction of Basic Fuel Properties of Binary and Ternary Fuel Blends

To predict fuel properties of fuel blends from the corresponding properties of their components, the measured values of the fuel properties of the blend were checked with Kay's mixing rule. It is more convenient to use mass fraction or volume fraction in place of molar fraction (x_i) in Equation (5.6), thus the equation is presented in the following form:

$$\varphi_B = \sum_i^n m_i \varphi_i \tag{5.12}$$

where φ_B is a property of the blend, φ_i is the corresponding property of pure component *i* and m_i is the mass fraction or volume fraction of component *i*. The agreement of the measured values and the values derived from Kay's mixing rule was determined by the value of absolute average deviation (*AAD*), defined as:

$$AAD = \frac{100}{N} \sum_i^n \left| \frac{\varphi_{Exp} - \varphi_{Cal.}}{\varphi_{Exp}} \right| \tag{5.13}$$

where N is the number of experiment data, φ_{Exp} is the experimental value of the measured property and $\varphi_{Cal.}$ is the predicted value of the property.

In this work, it was found that Kay's mixing rule could be applied for some properties of binary systems (Figures 5.19 and 5.20). Heating value, pH and ash content could be reasonably approximated by Kay's mixing rule using mass fraction instead of mole fraction. The using of mass fraction in Equation (5.12) gave a little less *AAD* than using volume fraction basis. The mean of *AAD* calculated by mass fraction for heating value, pH and ash content were 1.76%, 1.04% and 15%, respectively, whereas those calculated based on volume fraction were 2.58%, 1.91% and 19.4%, respectively. However, the computation based on using volume fraction works well for the density of the mixtures (1.37%*AAD* for volume fraction but 3.33%*AAD* for mass fraction). In addition, applying Kay's mixing rule for the ternary mixtures was found to be satisfactory for heating value, pH and density with the maximum *AAD* being about 3.9%, whereas that of ash content is relatively high of 42.7%. However, the calculations of other properties such as viscosity, flash point and pour point were not compatible with those estimated from Kay's mixing rule. It has been reported in the work of Joshi and Pegg (2006) that the measured values of pour point were better predicted by applying an empirical second-order polynomial equation than using a linear equation for biodiesel-diesel blends.

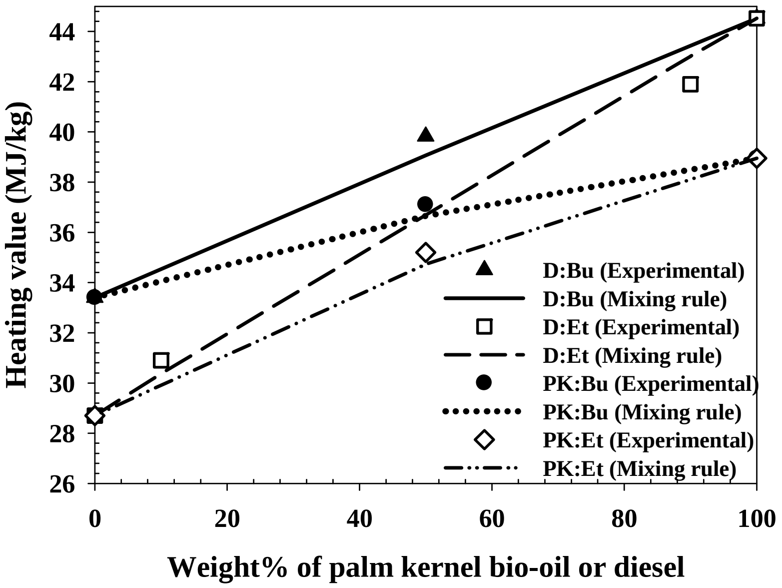

(a)

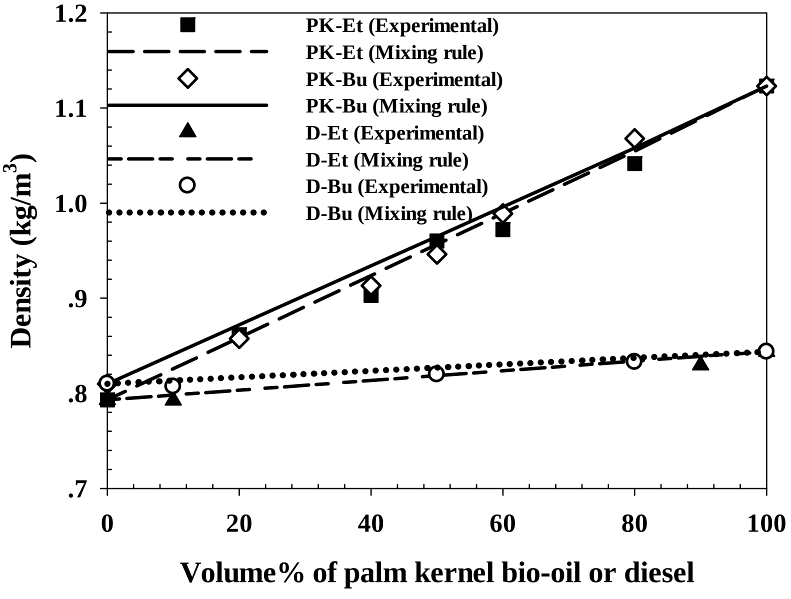

(b)

Figure 5.19 Fuel properties of blending fuels compared with those calculated by mixing rule; (a) heating value and (b) density (palm kernel bio-oil (PK), diesel (D), ethanol (Et) and butanol (Bu)).

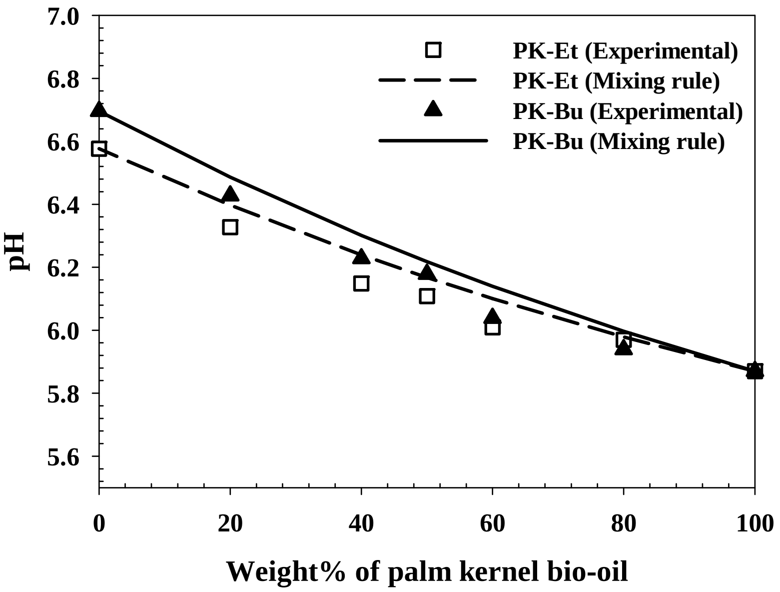

(a)

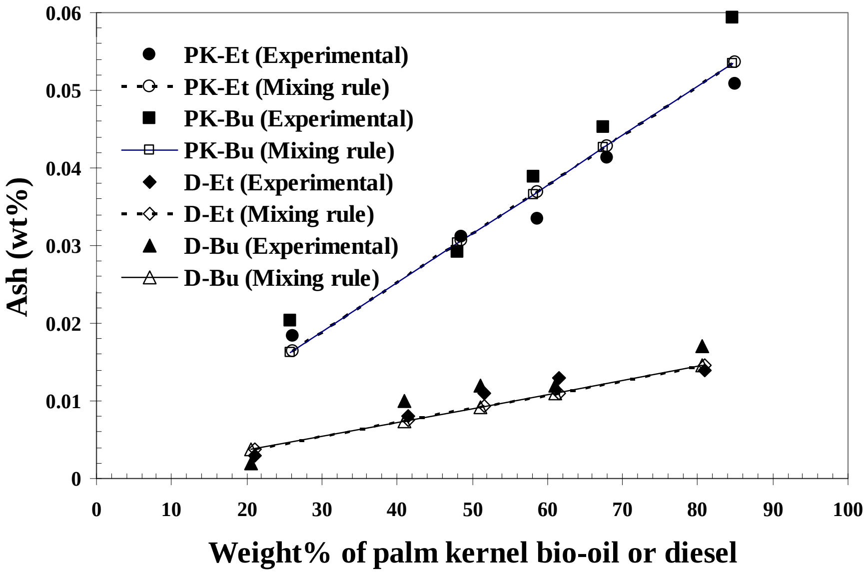

(b)

Figure 5.20 Fuel properties of blending fuels compared with those calculated by mixing rule; (a) pH and (b) ash content (palm kernel oil (PK), diesel (D), ethanol (Et) and butanol (Bu)).

5.4.4.4 Viscosity Estimation of Binary and Ternary Fuel Blends

In this work, the kinematic viscosities of pure components and the blends derived from various compositions of bio-oil-alcohol, diesel-alcohol and bio-oil-diesel-alcohol were measured as a function of temperature. For predicting viscosity of the blend at a desired temperature, Grunberg-Nissan equation was applied (Equation (5.7)). However, since in this work the kinematic viscosity was experimentally measured, it is more convenient to employ the volume fraction along with kinematic viscosity in Equation (5.7) instead of mole fraction and dynamic viscosity as originally used. Equation (5.7) now becomes

$$\ln \eta_B = \sum_i^n v_i \ln \eta_i + \sum_i^n \sum_j^n v_i v_j G_{ij} \tag{5.14}$$

where η_B is kinematic viscosity of the blend (mm^2/s), η_i is kinematic viscosity of pure component i (mm^2/s), v_i is volume fraction and G_{ij} is the interaction parameter, (G_{ij}=0 for $i = j$).

As to the effect of temperature on viscosity, the commonly recommended equation of Andrade equation (Equation (5.15)) was employed and rewritten as,

$$\eta = e^{(A+B/T+C/T^2)} \tag{5.15}$$

where η is the kinematic viscosity (mm^2/s), T is the absolute temperature (K) and A, B and C are constants.

To describe the viscosity-temperature characteristics of pure component fuels including bio-oil, diesel, ethanol and butanol, their measured viscosities were first fitted by Andrade equation. Figure 5.21 indicates that the viscosities of the pure components decreased non-linearly with increasing temperature. It is also found that the component having higher viscosities showed a more drastic decrease of viscosity with increasing temperature. The viscosity-temperature characteristics of these primary fuels were found to correlate very well with the Andrade equation and the derived constants A, B and C are listed in Table 5.12.

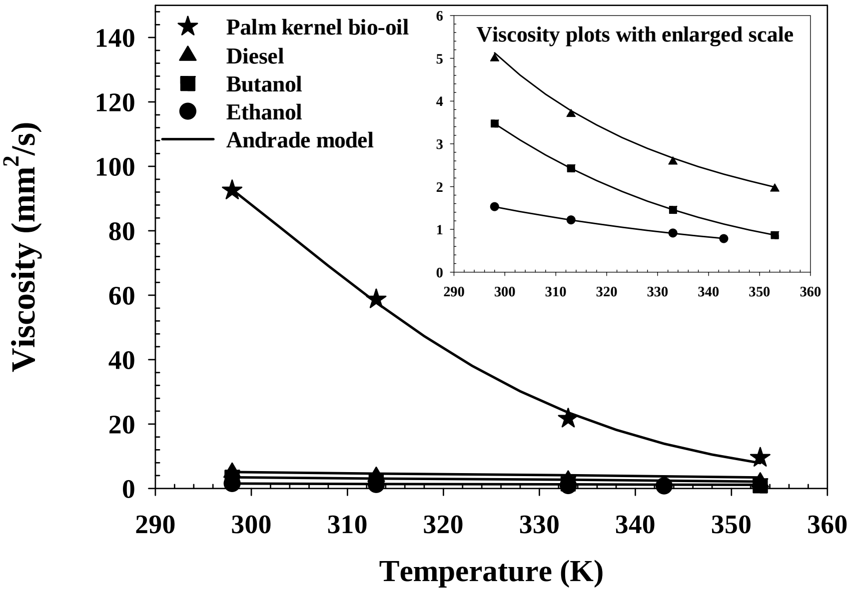

Figure 5.21 Viscosity-temperature characteristic of four pure chemicals with fitting by Andrade model.

Table 5.12 The fitted parameters derived from Andrade equation ($\eta = e^{(A+B/T+C/T^2)}$)

Fuel type	**A**	**B**	**C**	**R^2**	***AAD***
Palm kernel bio-oil	-57.5	3.48x10^4	-4.87x10^6	0.99828	6.99
Diesel	-2.00	2.21x10^2	2.57x10^5	0.99989	2.58
Butanol	-18.7	9.86x10^3	-1.16x10^6	0.99999	0.10
Ethanol	-8.29	3.85 x10^3	-3.74x10^5	1.00000	0.25

Next, on the viscosities of the blended fuels, the interaction parameters (G_{ij}) for the blends of bio-oil-ethanol, bio-oil-butanol, diesel-ethanol and diesel-butanol were determined by fitting the viscosity data with the modified Grunberg-Nissan equation (Equation (5.14)). The viscosities were also correlated by the modified Grunberg-Nissan equation without the effect of interaction parameter (G_{ij}=0) as shown by Equation (5.16).

$$\ln \eta_B = \sum_i^n v_i \ln \eta_i \qquad (5.16)$$

Figures 5.22 and 5.23 show the relationship between viscosity and composition of the binary system at different temperatures. It is observed that the modified Grunberg-Nissan equation with interaction parameter was capable of fitting the viscosity-composition relationship with the mean of *AAD* about 2.66%, whereas the modified Grunberg-Nissan equation without interaction parameter gave the higher mean of *AAD* about 18.53%. However, the application of Equation (5.16) gave better fitting at higher temperatures. As Table 5.13 shows, the mixture of bio-oil-ethanol gave the highest absolute value of interaction parameter compared to those of the blends of bio-oil-butanol, diesel-butanol and diesel-ethanol. The main reason for these differences could be ascribed to the difference in the degree of intermolecular interaction. The highest absolute value of interaction parameter derived from bio-oil-ethanol blend indicates the strong interaction of hydrogen bond of ethanol. The hydrogen atom of ethanol is able to bond with oxygen atom on carboxylic groups of some acids and aldehydes in the bio-oil. In the case of other binary mixtures, their interaction parameters were lower than that of bio-oil-ethanol blends. This could result from the smaller interaction force of van der Waal attraction among molecules. This hypothesis may be supported by considering the mutual solubility of ternary systems (Figure 5.16). Ethanol showed better miscibility in bio-oil but poorer miscibility in diesel as compared to the case of butanol. This is in agreement with the higher absolute value of G_{ij} of bio-oil-ethanol than that derived from bio-oil-butanol system. Similarly, the absolute value of G_{ij} derived from diesel-ethanol is lower than that derived from diesel-butanol. In addition, it is noted that all the fitting parameters have minus value and this agrees with the calculation of G_{ij} using group contribution method proposed by Isdale (Poling *et al.*, 2001). As to the temperature effect on the interaction parameters, their absolute values slightly decreased with increasing temperature. This trend is also in agreement with the equation suggested by Isdale (Poling *et al.*, 2001).

To estimate the effect of composition and temperature on the viscosity of ternary system of palm kernel bio-oil-diesel-alcohol blends, the modified Grunberg-Nissan equation and the Andrade equation were combined and the final equation is shown as display in Equation (5.17). In this equation, the viscosity of each fuel component ($\eta_{PK}, \eta_{D}, \eta_{Al}$) was derived from applying Andrade equation (Equation (5.15)) and the interaction parameters, G_{ij} were estimated from the binary systems (Table 5.13). Since the condition of no interaction between palm kernel bio-oil and diesel was assumed because of the full immiscibility characteristic, G_{PK-D} was thus taken as zero. The final viscosity equation now becomes

$$\ln \eta_{PK-D-Al} = v_{PK} \ln \eta_{PK} + v_D \ln \eta_D + v_{Al} \ln \eta_{Al} + v_{Al} v_{PK} G_{Al-PK} + v_{Al} v_D G_{Al-D} \tag{5.17}$$

where the subscripts of PK , D and Al represent the components of palm kernel bio-oil, diesel and alcohols (ethanol or butanol), respectively.

Figure 5.24 indicates that the predicted viscosities using Equation (5.17) agreed very well with the measured viscosities with the mean of *AAD* being 4.67%. If the interaction effect was omitted, the correlation gave higher mean of *AAD* of 11.1%. For this case, it is observed that the prediction of the bio-oil-diesel-ethanol mixture showed the largest deviation from the experimental data (8.47%*AAD*).

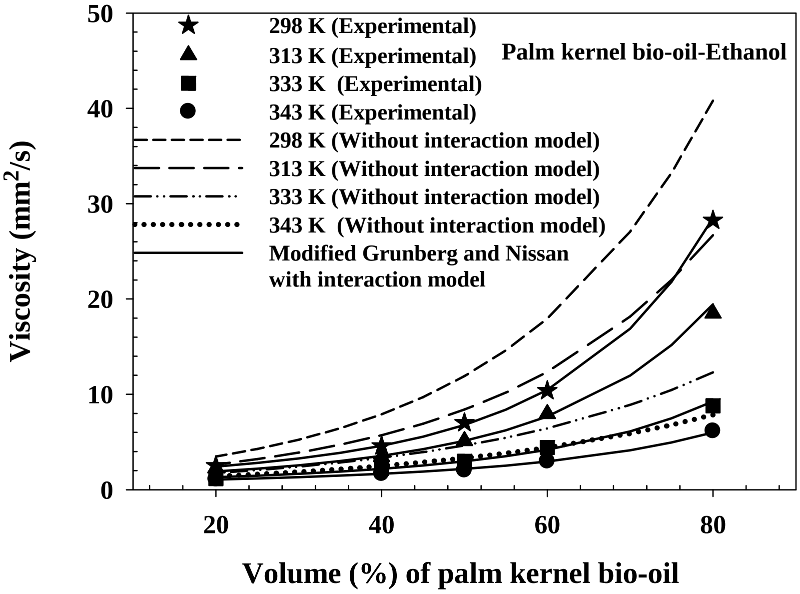

(a)

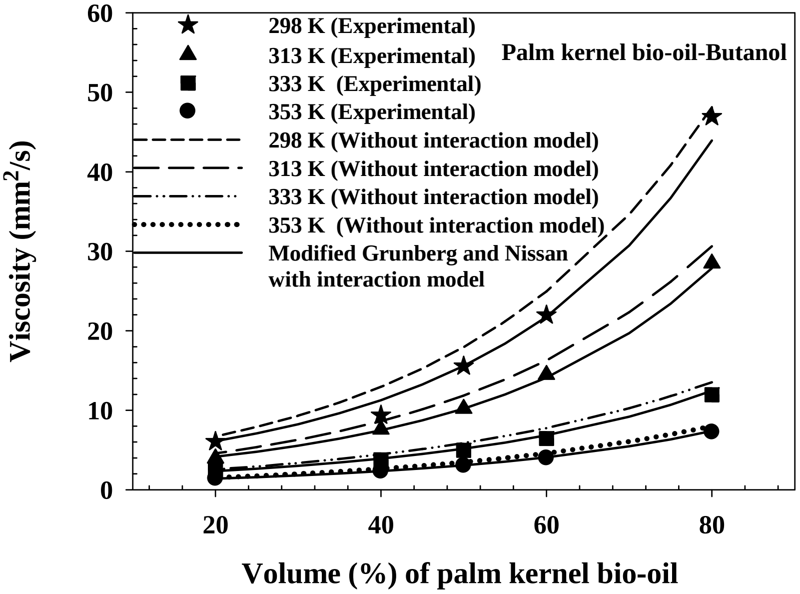

(b)

Figure 5.22 Kinematic viscosity of two component system at different temperatures; (a) palm kernel bio-oil-ethanol and (b) palm kernel bio-oil-butanol.

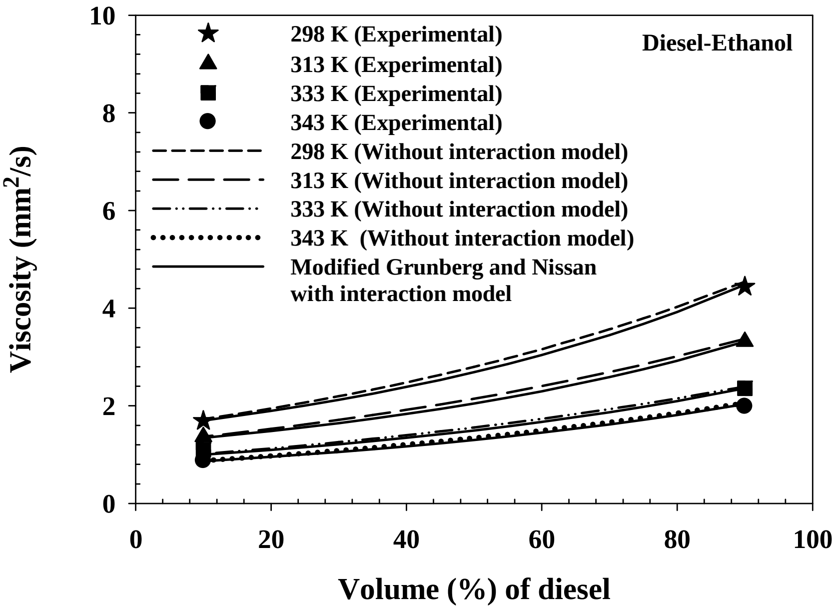

(a)

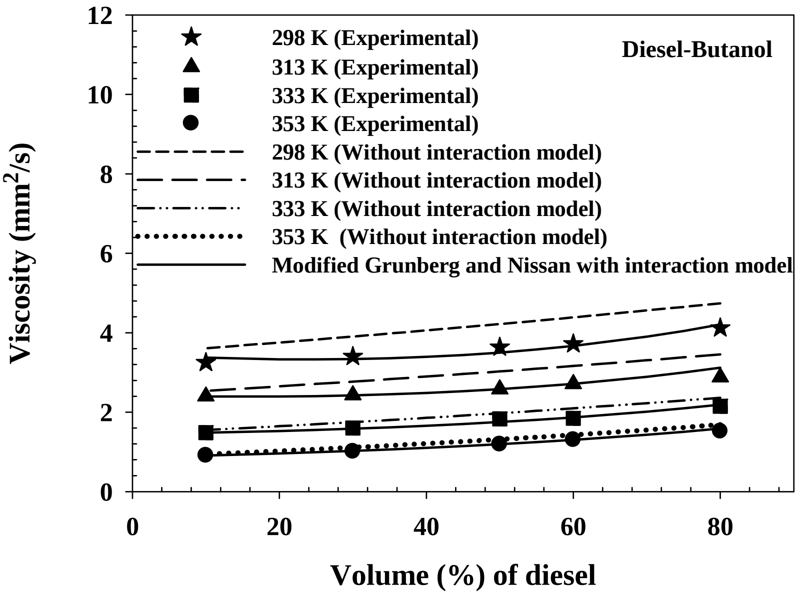

(b)

Figure 5.23 Kinematic viscosity of two component system at different temperatures; (a) diesel-ethanol and (b) diesel-butanol.

Table 5.13 Interaction parameters derived from fitting of modified Grunberg-Nissan equation ($\ln \eta_m = \sum_i^n x_i \ln \eta_i + \sum_i^n \sum_j^n x_i x_j G_{ij}$) (palm kernel bio-oil (PK), diesel (D), ethanol (Et) and butanol (Bu)).

Interaction parameter	**Chemical component**			
	PK+Et	**PK+Bu**	**D+Et***	**D+Bu**
G_{ij} at 298 K	-2.245	-0.568	-0.158	-0.745
G_{ij} at 313 K	-1.981	-0.59	-0.184	-0.634
G_{ij} at 333 K	-1.782	-0.515	-0.157	-0.473
G_{ij} at 343 K	-1.676	-	-0.125	-
G_{ij} at 353 K	-	-0.488	-	-0.378
AAD (with interaction)	3.80	1.75	2.75	2.32
AAD (without interaction)	49.81	11.75	2.04	10.50

Note: * = Fitted from two compositions varying in range of soluble solution

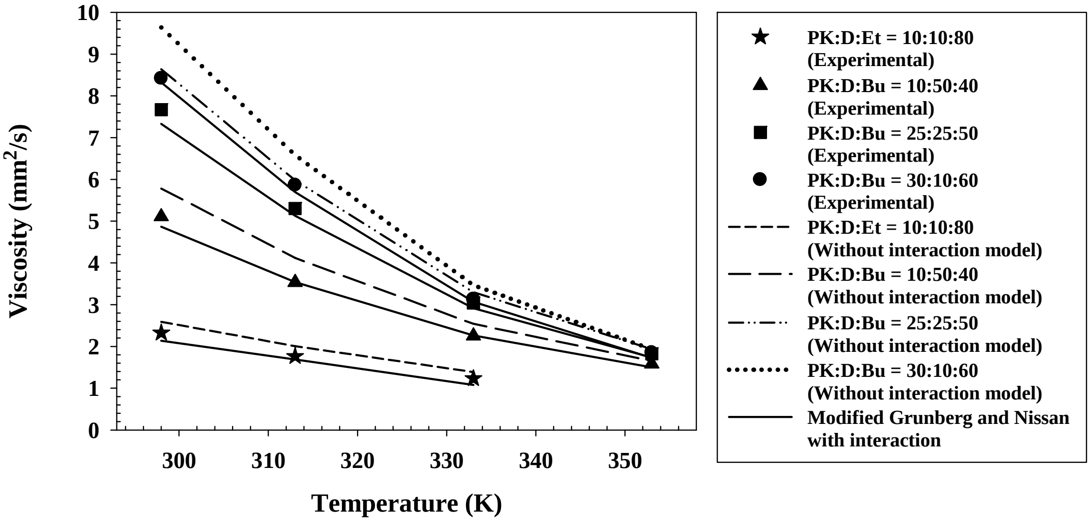

Figure 5.24 Kinematic viscosity of three component system at different temperatures (palm kernel oil (PK), diesel (D), ethanol (Et) and butanol (Bu)).

5.5 Esterification of Bio-Oil and Alcohol by Acid Catalysts

5.5.1 Introduction

Chemical components in bio-oil have strong effects on its physical and fuel properties. The presence of oxygenated compounds in the bio-oil is one of the main problems for its unsatisfactory use as an alternative fuel. Various processes such as hot-vapor filtration, catalytic hydrotreating and catalytic cracking have been applied to improve chemically the bio-oil properties (Bridgwater, 2003; Oasmaa and Czernik, 1994). However, catalytic upgrading processes give low yield of upgraded oils and produce undesirable products of coke deposit on the catalyst surface as well as high costs of product recovery (Demirbas and Balat, 2006). In addition, the bio-oil treated via hot-vapor filtration process at elevated temperature (~400-420°C) could accelerate polymerization reactions, thus increasing the rates of particle growth and agglomeration (Diebold, 2000). It was also reported that ageing effect could occur much faster at higher temperatures; the bio-oil stored at -20ºC showed the rate of viscosity increase of about 0.009 cP/day, but heating to 90ºC gave much higher rate of 300 cP/day. Esterification reaction is an upgrading method that can convert carboxylic acids in bio-oil to esters, leading to less corrosiveness and ageing problems of the bio-oil. This treatment could be an attractive method for improvement of bio-oil properties due to its ease of operation, low investment cost and avoiding secondary reactions that may occur at high operating temperatures.

In this work, dewatered palm shell oil with moderate heating value of 25.55 MJ/kg but relatively low pH of 2.92 was selected for the study of oil upgrading via the esterification process. The effects of alcohol type (methanol and ethanol), mole ratio of alcohol and carboxylic acids in bio-oil, catalyst type (solid acid catalyst, Amberlyst15 and liquid catalyst, 96 wt% H_2SO_4), catalyst amount (0, 5, 15 and 30 wt% of Amberlyst15), reaction temperature (25, 50 and 60°C) and reaction time (1, 5, 12 and 24 hr) on reaction conversion and product quality were investigated. The extent of esterification reaction was ascertained by the techniques of ^1H NMR and the titration with KOH and $NaHCO_3$. Moreover, basic fuel properties such as calorific value, density, viscosity, carbon residue and ash contents of the upgraded bio-oils were also measured.

5.5.2 Literature Reviews

5.5.2.1 Previous Studies

Although limited studies on bio-oil upgrading by esterification reaction have been reported thus far, this upgrading technique is still the topic of recent interests. Doshi *et al.* (2005) upgraded the bio-oil derived from fast pyolysis of sewage sludge via esterification using H_2SO_4 as an acid liquid catalyst. It was found that the odor of the treated oil was improved from an extremely annoying level to a not annoying level (ASTM D1833-87) with about four times reduction in viscosity and up to 9% increasing of heating value. However, suggestion of using solid catalyst in place of H_2SO_4 to reduce corrosion problem was also proposed. Moreover, increasing amount of alcohol can further reduce heating value of the upgraded oil, therefore alcohol separation by fractional distillation would be needed in this process. Later, several researchers have improved the process using various types of solid acid catalyst and/or recovery of the alcohol by distillation. Junming *et al.* (2008) and Mahfud *et al.* (2007) have used the technique of reactive distillation to remove water and alcohol solvent. In the work of Junming *et al.* (2008), it was reported that density and acidity were reduced (1.16 to about 0.93g/cm^3 for density and pH from 2.82 to 6.21) and the gross calorific value increased from 14.3 to 23 MJ/kg using ethanol as a reactant and SO_4^{2-}/ZrO_2 as a catalyst at the reaction temperature of 55-77°C. Mahfud *et al.* (2007) has treated the bio-oil with a higher boiling point alcohol of n-butanol in the presence of a solid acid catalyst of Nafion SAC13 at 50-80°C under reduced pressure of less than 10 kPa. The results indicated that the upgraded oil properties were improved particularly the heating value and viscosity but the acidity was still close to that of the raw bio-oil (pH of 3.2). In studying the effect of catalyst type, Zhang *et al.* (2006) used solid acid $40SiO_2/TiO_2$-SO_4^{2-} and solid base $30K_2CO_3/Al_2O_3$-NaOH to compare their effectiveness. It was found that acidity in the bio-oil was lowered by the action of both catalysts but the solid acid catalyst was capable of converting volatile and nonvolatile organic acids into more esters. However, the strong acidification of solid acid catalyst tended to intensify the acidity of bio-oil. Furthermore, the use of solid acid catalyst also promoted acetalization reaction of aldehydes and alcohol.

In conclusion, it is logical to infer that the esterification process has improved certain properties of bio-oil. It should be noted that there are a number of important parameters such as catalyst type and esterification conditions that can affect the effectiveness of bio-oil upgrading. Moreover, the complex compositions of bio-oil itself could be responsible for the occurrence of side reactions that may influence the properties of the upgraded oil. Thus, a detailed study of bio-oil upgrading by esterification for a specific bio-oil should be carried out.

5.5.2.2 Reactions Involving Constituents in Bio-oil

Generally, bio-oil contains many varieties of chemicals such as phenols, sugars, acetaldehyde, esters, ethers and carboxylic acids that can undergo various chemical reactions, leading to the deterioration of bio-oil properties during storage. Some important chemical reactions that can possibly take place from chemical constituents in bio-oil are presented as follows (Diebold, 2000).

(1) Esterification

Esterification is the reaction of organic acids with alcohols to form esters and water:

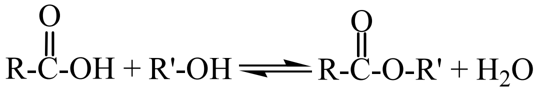

$$\mathrm{R\text{-}\overset{\overset{O}{\|}}{C}\text{-}OH + R'\text{-}OH \rightleftharpoons R\text{-}\overset{\overset{O}{\|}}{C}\text{-}O\text{-}R' + H_2O} \qquad (5.18)$$

where R is alkyl groups derived from acids and R' is alkyl groups derived from alcohols. This reaction can be catalyzed by an acid which is of interest in bio-oil upgrading because of the naturally low pH of bio-oil (2.3 to 3.0). In addition, the formation of esters from organic acids and alcohols is thermodynamically favored. For example, esterification of 1 N acetic acid with methanol is 50% complete after about 27 hrs at 70ºC with no catalyst added. Moreover, molecular sizes of the reactants have a significant effect on the reaction rate; the slower reaction rate is derived from the larger molecules.

(2) Transesterification

Transesterification reaction is the exchange of alkyl groups of acids (R and R") and alcohols (R' and R"') between a mixture of two or more esters as presented in Equation (5.19). This reaction can be also catalyzed also by acid similarly to esterification.

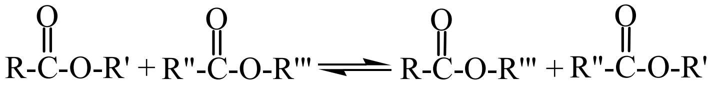

$$R\text{-}\overset{O}{\overset{\|}{C}}\text{-}O\text{-}R' + R''\text{-}\overset{O}{\overset{\|}{C}}\text{-}O\text{-}R''' \rightleftharpoons R\text{-}\overset{O}{\overset{\|}{C}}\text{-}O\text{-}R''' + R''\text{-}\overset{O}{\overset{\|}{C}}\text{-}O\text{-}R' \qquad (5.19)$$

(3) Hydration

Aldehydes or ketones can react with water to form hydrates, also referred to as glycols:

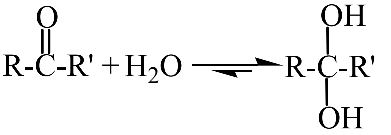

$$R\text{-}\overset{O}{\overset{\|}{C}}\text{-}R' + H_2O \rightleftharpoons R\text{-}\underset{\underset{OH}{|}}{\overset{\overset{OH}{|}}{C}}\text{-}R' \qquad (5.20)$$

where R and R' are hydrogen or alkyl groups. The rate of formation of aldehyde hydrates is quite rapid for formaldehyde in an excess of water. A bio-oil containing 25 wt% of water and 3 wt% of formaldehyde can form 99.9 mol% of formaldehyde hydrate at equilibrium, while 24 wt% of acetaldehyde hydrate can be obtained from the same bio-oil containing 3% acetaldehyde and the same bio-oil containing 3 wt% acetone in the oil gives only a trace of the acetone hydrate (0.04 wt%).

(4) Homopolymerization

Aldehydes can react with each other to form polyacetal oligomers and polymers, as shown in Equation (5.21):

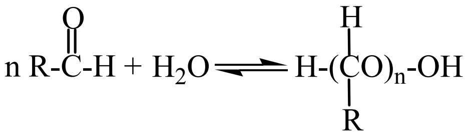

$$n\ R\text{-}\overset{\overset{O}{\|}}{C}\text{-}H + H_2O \rightleftharpoons H\text{-}(\underset{\underset{R}{|}}{\overset{\overset{H}{|}}{C}}O)_n\text{-}OH \qquad (5.21)$$

where R is alkyl groups. Organic acids such as formic, acetic, propionic, glycolic, benzoic, oxalic, etc are the catalyst for this reaction. The poly (oxymethylene) polymer derived has limited solubility in water. Solvents such as methanol, ethanol, propanol, isopropanol, glycols, and glycerol are used to stabilize aldehyde solutions and decrease the n value, with usually 6% to 15% of alcohol solvent.

(5) Acetalization

Aldehydes and alcohols can react to form acetals as shown by the following reaction:

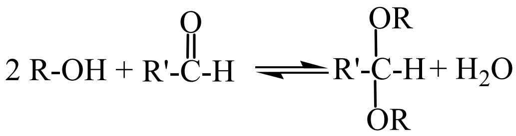

$$2\ R\text{-}OH + R'\text{-}\overset{\overset{O}{\|}}{C}\text{-}H \rightleftharpoons R'\text{-}\underset{\underset{OR}{|}}{\overset{\overset{OR}{|}}{C}}\text{-}H + H_2O \qquad (5.22)$$

where R is alkyl groups derived from alcohols, R' is alkyl groups derived from aldehydes. In the presence of acid catalysts, stable acetals are formed by the reaction of aldehydes and the hydroxyl groups of sugars, starches, and cellulose. Cellulose reacting with formaldehyde can also create a crosslinked polymer. Moreover, acetals can be also obtained from bio-oil producing process, especially the condition of a long residence time at the unit operations following the pyrolysis process such as cyclonic separators, hot-gas filters, or in the free-board volume above a fluidized bed. The catalysts used for acetal formation at lower temperatures include many salts potentially presenting in the ash of biomass such as chloride salts of aluminum, calcium, iron (ferric), lithium, magnesium, manganese and zinc.

(6) Phenol/Aldehyde Reactions

Phenol can act as an alcohol to react with formaldehyde to form the phenyl hemiformal in the absence of catalyst which its reaction rate is normally less than methanol. Afterward, phenyl hemiformal is changed to hydroxymethyl phenol in the presence of acid catalysts as shown in Equation (5.23). This reaction allows up to three units of formaldehyde to attach on a ring at ortho and para sites. The hydroxymethyl phenols can react with each other at free ortho or para site to form phenol-formaldehyde polymer.

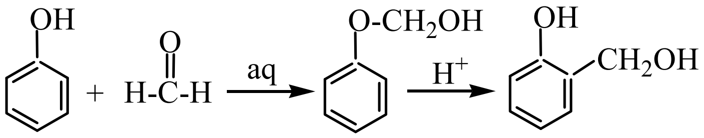

(5.23)

Phenyl hemiformal Hydroxymethyl phenol

In addition, phenols and substituted phenols can react with aldehyde hydrates to form novolak resins and water with the use of acid catalyst as follows:

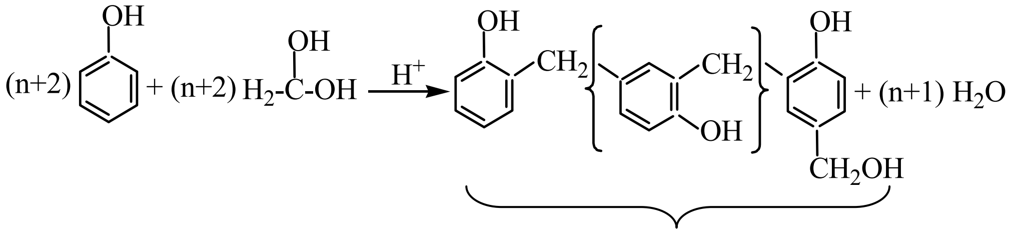

Novolak resin

(5.24)

The active sites for this reaction are at the 2, 4, and 6 positions such as the ortho and para positions. The 2, 6-dimethoxy phenols (syringols) have only the para site remaining to react with aldehydes resulting in chain-termination. Consequently, bio-oil from hardwood which contains higher amount of syringols than softwood bio-oils shows better properties after long storage time. In addition, these reactions of forming resins are irreversible under normal bio-oil storage conditions.

(7) Alcohol Addition into Unsaturated Organic Compounds

Very reactive reagents of unsaturated aldehydes such as acrolein can react with alcohols to form alkoxy aldehyde, unsaturated acetal, or alkoxy acetal using catalysts of acids or bases, as shown in Equation (5.25):

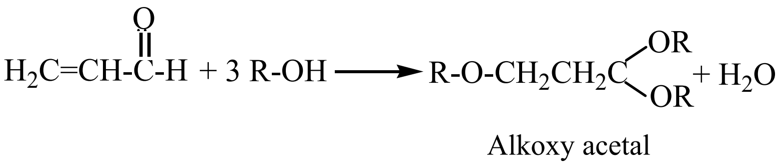

$$H_2C{=}CH\text{-}\overset{\overset{\displaystyle O}{\|}}{C}\text{-}H + 3\ R\text{-}OH \longrightarrow \underset{\text{Alkoxy acetal}}{R\text{-}O\text{-}CH_2CH_2C\begin{matrix}\diagup OR\\ \diagdown OR\end{matrix}} + H_2O \qquad (5.25)$$

where R is an alkyl groups of alcohol. Moreover, unsaturated compounds in bio-oil including acrolein, 2-butenone, propenyl substituted phenolics, and 2-propene-1-ol can react with each other to form polyolefins, with this reaction being catalyzed by anionic, cationic, or free-radical agents such as carboxylic acids.

(8) Oxidation

Alcohols and aldehydes in bio-oil when exposed to air can be oxidized to carboxylic acids. Moreover, an important reaction that takes place during bio-oil storage is that of forming hydroperoxides and alkylperoxides by autoxidation of bio-oil with air. These peroxides are very unstable and spontaneously decompose to form free-radicals. At high concentrations, many organic peroxides can be explosive. The active hydrocarbons in bio-oil that can form hydroperoxides follow the sequence n-alkanes< branched alkanes < aralkanes ~ alkenes < alkynes.

As mentioned earlier, esterification of bio-oil is a method that can change the bio-oil properties. It is not only able to change the radical agent as carboxylic acids to more stable chemicals of esters but also prohibit some reactions catalyzed by these carboxylic acids to occur. However, addition of alcohol and the existence of acid catalyst in the bio-oil containing complex chemical components could generate some other side reactions. For example, transesterification between alkyl alcohol groups of esters in bio-oil and alkyl groups of alcohol solvent can produce lower molecular weight esters (Equation (5.19)), aldehydes or ketones in bio-oil can be hydrated by water produced from esterification (Equation (5.20)), alcohol solvent can react with aldehydes to form acetals (Equation (5.22)), etc. In addition, it is observed that these side reactions could give an advantage in reducing aldehydes, leading to the reaction of oligomers or polymer formation from homopolymerization (Equation (5.21)), phenol/aldehyde reactions (Equation (5.24)), etc.

5.5.2.3 Chemical Analysis of Upgraded Bio-oil

Two methods namely ^{1}H NMR and titration were used to identify and quantify the ester product, respectively, after bio-oil upgrading by esterification. The principles of these techniques are briefly described here.

(1) ^{1}H NMR

^{1}H NMR is a technique widely used to identify esters occurring from esterification reaction in various previous works due to its effectiveness in elucidating the structure of organic chemicals and ease and low cost of operation (Reddy *et al.*, 2006; Soriano Jr *et al.*, 2009). The nuclear magnetic resonance (NMR) is based upon the measurement of resonant absorption of electromagnetic radiation in the radio-frequency region of roughly 4 to 900 MHz (Skoog *et al.*, 2007). The absorption of radio wave which is generated from the radiation of an electromagnetic field can change nuclear spin states of the sample molecules and this effect can be correlated with the molecular structure. ^{1}H is a nucleus that has been one of the greatest interest for biochemical structure analysis for it provides information of hydrogen's electronic environments derived from different chemical structures at slightly different frequencies. The number for locating the frequency occurring from spinning of nucleus relative to other nuclei is defined as chemical shift. For example, the correlation of common functional groups at different chemical shift is shown in Figure 5.25 (Lambert and Mazola, 2003).

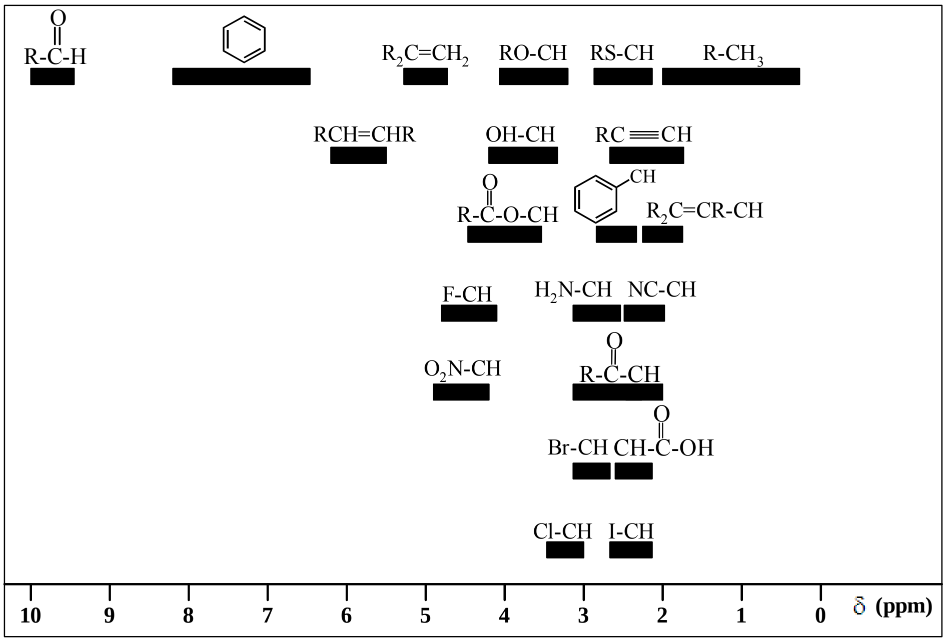

Figure 5.25 Chemical shift ranges of ^{1}H NMR spectra for common structural units. Symbol of CH is methyl, methylene, methane and R is a saturated alkyl groups (Lambert and Mazola, 2003).

(2) Bio-Oil Titration

Strong base of potassium hydroxide, KOH, is commonly used for determining acid number in petroleum products and lubricants according to the standard code of ASTM D664-07. In this work, this method is applied to quantify the content of carboxylic acids present in the bio-oil by titration at room temperature, the reaction of which is shown in Equation (5.26). However, phenol and its derivatives containing in the bio-oil can also react with KOH as presented by Equation (5.27). To achieve the correct amount of acid content for the calculation of esterification conversion, the bio-oil is also titrated with weak base of $NaHCO_3$ (Equation (5.28)) since $NaHCO_3$ does not react with phenols (Graham Solomons, 1997).

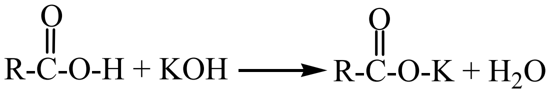

$$R\text{-}\overset{\overset{O}{\|}}{C}\text{-}O\text{-}H + KOH \longrightarrow R\text{-}\overset{\overset{O}{\|}}{C}\text{-}O\text{-}K + H_2O$$

(5.26)

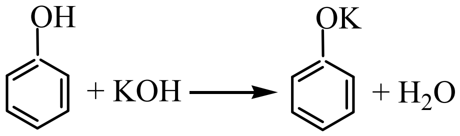

(5.27)

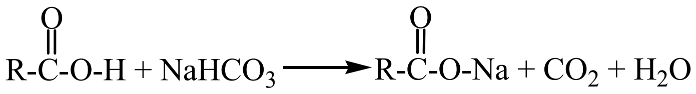

$$R\text{-}\overset{\overset{O}{\|}}{C}\text{-}O\text{-}H + NaHCO_3 \longrightarrow R\text{-}\overset{\overset{O}{\|}}{C}\text{-}O\text{-}Na + CO_2 + H_2O$$

(5.28)

Moreover, aldehydes with no α-hydrogen atom such as formaldehyde, benzaldehyde, 2, 2-dimethyl propanol, etc can react with alkali KOH. For example, formaldehyde can react with KOH at room temperature as given in Equation (5.29). However, this reaction was considered to be negligible for palm shell oil because typical raw oils derived from biomass pyrolysis have only slight amounts of these chemicals (Diebold, 1997; Milne *et al.*, 1997). This reasoning is based on the evidence that aldehydes with no α-hydrogen atom cannot be detected in palm shell oil with water removed by distillation (see Table 4.7 in Chapter IV).

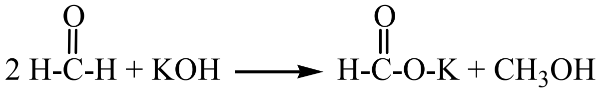

$$2\ \mathrm{H\text{-}\overset{\overset{O}{\|}}{C}\text{-}H} + \mathrm{KOH} \longrightarrow \mathrm{H\text{-}\overset{\overset{O}{\|}}{C}\text{-}O\text{-}K} + \mathrm{CH_3OH} \tag{5.29}$$

The equivalent point of titration depends on the types of titrant and analyte solution used (Wiggs, 2009). For instance, titration of 0.1 M acids at various K_a values with 0.1 M NaOH provides different pH values for achieving the equivalent point at the same NaOH volume (Figure 5.26). The equivalent point of weaker acids (lower K_a value) titrated with strong base of NaOH has higher pH than that of stronger acids. Since bio-oil contains very weak acids of free fatty acids (pH 7 (Schmid, 1996)), the volume of KOH corresponding to a nearly constant pH was thus taken as the equivalent point in this study.

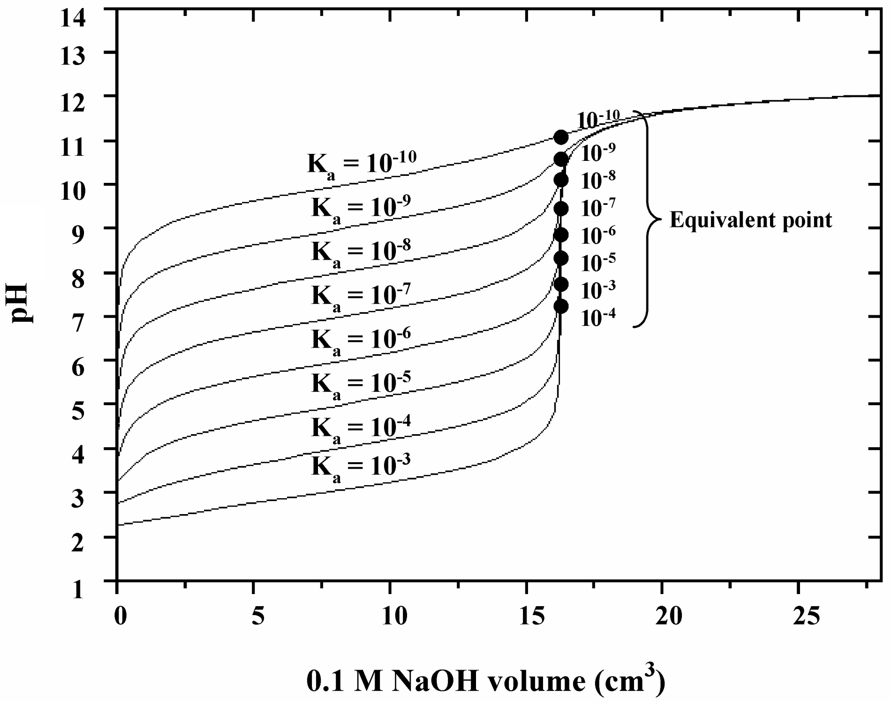

Figure 5.26 Titration curves of various acid types (different K_a values) with strong base of NaOH (Wiggs, 2009).

5.5.3 Materials and Methods

5.5.3.1 Materials

The oil sample used for esterification study was the oil phase separated by centrifugation (3000 rpm for 20 min) of the raw bio-oil derived from pyrolysis of palm shell (pyrolysis conditions: average palm shell size of 2.03 mm, pyrolysis temperature of 700°C, heating rate of 20°C/min and nitrogen flow of 200 cm^3/min). Two types of alcohol including methanol (99.9%) and ethanol (99.8%) were employed as starting reagents and were purchased from Carlo Erba Reagents Group. There are two types of catalysts used for this study including solid acid catalyst of Amberlyst15 and liquid catalyst of 96% sulfuric acid (H_2SO_4). They were acquired from Acros Organics Group and Carlo Erba Reagents Group, respectively. The Amberlyst15 catalyst is the dry type of sulfonic acid cation-exchange resin catalyst (H^+, ~4.7 meq/g), which is a macroreticular polymeric resin of crosslinked styrene divinybenzene copolymers.

5.5.3.2 Esterification Reaction

Fifteen test conditions as detailed in Table 5.14 were used to investigate the effect of process variables on the properties of upgraded bio-oils by esterification. Palm shell bio-oil and alcohol were mixed based on the required mole ratio of alcohol and carboxylic acid in the bio-oil and the catalyst was added as weight percentage of palm shell oil. It was found from a preliminary experimentation that 1 g of palm shell oil had acid content of 4.80 mmol/g oil based on the titration result of 403.0 mg $NaHCO_3$/g oil. The mixture reaction was carried out to upgrade the bio-oil under a controlled temperature using a water bath (P Selecta, Unitronic or) shaken at 50 rpm for the desired reaction time. To affect the increased conversion by shifting the reaction equilibrium, water produced was removed from the solution by adding 20 wt% molecular sieve 3A into the original mixture (Run no.15).

Table 5.14 Conditions for studying esterification of bio-oil from palm shell and alcohols.

Run No.	Parameters affecting esterification	Fixed conditions	Studied conditions
1	**Reaction temperature (°C)**	- 3.25:1 mole ratio of methanol to carboxylic acids in bio-oil - Reaction time of 24 hr - 5 wt% Amberlyst15	25
2			50
3			60
4	**Reaction time (hr)**	- 3.25:1 mole ratio of methanol to carboxylic acids in bio-oil - Reaction temperature of 60°C - 5 wt% Amberlyst15	1
5			5
6			12
3			24
7	**Catalyst amount (wt% of Amberlyst15)**	- 3.25:1 mole ratio of methanol to carboxylic acids in bio-oil - Reaction temperature of 60°C - Reaction time of 24 hr	0
3			5
8			15
9			30
10	**Catalyst type**	- 3.25:1 mole ratio of methanol to carboxylic acids in bio-oil - Reaction temperature of 60°C - Reaction time of 24 hr	5 wt% of H_2SO_4
11			5 wt% of recycled Amberlyst15
12			15 wt% of recycled Amberlyst15
3	**Mole ratio of methanol to carboxylic acids in bio-oil**	- Reaction temperature of 60°C - Reaction time of 24 hr - 5 wt% Amberlyst15	3.25:1
13			6.50:1
3	**Alcohol type**	- 3.25:1 mole ratio of alcohol to carboxylic acids in bio-oil - Reaction temperature of 60°C - Reaction time of 24 hr - 5 wt% Amberlyst15	Methanol
14			Ethanol
15	**Addition of molecular sieve 3A**	- 3.25:1 mole ratio of methanol to carboxylic acids in bio-oil - Reaction temperature of 60°C - Reaction time of 24 hr - 5 wt% Amberlyst15	20 wt% of molecular sieve 3A

5.5.3.3 Product Analysis

(1) ^{1}H NMR

The occurrence of esterification reaction was confirmed by analyzing the ^{1}H NMR spectra derived at a frequency of 300 MHz using a Varian Inova-300 NMR spectrometer. Samples were prepared for analysis by diluting 10 μl of the upgraded bio-oils in 990 μl of 99.8% deuterated chloroform, $CDCl_3$ (Wilmad-LabGlass, SP Industries Inc). Tetramethylsilane, TMS (99.7%, Merck Group) was also added into the sample solutions for use as an internal standard (Chemical shift at 0 ppm). In addition, the NMR spectrum of a mixture of raw bio-oil and methanol without catalyst was also derived. This information was used as a blank test for comparison with that of the upgraded bio-oils.

(2) Bio-oil Titration with KOH and $NaHCO_3$

To determine the esterification conversion of upgraded bio-oils from the amount of carboxylic acid left after the reaction, the oil sample weighing 5 g was titrated with 0.1 M KOH at room temperature. The volume of KOH used at the equivalent point was determined from the maximum volume at which the pH of sample solution became constant (see the titration curves in Figure 5.27). However, KOH could as well react with phenol and its derivatives. Thus, to obtain the actual amount of carboxylic acid in the raw bio-oil for the calculation of reaction conversion, $NaHCO_3$ was also used as a titrant for determining carboxylic acid content since it does not react with phenol and its derivatives. Further, there is a possibility that the acid catalyst may release proton from its active site and could react with the titrant base. To account for this effect, about 5 g of water that has been contacted with the pure catalyst under the same condition as that of bio-oil esterification was titrated with KOH and the acid content in the water determined. The required amounts of KOH and $NaHCO_3$ under all test conditions are presented in Table 5.15 and the conversion of the upgraded bio-oil ($X_{upgraded}$) was calculated based on the following equation.

$$X_{upgraded} = \frac{V_{KOH-raw} - (V_{KOH-upgraded} - V_{KOH-cat})}{V_{NaHCO_3-raw}} \tag{5.30}$$

where $V_{KOH\text{-}raw}$ is the volume of 0.1 M KOH titrated with the mixture of raw bio-oil and methanol without catalyst. $V_{KOH\text{-}upgraded}$ is the volume of 0.1 M KOH titrated with the upgraded bio-oil after esterification, $V_{KOH\text{-}cat}$ is the volume of 0.1 M KOH titrated with water after contacting with pure catalyst and $V_{NaHCO3\text{-}raw}$ is the volume of 0.1 M $NaHCO_3$ titrated with the mixture of raw bio-oil and methanol.

(3) Fuel Properties

Oil phase of palm shell oil, two alcohols (methanol and ethanol) and four types of upgraded bio-oil product (Run No. 3, 7, 13 and 14) were characterized for their basic fuel properties including calorific value (ASTM D240-92), density (Gay-Lussac bottle), viscosity (ASTM D445-96), pH (744 pH meter, Metrohm), carbon residue (ASTM D524-97), ash content (ASTM D482-95), flash point (ASTM D93-97) and pour point (ASTM D97-96a).

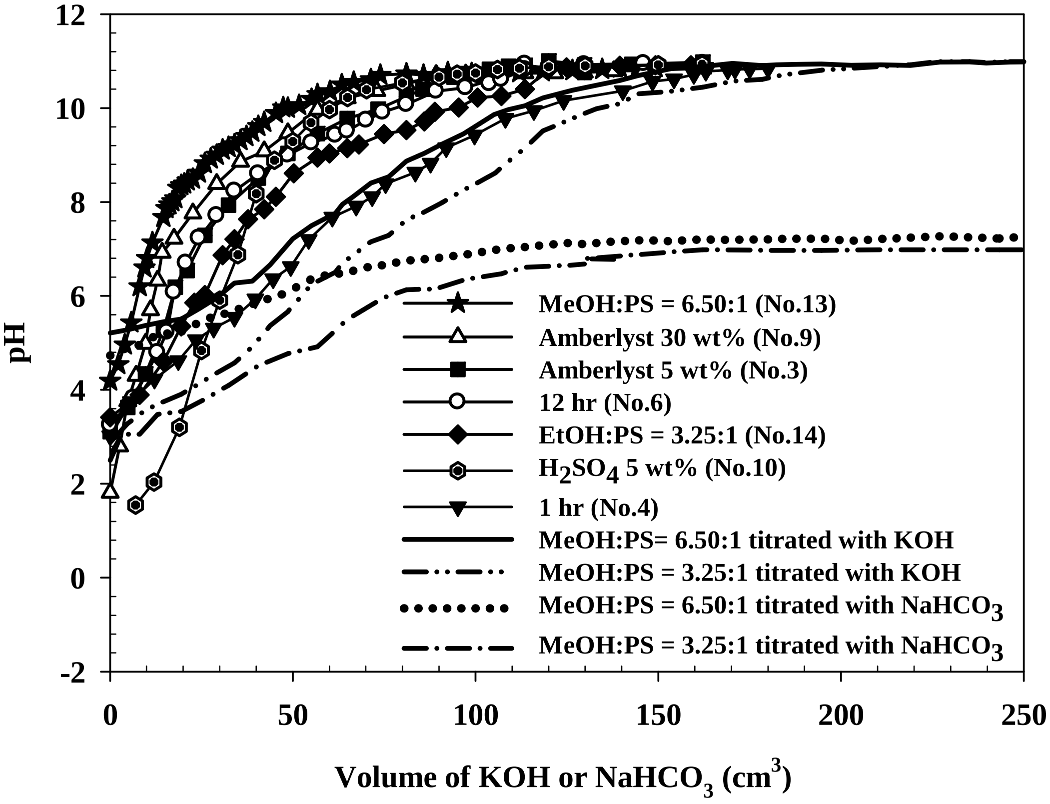

Figure 5.27 Titration curves derived from various upgraded bio-oils and mixtures of palm shell oil (PS) and methanol (MeOH).

Table 5.15 Volumes of base solution titrated with upgraded bio-oils and their calculated conversion and pH.

Run No.*	**Volume of 0.1 M KOH titrated with 5 g upgraded bio-oil (cm^3)**	**Volume of 0.1 M KOH titrated with 5 g extracted water (cm^3)**	**Volume (cm^3) of base solution titrated with 5 g of raw palm shell oil and alcohol**		**Conversion (%)**	**pH of sample after reaction**
			0.1 M KOH	**0.1 M $NaHCO_3$**		
1	170.0	0.43	225.5	160.0	34.96	3.15
2	132.0	0.43	225.5	160.0	58.71	3.22
3	108.5	0.43	225.5	160.0	73.39	3.31
4	165.5	0.43	225.5	160.0	37.77	3.02
5	126.0	0.43	225.5	160.0	62.46	2.98
6	113.0	0.43	225.5	160.0	70.58	3.20
7	204.5	0.00	225.5	160.0	13.13	4.32
8	101.0	1.32	225.5	160.0	78.64	2.74
9	89.0	2.49	225.5	160.0	86.87	1.81
10	111.5	36.00	225.5	160.0	93.75	**
11	119.0	0.26	225.5	160.0	66.73	3.48
12	112.5	0.46	225.5	160.0	70.91	3.36
13	74.9	0.32	169.0	124.5	75.81	4.31
14	122.2	0.43	197.0	140.0	54.80	3.42
15	161.0	0.43	225.5	160.0	40.58	3.11

Note: * = Run No. refers to esterification conditions given in Table 5.14

** = Not measurable

5.5.4 Results and Discussions

5.5.4.1 Raw Material Characterization

Dewatered bio-oil derived from centrifugation of the raw bio-oil from palm shell pyrolysis was used for esterification study. The separation of water by centrifugation is more economical than by distillation and the resulting bio-oil demonstrates a slower rate of ageing because centrifugation can be carried out at room temperature (Diebold, 2000). The bio-oil derived from centrifugation showed similar appearances and basic fuel properties to those of bio-oil with water removing by distillation and gave about 50% reduction in viscosity (9.14 cSt at 40°C by centrifugation and 20.38 cSt at 40°C by distillation). Results on chemical structures of the test bio-oils by ^{1}H NMR technique are shown in Figures 5.28 (a) and (b). The chemical structures can be identified as follows; chemical shift at 9.4-10.0 ppm is the groups of aldehydes, at 6.4-8.4 ppm is aromatics, at 5.0-6.4 ppm represents proton of aqueous solution left in the bio-oil, at 3.0-5.0 ppm is esters, ethers or alcohols, at 2.0-3.0 ppm is acids, ketones or alkynes and at 0.8-2.0 ppm is saturated alkanes. When water was removed from the raw oil by distillation compared with by centrifugation, the NMR results of bio-oils (Figures 5.28 (a)) show that the peak at 3.4-3.6 and 9.0-10.0 ppm disappeared and the peak area at chemical shift 0.8-1.5 ppm has increased for ^{1}H spectrum. This indicates the removal of some functional groups such as ethers, alcohols and aldehydes with increasing composition of saturated alkanes when water was removed from the raw bio-oil by thermal distillation.

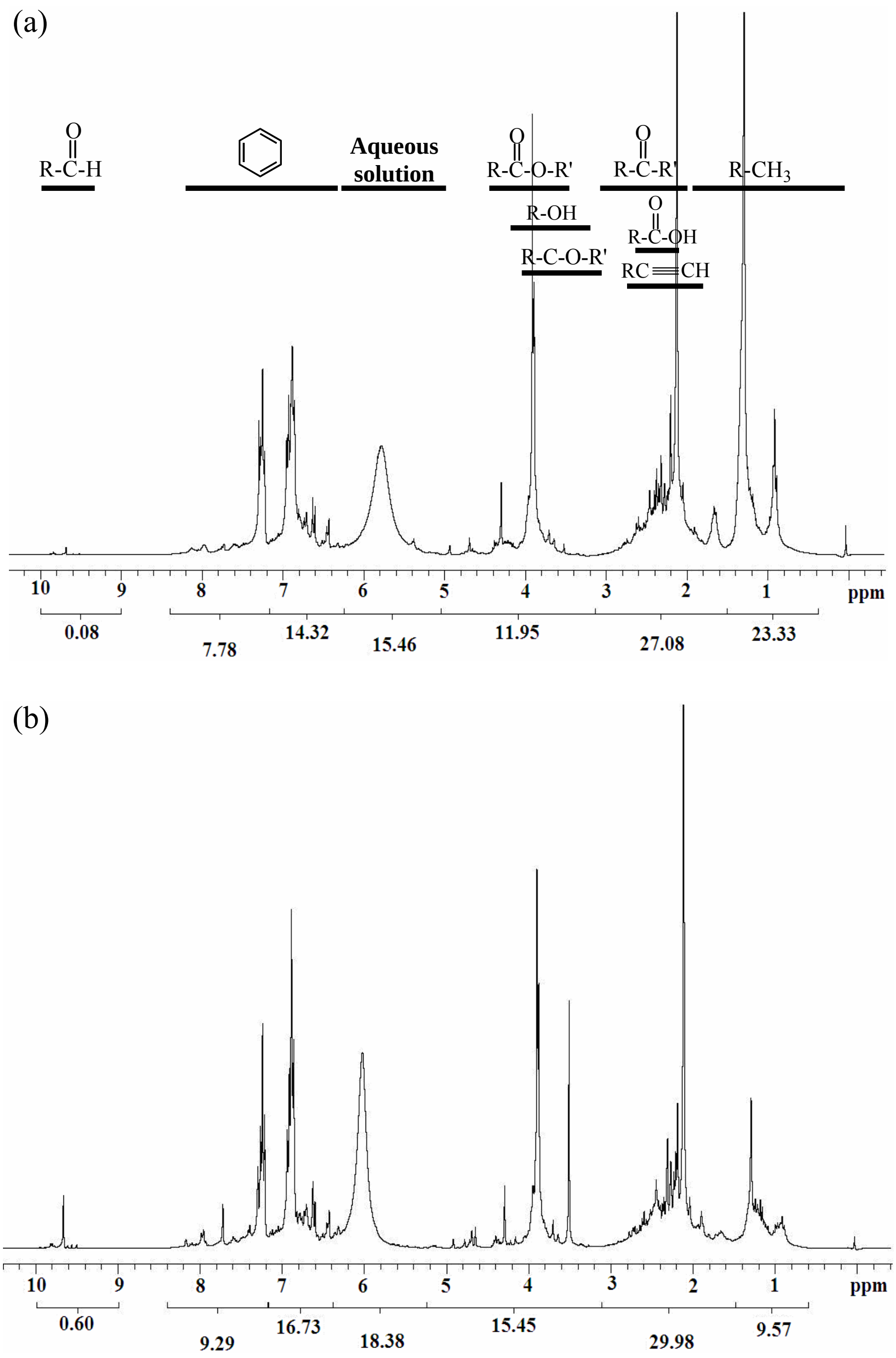

Figure 5.28 ^{1}H NMR spectra of (a) palm shell bio-oil with water removed by distillation (b) palm shell bio-oil with water removed by centrifugation.

5.5.4.2 Effect of Esterification Conditions on Upgraded Bio-oils

The original unreacted bio-oil and alcohol mixture was also analyzed with ^1H NMR in order to compare the spectra results with those of the upgraded bio-oils. Figure 5.29 (a) shows the results from the analysis. If an ester group exists in the solution, NMR analysis will show a sharp high peak at the chemical shift in the range 3.6-5.0 ppm. It is noted, however, that in the same range of chemical shift an unreacted mixture of bio-oil and methanol show a rather broad peak of NMR spectra as displayed in Figure 5.29 (a). The rather broad peak of NMR spectra of pure methanol shown in Figure 5.29 (b) has contributed also to the broad peak appearance of the bio-oil and alcohol mixture, as mentioned earlier.

The effects of esterification conditions including reaction temperature, reaction time, catalyst loading, catalyst type, alcohol type and alcohol to carboxylic acids mole ratio on the reaction conversation and properties of the upgraded oil were studied. ^1H NMR is the technique used to trace the existence of ester groups produced from the esterification reaction for which the NMR spectra occur at chemical shift of 3.6-5.0 ppm. Titration of bio-oil with KOH or $NaHCO_3$ was used to determine the amount of acids left in the upgraded bio-oils, thus enabling the estimation of percent conversion of acids to esters.

The effect of reaction temperature was investigated by studying esterification of the bio-oil and methanol under the following conditions: 3.25:1 mole ratio of methanol to carboxylic acids in bio-oil, reaction temperature from 25-60°C, 5 wt% Amberlyst15 catalyst and reaction time of 24 hr. The results presented in Table 5.15 indicate that the conversion increased with increasing reaction temperature and the highest temperature studied gave the highest esterification conversion. Also as

Figure 5.30 shows, the sharpness of esters spectra at chemical shift 3.6-5.0 ppm is progressively increasing with increasing reaction temperature from 25 to 60°C. Theses results support the increasing conversion of acids in the bio-oil with temperature as previously mentioned.

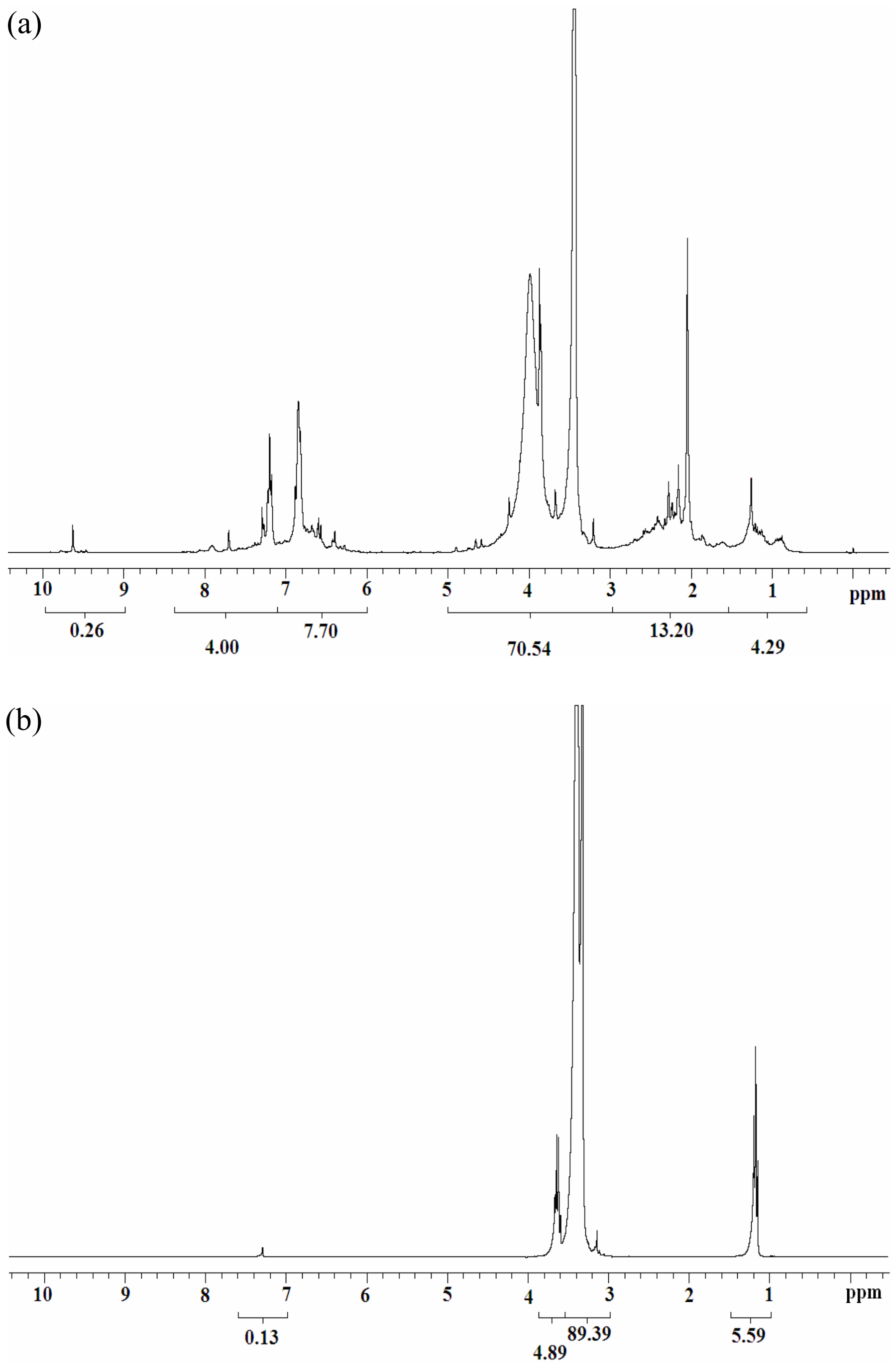

Figure 5.29 ^{1}H NMR spectra of (a) mixture of palm shell oil and methanol (unreacted) with 3.25:1 mole ratio of methanol to carboxylic acids in bio-oil and (b) pure methanol.

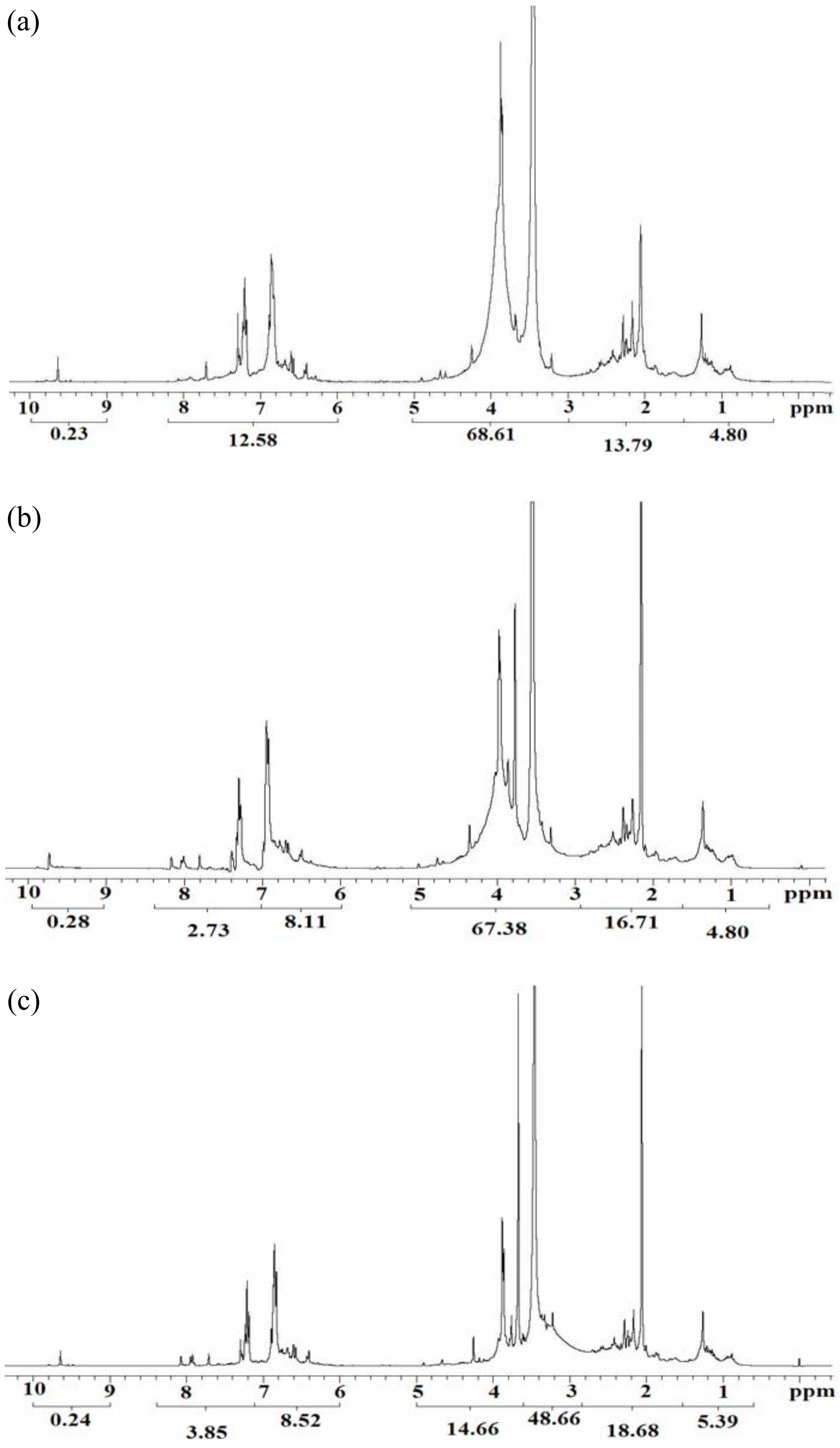

Figure 5.30 ^{1}H NMR spectra of upgraded bio-oils derived from different reaction temperatures of (a) 25°C, (b) 50°C and (c) 60°C (Run no. 1, 2 and 3).

For the effect of reaction time, Table 5.15 and Figure 5.31 show that longer reaction time provided higher esterification conversion for the conditions of 3.25:1 mole ratio of methanol and carboxylic acids in bio-oil, 5 wt% of Amberlyst15 and reaction temperature of 60°C. However, the reaction rate (slop of the curve) decreased with increasing time and finally the conversion approached a relatively constant value after the reaction time of about 12 hr (Figure 5.31). As shown in Figure 5.32, the sharpness of ^{1}H NMR peaks in the range of 3.6-5.0 ppm increased with increasing reaction time, corresponding with the increased reaction conversion. However, almost similar spectra at chemical shift of 3.6-5.0 ppm were observed for reaction times at 12 and 24 hrs, indicating the establishment of chemical reaction equilibrium.

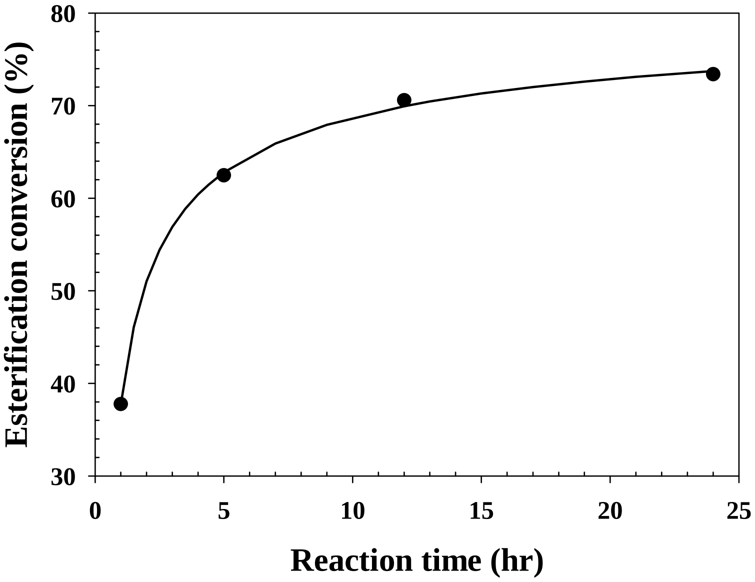

Figure 5.31 Effect of reaction time on conversion of esterification reaction for esterification conditions of 3.25:1 mole ratio of methanol to carboxylic acids in bio-oil, 5 wt% of Amberlyst15 and reaction temperature of 60°C.

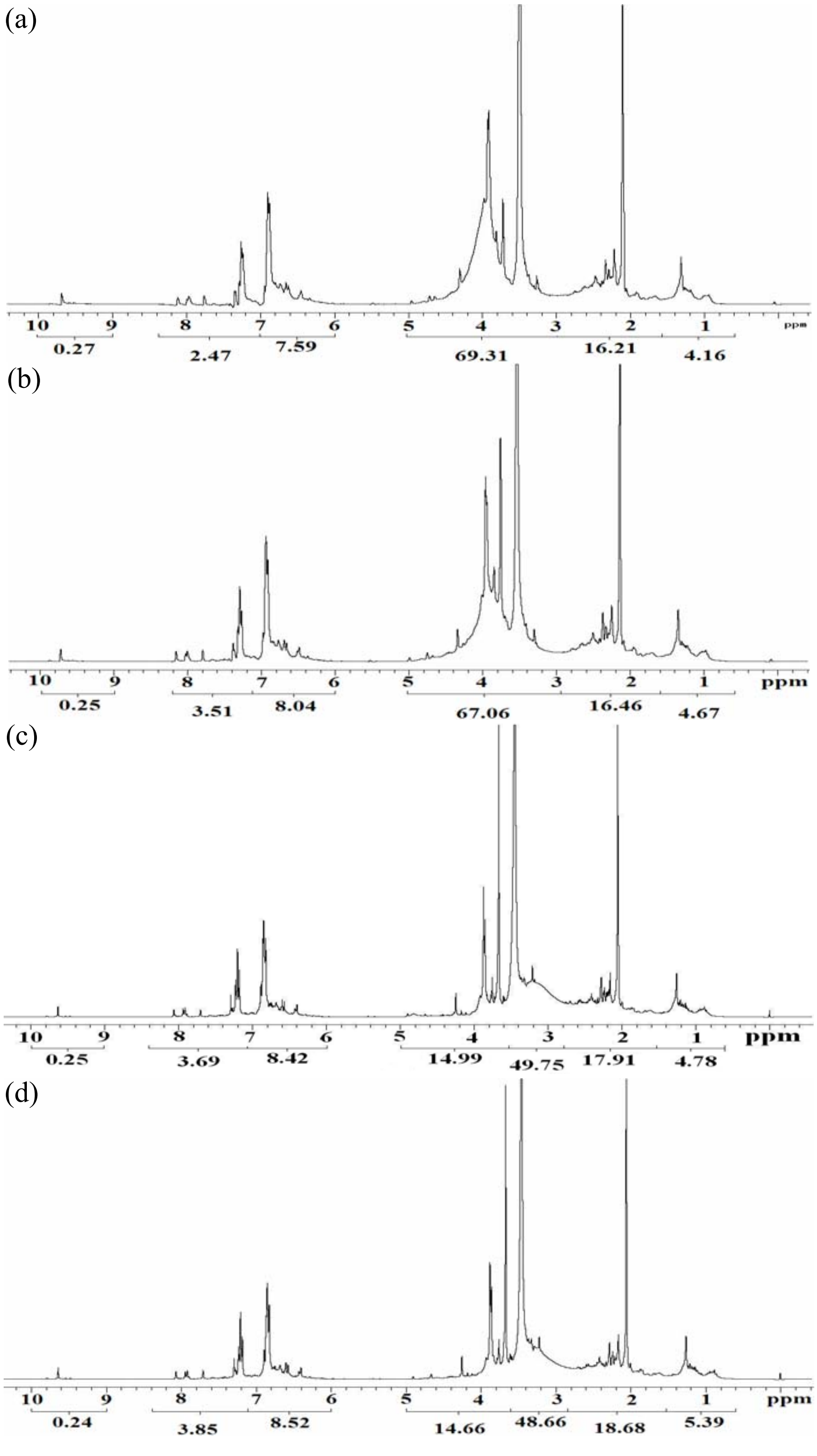

Figure 5.32 ^{1}H NMR spectra of upgraded bio-oils derived from different reaction times of (a) 1 hr, (b) 5 hr, (c) 12 hr and (d) 24 hrs (Run no. 4, 5, 6 and 3).

The effects of catalyst amount and catalyst type on the formation of ester products were investigated for the esterification conditions of 3.25:1 mole ratio of methanol to carboxylic acids in bio-oil, reaction temperature of 60°C and reaction time of 24 hrs. Solid acid catalyst of Amberlyst15 was used for studying the effect of catalyst amount and the results are listed in Table 5.15 and Figure 5.33. It was discovered that the upgraded bio-oil without addition of catalyst gave only 13.13% of esterification conversion and showed similar ^{1}H NMR spectra to that of the original unreacted bio-oil and alcohol mixture (comparing Figure 5.29 (a) and Figure 5.33 (a)). However, the presence of only 5 wt% Amberlyst15 catalyst could provide a 60% increase of conversion compared with the case of without using catalyst and the increase of catalyst amount appeared to increase the conversion. This is observed from Figure 5.33 that the clear sharp peaks of ^{1}H NMR spectra in the range of 3.6-5.0 ppm were obtained with the use of 5-30 wt% Amberlyst15 and the area under the curves tended to increase with increasing the amount of catalyst used.

On the effect of catalyst type, Table 5.15 indicates that the use of 5 wt% of H_2SO_4 gave the maximum conversion of 93.75%, while 30 wt% Amberlyst15 gave lower conversion of 86.87%, even though the H^+ amount of 30 wt% Amberlyst15 is higher than that of 5 wt% of H_2SO_4 (1.41 meq/g oil for 30 wt% Amberlyst15 versus 1.02 meq/g oil for 5 wt% of H_2SO_4). This difference may be attributed to mass transfer limitation inside the pores of Amberlyst15. The reactants must transport to hydrogen ion sites located in macroreticular pore of Amberlyst15 catalyst, while liquid catalyst of H_2SO_4 can readily react with molecules of fatty acids in the bulk liquid phase. It is noted that the spectra at chemical shift of 9.0-10.0 ppm (Figure 5.34) indicates the disappearance of aldehyde group (only 0.02% of area under the curve remained) when 5 wt% of H_2SO_4 was used as the catalyst, whereas the area reduction at this position was observed only when more than 15wt% of Amberlyst15 was used (Figure 5.33). Thus, this finding appears to indicate that active H^+ of catalysts can also decrease aldehyde contents possibly by inducing the side reaction of acetalization (Equation (5.22)). The formation of acetals via this reaction could contribute advantageous effects for both reducing aldehyde content and shifting away the formation of acetaldehyde hydrates (Equation (5.20)) to produce polymeric resins (Equation (5.24)). Furthermore, in this study the effectiveness of used solid catalyst was compared to that of the fresh catalyst. It was found that the reusing of Amberlyst15 catalyst gave lower conversion than that of the fresh catalyst (Table 5.15). It is possible that the used catalyst could have lower amount of active H^+ because it may have lost in the bio-oil during the upgrading reaction. This is supported by the evidence from Table 5.15 which shows that the pH of the bio-oil upgraded by solid catalyst (Run No.3) is lower than that derived from without using catalyst (Run No.7). It should be also observed that the pH value decreased significantly with increasing amount of Amberlyst15 catalyst (Table 5.15). The high acid character of upgraded bio-oil derived from using solid acid catalyst still persist and is a significant problem inherent with this treatment method. This characteristic was also reported for applying other types of solid acid catalysts such as Nafion SAC13 and $40SiO_2/TiO_2\text{-}SO_4^{2}$ (Mahfud *et al.,* 2007; Zhang *et al.,* 2006).

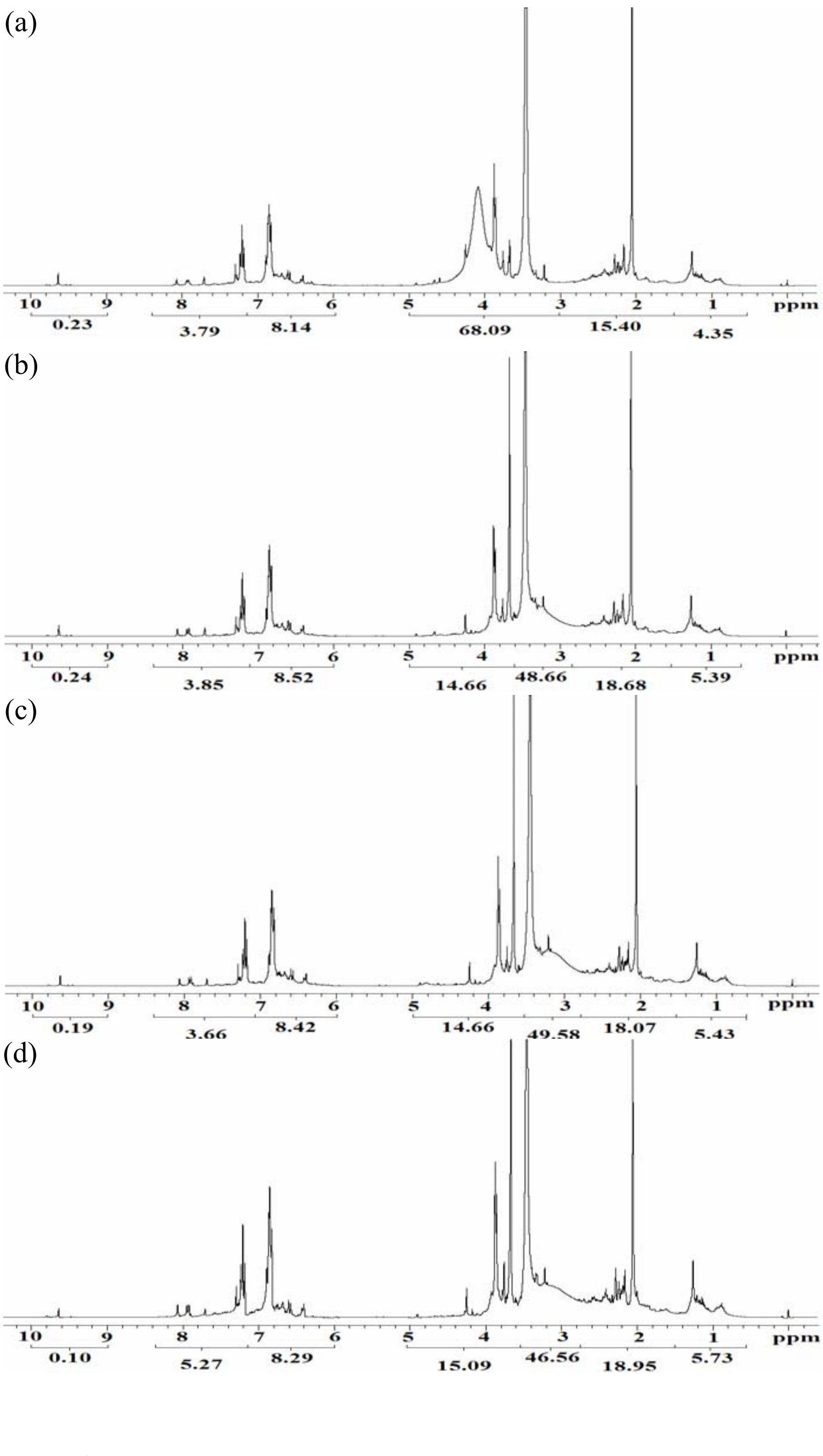

Figure 5.33 ^{1}H NMR spectra of upgraded bio-oils derived from different catalyst amounts (Amberlyst15) of (a) 0 wt%, (b) 5 wt% (c) 15 wt% and (d) 30 wt% (Run no. 7, 3, 8 and 9).

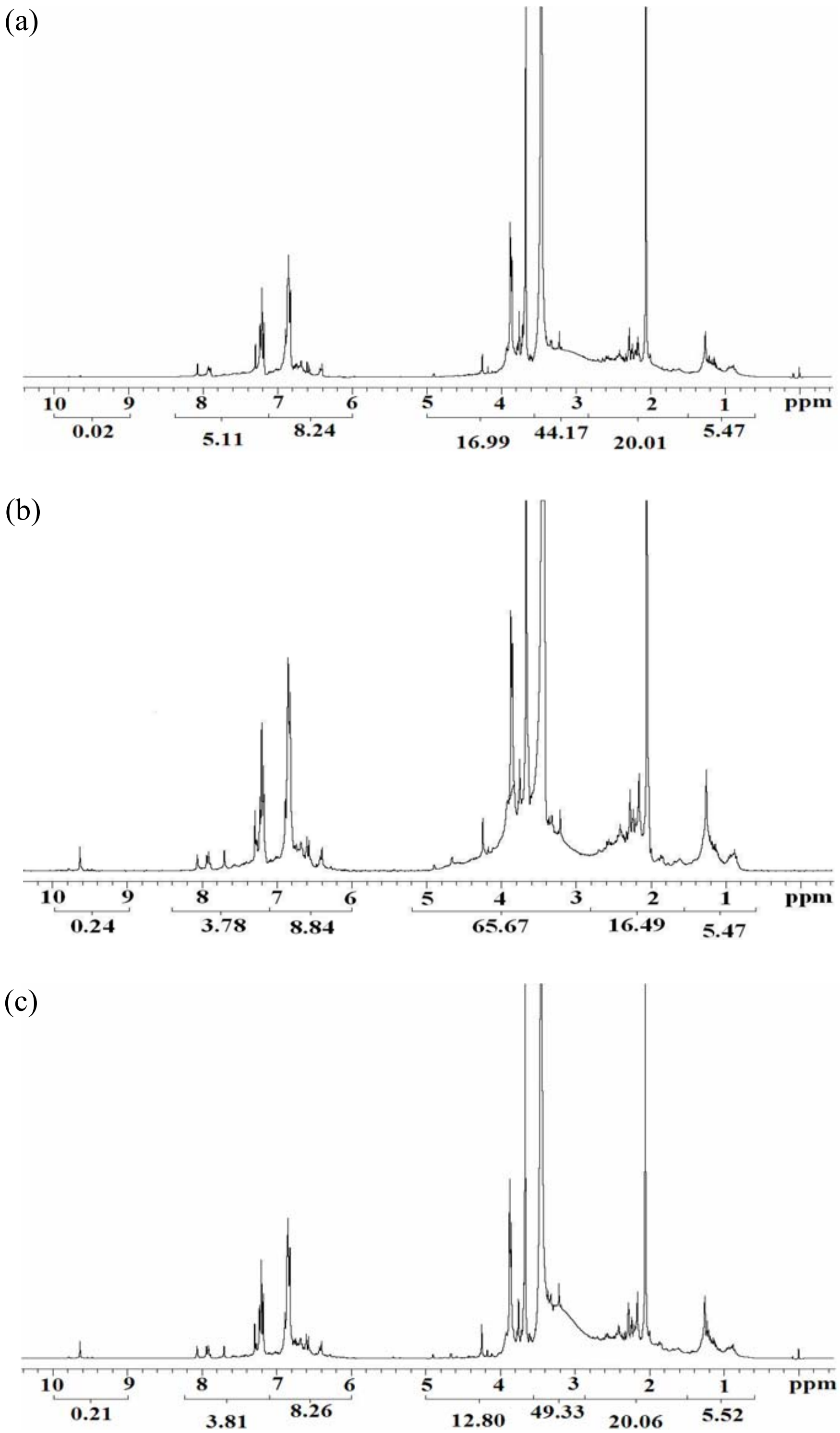

Figure 5.34 ^{1}H NMR spectra of upgraded bio-oils derived from different catalyst types of (a) 5 wt% H_2SO_4 (b) 5 wt% recycled Amberlyst15 and (c) 15 wt% recycled Amberlyst15 (Run no. 10, 11 and 12)

The effects of alcohol content and alcohol type were investigated by studying esterification with 5 wt% of Amberlyst15 at 60°C for 24 hrs. Generally, higher amount of alcohol can shift the esterification reaction in the forward direction to obtain higher conversion (Kirumakki *et al.*, 2006). The results shown in Table 5.15 indicate that increasing alcohol content gave higher esterification conversion but the conversion was increased only 2.42% for a twofold increase of mole ratio of methanol to carboxylic acids. Thus, it may be inferred that the mole ratio of 3.25:1 of methanol to carboxylic acid is probably adequate to achieve reasonably high conversion (~73%) under the condition tested. For the effect of alcohol type, Table 5.15 shows that the bio-oil upgraded using methanol exhibited higher conversion of 73.39% compared with the use of ethanol which gave only 54.80% conversion. This may be ascribed to the effect of the size of alkyl group of alcohol on the reaction rate; higher active reagent of shorter carbon-chain alcohol and greater solubility between this alcohol and the bio-oil could promote a faster reaction (Marchetti and Errazu, 2008). The esterification of bio-oil and ethanol could be operated at a higher temperature to attain higher esterification conversion. The work of Doshi *et al.* (2005) showed that bio-oil derived from fast pyolysis of sewage sludge via esterification with ethanol using H_2SO_4 produced faster reaction rate when the reaction temperature was increased from 50 to 75°C. In addition, it should be noted that the ester group of upgraded oil derived from esterification of palm shell oil and ethanol cannot be directly identified by ^{1}H NMR technique because of the interfering of a major broad peak of the remaining ethanol positioning at chemical shift of 3.6-5.0 ppm (Figures 5.35 (a) and (b)).

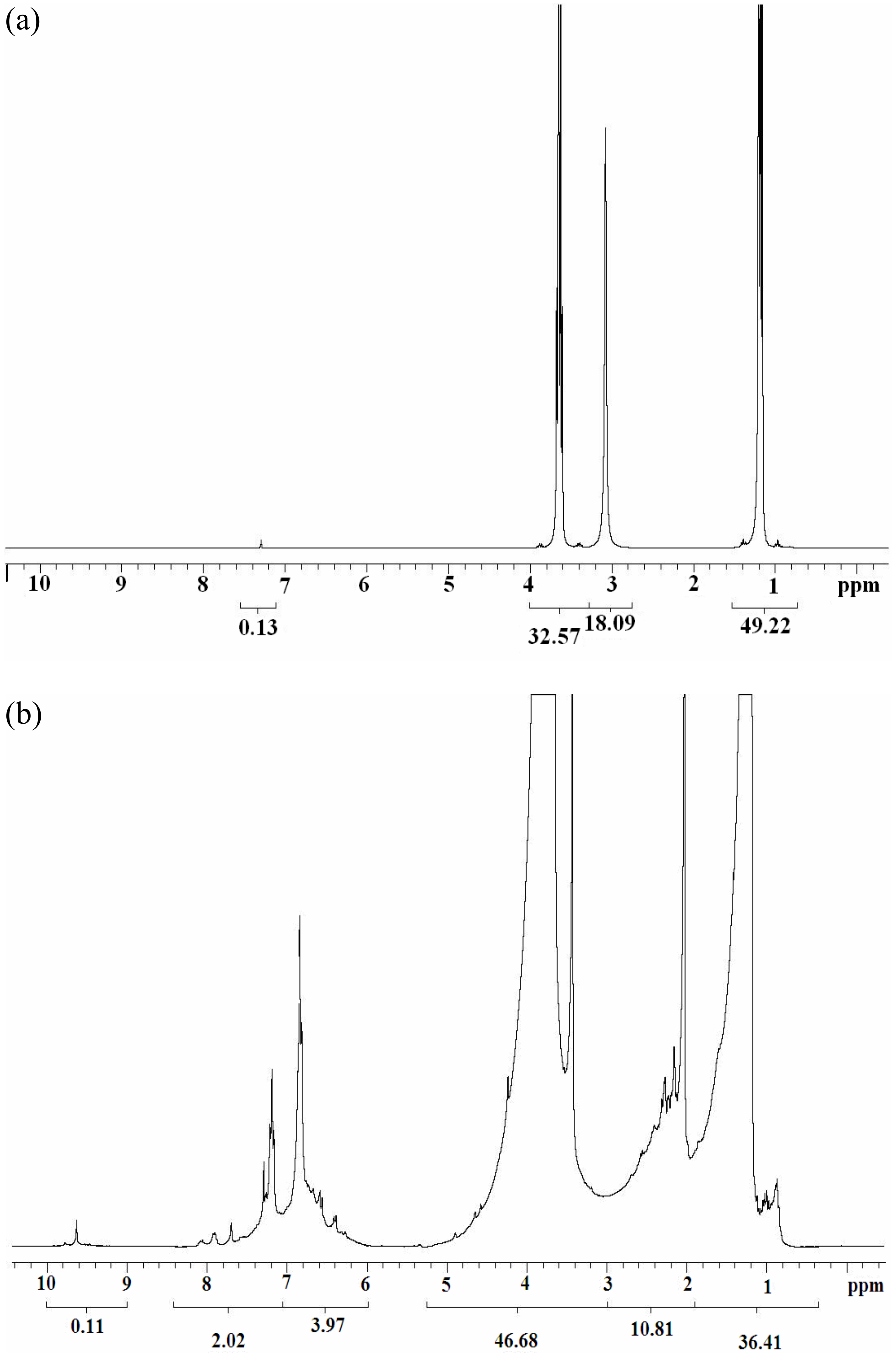

Figure 5.35 ^{1}H NMR spectra of (a) ethanol and (b) upgraded bio-oil for the esterification conditions of 3.25:1 mole ratio of ethanol to carboxylic acids in bio-oil, reaction temperature of 60°C and reaction time of 24 hr (Run No. 14).

Finally, to enhance the esterification conversion, 20 wt% molecular sieve 3A was added to adsorb the produced water in order to shift the reaction forward. The amount of molecular sieve 3A used was calculated based on the amount of water produced from converting 100% acids in the raw bio-oil. However, it was found that the addition of molecular sieve 3A provided less sharp peaks at chemical shift of 3.6-5.0 ppm and with lower conversion than that derived from without adding molecular sieve 3A at the same conditions (Run No. 3 and 15, shown in Table 5.15 and Figure 5.36). This may result from the possible adsorption of methanol molecules by molecular sieve 3A, thus giving less amount of alcohol available for the reaction. Although molecular sieve 3A is commercially used as an adsorbent for drying of liquid alcohol, it was observed experimentally in this work that this adsorbent is capable of alcohol adsorption with the capacity of only 0.3 ml methanol per gram of adsorbent. Thus, this could support the reason of achieving much lower conversion (40.58%) with the addition of molecular sieve 3A.

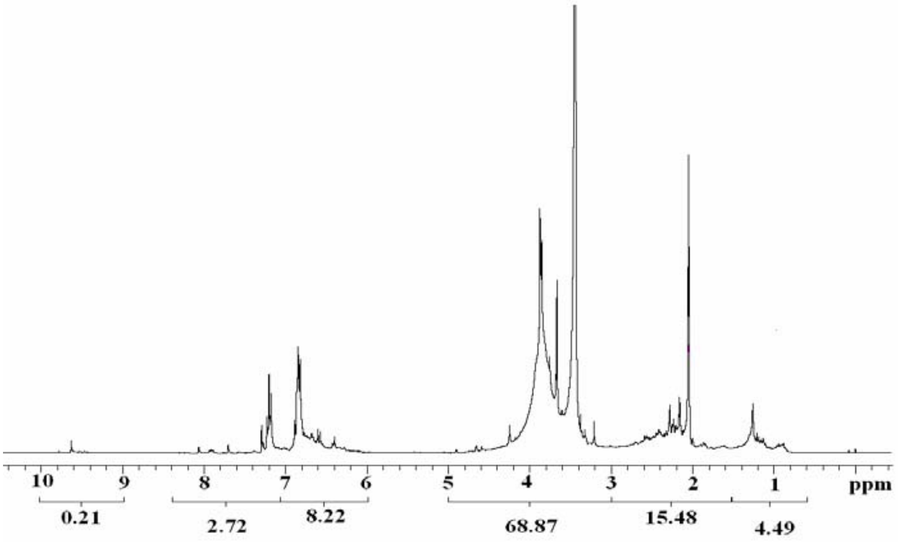

Figure 5.36 ^{1}H NMR spectra of upgraded bio-oils derived from palm shell oil-methanol esterification with addition of molecular sieve 3A (Run no. 15).

5.5.4.3 Fuel Properties of Upgraded Bio-oils

It was previously reported that the presence of alcohol in bio-oil can help stabilizing the bio-oil by four different reactions (Diebold, 2000) including (1) reduction of the reactive aldehydes concentration by converting them to less reactive components such as hemiacetals and acetals, (2) transacetalization of large hemiacetals and acetals to form lower molecular weight hemiacetals and acetals, (3) conversion of organic acids to esters by esterification and (4) transesterification of higher molecular weight esters to form lower molecular weight esters. Based on these positive effects, the upgraded bio-oils were characterized without the removal of remaining alcohol. Four upgraded oils were selected for the measurement of their basic fuel properties and the results are shown in Table 5.16.

It was further found that after esterification, the bio-oils have heating value lower than that of the raw bio-oil, resulting from the presence of remaining alcohol solvent in the products. It was also observed that the use of different alcohol type showed an effect on the heating value of the upgraded bio-oils. Relatively constant values of heating value in the range of 23.10-23.78 MJ/kg were obtained with methanol at different esterification conditions (Run No.3, 7, and 13) and the upgraded bio-oil using ethanol (Run No.14) gave slightly higher value of 25.40 MJ/kg. The upgraded bio-oils improved certain fuel properties i.e., giving lower values of viscosity, ash content, %carbon residue content and pour point. However, the presence of alcohol solvent in the upgraded bio-oils gave unsatisfactory properties of lowering energy density and flash point. The upgraded oils which have lower density caused energy density to be less than that of the raw bio-oil (21.55-25.20 GJ/m^3 for upgraded oils and 28.87 GJ/m^3 for raw bio-oil) and their flash points being in the range 22-35°C, indicating that the use of upgraded oils should require more attention of safety even at room temperature. In addition, the pH of upgraded oils was increased slightly compared with that of the raw oil. It is also noted that the upgraded oils from using Amberlyst15 catalyst (Run No. 3) showed lower pH values than that of upgraded oils without addition of catalyst (Run No. 7) at the same esterification conditions: 3.25:1 mole ratio of methanol to carboxylic acids in bio-oil, reaction temperature of 60°C and reaction time of 24 hr. This is possibly due to the release of active H^+ from Amberlyst15 catalyst into the bio-oils during the course of reaction.

Table 5.16 Fuel properties of raw bio-oil and upgraded bio-oils

Fuel properties	**Methanol**	**Ethanol**	**Dewater palm shell oil**	**Upgraded palm shell oil Run No.**			
				3	**7**	**13**	**14**
Calorific value (MJ/kg)	22.62	28.73	25.55	23.78	23.73	23.10	25.40
Density at 25°C (g/cm^3)	0.791	0.793	1.130	0.985	0.987	0.933	0.992
Viscosity at 40°C (mm^2/s)	0.577	1.22	9.14	1.19	1.27	0.97	1.54
pH	6.63	6.58	2.92	3.31	4.32	4.21	3.42
Ramsbottom carbon residue (wt%)	0.019	0.021	6.35	4.31	4.56	2.93	4.74
Ash (wt%)	-	-	0.089	0.066	0.071	0.038	0.051
Flash point (°C)	11*	14*	88	35	35	22	28
Pour point (°C)	-98.0**	-114.0**	-18	<-20	<-20	<-20	<-20

Note: * = Flash point (Oxford University 2005b; 2008)

** = Freezing point (Oxford University 2005b; 2008)

5.6 Conclusions

Results on studying bio-oil upgrading by three different methods to improve bio-oil characteristics can be concluded as follows.

5.6.1 Rheology and Fuel Properties of Char-Bio-oil Slurries

- On studying time effect during shearing of cassava residue char-raw oil slurry at solid concentrations lower than 30 wt% and shear rates less than 345 s^{-1}, the shear stress remained substantially constant independent of shearing time but at higher solid concentration of 40 wt% and shear rates higher than 345 s^{-1} the shear stress tended to decrease with time and eventually attaining a constant value at a longer time.

- All slurry types derived from different types of char and suspending media can be well described by the power law model with yield stress. Both slurries of cassava pulp residue char-raw oil and palm shell char-aqueous solution showed rheological characteristics of pseudoplastic fluids. However, palm shell char-oil slurry presented a flow transition from pseudoplastic to dilatant behavior at a certain shear rate and cassava pulp residue char-water slurry exhibited the flow curve close to a Newtonian fluid.

- For cassava pulp residue char-raw oil slurry, increase of solid content in range of 10-40 wt% gave higher yield stress, higher consistency index and increasing degree of pseudoplastic and maximum solid loading of this slurry was limited to be less than 40 wt% to maintain the fluid flow character. For palm shell char-oil slurry, increase of solid concentration from 30 to 40 wt% shifted the shear rates at which the flow characteristic was changed from pseudoplastic to dilatant to a lower value of shear rate from 445 to 50 s^{-1}.

- Particle size distribution and mean particle size of char in the slurry showed a significant effect on rheological behavior of cassava pulp residue char-raw oil slurry. The larger mean size offered higher shear stress and viscosity but wider size distribution provided lower values of yield stress and consistency index and exhibiting flow behavior closer to a Newtonian fluid.

- Decrease of shear stress was observed with increasing temperature in range of 15-45°C but slurry temperature showed slight effect on apparent viscosity. It should be noted that maximum temperature for operating cassava pulp residue-bio-oil slurry should be less than 45°C to prevent the evaporation of the suspending medium.

- Fuel properties of char-bio-oil slurries at 30 wt% solid concentration are as follows: density at 25°C, 1.26-1.30 g/cm^3; viscosity at 25°C with shear rate of 100 s^{-1}, 179-351 mPas; pH, 3.54-3.98 and ash content, 3.85-6.64 wt%. Their calorific values are in range of 18.0-31.7 MJ/kg but the calorific value of cassava pulp residue char-water slurry cannot be determined. The increase of solid loading in the slurry contributed to higher values of these fuel properties. For combustion characteristic, the char-bio-oil slurries gave combustion temperature in range 280-560°C with no ignition delay compared with their solid chars.

5.6.2 Phase Behaviors and Fuel Properties of Bio-oil-Diesel-Alcohol Blends

Blending of dewatered palm kernel bio-oil with diesel using alcohol (ethanol or butanol) as a cosolvent is a promising alternative to avoid the problems associated with direct use of palm kernel bio-oil as a fuel. The following conclusions can be drawn from studying phase behaviors and basic fuel properties of binary (bio-oil-alcohol) and ternary (bio-oil-diesel-alcohol) mixtures.

- Alcohol types showed a significant influence on the phase characteristics; palm kernel bio-oil-diesel-butanol system gave larger soluble area than that of palm kernel bio-oil-diesel-ethanol system.
- The blended fuels of these ternary systems gave satisfactory fuel properties in spite of relatively high amounts of alcohol being required for phase stability and use of butanol as a cosolvent showed better characteristics of phase behavior and fuel properties than using ethanol.
- The binary mixture of palm kernel bio-oil and butanol showed also a potentiality as a renewable fuel because it can mitigate some undesirable bio-oil properties and yet giving reasonably high heating value.
- Blended fuels of both binary and ternary systems showed superior properties including lower values of viscosity (1.77-9.21 mm^2/s at 40°C), carbon residue content (1.02-4.66 wt%), ash content (0.016-0.039 wt%) and pour point (<-25 to -6 °C), higher pH value (~6.4) and giving reasonable heating values in range 32.5-41.2 MJ/kg. However, high alcohol content in the blended fuels gave large difference of distillation temperature at low and high amount of distillate volume, with the

marked rising of the distillation curve after the complete distillation of alcohol. This could result in longer warming-up time for the engines.

- Some fuel properties of the blends including heating value, density, ash content and pH could be well described by the Kay's mixing rule, whereas the modified Grunberg-Nissan equation and Andrade equation gave good prediction for mixture viscosities at different temperatures.

- To minimize the amount of cosolvent used, it is suggested that a mixture of miscible solvents such as ethanol-butanol should be tried for ternary system of bio-oil-diesel-alcohol.

5.6.3 Esterification of Bio-Oil and Alcohol by Acid Catalysts

The upgrading of bio-oil (separated oil phase) from palm shell pyrolysis by esterification has led to the following conclusions.

- Under conditions studied, maximum conversion of 93.75% was obtained from the following esterification conditions: 3.25:1 mole ratio of alcohol and carboxylic acids in bio-oil, catalyst amount of 5 wt% H_2SO_4, reaction temperature of 60°C and reaction time of 24 hr. However, under the same conditions, maximum conversion of bio-oil upgraded by 30 wt% Amberlyst15 (a solid catalyst) was about 86.87%.

- Higher reaction temperature in the range of 25-60°C gave higher esterification conversion with an almost linear increase with increasing temperature, while higher reaction time showed higher conversion and approached a constant value after 12 hr of reaction time.

- The use of merely 5 wt% Amberlyst15 catalyst can increase bio-oil conversion by almost six times compared with case of without catalyst and higher conversion was achieved with increasing amount of catalyst. When compared with liquid catalyst of H_2SO_4, higher active H^+ of 30 wt% Amberlyst15 gave lower bio-oil conversion than that achievable with 5 wt% H_2SO_4 having lower H^+ exchange.

- Higher weight ratio of methanol to acids resulted in higher conversion but the increase was only 2.42% when increasing the ratio from 3.25:1 to 6.50:1. When comparing effect of alcohol type, smaller molecule of methanol showed higher conversion than that derived from ethanol, being about 73.39% for methanol and 54.80% for ethanol.

- Addition of 20 wt% molecular sieve 3A to increase reaction conversion gave only 40.58% conversion which was lower than that without addition of molecular sieve 3A at the same esterification conditions.

- The upgraded oils had similar heating values (23.10-25.40 MJ/kg) compared with that of the raw bio-oil but showed improved properties of lower values of viscosities, carbon residue content, ash content and pour point and higher value of pH.

- It should be noted that Amberlyst15 appeared to be an effective catalyst for esterification reaction but it had a weak point of releasing active H^+ during esterification reaction, causing the lowering of pH value of upgraded oil. Thus, a suitable catalyst that has a characteristic of high proton affinity on the support should be a viable alternative for bio-oil upgrading by the process of esterification.

- Two analytical techniques including ^1H NMR and bio-oil titration are proved to be satisfactory for determining conversion of bio-oil by esterification reaction. To further understand the underlying mechanisms of esterification and other side reactions on product compositions, other analytical techniques such as GC-MS should be further carried out.

5.7 References

Anandha Rao, M. (1999). **Rheology of fluid and semisolid foods: Principles and applications**. United State of America: Aspen Publishers.

Benjumea, P., Agudelo, J., and Agudelo, A. (2008). Basic properties of palm oil biodiesel-diesel blends. **Fuel** 87(10-11): 2069-2075.

Benter, M. M., Gilmour, I. A., and Arnoux, L. (1997). Biomass-oil slurry fuels: an investigation into their preparation and formulation. **Biomass and Bioenergy** 12 (4): 253 261.

Bertoli, C., D'Alessio, J., Del Giacomo, N., Lazzaro, M., Massoli, P., and Moccia, V. (2000). Running light-duty DI diesel engines with wood pyrolysis oil. Paper presented at **International Fall Fuels and Lubricants Meeting and Exposition** (SAE paper 2000-01-2975), Baltimore, MD.

Bird, R. B., Stewart, W. E., and Lightfoot E. N. (2002). **Transport phenomena** (2nd ed.). United States of America: John Wiley & Sons.

Bridgwater A. V. (2002). The future for biomass pyrolysis and gasification: status, opportunities and policies for Europe. **ALTENER programme**, Contract No: 4.1030/S/01-009/2001.

Bridgwater, A V. (2003). Renewable fuels and chemicals by thermal processing of biomass. **Chemical Engineering Journal** 91 (2-3): 87-102.

Chiaramonti, D., Bonini, M., Fratini, E., Tondi, G., Gartner, K., Bridgwater, A. V., Grimm, H. P., Soldaini, I., Webster, A., and Baglioni, P. (2003a). Development of emulsions from biomass pyrolysis liquid and diesel and their use in engines-Part 1: emulsion production. **Biomass and Bioenergy** 25: 85-99.

Chiaramonti, D., Bonini, M., Fratini, E., Tondi, G., Gartner, K., Bridgwater, A. V., Grimm, H. P., Soldaini, I., Webster, A., and Baglioni, P. (2003b). Development of emulsions from biomass pyrolysis liquid and diesel and their use in engines-Part 2: tests in diesel engines. **Biomass and Bioenergy** 25: 101-111.

Cheng, J., Zhou, J., Li, Y., Liu, J., and Cen, K. (2008). Effects of pore fractal structures of ultrafine coal water slurries on rheological behaviors and combustion dynamics. **Fuel** 87 (12): 2620-2627.

Cui, L., An, L., and Jiang, H. (2008). A novel process for preparation of ultra-clean superfine coal-oil slurry. **Fuel** (10-11) 87: 2296-2303.

Czernik, S., and Bridgwater, A. V. (2004). Overview of applications of biomass fast pyrolysis oil. **Energy & Fuels** 18: 590-598.

Demirbas, M. F., and Balat, M. (2006). Recent advances on the production and utilization trends of bio-fuels: A global perspective. **Energy Conversion and Management** 47 (15-16): 2371-2381.

Diebold, J. P. (1997). A review of the toxicity of biomass pyrolysis liquids formed at low temperatures. **National Renewable Energy Laboratory**, NREL/TP-430-22739.

Diebold, J. P. (2000). A review of the chemical and physical mechanisms of the storage stability of fast pyrolysis bio-oils. **National Renewable Energy Laboratory,** NREL/SR-570-27613.

Dinger, D. R. (2002). **Rheology for ceramists**. United State of America: Morris Publishing.

Dynamotive Energy Systems Corporation (2009). Technology [On-line]. Available: **http://www.dynamotive.com/.**

Dominguez, M., Pardo, J. I., Gascon, I., Royo, F. M., and Urieta, J. S. (2000). Viscosities of the ternary mixture (2-butanol+n-hexane+1-butylmine) at 298.15 and 313.15 K. **Fluid Phase Equilibria** 169: 277-292.

Doshi, V. A., Vuthaluru, H. B., and Bastow, T. (2005). Investigations into the control of odour and viscosity of biomass oil derived from pyrolysis of sewage sludge. **Fuel Processing Technology** 86 (8): 885-897.

Food and Agriculture Organization of the United Nations (2009). The research progress of biomass pyrolysis processes [On-line]. Available: **http://www.fao.org/docrep/t4470E/t4470e0a.htm.**

Gammon, E. (2002). **General chemistry**. United State of America: Houghton Mifflin Company.

Graham Solomons, T. W. (1997). **Fundamentals of organic chemistry**. United States of America: John Wiley & Sons.

Gu, T. Y., Wu, G. G., Li, Q. H., Sun, Z. Q., Zeng, F., Wang, G. Y., and Meng, X. L. (2008). Blended coals for improved coal water slurries. **Journal of China University of Mining & Technology** 18 (1): 50-54.

Guo, D. H., Li, X. C., Yuan, J. S., and Jiang, L. (1998). Rheological behavior of oil-based heavy oil, coal and water multiphase slurries. **Fuel** 77 (3): 209-210.

He, M., Wang, Y., and Forssberg, E. (2004) Slurry rheology in wet ultrafine grinding of industrial minerals: a review. **Powder Technology** 147 (1-3): 94-112.

Ikura, M., Stanciulescu, M., and Hogan, E. (2003). Emulsification of pyrolysis derived bio-oil in diesel fuel. **Biomass and Bioenergy** 24 (3): 221-232.

Joshi, R. M., and Pegg, M. J. (2007). Flow properties of biodiesel fuel blends at low temperatures. **Fuel**. 86 (1-2): 143-151.

Junming, X., Jianchun, J., Yunjuan, S., and Yanju, L. (2008). Bio-oil upgrading by means of ethyl ester production in reactive distillation to remove water and to improve storage and fuel characteristics. **Biomass and Bioenergy** 32 (11): 1056-1061.

Karabektas, M., and Hosoz, M. (2009). Performance and emission characteristics of a diesel engine using isobutanol-diesel fuel blends. **Renewable Energy** 34 (6): 1554-1559.

Kirumakki, S, R., Nagaraju, N., and Chary, K. V. R. (2006). Esterification of alcohols with acetic acid over zeolites Hβ, HY and HZSM5. **Applied Catalysis A: General** 299: 185-192.

Kyle, B.G (1999). **Chemical and process thermodynamics**. New Jersey: Prentice-Hall Inc International.

Lambert, J. B. and Mazola, E. P. (2003). **Nuclear magnetic resonance spectroscopy: An introduction to principles applications and experimental methods**. New Jersy: Prentice Hall.

Levine, I. N. (2001). **Physical Chemistry** (5th ed.). Boston: McGraw-Hill.

Logos, C., and Nguyen, Q. D. (1996). Effect of particle size on the flow properties of a South Australian coal-water slurry. **Powder Technology** 88 (1): 55-58.

Mahfud, F. H., Melian-Cabrera, I., Manurung, R., and Heeres, H. J. (2007). Biomass to fuels upgrading of flash pyrolysis oil by reactive distillation using a high boiling alcohol and acid catalysts. **Process Safety and Environmental Protection** 85 (B5): 466-472.

Majumder, S. K., Chandna, K., De, D. S., and Kundu, G. (2006). Studies on flow characteristics of coal-oil-water slurry system. **International Journal of Mineral Processing** 79 (4): 217-224.

Marchetti, J. M., and Errazu, A. F. (2008). Comparison of different heterogeneous catalysts and different alcohols for the esterification reaction of oleic acid. **Fuel** 87 (15-16): 3477-3480.

Miller, S. F., and Schobert, H. H. (1993). Effect of fuel particle and droplet size distribution on particle size distribution of char and ash during pilot-scale combustion of pulverized coal and coal-water slurry fuels. **Energy & Fuels** 7 (4): 520-531.

Milne, T. A., Agblevor, F., Davis, M., Deutch, S., and Johnson, D. (1997). A review of the chemical composition of fast pyrolysis oils, in developments in thermal biomass conversion. In Bridgwater, A. V. and Boocock, D. G. B. (eds.) (pp. 409-424). London: Blackie Academic and Professional.

Natarajan, V., and Suppes, G. (1997). Rheological studies on a slurry biofuel to aid in evaluating its suitability as a fuel. **Fuel** 76(14-15), 1527-1535.

Nguyen, D., and Honnery, D. (2008). Combustion of bio-oil ethanol blends at elevated pressure. **Fuel** 87 (2): 232-243.

Oasmaa, A., and Czernik, S. (1994). Fuel oil quality of biomass pyrolysis oils-state of the art for the end users. **Energy & Fuels** 13 (4): 914-921.

Oxford University (2005a). Safety data for 1-butanol [On-line] Available: **http://msds.chem.ox.ac.uk/BU/1-butanol.html**.

Oxford University (2005b). Safety data for methyl alcohol [On-line] Available: **http://msds.chem.ox.ac.uk/ME/methyl_alcohol.html**.

Oxford University (2008). Safety data for ethyl alcohol absolute [On-line] Available: **http://msds.chem.ox.ac.uk/ET/ethyl_alcohol.html**.

Papachristodoulou, G., and Trass, O. (1987). Coal slurry fuel technology. **The Canadian Journal of Chemical Engineering** 65 (2): 177-201.

Poling, B. E., Prausnitz, J. M. and O'Connell, J. P. (2001). **The properties of gases and liquids**. New York: McGraw-Hill.

Reddy, C. V. R., Oshel, R., and Verkade J. G. (2006). Room-temperature conversion of soybean oil and poultry fat to biodiesel catalyzed by nanocrystalline calcium oxides. **Energy & Fuels** 20 (3): 1310-1314.

Schmid, G. H. (1996). **Organic chemistry**. United States of America: Mosby.

Schramm, G. (1994). **A practical approach to rheology and rheometry.** Germany: Gebrueder HAAKE GmbH.

Schramm, L. L. (2005). **Emulsions, foams, and suspensions: Fundamental and application**. Weinheim:Wiley-VCH.

Shin, Y. J., and Shen, Y. H. (2007). Preparation of coal slurry with organic solvents. **Chemosphere** 68 (2): 389-393.

Sittichaitaweekul, Y. (2003). **Fuel properties and the treatment of vegetable oil for the use in a diesel engine**. M.S. Thesis, Suranaree University of Technology, Nakhon Ratchasrima, Thailand.

Skoog, A. D., Holler, F. J., and Crouch, S. R. (2007). **Principles of instrumental analysis**. Canada: Thomsom Brooks/Cole.

Slagle, D. J., Shah, Y. T., Kllnzlng, G. E., and Walters, J. G. (1978). Settling of coal in coal-oil slurries. **Industrial and Engineering Chemistry Process Design and Development** 17 (4): 500-504.

Soriano Jr, N. U., Venditti, R., and Argyropoulos, D. S. (2009). Biodiesel synthesis via homogeneous Lewis acid-catalyzed transesterification. **Fuel** 88 (3): 560-565.

Stamatov, V., Honnery, D., and Soria, J. (2006). Combustion properties of slow pyrolysis bio-oil produced from indigenous Australian species. **Renewable Energy** 31: 2108-2121.

Steffe, J. F. (1996). **Rheological methods in food process engineering** (2nd ed.). United State of America: Freeman Press.

Tangsathitkulchai, C. (1987). **The effect of slurry density and rheology on wet grinding characteristics in a tumbling ball mill**. Ph.D. Dissertation, The Pennsylvania State University.

Tanner, R.I. (2000). **Engineering rheology** (2nd ed.). United State of America: Oxford University.

Wiggs, M. (2009). Titrations [On-line] Available: **http://www.chemistry.nmsu.edu/studntres/chem116/notes/titrations.html**.

Xu, R., He, Q., Cai J., Pan, Y., Shen, J., and Hu, B. (2008). Effects of chemicals and blending petroleum coke on the properties of low-rank Indonesian coal water mixtures. **Fuel Processing Technology** 89 (3): 249-253.

Zhang, Q., Chang, J., Wang T., and Xu, Y. (2006). Upgrading bio-oil over different solid catalysts. **Energy & Fuels** 20 (6): 2717-2720.

Zhang, Q., Chang, J., Wang, T., and Xu, Y. (2007). Review of biomass pyrolysis oil properties and upgrading research. **Energy Conversion and Management** 48 (1): 87-92.

CHAPTER VI

EFFECTS OF GASIFYING CONDITIONS AND BED MATERIALS ON FLUIDIZED-BED STEAM GASIFICATION OF WOOD BIOMASS

6.1 Abstract

The effect of steam gasification conditions on products properties was investigated in a bubbling fluidized bed reactor, using larch wood as starting material. For bed material effect, calcined limestone and calcined waste concrete gave high content of H_2 and CO_2, while silica sand provided high content of CO. At 650°C, calcined limestone was proved to be most effective for tar adsorption and showed high ability to adsorb CO_2 in bed. However, at 750°C it could not capture CO_2 but still gave the highest cold gas efficiency (%LHV) of 79.61% and lowest tar emission of 3.23% or 10.03 g-carbon/Nm^3 of produced gas. Calcined waste concrete was reasonably effective in the steam gasification process, giving high cold gas efficiency of 68.46% with moderately higher tar emission of 9.62% or 38.75 g-carbon/Nm^3 of produced gas at 750°C. Biomass pyrolysis under N_2 atmosphere using calcined limestone as the bed material gave about half of gas products, lower H_2/CO ratio and higher tar content as compared with steam gasification. Combined use of calcined limestone and calcined waste concrete with equal proportion contributed relatively same gas composition, gas yield and cold gas efficiency as those of calcined limestone, but

showed less attrition, sintering, and agglomeration propensities similar to the use of calcined waste concrete alone.

6.2 Introduction

Gasification is an attractive technology to convert carbonaceous materials to a combustible or synthetic gas. It has an ability to produce consistent products for the generation of electricity and the manufacturer of chemicals and transportation fuels. In addition, this process offers advantages over combustion process including giving lower emission of sulfur, nitrogen oxides and particulates and producing very less amount of furan and dioxin compounds (Rezaiyan and Cheremisinoff, 2005). Therefore, it is interesting to apply this process for the conversion of biomass to a potential clean energy source. This work focused on the development of gasification process to give high gas yield and cold gas efficiency and minimum emission of tar components via steam gasification of biomass (larch). Waste concrete, which is a disposed material containing CaO in the form of calcium silicate, calcium aluminate, and tetracalcium aluminoferrite, was proposed to be used as the bed material for tar adsorption and CO_2 capture to give high yield of fuel gas. The effects of gasification conditions including types of bed material (silica sand, calcined limestone and calcined waste concrete), temperature (650 and 750°C) and gasifying agents (steam and N_2) on gasification products were investigated. Analytical techniques of thermogravimetric analysis (TGA), X-ray diffraction (XRD) and scanning electron microscope (SEM) were used to investigate CO_2 adsorption and physical deterioration of bed material at the end of gasification operation. In addition, the combined use of calcined limestone and calcined waste concrete as a new bed material in the steam gasification process was also studied.

6.3 Literature Reviews

6.3.1 Biomass Gasification

It is well recognized that gasification is a viable route for converting biomass to simple fuel gases. The gases produced can be utilized directly as fuels for electricity and power generation or as chemical feedstocks for manufacturing methanol, dimethyl ether, Fischer-Tropsch oils, etc (Han and Kim, 2008; McKendry, 2002; Wei *et al.*, 2007). Main chemical reactions of biomass gasification are typically shown as in Equations (6.1)-(6.13) (Florin and Harris, 2006; Mahishi and Goswami, 2007; Sutton *et al.*, 2001; Wang *et al.*, 2008; Xu *et al.*, 2005).

$$\text{Biomass} \rightarrow \text{char}+H_2+CO+CO_2+CH_4+C_nH_m+\text{Tars}+\ldots, \qquad \Delta H_{298} > 0 \quad (6.1)$$

$$C+0.5O_2 \rightarrow CO, \qquad \Delta H_{298} = -111 \text{ kJ/mol} \quad (6.2)$$

$$CO+0.5O_2 \rightarrow CO_2, \qquad \Delta H_{298} = -254 \text{ kJ/mol} \quad (6.3)$$

$$H_2+0.5O_2 \rightarrow H_2O, \qquad \Delta H_{298} = -242 \text{ kJ/mol} \quad (6.4)$$

$$C+CO_2 \rightarrow 2CO, \qquad \Delta H_{298} = +172 \text{ kJ/mol} \quad (6.5)$$

$$C+2H_2 \rightarrow CH_4, \qquad \Delta H_{298} = -75 \text{ kJ/mol} \quad (6.6)$$

$$C+H_2O \rightarrow CO+H_2, \qquad \Delta H_{298} = +131 \text{ kJ/mol} \quad (6.7)$$

$$C+2H_2O\rightarrow CO_2+2H_2, \qquad \Delta H_{298} = +100 \text{ kJ/mol} \qquad (6.8)$$

$$CH_4+H_2O \rightarrow CO+3H_2, \qquad \Delta H_{298} = +206 \text{ kJ/mol} \qquad (6.9)$$

$$CH_4+2H_2O \rightarrow CO_2+4H_2, \qquad \Delta H_{298} = +165 \text{ kJ/mol} \qquad (6.10)$$

$$CO+H_2O\rightarrow CO_2+H_2, \qquad \Delta H_{298} = -41 \text{ kJ/mol} \qquad (6.11)$$

$$C_nH_m+nH_2O\rightarrow nCO+ (n+\frac{1}{2} m)\ H_2, \qquad \Delta H_{298} >0 \qquad (6.12)$$

$$\text{Tars}+ H_2O \rightarrow H_2+CO_2+CO+\text{lower hydrocarbons}+\ldots, \qquad \Delta H_{298} >0 \qquad (6.13)$$

6.3.2 Effect of Gasification Conditions

Compositions of gases produced from the gasification process are governed by operating conditions including reaction temperature, pressure, gasifying medium, type and amount of catalyst, particle size of biomass and catalyst (McKendry, 2002).

6.3.2.1 Gasification Temperature

Temperature is a significant factor in thermal conversion processes. Previous works (Franco *et al.*, 2003; Wei *et al.*, 2007) showed that increasing of temperature gave higher gas yields and lower contents of char and tar. Franco *et al.* (2003) has proposed three reactions for the increase of gas yield with increasing temperature; pyrolysis reaction, endothermic reaction of char gasification and steam reforming and cracking of hydrocarbon and tars. Moreover, the gas product distribution also depends on the reaction temperature. At low gasification temperature, the exothermic reaction favors the formation of reaction products, while at the high temperature the reactants are dominantly formed in endothermic reactions. For example, for the endothermic reactions of methane/steam reforming (Equations (6.9) and (6.10)), it was reported that the amount of H_2 increased and CH_4 decreased with increasing temperature in the range of 300-900°C (Franco *et al.*, 2003; Lv *et al.* 2004; Moghtaderi, 2007).

6.3.2.2 Particle Size of Biomass and Catalyst

Particle sizes of both biomass and catalyst play an important role on product gas quality. It has been suggested that the particle size of feedstock material should be in the order of 10-20% of hearth diameter (McKendry, 2002). A larger size can form bridges which obstruct the flow of feedstock, whereas a smaller size can clog and lead to high pressure drop causing shutting down of the system. Lv *et al.* (2004) found that higher values of gas yield, calorific value of gas product and carbon conversion efficiency were obtained with decreasing particle size of biomass. Smaller particle size of biomass gives better advantages of larger surface area, shorter diffusion path, and fast heating rate, thus the rate limiting step is mainly controlled by reaction kinetic. For the effect of catalyst size, smaller particle size of olivine and dolomite catalyst (0.25-0.42 mm) could produce higher gas yield and higher syngas contents than that derived from larger size of catalyst (0.42-0.84 mm) (Hu *et al.*, 2006).

6.3.2.3 Gasifying Agent

Gasifying agents affects strongly the compositions and colorific value (CV) of gas products (Hu *et al.*, 2006; Mahishi *et al.*, 2007). The use of hydrogen gas as a gasifying agent produces high CV (40 MJ/Nm^3) of gas product, whereas medium CV (12-18 MJ/Nm^3) and low CV (4-6 MJ/Nm^3) are obtained from using oxygen, steam and air or steam/air, respectively (Mahishi *et al.*, 2007). In addition, the gasifying agent should be so selected to suit individual process because it gives different advantages and disadvantages. Using air as a gasifying medium gives lower operating cost but low heating value gas is obtained due to the dilution of nitrogen in air. The use of oxygen provides syngas of medium heating value but a large investment cost for oxygen production is required. For steam gasification, it needs more heat supply because of endothermic reaction of water gas reaction (Equations (6.7) and (6.8)) but it gives the advantage of easy separation of excess steam by condensation (Devi *et al.*, 2003; McKendry, 2002). In addition, this process is an attractive process for producing H_2-rich gas and reducing undesirable products consisting of tar, char and coke on the catalyst (Franco *et al.*, 2003; Ross *et al.*, 2007; Taralas and Kontominas, 2006).

6.3.2.4 Catalyst Type

The significant parameter that affects the gas quality from gasification processes is indeed the catalyst type. Sutton *et al.* (2001) has given criteria for assessing the effectiveness of catalysts. They are effective tar removal, capability of generating a suitable syngas ratio, resistance to deactivation as a result of carbon fouling and sintering, simple regeneration, and low price. Catalysts used in gasification processes are divided into two classes including mineral and synthetic catalysts (Abu El-Rub *et al.*, 2004). Calcined rocks are the mineral catalysts that contain alkaline earth metal oxides. Simell *et al.* (1992) have classified them based on CaO/MgO ratio; limestone (>50), dolomitic limestone (4-50), calcite dolomite (1.5-4) and dolomite (1.5). They found that improvement of the activity of these rocks was achieved by increasing the Ca/Mg ratio, decreasing the grain size, and increasing the active metal content such as iron. The most commonly used calcined rock catalyst is dolomites (Abu El-Rub *et al.*, 2004; Devi *et al.*, 2003). Dolomites are most active in acting as a primary catalytic bed for the removal of heavy hydrocarbons prior to the reforming of the lighter hydrocarbons to produce syngas (Devi *et al.*, 2003; Hu *et al.*, 2006). Olivine was reported to eliminate tar as effectively as dolomite but its attrition resistance is higher than that of dolomite (Rapagná *et al.*, 2000). Clays minerals can reduce tar quite effectively as they contain strong acid sites and have suitable pore diameters (Abu El-Rub *et al.*, 2004). In addition, it was noted that the reduction of iron oxide (Fe_2O_3) in clay to the more reactive form of magnetite (Fe_3O_4) can reduce C_2-C_3 content emissions during air/steam gasification of biomasses (Ross *et al.*, 2007). For synthetic catalysts, alkali catalysts (Li, Na, K, Rb, Cs and Fr) can increase the rate of gasification dramatically and also reduce tar content in the gas product. However, the disadvantages associated with this type of catalyst are the difficulty in recovery, high cost and agglomeration problem at high temperatures (Abu El-Rub *et al.*, 2004; Sutton *et al.*, 2001). For transition metal-based catalysts, nickel catalyst has been known as the most important catalyst in hot gas cleaning processes. It is sufficiently active to remove tar and improve the content of syngas and less expensive than noble metal catalysts such as Ru, Pt, and Rh. Deactivation of the nickel catalysts are mainly due to carbon deposition and nickel particle growth. Char is an attractive synthetic catalyst due to its low price, being the direct by-product from gasification processes. Char has ample catalytic activity to eliminate tar but it can be deactivated by coke formation and loss of char mass in steam and dry reformation reactions (Abu El-Rub *et al.*, 2004).

6.3.3 H_2 Production Coupled with Simultaneous Capture of CO_2 for Steam Gasification Process

Hydrogen is an important feedstock material in various processes such as electronics industry, ammonia manufacturing, petroleum refining and petrochemical production (Saxena *et al.*, 2008). The hydrogen content required for ordinary synthesis process, such as methanol and fuel hydrogen syntheses in terms of H_2/CO stoichiometric mole ratio should be greater than 2 (Kumabe *et al.*, 2007). As mentioned previously, steam gasification has a merit of producing high H_2 content and low amounts of tar and char with decreasing rate of coke formation on catalysts (Franco *et al.*, 2003; Rapagná *et al.*, 2002; Ross *et al.*, 2007; Taralas and Kontominas, 2006). However, the undesired component of CO_2 is also simultaneously generated during steam gasification process. To enhance the efficiency of steam gasification, considerable efforts have been devoted to produce high yield of H_2 by simultaneous capture of CO_2. It has been reported (Florin and Harris, 2006) that the CaO introduced could capture CO_2 via Equation (6.14) during gasification reaction, thus shifting the equilibrium reactions of the water-gas reaction by Equation (6.8), methane reforming by Equation (6.10) and water-gas shift reaction by Equation (6.11) to promote a H_2-rich gas product. Moreover, CaO could act as a catalyst to eliminate tars in the gas product by Equation (6.13) (Mahishi and Goswami, 2007; Simell *et al.*, 1992). The chemical reaction involving the capture of CO_2 by CaO is

$$CaO + CO_2 \rightarrow CaCO_3 \qquad \Delta H_{298} = -170.5\ \text{kJ/mol} \quad (6.14)$$

Lin *et al.* (2002; 2006); Sato *et al.* (2003) have developed HyPr-RING (hydrogen production by reaction-integrated novel gasification) which used calcium oxide (CaO) and/or calcium hydroxide ($Ca(OH)_2$) as the CO_2 adsorbent.

However, this process had to be operated at a high steam pressure. From the limitations of capital and operating costs for high pressure processes, hydrogen production with CO_2 capture at atmospheric pressure should be more desirable. Hughes *et al.* (2005) have shown that at atmospheric pressure, the optimum temperature for carbonation of CaO should be in the range 650-750°C. Furthermore, the capability of $CaCO_3$ formation at the respective temperature depended on CO_2 partial pressure; CO_2 can be best adsorbed at a suitable partial pressure for a given system temperature (Xu *et al.*, 2005).

It should be noted that CaO is an attractive material that can play the combined roles of catalyst and adsorbent in a steam gasification process. There are several CaO containing materials such as calcined limestone, calcite, dolomite, wallastonite, and blast furnace slag. Limestone is a commonly used material in the gasification process and CO_2 adsorption. However, it was reported that there were particle attrition and deactivation problems for long operation time and at temperatures higher than 650°C (Florin and Harris, 2008). In this study, we propose to use waste concrete as another potential material in a steam gasification process. Because of its being a material left for disposal after the concrete structures such as buildings, bridges, dams, road surfaces are demolished and containing active composition of CaO in the forms of tricalcium silicate ($3CaO \cdot SiO_2$), dicalcium silicate ($2CaO \cdot SiO_2$), tricalcium aluminate ($3CaO \cdot Al_2O_3$) and tetracalcium aluminoferrite ($4CaO \cdot Al_2O_3 \cdot Fe_2O_3$) (Department of Materials Science and Engineering, University of Illinois Urbana-Champaign, 2008; Mindess *et al.*, 2003), thus it is very attractive to use this waste material as an effective bed material in a fluidzed-bed gasifier.

6.4 Materials and Methods

6.4.1 Raw Materials

Biomass feedstock used in this study was larch, which is one species of coniferous tree classified in the genus Larix of the family Pinaceae. Larch was supplied by Kuzumaki-ringyo Co., Ltd. in the form of pellet (0.7 cm in diameter and 4.0 cm long). It was milled, sieved to the size fraction of 250-600 µm (20x60 mesh) and packed into a cellulose capsule (Matsuya Corporation: size no. 3 and weighing 0.05 g). Four alumina balls (2 mm in diameter) were also put inside the cellulose capsule to make the capsule sufficiently heavy to sink quickly downward in the fluidized bed after being fed into the gasifier, thus avoiding overbed gasification of the biomass. The larch pellet and the cellulose capsule were analyzed for their elemental compositions (A JM10 Micro Corder-CHN analyzer: J-Science Lab Co., Ltd.), proximate analysis for moisture content (ASTM D2867-95), volatile content (ASTM D5832-95), ash content (ASTM D2866-94) and fixed carbon content (by difference), and calorific values (Gallenkamp Bomb Calorimeter: Weiss Gallenkamp Ltd.).

Silica sand, limestone and waste concrete were used as bed materials in this study. Silica sand and limestone were acquired from Toyoura Keiseki Kogyo Co., Ltd. and Chichibu lime industry Co., Ltd., respectively. The waste concrete abandoned from remnants of the residential structures was received from a waste recycling company (Jobu eco-clean Co., Ltd.). These bed materials were crushed and sieved to obtain the particle size in the range of 150-250 µm (60x100 mesh). In addition, for limestone and waste concrete, they were further calcined at the temperature of 900°C for 3 hrs prior to running the gasification experiments.

Apparently, there was no observed change in the particle sizes of the bed materials after the calcination treatment. The physical properties of bed materials including particle density, pore volume, and surface area, were analyzed by a mercury porosimeter (Pore Sizer 9310: Micromeritics). Chemical compositions of the bed materials were identified and quantified by inductively coupled plasma emission spectroscopy (ICP-ES) (ICPS-7500 Sequential plasma spectrometer: Shimadzu Corporation).

6.4.2 Biomass Gasification

Biomass gasification was performed in a fluidized bed gasifier at atmospheric pressure. Figure 6.1 shows the schematic diagram of the experimental apparatus. Each bed material (125 g of calcined limestone, 125 g of calcined waste concrete, 125 g of a 50: 50 wt% mixture of calcined limestone and calcined waste concrete, and 225 g of silica sand) was packed to a height of 8.0 cm inside a heated fluidized bed column made of stainless steel pipe (4.2 cm I.D. and 57.5 cm high). A mixture of 85 vol% steam and 15 vol% N_2 was introduced into the outer stainless steel pipe, and then flowed upwardly through the distributor (a sintered porous plate) with the superficial gas velocity of about five times the minimum fluidizing velocity ($U_0 = 5U_{mf}$) to ensure intense mixing and uniform bed temperature. The minimum fluidizing velocities for various gasification conditions were estimated by both visual observation and the traditional pressure drop-velocity diagram measured at the gasification temperatures. When the system was heated from room temperature to the desired gasification temperature at 650 or 750°C, capsules containing biomass were dropped one by one into the gasifier through the nitrogen purged lockhopper at the rate of 0.21 g/min for a total of 3 g of biomass. In all experimental runs the total reaction time was 60 min. Over the course of steam gasification, the product gases passed through two tar trapping tubes packed with 2 mm of alumina balls and maintained at 200°C and 100°C, respectively. Subsequently, steam and tar of some light molecular weights were condensed in the three bottles connected in series. A volume of 300 cm^3 of distilled water was filled in each bottle and the temperature was controlled at 0-5°C. Non-condensable gases were collected in teflon sample bags for subsequent gas composition analysis. The experimental gasification conditions used are listed in Table 6.1.

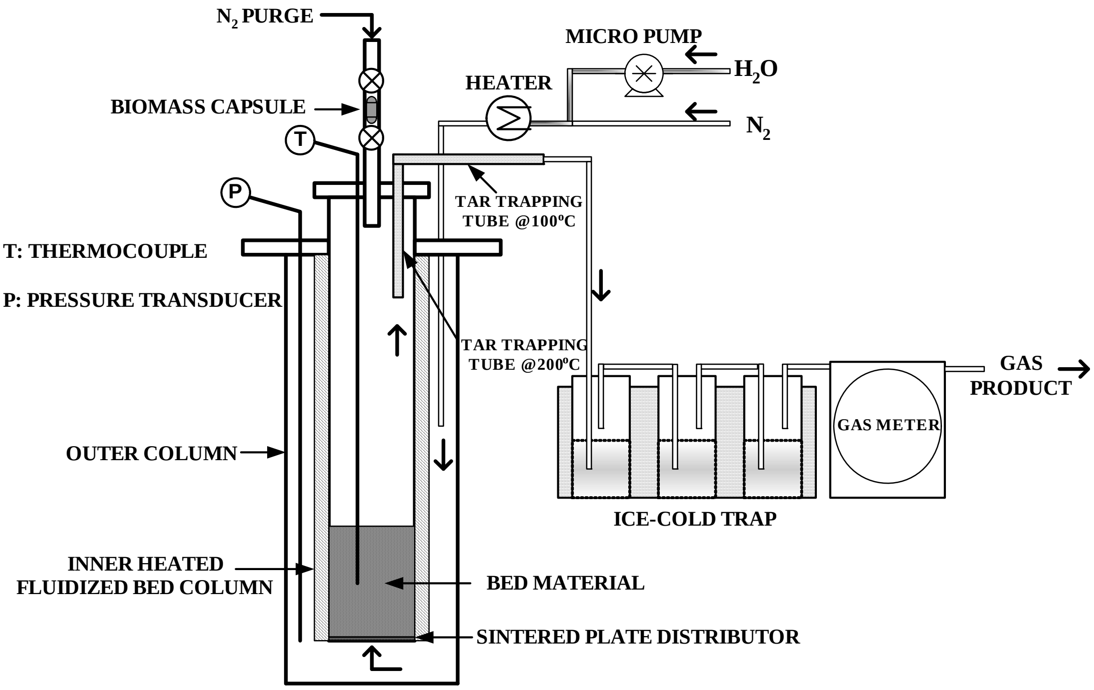

Figure 6.1 Experimental fluidized-bed gasification system.

Table 6.1 Experimental conditions used in fluidized-bed steam gasification of biomass.

Run No.	**1**	**2**	**3**	**4**	**5**	**6**	**7**
Bed material	Silica sand	Calcined limestone	Calcined waste concrete	Calcined limestone (100%N_2)	Calcined limestone	Calcined waste concrete	Mixed bed material*
Temperature (°C)	650	650	650	750	750	750	750
Steam (vol%)	85	85	85	-	85	85	85
Minimum fluidizing velocity : U_{mf} (m/s)	0.0216	0.0197	0.0203	0.0147	0.0179	0.0184	0.0181
Superficial gas velocity : U_0 (m/s)	0.1016	0.0997	0.1003	0.0947	0.0979	0.0984	0.0981
Biomass feed rate (g/min)	0.21	0.21	0.21	0.21	0.21	0.21	0.21
Total feedstock (larch wood and capsule) (g)	3.00	3.00	3.00	3.00	3.00	3.00	3.00
Bed height (cm)	8.0	8.0	8.0	8.0	8.0	8.0	8.0

Note: * = 50:50 wt% mixture of calcined limestone and calcined waste concrete

6.4.3 Product Analyses

After the gasification test was completed, total gas product collected was analyzed by Micro GC (Agilent 3000: Agilent Technology) with a thermal conductivity detector. The micro GC consists of two independent capillary columns of PoraPLOT Q for CO_2, C_2H_4 and C_2H_6 and Molecular Sieve 5A with PoraPLOT U pre-column for H_2, O_2, N_2, CH_4 and CO. Knowing the product gas compositions and the volume collected, the cold gas efficiency (%LHV) can be computed as the percentage ratio of lower heating value (LHV) of the gas product and that of the starting feedstock.

Char (250-650 μm) and the bed material (150-250 μm) were first separated by careful hand sieving using a 60 mesh (250 μm) screen. Char retaining on the screen with a small amount of bed material adhering on the char particles were weighed and ground to fine sizes and its total carbon content was determined using a CHN analyzer (JM10 Micro Corder: J-Science Lab). Materials passing the screen which consisted mainly of the bed material plus little amount of fine char particles were distributed uniformly on a tray and about 100 g of the sample was randomly collected for determining carbon content in the bed material by CHN analyzer. No attempt was made to separate completely the bed material and the char particles in the oversize and undersize screen fractions for the contamination in each fraction was considered to be insignificantly small. Total volume of condensed water was measured and its carbon content was analyzed by total organic carbon analyzer (TOC-2000, Hiranuma). The spent alumina balls packed in the 200°C and 100°C tar trapping tubes were combusted at 800°C in a horizontal tube furnace. The generated CO_2 was then collected in a teflon gas bag and the amount of CO_2 was quantified by a micro GC. From the known gas volume of CO_2 and its composition, the carbon contents of tar at 200°C and 100°C were thus determined. As a result, carbon distributions of gasification products in gas, char and tar (collected in bed material, trapped tar at 200°C and 100°C and condensed water) could be determined.

Evidence for CO_2 adsorption by the bed materials was evaluated by X-ray Diffraction technique (RINT-2000-XRD: Rigaku Corporation) and a thermogravimetric analyzer (TG-DTA 2000S: Material analysis and characterization). For thermogravimetric analysis, a sample of 10-15 mg of spent bed material was heated from room temperature to 1000°C with the heating rate of 30°C/min under a constant nitrogen flow rate of 100 cm^3/min. Physical deterioration of bed materials after gasification was examined by a field emission scanning electron microscope (FE-SEM) (JSM-6330FS: JEOL).

6.5 Results and Discussions

6.5.1 Raw Material Properties

6.5.1.1 Feedstock

Table 6.2 shows the basic chemical compositions and calorific values of the feedstocks used in this work. The elemental compositions of larch and capsule are relatively similar; carbon and oxygen are the major elements with the values varying between 44-49 wt%. However, the results of proximate analysis show that cellulose capsule contains much higher volatile and lower fixed carbon than those of larch pellet. The lower heating values of both feedstocks are approximately 20 MJ/kg.

Table 6.2 Feedstock properties.

Properties	**Materials**	
	Larch wood	**Cellulose capsule**
Elemental analysis (wt%)		
C	44.18	48.83
H	6.38	6.71
N	0.12	0.17
O (by difference)	49.32	44.29
Chemical formula	$CH_{1.723}N_{0.002}O_{0.837}$	$CH_{1.816}N_{0.003}O_{0.749}$
Proximate analysis (wt%)		
Moisture	8.16	2.51
Volatile	76.86	96.13
Ash	0.12	0.51
Fixed carbon (by difference)	14.86	0.85
Lower heating value (MJ/kg)	19.45	20.16

6.5.1.2 Bed Materials

The physical properties of the three bed materials are shown in Table 6.3. Their particle densities are in the range of 2,600-2,800 kg/m^3. The bulk density of silica sand is highest (~1,900 kg/m^3) and that of calcined limestone and calcined waste concrete are approximately the same of 1,100 kg/m^3. The magnitude of pore volume and surface area of the three bed materials are in the following order: calcined limestone > calcined waste concrete > silica sand. The pore size distribution data of the three bed materials are shown in Figure 6.2. It indicates that the pore sizes of all bed materials distribute mostly within the macro pore size range (>50 nm). Silica sand shows almost no pore volume distribution and total pore volume is extremely low, indicating that it is almost non-porous. The pore sizes of calcined waste concrete vary widely in the range of 20-40,000 nm with a bimodal distribution characteristic. Calcined limestone shows a much narrower distribution between 50-

10,000 nm with the smallest average pore size. The order of average pore size for the three bed materials is as follows: calcined waste concrete (933 nm) > calcined limestone (192 nm) > silica sand (181 nm).

The chemical compositions of bed materials were identified by X-ray diffraction and inductively coupled plasma emission spectroscopy (ICP-ES). The XRD patterns as shown in Figures. 6.3 (a), (c) and (e) indicate that the main identified components of waste concrete are in the form of SiO_2, CaO and $CaCO_3$, while $CaCO_3$ and SiO_2 are detected in limestone and silica sand, respectively. After calcination of limestone and waste concrete, the results illustrate that CO_2 was removed leaving only the presence of CaO (Figures. 6.3 (b) and (d)). The amounts of oxide compositions derived from the three bed materials are shown in Table 6.3. Silica sand consists mainly of SiO_2 (92.64 wt%), as expected. Calcined limestone consists virtually of CaO (99.26 wt%) with trace amounts of Al_2O_3 and MgO. The major compositions of calcined waste concrete are SiO_2 (69.61 wt%) and CaO (14.80 wt%).

Table 6.3 Properties of bed materials.

Properties	Silica sand	Calcined limestone	Calcined waste concrete
Physical properties			
Particle density (kg/m^3)	2,790	2,551	2,623
Bulk density (kg/m^3)	1,900	1,089	1,106
Pore volume (cm^3/g)	0.01	0.28	0.19
Surface area (m^2/g)	0.19	5.86	1.72
Average pore diameter	181	192	933
Chemical composition			
CaO	0.52	99.26	14.80
SiO_2	92.64	0.00	69.61
Al_2O_3	3.71	0.36	5.34
Fe_2O_3	0.73	0.00	4.05
MgO	0.19	0.37	1.80
Total	97.79	100.00	95.60

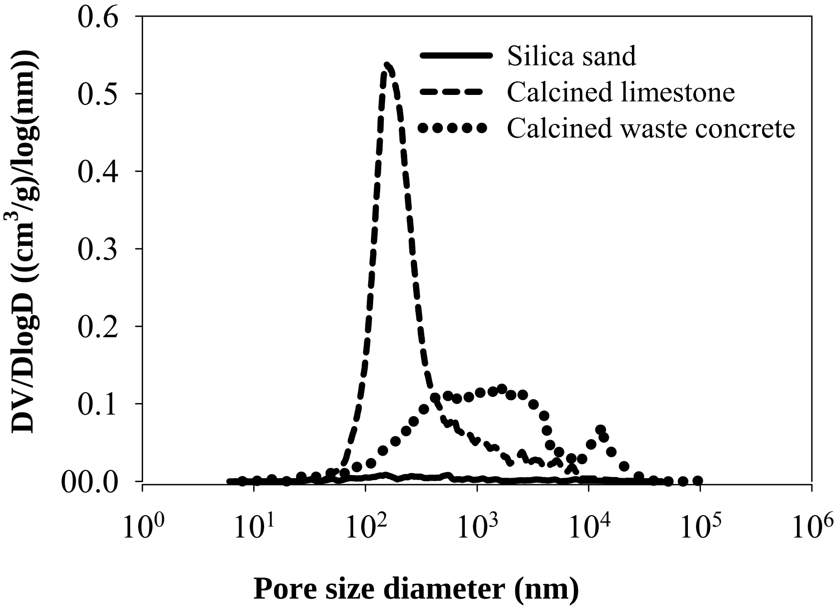

Figure 6.2 Pore size distributions of the test bed materials.

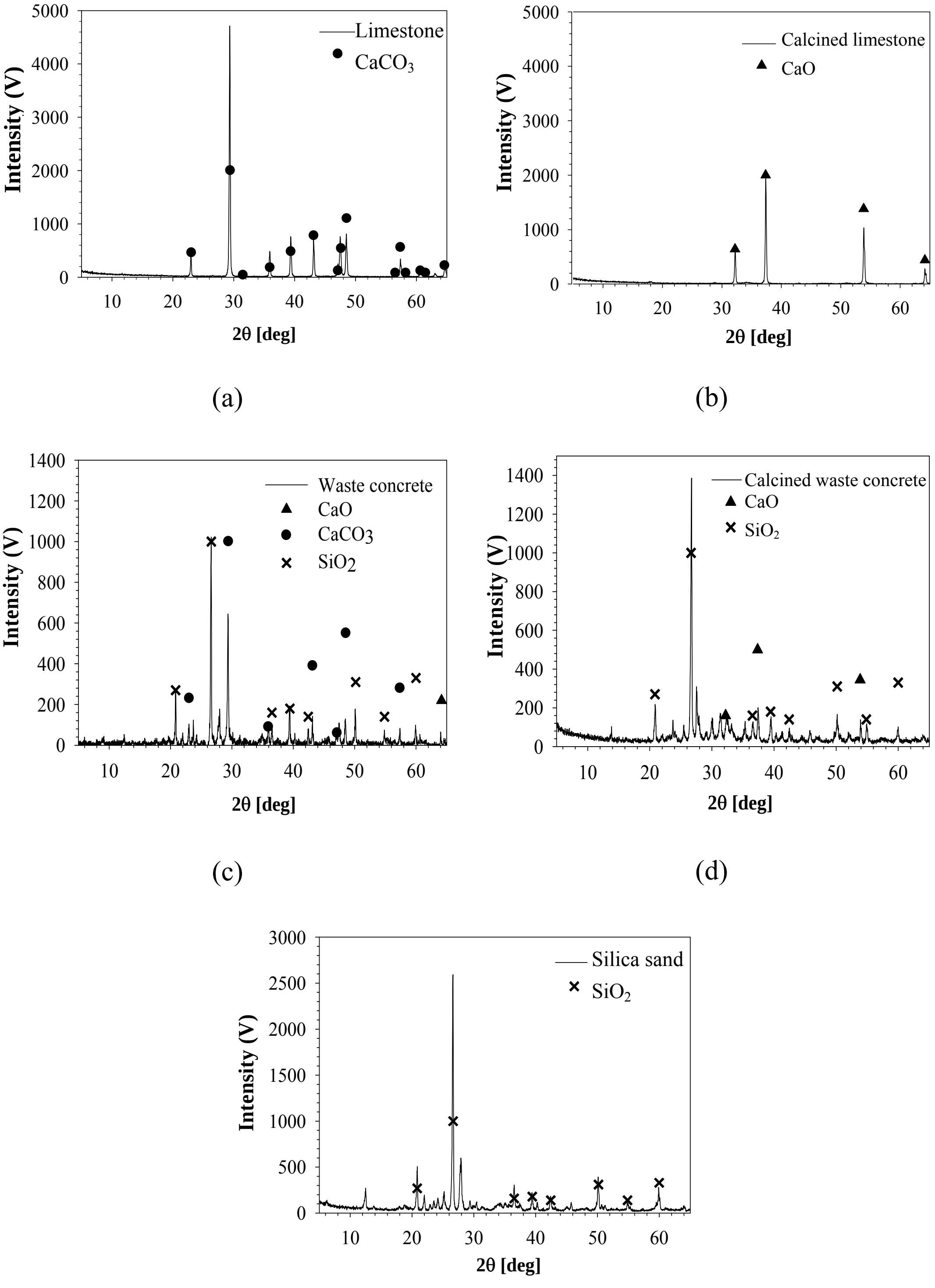

(a) (b)

(c) (d)

(e)

Figure 6.3 XRD patterns of bed materials: (a) limestone b) calcined limestone (c) waste concrete (d) calcined waste concrete and (e) silica sand.

6.5.2 Biomass Gasification

6.5.2.1 Effect of Bed Material Types

The three bed materials including silica sand, calcined limestone and calcined waste concrete were used to study the effect of bed materials on the produced gas compositions, carbon distribution of products and cold gas efficiency (%LHV) for steam gasification at 650°C. The results are presented in Figure 6.4 and Table 6.4.

As observed, the type of bed material had a strong influence on the yield and composition of gas produced from the gasification process. Silica sand provided the lowest amount of gas (18.39 mmol/g or 412 cm^3/g) but gave a maximum in CO content (8.28 mmol/g or 45.0 vol%). The largest volume of gas (47.53 mmol/g or 1065 cm^3/g) was produced from gasification using calcined limestone as the bed material. For this case, the major components of product gas were H_2 (30.21 mmol/g or 63.56 vol%) and CO_2 (11.77 mmol/g or 24.75 vol%). Overall, calcined waste concrete gave intermediate amount of produced gas of 33.18 mmol/g or 743 cm^3/g and yielded similar major gases of H_2 (15.57 mmol/g or 46.94 vol%) and CO_2 (10.14 mmol/g or 30.55 vol%) but with a higher concentration of CO (4.70 mmol/g or 14.18 vol%) compared with calcined limestone. Also from Figure 6.4, the effect of bed material on the cold gas efficiency (%LHV) followed the same trend as the effect on the amount of gas produced. The following order of %LHV was observed: calcined limestone (56.47%) > calcined waste concrete (39.40%) > silica sand (33.37%).

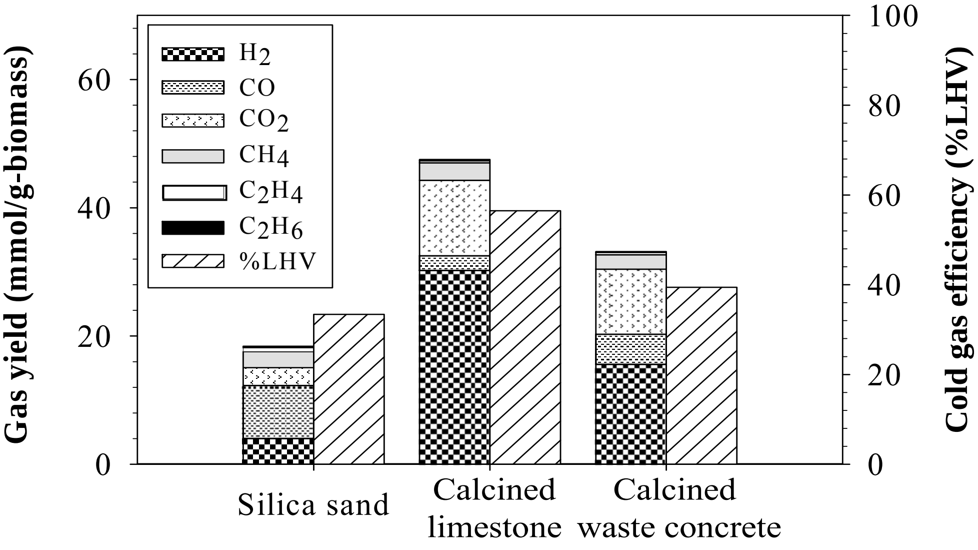

(a)

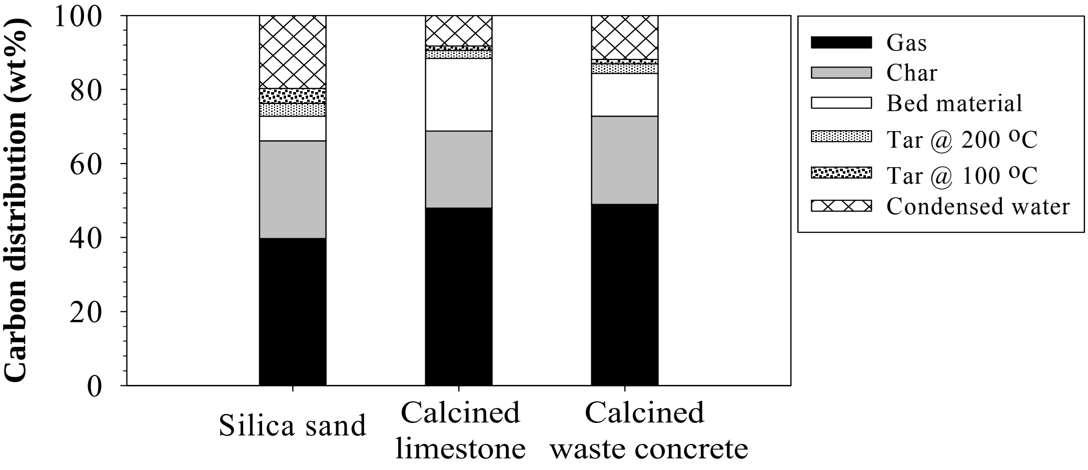

(b)

Figure 6.4 Effect of bed materials on (a) gas compositions and (b) carbon distribution of products for steam gasification at 650°C.

Table 6.4 Gasification results obtained under various conditions.

Run No.		**1**	**2**	**3**	**4**	**5**	**6**	**7**
Bed material		Silica sand	Calcined limestone	Calcined waste concrete	Calcined limestone (100%N_2)	Calcined limestone	Calcined Waste concrete	Mixed bed material*
Temperature (°C)		650	650	650	750	750	750	750
Steam (vol%)		85	85	85	-	85	85	85
[Ca]/[C] mole ratio		-	19.83	2.94	19.39	20.01	2.99	11.58
Gas composition (vol%)	**H_2**	21.84	63.56	46.94	38.03	55.97	48.26	55.68
	CO	45.00	4.85	14.18	35.54	7.71	15.17	7.40
	CO_2	14.99	24.75	30.55	12.16	29.23	27.14	29.57
	CH_4	13.61	5.75	6.81	9.93	5.72	7.18	5.91
	C_2H_4	3.34	0.66	1.05	1.74	1.06	1.85	1.10
	C_2H_6	1.22	0.43	0.46	2.59	0.32	0.41	0.35
H_2/CO mole ratio		0.49	13.12	3.31	1.07	7.28	3.18	7.53
Gas formation (cm^3/g)		412	1,065	743	692	1,549	1,194	1,470
Lower heating value (MJ/kg)		6.49	10.98	7.66	10.35	15.48	13.32	14.76
Cold gas efficiency (%LHV)**		33.37	56.47	39.40	53.19	79.61	68.46	75.88
Carbon distribution (wt%)	**Gas products**	39.75	47.91	48.95	52.78	78.75	76.09	79.91
	Char	26.37	20.85	23.87	20.61	3.05	2.32	3.51
	Bed material	6.68	19.68	11.52	23.36	14.97	11.96	12.13
	Tar at 200°C	3.47	2.16	2.57	0.33	0.35	2.83	0.93
	Tar at 100°C	4.00	1.16	1.19	0.38	0.34	2.07	0.86
	Condensed water	19.73	8.24	11.89	2.55	2.54	4.72	2.67
Tar emission (g-carbon/Nm^3 of produced gas)		317.55	52.21	101.31	22.66	10.03	38.75	14.59
Carbon conversion (%)		73.63	79.15	76.13	79.39	96.95	97.68	96.49

Note: * = Combination of bed materials (50:50 wt% of calcined limestone and calcined waste concrete)

** = Cold gas efficiency (%LHV) = (Lower heating value of gas product/ Lower heating value of feedstock)x100

It has been reported that CaO could act as a catalyst to produce the H_2 rich gas (Florin and Harris, 2006; Franco *et al.*, 2003; Rapagná *et al.*, 2002; Ross *et al.*, 2007). It can be observed from Table 6.3 that the three bed materials used in this study contain different contents of CaO and this could affect the compositions of the gas products (Table 6.4). As observed from the above results, the bed material containing higher content of CaO could produce higher content of H_2 and CO_2 and lower amount of CO, presumably because of the catalytic role of CaO in converting CO to H_2 and CO_2 via water gas shift reaction of Equation (6.11) (normally the reaction is appreciable at above 1000°C (Sato *et al.*, 2003)). The H_2/CO ratio derived from using different bed materials followed the sequence: calcined limestone (13.12) > calcined waste concrete (3.31) > silica sand (0.49). Moreover, it was observed that the content of light hydrocarbons of C_2H_4 and C_2H_6 derived from calcined limestone and calcined waste concrete was less than that of using silica sand as the bed material. This may result from the presence of CaO in calcined limestone and calcined waste concrete that could facilitate the conversion of these light hydrocarbon gases to CO and H_2 by Equation (6.12) (Wang *et al.*, 2007).

As Table 6.4 shows, the types of bed material exerted relatively little influence on the carbon distribution in the char and tar. Percentage of carbon distributing in the char for the three bed materials varied in the range of 20.85-26.37 wt%, whereas total tar yield (carbon in bed material, condensed water and trapped tar at 200 and 100°C) were 27.17-33.88 wt%. The results also indicate that calcined limestone is the most effective catalyst for carbon conversion with less tar emission (lowest %carbon in condensed water and trapped tar at 200 and 100°C, 11.56 wt% or 52.21 g-carbon/Nm^3 of produced gas). This is consistent with the results of previous works (Franco *et al.*, 2003; Mahishi and Goswami, 2007; Simell *et al.*, 1992) which suggested that CaO enhanced the conversion of char and tar in steam gasification. Moreover, calcined limestone showed the highest percentage of tar removal by bed adsorption (19.68 wt% of carbon in bed material), as compared to 11.52 wt% for calcined waste concrete and 6.68 wt% for silica sand. The work of Ito *et al.* (2003) has shown that tar capture in the bed material depends on specific pore surface area and pore volume of the particle. Therefore, the significantly improved adsorption capacity of calcined limestone over the other two bed materials is obviously due to its larger pore volume and surface area.

The evidence of CO_2 adsorption by the bed material may be traced from examining the content of CO_2 in the gas products. During gasification, CO_2, H_2 and CO were generated simultaneously by several reactions such as the reactions of pyrolysis (Equation (6.1)), water gas (Equations (6.7) and (6.8)), steam reforming (Equations. (6.9), (6.10), (6.12) and (6.13)) and water gas shift (Equation (6.11)). According to these reactions, the higher H_2 contents observed with the use of calcined limestone was expected to be accompanied by the correspondingly higher CO_2 contents. It was noted, however, that the use of calcined limestone produced relatively the same amount of CO_2 in the gas product as in the case of calcined waste concrete although its H_2 content is higher (63.56% vs 46.94%). Thus, the disappearance of CO_2 during gasification in the fluidized bed using calcined limestone might be due to the effect of gas adsorption by the limestone bed. This hypothesis was tested by examining the XRD-patterns of calcined limestone and calcined waste concrete after gasification. The XRD-pattern of calcined limestone after gasification at 650°C (Figure 6.5 (a)) shows the existence of some additional peaks of $CaCO_3$ and $Ca(OH)_2$, indicating the possible incorporation of CO_2 and H_2O by the bed material, while that of calcined waste concrete gave the same peak pattern before and after gasification (Figures 6.3 (d) and 6.5 (c)). Furthermore, TG curves of Figure 6.6 demonstrates that there were weight losses of calcined limestone after gasification at the temperature of 300-370°C and 550-700°C, conforming to the decomposition of $Ca(OH)_2$ and $CaCO_3$, respectively (Lin *et al.*, 2006). Therefore, the ability of calcined limestone in capturing CO_2 during gasification was substantiated. In comparison, no capture of CO_2 by calcined waste concrete was observed from XRD results. This may be reasoned that calcined waste concrete contains much less content of CaO and lower available surface area and pore volume for CO_2 capture (Table 6.3).

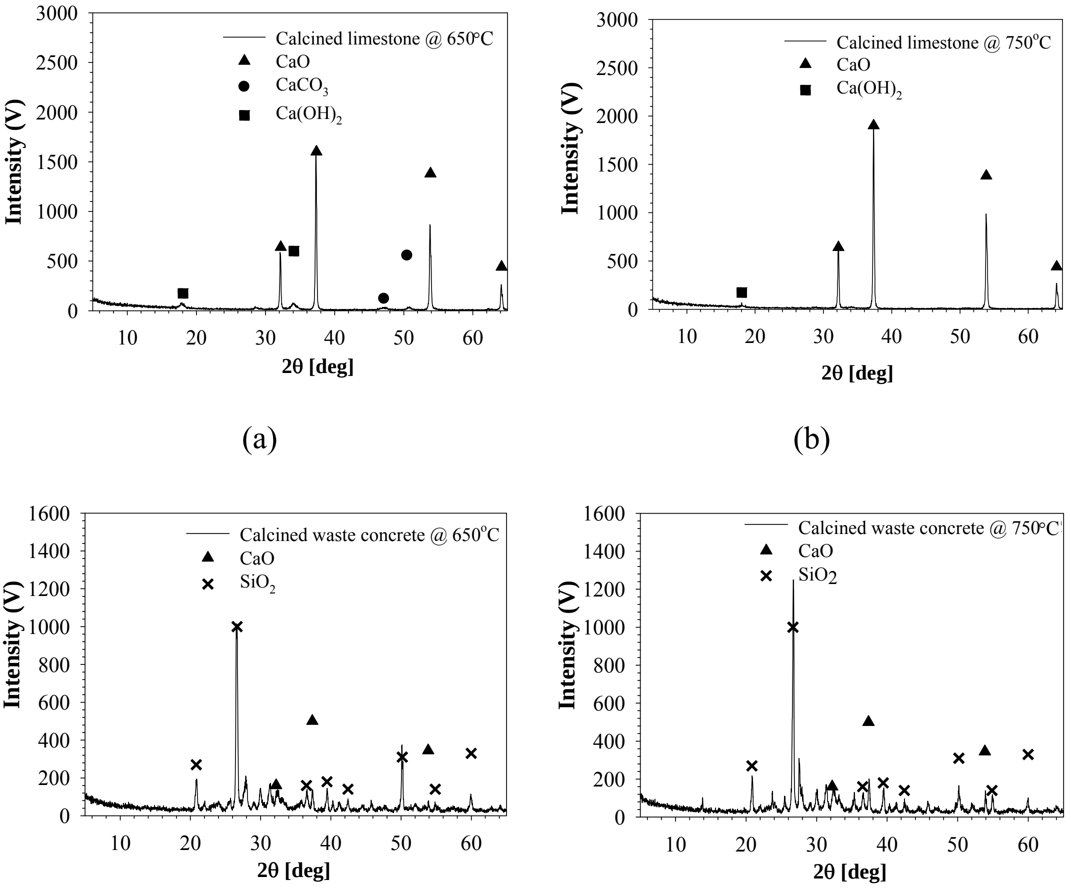

(a) (b)

(c) (d)

Figure 6.5 XRD patterns of bed materials after gasification: (a) calcined limestone at 650°C (b) calcined limestone at 750°C (c) calcined waste concrete at 650°C and (d) calcined waste concrete at 750°C.

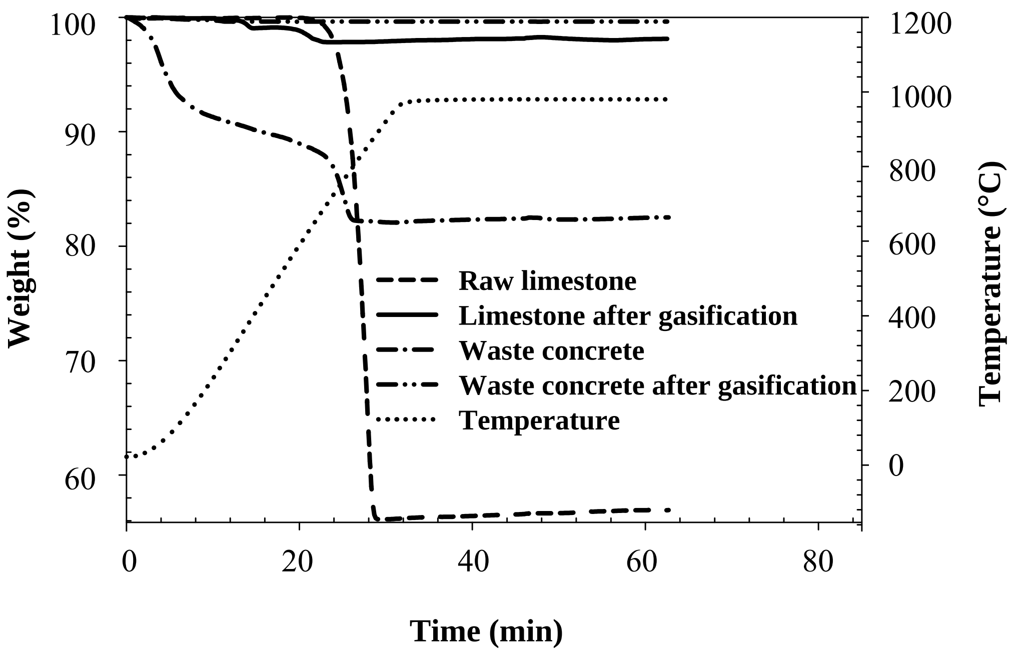

Figure 6.6 TGA curves of bed materials after steam gasification at 650°C.

6.5.2.2 Effect of Gasification Temperature

Typically, biomass gasification in a fluidized-bed system is operated at temperatures in the range of 800-900°C (Saxena *et al.*, 2008). However, for the purpose of studying the effect of CaO on the inbed capture of CO_2 to affect the gas yield and composition, it is necessary to operate the gasifier at a lower temperature range (Hughes *et al.*, 2005). For this reason, the gasification temperatures of 650 and 750°C were chosen in the present work. Figure 6.7 and Table 6.4 show results on gas compositions and carbon distribution of the gasification products. The increase of gasification temperature from 650 to 750°C had considerable effect on the gas yield and composition, carbon distribution of products and cold gas efficiency (%LHV). The increase in gas yield either with calcined limestone or calcined waste concrete was about 21 mmol/g-biomass as the gasification temperature was increased. The increase in %LHV was 23.14% and 29.06% for calcined limestone and calcined waste concrete, respectively. In addition, %carbon in char product and total tars (in bed material, trapped tar at 200 and 100°C and condensed water) decreased markedly when the gasification temperature was increased. The decrease in char production for the two bed materials was almost the same, 17.80 and 21.55% for calcined limestone and calcined waste concrete, respectively. The amounts of total carbon in tars decreased by about 13.04% for calcined limestone and 5.59% for calcined waste concrete. Considering tar emission per gas volume (g-carbon/Nm^3 of produced gas), increasing gasification temperature gave a reduction of 60-80% emission per gas volume. It should be observed that the lowering of tar and char production gave rise to the increased carbon content in the product gas when the temperature was increased, as anticipated from the gas production from endothermic reactions of char decompositions via Equations. (6.7) and (6.8) and steam reforming of hydrocarbon tar via Equation (6.13). Gasification using calcined limestone at 750°C generated the least tar emission (condensed water and trapped tar at 200 and 100°C) among other conditions, 3.23 wt% or 10.03 g-carbon/Nm^3 of produced gas. However, the increasing of temperature did not affect tar contents of high molecular weight (trapped tar at 200 and 100°C) obtained from using calcined waste concrete as the bed material. This may result from the fact that calcined waste concrete contains much less amount of CaO than limestone to affect the following catalytic tar reforming reaction.

Concerning the effect of temperature on the composition of gas product, it was found that calcined waste concrete provided similar gas composition at the two gasification temperatures of 650 and 750°C (Table 6.4). In addition, for calcined waste concrete the H_2/CO ratio obtained at these two temperatures did not change much (3.18-3.31). When calcined limestone was used as the bed material, the H_2/CO molar ratios were 13.12 and 7.28 at the gasification temperatures of 650 and 750°C, respectively (Table 6.4 and Figure 6.8). This implies that the efficiency of converting CO to H_2 via water gas shift reaction (Equation (6.11)) at 750°C is lower than that at the lower temperature of 650°C when calcined limestone was used. This result is in agreement with the work of Florin and Harris (2006) in that the exothermic water-gas shift reaction is favored at a lower temperature. In addition, the decrease of H_2 concentration may result from the deactivation of CaO sorbent at the temperature higher than 650°C (Florin and Harris, 2008). This was supported by the XRD results at the higher temperature of 750°C, as shown in Figures 6.5 (b) and (d), where they did not adsorb much CO_2 at this higher temperature (no significant peaks of $CaCO_3$ were observed). When the lowering of CO_2 capture by CaO is observed, it means the lower capability of CaO to shift the equilibriums of the water-gas reaction via Equation (6.8), steam reforming via Equations (6.10) and (6.13) and water-gas shift reaction via Equation (6.11).

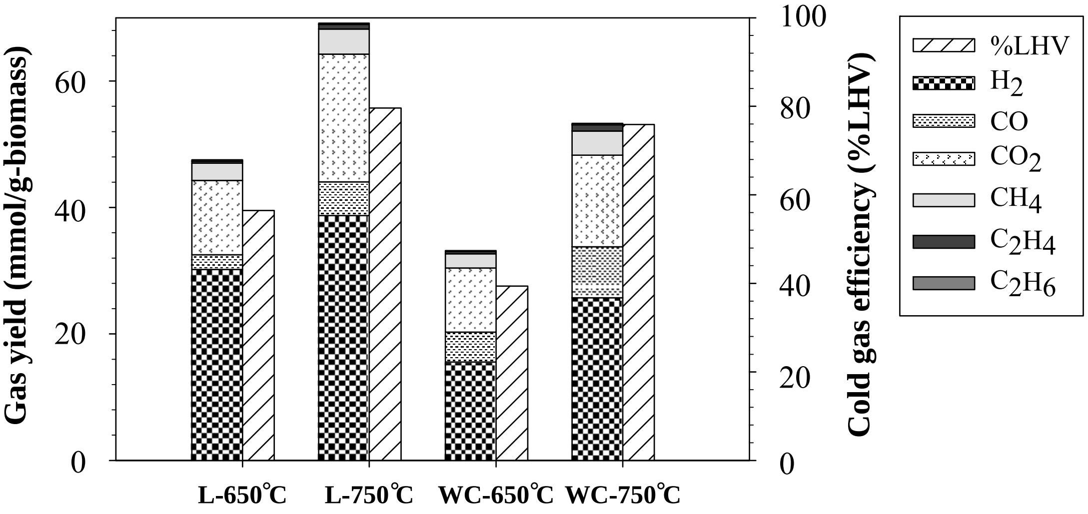

(a)

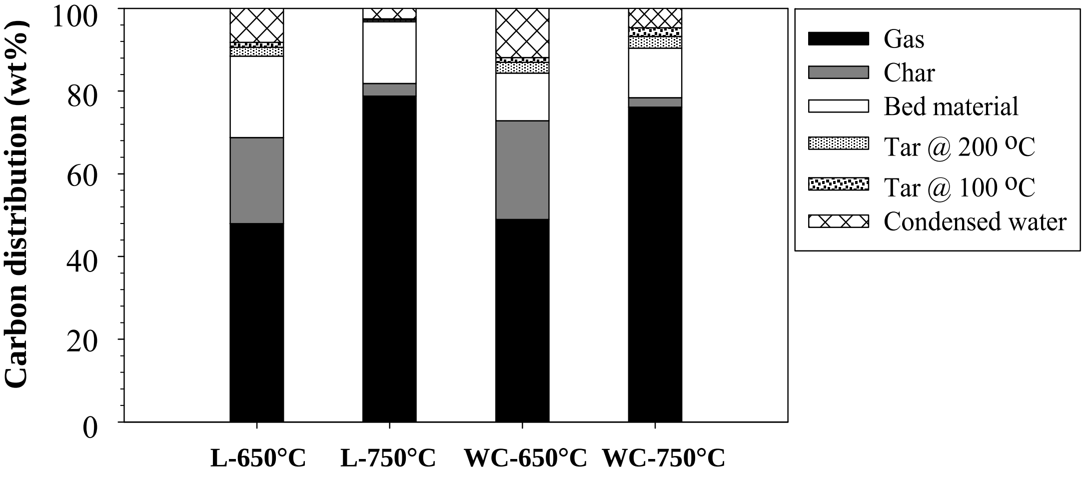

(b)

Figure 6.7 Effect of gasification temperature on (a) gas yield and (b) carbon distribution of products derived from using calcined limestone and calcined waste concrete (L: calcined limestone and WC: calcined waste concrete).

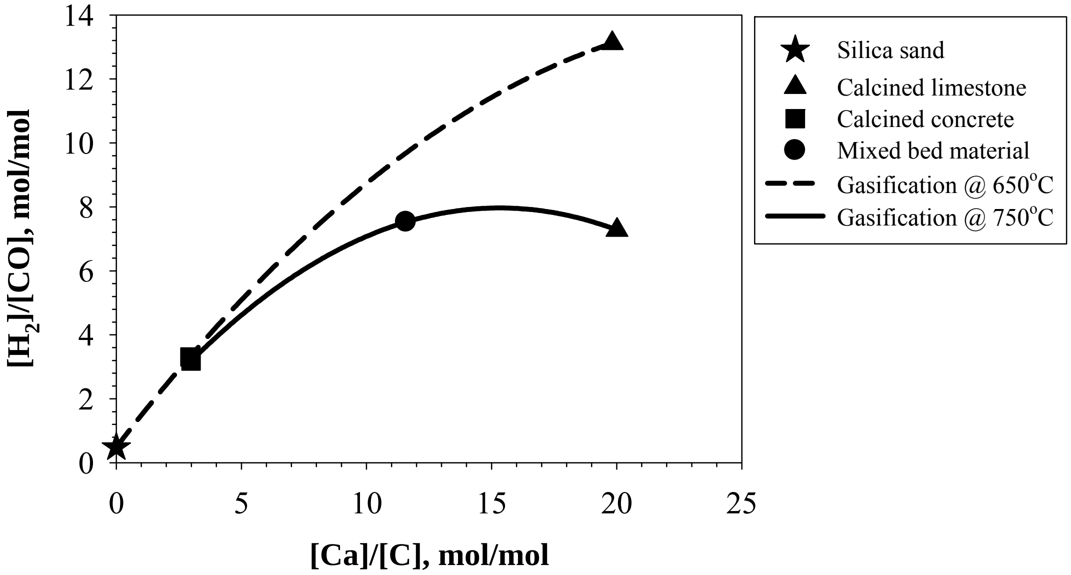

Figure 6.8 The relationships between $[H_2]/[CO]$ and [Ca]/[C] at gasification temperatures of 650 and 750°C.

6.5.2.3 Effect of Gasifying Agents

Pure N_2 (pyrolysis) and mixture of 85% steam and 15% N_2 (steam gasification) were used to compare the effect of gasifying agent using calcined limestone as bed material at 750°C. It was found that amount of total gas produced from steam gasification was higher than that obtained from pyrolysis process by about twofold (Figure 6.9 (a)). A plausible explanation to this result could be the increased reaction conversion of ligno-cellulose biomass in the steam atmosphere (Haykiri-Acma and Yaman, 2008). Moreover, much lower carbon content of char and tar in the bed material from steam gasification as compared to pyrolysis process (Table 6.4 and Figure 6.9 (b)) may be attributed to the contributions from char and tar decomposition reactions to produce more gas products when the steam was used. The carbon conversion in steam gasification reached 96.95%, whereas pyrolysis process could convert up to only 79.39% (Table 6.4). Percent of carbon in the bed material derived from steam gasification process was less than that of pyrolysis process by about 8.39%. As compared with pyrolysis, steam gasification provided similar value of tar emission (trapped tar at 200 and 100°C and in condensed water,) on a weight basis of ~3.25wt% carbon but gave about haft in terms of tar emission per gas volume (10.03 g-carbon/Nm^3 of produced gas vs 22.66 g-carbon/Nm^3 of produced gas).

As observed from Figure 6.9 (a), it was noted that there are differences in the gas compositions derived from the two different gasifying agents. The main gas product of steam gasification was H_2 (38.71 mmol/g) and CO_2 (20.21 mmol/g), while H_2 (11.76 mmol/g) and CO (10.99 mmol/g) were the major gas components in the pyrolysis process. For steam gasification, the significant increasing of H_2 and CO_2 content may be attributed to the char decompositions (Equations (6.7) and (6.8)), reforming of hydrocarbon gases and tars (Equations. (6.9), (6.10), (6.12) and (6.13)) and reactions of water-gas shift reaction (Equation (6.11)). It may be also expected that the amount of CO should be increased through steam reforming reactions of hydrocarbon gases and tars (Equations (6.9), (6.12) and (6.13)) and char decompositions (Equation (6.7)). However, the lower content of CO derived from steam gasification was observed in this work and this may be due to the conversion of CO by water gas shift reaction (Equation (6.11)) to produce more H_2 and CO_2. In this study, steam gasification gave H_2/CO mole ratio about seven times higher than that obtained from the pyrolysis process (Table 6.4).

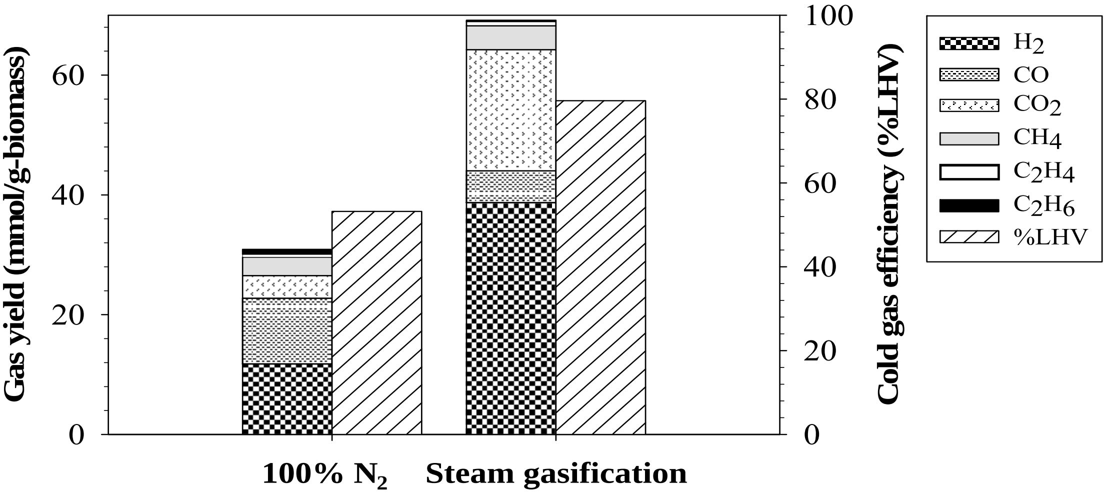

(a)

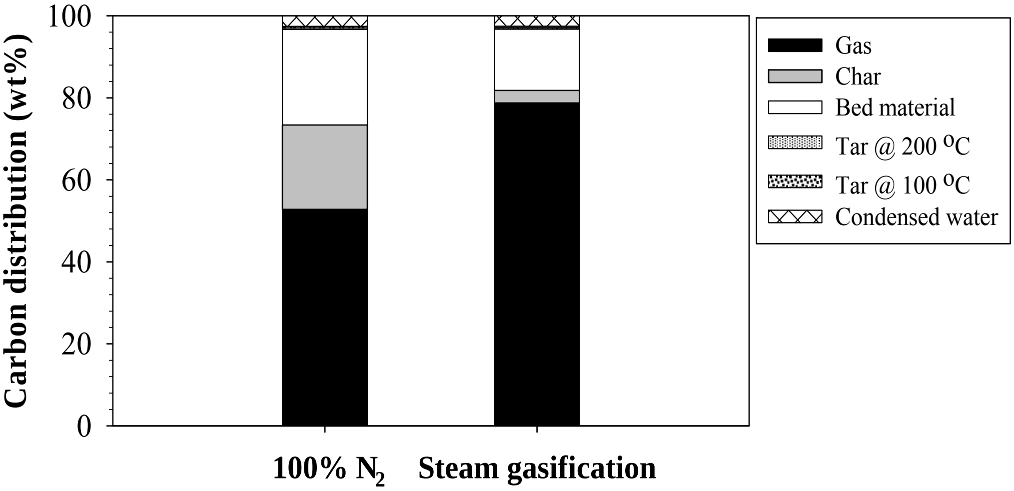

(b)

Figure 6.9 Effect of gasifying agents on (a) gas yield and (b) carbon distribution of products for 100% N_2 and steam gasification at 750°C with calcined limestone as the bed material.

6.5.2.4 Effect of Mixed Bed Materials

As discussed earlier, the steam gasification with calcined limestone gave the highest cold gas efficiency (%LHV), H_2/CO ratio, and the lowest tar generation. However, limestone presented some disadvantages after being calcined and after steam gasification. It had a tendency to break, agglomerate and sinter; the resulting fine strong particle would cause the plugging and blocking of gas passage route such as parts of the trapped tar tubes used in this work. This problem could be intensified because of the increased temperature and higher contents of CO_2 and H_2O in the process (Florin and Harris, 2008). Figure 6.10 (a) evidently shows the existence of small fragments of limestone particles after gasification. Figure 6.10 (b) shows that the breakage of waste concrete particles into smaller sizes did not occur even at the high gasification temperature of 750°C. It is thus expected that calcined waste concrete can be applied at a high temperature and for a long period of gasification operation. In this respect, although waste concrete possesses the advantage of physical durability, it provides lower cold gas efficiency (%LHV) and higher tar emission than for the case of using calcined limestone.

To decrease the attrition and the agglomeration propensities during gasification operation and still maintaining reasonably high quality of gas product, the use of mixed bed materials was proposed in this work. An equal amount of calcined limestone and calcined waste concrete was mixed to give a 50:50 wt% mixture which was used in steam gasification at 750°C. Figure 6.11 and Table 6.4 show the gas compositions and carbon distribution of products derived from using the mixture of calcined limestone and calcined waste concrete. It demonstrates that using the mixed bed materials gave comparable composition, amount of gas produced

(65.62 mmol/g-biomass or 1,470 cm^3/g) and cold gas efficiency (75.88%LHV) to those of calcined limestone, but with less tar adsorption by bed material and slightly higher tar emission (trapped tar and condensed water). This can be explained on the ground that the use of mixed bed materials changed the [Ca]/[C] (Table 6.4 and Figure 6.8), which in turn affected the gas composition and tar emission. However, it is interesting to note that although mixed bed materials had lower [Ca]/[C] ratio but its H_2/CO molar ratio was still similar to that of calcined limestone (Table 6.4). In addition, in using the mixed bed material, the problems of attrition, sintering, and agglomeration became less than those of using calcined limestone alone (Figure 6.10 (c)). Therefore, a mixture of calcined limestone and calcined waste concrete should be a satisfactory bed material for steam gasification to provide high cold gas efficiency (%LHV) comparable to calcined limestone and yet giving longer physical durability.

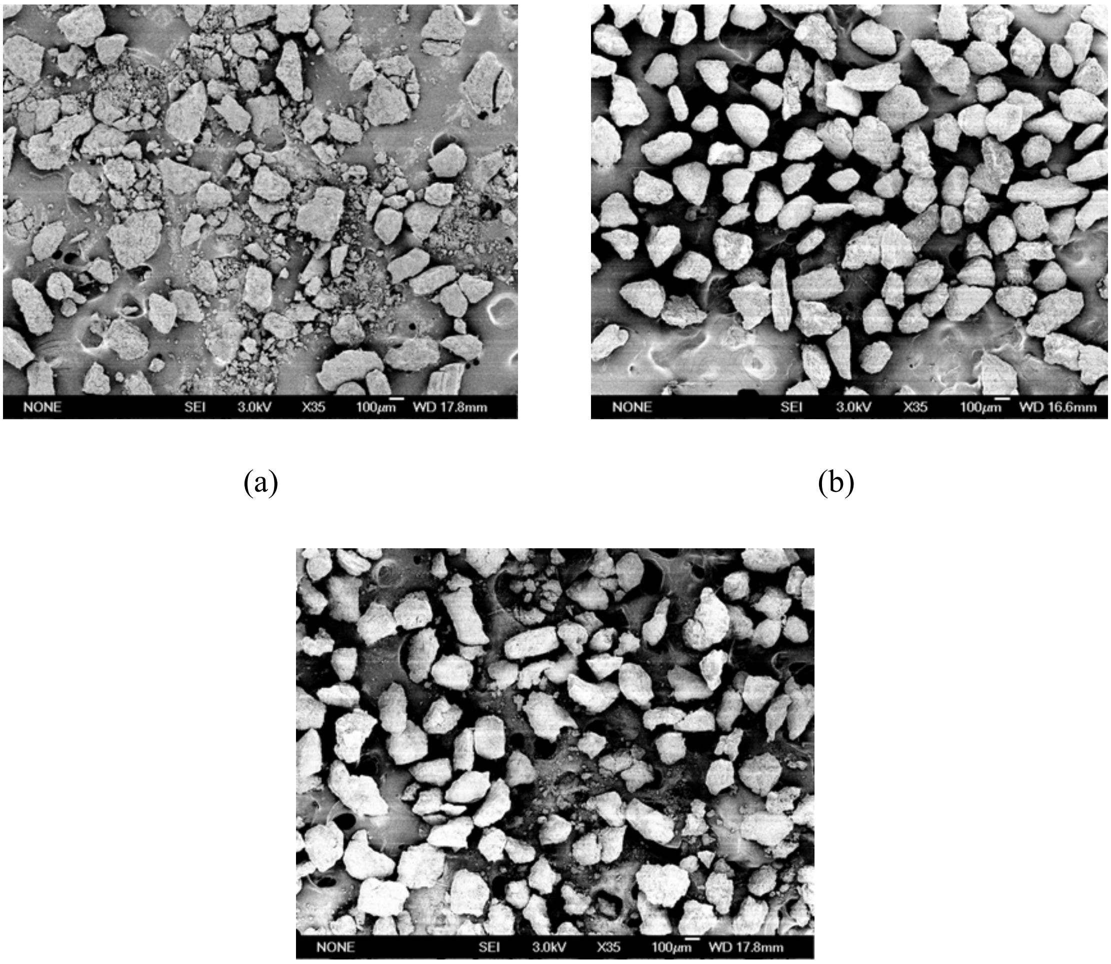

(a) (b)

(c)

Figure 6.10 SEM photographs of bed materials after steam gasification at 750°C: (a) calcined limestone, (b) calcined waste concrete, and (c) mixed bed material of calcined limestone and calcined waste concrete.

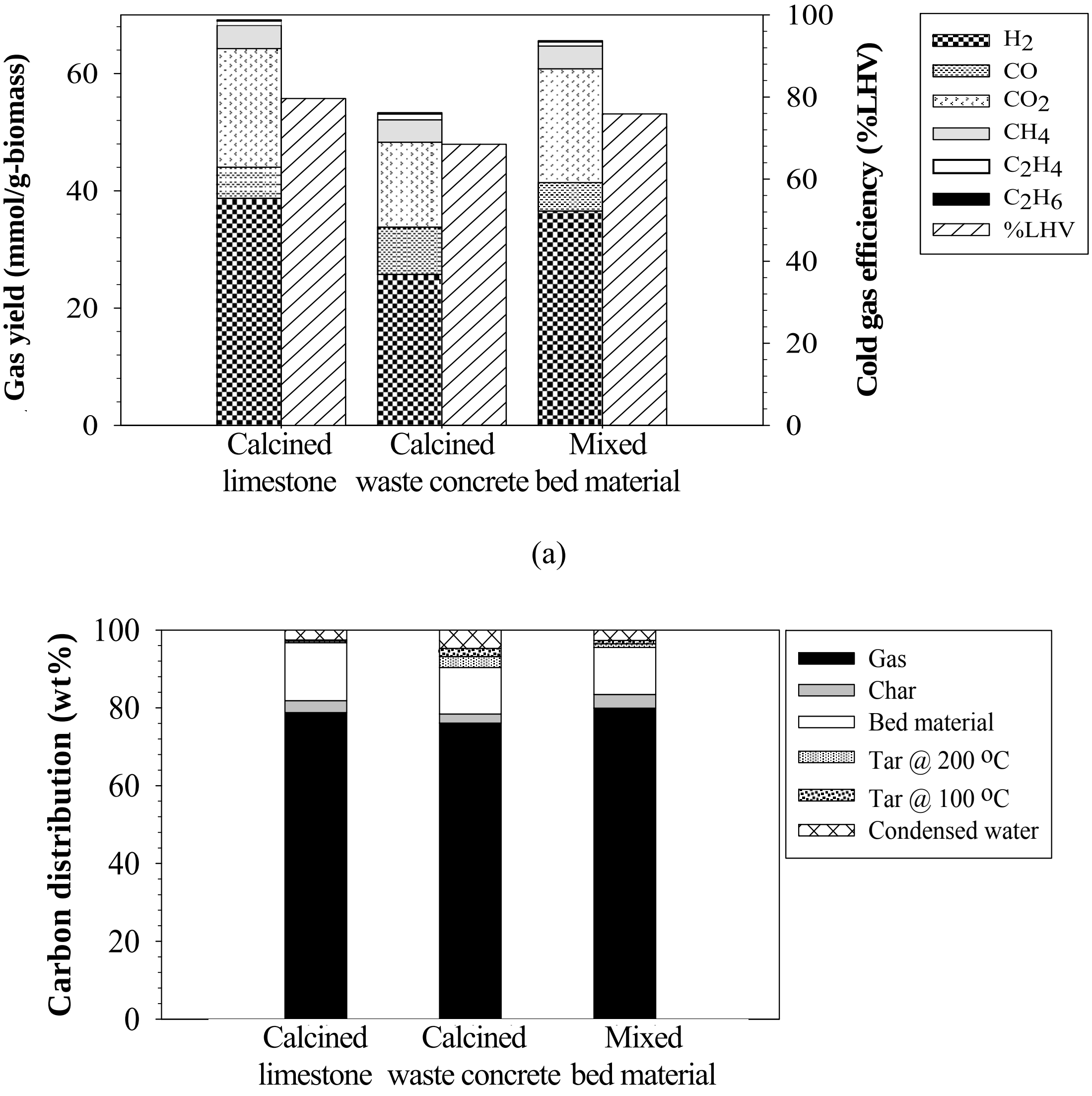

(a)

(b)

Figure 6.11 Effect of mixed bed materials on (a) gas yield and (b) carbon distribution of products for steam gasification at 750°C.

6.6 Conclusions

The running of a shallow fluidized bed steam gasifier used in this study indicated that the gasification conditions had a strong influence on gasification products derived from larch biomass. The results derived from this study are summarized as follows.

- Different bed material gave the different gas compositions; major compositions of gas products observed from using calcined limestone or calcined waste concrete were H_2 and CO_2, while the highest CO concentration was obtained from using silica sand.

- Increasing gasification temperature from 650 to 750°C caused the increase of %LHV by about 23.14-29.06% and the decrease of total tar by about 5.59-13.04%. However, efficiency of CO_2 capture by calcined limestone bed and its ability in converting CO to H_2 and CO_2 via water gas shift reaction declined with increasing of gasification temperature.

- Steam utilization in the gasification process caused an increase in amount of gas product and higher H_2/CO ratio as compared to pyrolysis in 100% N_2. Steam gasification at 750°C using calcined limestone generated the least tar emission of 3.23% or 10.03 g-carbon/Nm^3 of produced gas and the highest cold gas efficiency of 79.61%, while calcined waste concrete gave reasonably high cold gas efficiency of 68.46% with moderately higher tar emission of 9.62% or 38.75 g-carbon/Nm^3 of produced gas.

- A mixture of 50:50 wt% of calcined limestone and calcined waste concrete was proved to be most advantageous for providing high cold gas efficiency (75.88 %LHV) and longer physical durability than the use of calcined limestone alone.

However, the use of only waste concrete as a bed material may be an attractive choice, considering its solving disposal problem and yet reasonably effective in the steam gasification process.

6.7 References

Abu El-Rub, Z., Bramer, E. A., and Brem, G. (2004). Review of catalysts for tar elimination in biomass gasification processes. **Industrial & Engineering Chemistry Research** 43 (2): 6911-6919.

Department of Materials Science and Engineering, University of Illinois Urbana-Champaign, (2008). Scientific Principles [On-line]. Available: **http://matse1.mse.uiuc.edu/concrete/prin.html**.

Devi, L., Ptasinski, K. J., and Janssen, F. J. J. G. (2003). A review of the primary measures for tar elimination in biomass gasification processes. **Biomass & Bioenergy** 24 (2): 125-140.

Florin, N. H., and Harris, A. T. (2006). Hydrogen production from biomass coupled with carbon dioxide capture: The implications of thermodynamic equilibrium. **International Journal of Hydrogen Energy** 31 (17): 945-952.

Florin, N. H., and Harris, A. T. (2008). Enhanced hydrogen production from biomass with in situ carbon dioxide capture using calcium oxide sorbents. **Chemical Engineering Science** 63 (2): 287-316.

Franco, C., Pinto, F., Gulyurtlu, I., and Cabrita, I., (2003). The study of reactions influencing the biomass steam gasification process. **Fuel** 82 (7): 835-842.

Han, J., and Kim, H. (2008). The reduction and control technology of tar during biomass gasification/pyrolysis: an overview. **Renewable and Sustainable Energy Reviews** 12 (2): 397-416.

Haykiri-Acma, H., and Yaman, S., (2008). Thermal reactivity of rapeseed (Brassica napus L.) under different gas atmospheres. **Bioresource Technology** 99 (2): 237-242.

Hughes, R. W., Lu, D. Y., Anthony, E. J., and Macchi. A. (2005). Design, process simulation and construction of an atmospheric dual fluidized bed combustion system for in situ CO_2 capture using high-temperature sorbents. **Fuel Processing Technology** 86 (14-15): 1523-1531.

Hu, G., Xu, S., Li, S., Xiao, C., and Liu, S. (2006). Steam gasification of apricot stones with olivine and dolomite as downstream catalysts. **Fuel Processing Technology** 87 (5): 375-382.

Ito, K., Moritomi, H., Yoshiie, R., Uemiya, S., and Nishimura, M. (2003). Tar capture effect of porous particles for biomass fuel under pyrolysis conditions. **Journal of Chemical Engineering of Japan** 36 (7): 840-845.

Kumabe, K., Hanaoka, T., Fujimoto, S., Minowa, T., and Sakanishi, K. (2007). Co-gasification of woody biomass and coal with air and steam. **Fuel** 86 (5-6): 684-689.

Lin, S., Suzuki, Y., Hatano, H., and Harada M. (2002). Developing an innovative method, HyPr-RING, to produce hydrogen from hydrocarbons. **Energy Conversion and Management** 43 (9-12): 1283-1290.

Lin, S., Suzuki, Y., Hatano, H., and Harada M. (2006). Continuous experiment regarding hydrogen production by coal/CaO reaction with steam (II) solid formation. **Fuel** 85 (7-8): 1143-1150.

Lv, P., Xiong, Z., Chang, J., Wu, C., Chen, Y., and Zhu, J. (2004). An experimental study on biomass air-steam gasification in a fluidized bed. **Bioresource Technology** 95 (1): 95-101.

Mahishi, M., and Goswami, D. (2007). An experimental study of hydrogen production by gasification of biomass in the presence of a CO_2 sorbent. **International Journal of Hydrogen Energy** 32 (14): 2803-2808.

McKendry, P. (2002). Energy production from biomass (part 3): gasification technologies. **Bioresource Technology** 83 (1): 55-63.

Mindess, S., Young, J. F., and Darwin, D. (2003). **Concrete** (2nd ed). Prentice Hall, United State of America.

Moghtaderi, B. (2007). Effects of controlling parameters on production of hydrogen by catalytic steam gasification of biomass at low temperatures. **Fuel** 86 (15): 2422-2430.

Rapagná, S., Jand, N., Kiennemann, A., and Foscolo, P. (2000). Steam gasification of biomass in a fluidized-bed of olivine particles. **Biomass&Bioenergy** 19 (3): 187-197.

Rapagná, S., Provendier, H., Petit, C., Kiennemann, A., and Foscolo, P. (2002). Development of catalysts suitable for hydrogen or syn-gas production from biomass gasification. **Biomass&Bioenergy** 22 (5): 377-388.

Rezaiyan, J., and Cheremisinoff, N. P. (2005). **Gasification technologies: a primer for engineers and scientists**. United State of America: Taylor & Francis Group.

Ross, D., Noda, R., Horio, M., Kosminski, A., Ashman, P., and Mullinger, P. (2007). Axial gas profiles in a bubbling fluidized bed biomass gasifier. **Fuel** 86 (10-11): 1417-1429.

Sato, S., Lin, S.-Y., Suzuki, Y., and Hatano, H. (2003). Hydrogen production from heavy oil in the presence of calcium hydroxide. **Fuel** 82 (5): 561-567.

Saxena, R. C., Seal, D., Kumar, S., and Goyal, H. B. (2008). Thermo-chemical routes for hydrogen rich gas from biomass: a review. **Renewable and Sustainable Energy Reviews** 12 (7): 1909-1927.

Simell, P., Leppalahti, J., and Bredenberg, J. (1992). Catalytic purification of tarry fuel gas with carbonate rocks and ferrous materials. **Fuel** 71 (2): 211-218.

Sutton, D., Kelleher, B., and Ross, J. (2001). Review of literature on catalysts for biomass gasification. **Fuel Processing Technology** 73 (3): 155-173.

Taralas, G., and Kontominas, M. (2006). Pyrolysis of solid residues commencing from the olive oil food industry for potential hydrogen production. **Journal of Analytical and Applied Pyrolysis** 76 (1-2): 109-116.

Wang, Y., Yoshikawa, K., Namioka, T., and Hashimoto, Y. (2007). Performance optimization of two-staged gasification system for woody biomass. **Fuel Processing Technology** 88 (3): 243-250.

Wei, L., Xu, S., Zhang, L., Liu, C., Zhu, H., and Liu, S. (2007). Steam gasification of biomass for hydrogen-rich gas in a free-fall reactor. **International Journal of Hydrogen Energy** 32 (1): 24-31.

Xu, G., Murakami, T., Suda, T., Kusama, S., and Fujimori, T. (2005). Distinctive effects of CaO additive on atmospheric gasification of biomass at different temperatures. **Industrial & Engineering Chemistry Research** 44 (15): 5864-5868.

CHAPTER VII

CONCLUSIONS AND RECOMMENDATIONS

7.1 Conclusions

This work focused on studies of thermochemical processes for converting biomasses to synthetic fuels. Gasification and pyrolysis which offer great promise for producing gaseous and liquid fuels for the generation of heat and powers were adopted in this study. Various biomasses which are agricultural wastes left from processing plants including cassava pulp residue, palm kernel cake, palm shell, coconut shell and longan fruit seed were used for study of slow pyrolysis process, whereas larch, a fast-growing tree, was used for studying steam gasification. The research commenced with study of pyrolysis kinetic of biomasses. Effects of biomass type, particle size and heating rate on these non-isothermal pyrolysis characteristics were investigated using a thermogravimetric analyzer (TGA). In addition, five kinetic models based on three pyrolysis schemes were employed for describing pyrolysis behaviors of cassava pulp residue for different particle sizes and heating rates. The next task involved study of biomass pyrolysis in a small fixed-bed reactor. Effects of biomass type and pyrolyis conditions on product yields were examined and derived products were characterized for their chemical and fuel properties. However, bio-oil which has potential to be used as a liquid fuel possesses undesirable properties such as low heating value, corrosiveness, high viscosity and ageing characteristics. Thus, a study on improvement of bio-oil properties by various methods has been also attempted. There were three simple methods for upgrading three different bio-oils, namely using bio-oil from cassava pulp residue in form of char-bio-oil slurry fuel, blending of dewatered palm kernel bio-oil with diesel and alcohol and conversion of carboxylic acids in dewatered palm shell oil to esters via esterificaton reaction. Finally, steam gasification of larch wood using different bed materials to affect gas product qualities were performed in a bubbling atmospheric fluidized-bed reactor. The effects of gasification conditions including types of bed material, temperature and types of gasifying agent on the yield and composition of gasification products were investigated. The conclusions drawn from this work can be summarized as follows.

On studying pyrolysis kinetic, all biomasses showed sigmoid shape of thermograms presenting as weight remaining with respect to increasing pyrolysis temperature (TGA curves) and main decomposition occurred at approximately the same range of 250-400°C. However, different biomasses displayed different characteristics of the first derivative thermograms (DTG curves). For cassava pulp residue sample, particle size between 106 and 1325 µm gave almost no effect on the pyrolysis behavior but heating rate in range of 5-40°C/min showed a strong influence on decomposition temperature range and decomposition rate. The best fitting for describing pyrolysis behavior of cassava pulp residue for different particle sizes and heating rates was obtained from the two-parallel reactions model (3.55% in maximum error). The one-step global model assuming nth order reaction and the two-step consecutive reaction model with allowance for stoichiometric coefficient gave satisfactory prediction. However, the one-step global model assuming 1st order reaction and the two-step consecutive reaction model of Guo and Lua showed relatively large deviation between predicted and experimental results. Under the conditions investigated, fitting parameters derived from the two-parallel reactions model can be summarized as follows. The mass fraction of the first component with first-order decomposition reaction was found to be 0.51, while that of the second fraction following nth order decomposition reaction was found to be 0.49. The frequency factor (*A*) and activation energy (*E*) of the first fraction were in the range of 1.03×10^{8}-4.14×10^{9} s^{-1} and 1.06×10^{2}-1.27×10^{2} kJ/mol, respectively, and those of the second fraction were 2.05×10^{16}-9.31×10^{20} s^{-1} and 1.80×10^{2}-2.47×10^{2} kJ/mol, respectively.

On studying the slow pyrolysis in a fixed-bed reactor, biomass type, pyrolysis temperature (300-700°C) and average particle size in range of 0.71-2.03 mm exerted a great influence on product yields of liquid, gas and char, while N_2 purge rate (200-600 cm^3/min) and heating rate (5-20°C/min) gave almost insignificant effect. The maximum liquid product yields for different biomasses varied in the range of 42.4-54.3 wt%. Dewatered palm kernel bio-oil showed most promising, giving the highest heating value (40 MJ/kg), lowest acidity (pH of 5.62) and its boiling range distribution was closest to that of diesel oil. However, other bio-oils gave heating values only in the range 14-28 MJ/kg and possessed serious problem of high acidity (2.11-4.06). The crude bio-oils contained main functional groups of alcohols, ketones, ethers, esters, aldehydes and carboxylic acids, with groups of alkanes, alkenes and aromatics being dominantly detected after the removal of water from the oil. On GC-MS analysis, major compounds detected in dewatered oils from palm kernel cake and palm shell were acid groups of n-C_8-C_{18}, ester groups and phenolics, while dewatered cassava pulp residue oil showed higher content of ethers, ketones, aldehydes plus the highest amounts of polar fraction and non-volatile compounds derived from methanol extracted fraction. Pyrolysis temperature showed a strong effect on some oxygenated and hydrocarbon compounds of bio-oils, with higher pyrolysis temperature of 700°C giving lower amounts of esters and phenol and higher contents of high molecular weights of n-alkanes and polycyclic aromatic hydrocarbons (PAH). The derived chars had high calorific value (29-35 MJ/kg) and chars from palm kernel cake and palm shell showed a characteristic of reasonably high porosity (BET surface area of about 209 and 367 m^2/g, respectively). Biomass type and pyrolysis temperature affected significantly both gas yields and compositions. Heating values of gases produced from various biomass pyrolysis at 500 and 700°C were in the range of 1.14-4.42 MJ/kg-biomass.

On studying bio-oil upgrading, three approaches were investigated, including rheology and fuel properties of char-bio-oil slurries, phase behaviors and fuel properties of bio-oil-diesel-alcohol blends, and esterification of bio-oil and alcohol by acid catalysts. The results indicated that cassava pulp residue char-raw oil slurry exhibited a good characteristic of slurry transport, that is, it showed pseudoplastic behavior with a reduction in the apparent viscosity with increasing shear rate. This behavior was also found in palm shell char-aqueous solution slurries. On the other hand, slurry of palm shell char and its oil phase presented a flow transition from pseudoplastic to dilatant behavior at a certain shear rate and this would give a marked rise of viscosity at high shear rate that could create pump and injector blockages and poor atomization in burners. It should be also noted that the maximum solid concentration in cassava pulp residue char-raw oil slurry should be limited to 40 wt% and the maximum temperature of 45°C. In addition, it was suggested that natural size distribution of <38 μm for slurry preparation provided the best packing of char particles for cassava pulp residue char-raw oil slurry, thus showing the lowest shear stress and slurry viscosity. Fuel properties of all slurries and pH values were improved over those of bio-oils. Char-bio-oil slurries at 30 wt% solid had moderate calorific value of 18-32 MJ/kg, while that of char-water slurry at the same solid concentration could not be determined. The viscosity of the char-bio-oil slurry with 30 wt% solid loading varied between 179-351 mPas at the shear rate of 100 s^{-1}. For combustion behavior, the combustion temperatures of char-bio-oil slurries occurred between 280 and 560°C with no ignition delay compared with their solid chars.

On upgrading dewatered palm kernel bio-oil by blending with diesel and alcohol, alcohol types showed a profound effect on phase stability and fuel properties of the blended fuels. The use of butanol as a cosolvent gave better characteristics of phase behavior and fuel properties than by using ethanol for palm kernel bio-oil-diesel-alcohol system. A blend of bio-oil and butanol can alleviate some unsatisfied properties of bio-oil and offered reasonable heating value. The ranges of fuel properties of binary and ternary blended fuels are as follows; heating value, 33-41 MJ/kg; density at 25°C, 0.83-0.96 g/cm^3; viscosity at 40°C, 1.77-9.21 mm^2/s; carbon residue content, 1.02-4.66 wt%; ash content, 0.016-0.039 wt%; pour point, <-25 to -6°C; flash point, 19-42°C and pH, 6.1-6.5. Satisfactory prediction of some fuel properties of the fuel mixtures were obtained by using Kay’s mixing rule, modified Grunberg-Nissan equation and Andrade equation. In addition, interaction parameter derived from modified Grunberg-Nissan equation (G_{ij}) is indicative of a pair component affinity that helps to determine a proper co-solvent for a ternary composition system.

For the final part of bio-oil upgrading, esterification reaction using solid acid catalyst of Amberlyst15 was successful in converting organic acids to esters and reduced amount of active aldehydes. The use of H_2SO_4 liquid catalyst showed higher conversion at the same reaction condition. On effect of esterification conditions, higher esterification conversion was obtained from higher reaction temperature and longer reaction time, higher amounts of catalyst and alcohol and the use of shorter hydrocarbon chain of alcohol. The upgraded bio-oils showed lower amounts of active chemicals such as acids and aldehydes that could help to lessen ageing rate of bio-oil. It also gave a moderate heating value of 23-25 MJ/kg and improved fuel properties by lowering of density, viscosity, carbon residue content, ash content and pour point as well as giving higher value of pH. However, it was also noted that the application of Amberlyst15 can release active H^+ located on resin catalyst that could inevitably increase the acidity of bio-oil.

Finally, results from studying steam gasification of larch wood in a shallow fluidized bed gasifier indicated that type of bed material, gasification temperature and gasifying reagent had strong influence on qualities of gas products. Calcined limestone gave the highest gas yield, cold gas efficiency and tar removal. Additionally, it showed high ability to adsorb CO_2 in bed at 650°C. The use of calcined waste concrete was reasonably effective in steam gasification process but the use of silica sand offered only half of gas heating value and tar adsorption compared to those of calcined limestone. At the higher temperature of 750°C, calcined limestone still gave better gas qualities but with declining efficiency of CO_2 capture. The use of steam as a gasifying agent gave higher amount of gas product and higher H_2/CO ratio as compared to pyrolysis in the inert gas of 100% N_2. However, using calcined limestone in steam gasification process presented a tendency to break, agglomerate and sinter resulting in plugging and blocking of gas passage route. Using a mixture of 50:50 wt% of calcined limestone and calcined waste concrete has proved to mitigate theses problems and provided reasonably high cold gas efficiency (75.88 %LHV).

7.2 Outlooks of Gasification and Pyrolysis and a Note on Potential Biomasses in Thailand

Apart from petroleum fuels, various renewable energy sources should play an important role in supporting a continued increase of energy demand. Biomass has been proved to be the most promising energy-carrying agent that satisfies the environmental concerns. It is considered as an important renewable energy source for agriculture-based countries. Particularly, Thailand which has abundant supply of many indigenous biomasses, the use of biomass as an alternative source of energy should be certainly promoted.

Gasification and pyrolysis are the viable thermal conversion processes that can convert biomass into various forms of energy. However, the two processes differ in their basic operations and give different applications of products. For process selection, various factors need to be considered, for example, type, properties and quantity of biomass feedstock, form of required fuel, economic conditions, etc. For gasification process, main products are combustible gases or synthetic gases which can be used as a gas fuel or a starting feedstock for production of chemicals or transport fuels. The application of gas product is dictated by the gas quality (gas composition, tar emission and cold gas efficiency), which in turn depends on biomass type and process conditions. However, gas products from a gasification process have some limitations of market application and flexibility. The use of gas products needs huge costs for handling, transportation and storage. Therefore, it is best to use product gases on-site immediately, for instance, gasification process coupled with Fischer-Tropsch unit to produce biomass-to-liquid chemicals and integrated gasification combined cycle (IGCC) to give higher efficiencies and lower emissions for electricity generation. In addition, gasification plants should be located closer to source of biomass supply to reduce transportation costs and biomass collection. These restrictions thus determine the maximum capacity of a gasification plant. Moreover, gasifier type should also be taken into consideration. A simple and reliable technology such as an atmospheric downdraft reactor should be appropriate for a small gasification plant. With higher throughput, bubbling or circulating fluidized bed gasifiers should be more economical for scaling up. A pressurized reactor could be a better choice for IGCC because it is more attractive to pressurize the feed to a gasifier than to pressurize the syngas product.

Pyrolysis can convert biomass to various forms of valuable products but has an advantage over other processes in that it can directly produce a liquid fuel. The liquid fuel or bio-oil gives higher energy density than its original biomass. Thus, it is more convenient and cheaper for storage and transportation. Moreover, it has been proved to be reliable for using in boilers, furnaces, kilns and turbines for heat and power productions. Apart from the bio-oil product, solid and gas products can also be used as a source of energy. However, pyrolysis process has a certain disadvantage of requiring various auxiliary process technologies such as feed preparation, heat supply systems, liquid collection, etc. To approach the high profit and high efficiency for converting biomass via the pyrolysis process, proper managements of resource and energy supplies are a mandatory. Two possible options for applying pyrolysis process are suggested to effectively convert biomass into energy products. The first process is the integrated pyrocycling combined cycle (IPCC) that gives an increased efficiency and lowering costs for power generation. Pyrolysis products from a pyrolysis plant can be used as a fuel to supply the close-coupled power plant. The possible pyrolysis products including bio-oil, char and aqueous solution and char in form of slurry may be used as fuels for turbine engines to generate electricity. The derived exhaust heat could be used to generate steam for producing additional electricity or for supplying heat for the pyrolysis process itself. A pyrolysis plant should be situated close to a large source of biomass and pyolysis process should be designed to provide high efficiency of bio-oil production for supplying the power plant. The reactor type that has high specific capacity, ability of scaling up and simple construction and operation such as fluidized bed should be the first choice for IPCC. For the second option, pyrolysis products produced from a central pyrolysis plant can be supplied directly to various end-users. They can be used as various forms of energy sources or as starting feedstock for manufacture of various valuable products. Transportable fuels including bio-oil and char-bio-oil slurry should be the primary fuels for several energy users such as power plants and industrial factories. They can be also used to support biomass gasification plants that have a limitation of biomass logistics. Derived gases and char could be used as fuels for the pyrolysis process. Moreover, char may be sold as a solid fuel or a precursor for the production of activated carbon adsorbents. Apart from using aqueous solution in the form of slurry fuel, aqueous solution which contains light oxygenated compounds could be valuable for the production of food flavorings, pesticides, fertilizers, and emission control agents. This route can be adopted in varying plant scale, depending on various factors such as biomass quantity, requirement of products and logistics of product to users. In the case of scattered biomass availability, several small plants could supply pyrolysis products to local users. For a small plant scale, simple operation and a simple reactor such as a moving bed reactor should be applied.

Biomass type is a significant parameter that should be considered for energy generation via a thermochemical process. Although the thermochemical processes can accommodate a wide variety of biomass, the product quality depends specifically on biomass type. On gasification process, biomass type which possesses different chemical components has a strong effect on gas yield and compositions. Cellulose and hemicellulose can generate higher gas product than lignin which favors the formation of char product. Considering gas composition, high contents of CO and CO_2 are generally derived from cellulose and hemicellulose, while lignin gives high content of H_2 and CH_4. For generation of heat and power, biomass which can produce high gas yield and high calorific value at low gasification temperatures is more attractive in terms of economic benefit. On pyrolysis process, bio-oil is the most promising product to be used as an energy source. To attain acceptable characteristics of bio-oil, suitable biomass type should be considered. In this respect, this work has clearly demonstrated that biomass type not only had important effects on product distribution and product properties but it also affected the bio-oil upgrading method. Results from this study showed that palm kernel bio-oil from the slow pyrolysis process has high potentiality to substitute petroleum-based fuels. The dewatered palm kernel bio-oil has high heat content of 40 MJ/kg and gives the closest boiling range distribution to that of diesel fuel. In addition, pyrolysis of palm kernel cake is quite practical and economical for bio-oil production. High yields of palm kernel bio-oil can be obtained at a low pyrolysis temperature (about 500°C) and oil and aqueous phases can be easily separated by decanting. However, palm kernel oil has undesirable properties of high viscosity and slight acidity. Simple pretreatments such as solvent addition or blending with alcohol and diesel to reduce viscosity and acidity are satisfactory, enabling the possible use of the upgraded oil in various combustion systems. Moreover, palm kernel bio-oil should be attractive for converting it into synthetic mobile fuels via chemical/catalysis upgrading processes because it has the high contents of hydrocarbons among typical bio-oils. Palm shell and coconut shell could be attractive potential biomasses to produce a promising bio-oil. About 50 wt% of liquid yields from these bio-oils could be derived at the low temperature of about 500°C. In addition, aqueous solution dispersed in crude bio-oil can be easily separated by centrifugation and the dewatered bio-oils have moderate heating value of ~26 MJ/kg. However, both bio-oils have an important problem of high acidity that could prevent their direct uses in general processes. It may damage common construction materials such as carbon steel and aluminum and some sealing materials. Esterification is a simple method used successfully in converting acids in the bio-oil to esters. This method does not only decrease acidity in the bio-oil but helps to reduce ageing rate and viscosity of bio-oil resulting from alcohol addition. For cassava pulp residue and longan fruit seed, these biomasses gave lower liquid yield among others and their bio-oils possesses relatively low heating value (~14 MJ/kg, lower than biomass feedstock) as well as high acidity. The uses of these bio-oils in the form of char-bio-oil slurry fuel or the whole bio-oil as useful bulk chemicals should be more practical and economical. Apart from its effect on bio-oil properties, biomass type also affects significantly the char and gas products. Chars derived from palm kernel cake and palm shell gave a good characteristic of reasonably high porosity structure that may be further used as a starting precursor for activated carbon production. On the other hand, cassava pulp residue and longan fruit seed showed superiority to other biomasses in that they could produce high gas yield and heating value at low pyrolyis temperatures.

We can infer from this study that pyrolysis of palm kernel cake, palm shell and coconut shell have potentiality for energy production. In terms of biomass availability, they are produced approximately 800 ktonnes annually. The pyrolysis plant should be located close to industries that produce these wastes such as around central or southern part of Thailand. In addition, it should be noted that other available biomasses that offer similar properties of bio-oil could be co-pyrolyzed to increase feasibility of plant capacity and reduce cost of biomass transportation. Cassava pulp residue and longan fruit seed that give relatively high yields and high heating values of gas product should be used as feedstock for a gasification process. Annual production of cassava pulp residue left from starch industries may warrant the set up of conventional power plants at the central or northern regions. However, longan fruit seed, with low annual production, could be used as a co-biomass for a gasification plant for power generation or pyrolysis plant for production of chemicals or slurry fuels.

Apart from considering the potentiality of biomass available in Thailand, process technologies must also be taken into consideration for converting biomass via the two thermal conversion processes. A simple and low cost process should be a viable choice for the process selection. Biomass gasification with combined heat and power generation system should be most promising to provide the highest efficiency for simultaneous generation of electricity and heat. Low calorific value gas containing certain tar and particulate levels from biomass gasification can be directly combusted in simple systems such as boiler or gas engine. However, for IGCC, the use of fuel gas in fuel cell or synthesis of transport fuels that require rather high technologies of gasification and gas cleaning processes are still less attractive in this country. For biomass pyrolysis, it is far less competitive processes for energy production due to the low fuel quality of bio-oil and requiring various units and reliable technologies for process operation. To initiate this technological process, several small plants supplying pyrolysis products to local users could be the best alternative. The adoption of a simple process operation, for example, a moving bed pyrolysis reactor located in various areas where sufficiently supply of biomass can be realized. In addition, all useful products derived from the pyrolysis process should be fully used as both transportable fuels and valuable feedstocks to gain the maximum benefits from this process.

7.3 Recommendations for Further Studies

7.3.1 Biomass Pyrolysis and Applications

- A continuous process of slow pyrolysis on a larger scale unit should be investigated. A moving bed reactor should be a suitable reactor for this purpose due to its simple operation and construction. The pyrolysis system should be designed in such a way to save resource and energy consumptions. The amount of N_2 sweep gas flow can be minimized by using recycled carrier gas. The possibility of this route should be investigated by studying the effect of the use of recycled carrier gas on product yield and compositions. In addition, a simple condenser system should be applied and the lowest condensing temperature used could be higher than that used in this study because almost 95 wt% of liquid product was derived from the first condenser maintaining at -6 to -8°C and at the second condenser light oxygenated compounds were obtained.

- There are various undesirable properties of bio-oil affecting the operations of an engine and fuel system equipment. For example, low energy density of bio-oil requires a fuel system that can provide higher feed flow rate to achieve the same energy output as that of typical petroleum fuels, its high viscosity cause deleterious effect on fuel atomization and low pH of bio-oil demands the use of stainless steel or polymer materials for all components wetted by the bio-oil. Improvement of bio-oil properties for using in commercial engines should be more beneficial than by the modification of the engine. However, the complicated upgrading methods to convert bio-oil to transport fuels are still costly compared with other renewable fuels such as biodiesel or gasohol that are available in Thailand. Simple methods of bio-oil upgrading could be employed but it may need a series of steps to achieve the final required fuel properties. For instance, oil phase and aqueous phase of bio-oil should be first separated by a simple basic method such as decanting or centrifugation before the pH of bio-oil is further adjusted via esterification to obtain lower acidity and reduced viscosity, followed by filtration to reduce carbon residue content and addition of a certain additive to reduce ash content. Each simple upgrading method proposed in this research should be further investigated as follows:

Char-bio-oil slurry - Blending the raw bio-oil with its co-product char in the form of slurry has improved calorific value and acidity of bio-oil but pH value of slurry is still low. The combined use of bio-oil and waste solvents or alcohols obtained from renewable sources as a co-suspending medium could give a satisfactory pH value of the slurry fuel. In this regard, effects of solvent type and amount of added solvent on the rheological behavior and fuel properties of a given slurry should be also undertaken.

Bio-oil-Diesel-Alcohol blends - To fully utilize bio-oil in any combustion system, optimum ratio of these three components should be explored. An added alcohol can improve various properties of bio-oil and diesel such as reducing the high viscosity of bio-oil, black smoke and emissions of CO and NO_x of diesel, etc. However, large quantity of alcohol solvent required to achieve a single phase of the mixture can cause undesirable properties such as a marked difference of boiling distillation temperature, resulting in longer warming-up time of engines and relatively and low flash point, thus giving increased likelihood of self ignition during storage. The amount of alcohol could be reduced by adding an additive to increase affinity between bio-oil and diesel. Moreover, a mixed co-solvent of different chain length of alcohol could give different polarity, enabling better miscibility of bio-oil and diesel.

Esterification - Catalyst plays a major role in this esterification upgrading method. A more effective catalyst that could give a complete conversion with low usage of added alcohol and without the release of proton from catalyst active site should be further investigated. Process conditions that can minimize the amount of alcohol should be also explored. This is because the presence of alcohol in the upgraded bio-oil will give its flash point getting close to room temperature and this could affect the combustion characteristics. In addition, the improved ageing characteristic of upgraded bio-oils from esterification process should be further studied.

- Bio-oils derived from different biomass types and different upgrading methods and the prepared char-bio-oil slurries should be tested with various combustion engines to assess their possibilities for applying in the real systems and to obtain useful information for the development of further upgrading methods. Furthermore, long term operation with various bio-oils and char-bio-oil slurries should be undertaken.
- Apart from the application of bio-oil in energy utilization, by-products consisting of aqueous solution and char should be served as a source of several valuable products to provide further benefits of the pyrolysis process. Further studies should be made on the use of aqueous solution from bio-oils as food flavorings, pesticides and fertilizers, the combined use of char and aqueous solution to improve soil qualities, etc.
- Possibility of running pyrolysis plant with two different routes including integrated pyrocycling combined cycle (IPCC) for electricity generation and a central pyrolysis plant to produce various forms of energy sources and valuable products should be intensively assessed. The assessment should be conducted on various important factors such as biomass availability, product applications, plant capacity, reliability of process, ease of operation and cost and energy saving. Moreover, economic competitiveness including fuel prices, taxes and incentives should be also considered.

7.3.2 Biomass Gasification

- For the study of biomass gasification, bed materials including calcined limestone, calcined waste concrete and mixed bed material of calcined limestone and calcined waste concrete gave reasonable gas quality for a batch fluidized bed gasifier. However, efficiency and reliability of these bed materials should be also confirmed and tested in a larger scale gasification process. In this work, N_2 which is used as a gas carrier for steam gasification could be substituted with air carrier gas to reduce cost from using pure N_2 gas. The effect of carrier gas on gasification products should thus be further studied.

- Commercial plants of biomass gasification for electricity generation have been operated in Thailand. However, the improvement in the efficiency of a gasification process should be required and several potential biomasses available in Thailand should be further tested and assessed to provide additional energy sources for the country.

APPENDIX

LIST OF PUBLICATIONS

LIST OF PUBLICATIONS

1. Referred Journals

Weerachanchai, P., Horio, M., and Tangsathitkulchai, C. (2009). Effects of gasifying conditions and bed materials on fluidized-bed steam gasification of wood biomass. **Bioresource Technology** 100: 1419–1427.

2. Conference Proceedings

Weerachanchai, P., Tangsathitkulchai, C., and Tangsathitkulchai, M. (2006). Characteristics of bio-oil from biomass pyrolysis. **2nd Energy Technology Network of Thailand (E-NETT2006)**.

Weerachanchai, P., Tangsathitkulchai, C., and Tangsathitkulchai, M. (2007). Fuel properties and chemical compositions of bio-oils from biomass pyrolysis. **JSAE/SAE International Fuels and Lubricants Meeting (JSAE/SAE2007)**.

Weerachanchai, P., Tangsathitkulchai, C., and Tangsathitkulchai, M. (2009). Phase behaviors and fuel properties of bio-oil-diesel-alcohol blends. **International Conference on Energy and Environment (ICEE2009).**

3. Conference Abstracts

Weerachanchai, P., Tangsathitkulchai, C., and Tangsathitkulchai, M. (2006). Fuel properties of bio-oil from pyrolysis of biomasses. **RGJ-Ph.D. Congress VII.**

3. Conference Abstracts (Continued)

Weerachanchai, P., Tangsathitkulchai, C., and Tangsathitkulchai, M. (2008). Products from slow pyrolysis of biomasses. **The 18th Thailand Chemical Engineering and Applied Chemistry Conference (TIChE18-2008).**

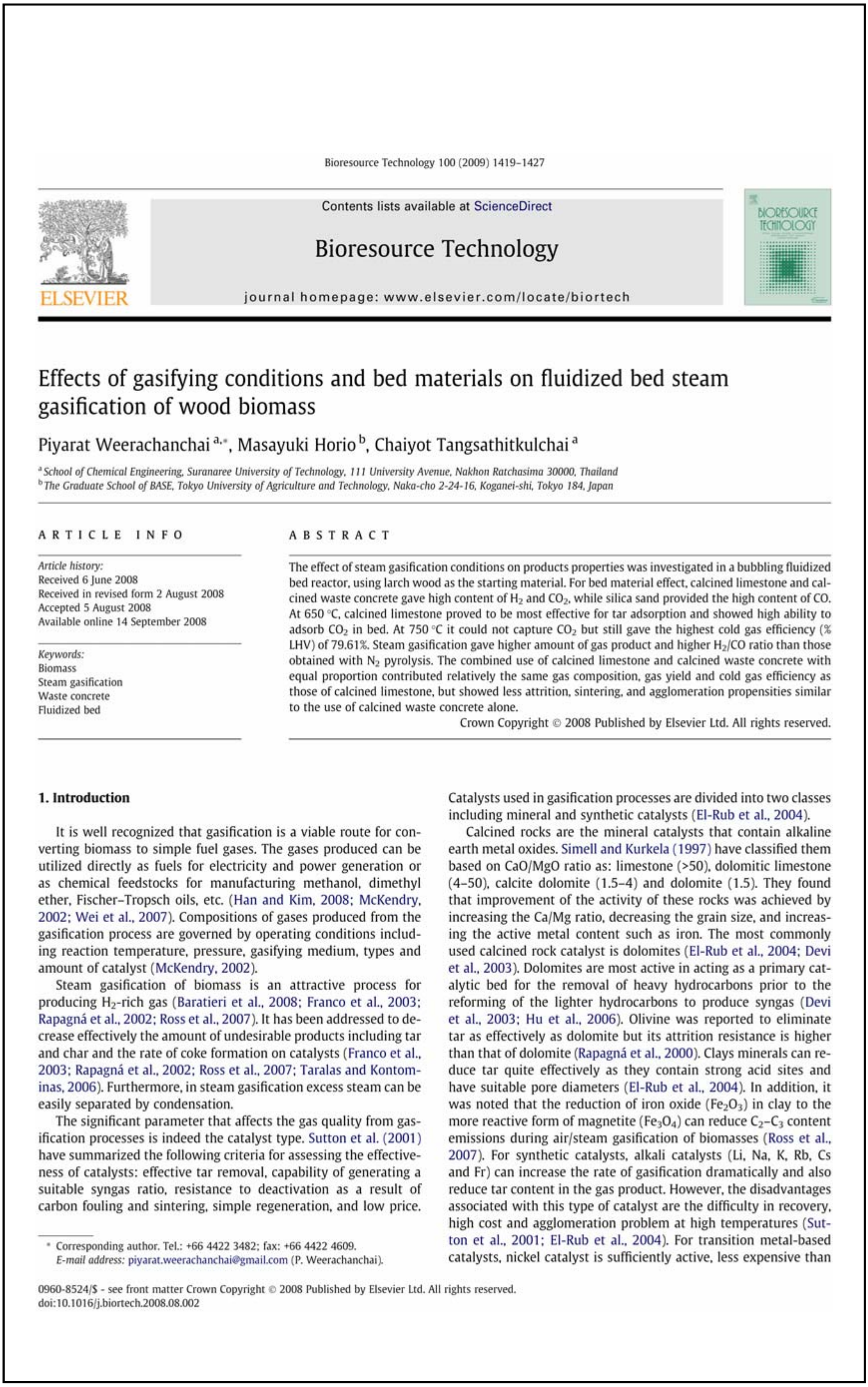

Bioresource Technology 100 (2009) 1419–1427

Contents lists available at ScienceDirect

Bioresource Technology

journal homepage: www.elsevier.com/locate/biortech

Effects of gasifying conditions and bed materials on fluidized bed steam gasification of wood biomass

Piyarat Weerachanchai [a,*], Masayuki Horio [b], Chaiyot Tangsathitkulchai [a]

[a] *School of Chemical Engineering, Suranaree University of Technology, 111 University Avenue, Nakhon Ratchasima 30000, Thailand*
[b] *The Graduate School of BASE, Tokyo University of Agriculture and Technology, Naka-cho 2-24-16, Koganei-shi, Tokyo 184, Japan*

ARTICLE INFO

Article history:
Received 6 June 2008
Received in revised form 2 August 2008
Accepted 5 August 2008
Available online 14 September 2008

Keywords:
Biomass
Steam gasification
Waste concrete
Fluidized bed

ABSTRACT

The effect of steam gasification conditions on products properties was investigated in a bubbling fluidized bed reactor, using larch wood as the starting material. For bed material effect, calcined limestone and calcined waste concrete gave high content of H_2 and CO_2, while silica sand provided the high content of CO. At 650 °C, calcined limestone proved to be most effective for tar adsorption and showed high ability to adsorb CO_2 in bed. At 750 °C it could not capture CO_2 but still gave the highest cold gas efficiency (% LHV) of 79.61%. Steam gasification gave higher amount of gas product and higher H_2/CO ratio than those obtained with N_2 pyrolysis. The combined use of calcined limestone and calcined waste concrete with equal proportion contributed relatively the same gas composition, gas yield and cold gas efficiency as those of calcined limestone, but showed less attrition, sintering, and agglomeration propensities similar to the use of calcined waste concrete alone.

1. Introduction

It is well recognized that gasification is a viable route for converting biomass to simple fuel gases. The gases produced can be utilized directly as fuels for electricity and power generation or as chemical feedstocks for manufacturing methanol, dimethyl ether, Fischer–Tropsch oils, etc. (Han and Kim, 2008; McKendry, 2002; Wei et al., 2007). Compositions of gases produced from the gasification process are governed by operating conditions including reaction temperature, pressure, gasifying medium, types and amount of catalyst (McKendry, 2002).

Steam gasification of biomass is an attractive process for producing H_2-rich gas (Baratieri et al., 2008; Franco et al., 2003; Rapagná et al., 2002; Ross et al., 2007). It has been addressed to decrease effectively the amount of undesirable products including tar and char and the rate of coke formation on catalysts (Franco et al., 2003; Rapagná et al., 2002; Ross et al., 2007; Taralas and Kontominas, 2006). Furthermore, in steam gasification excess steam can be easily separated by condensation.

The significant parameter that affects the gas quality from gasification processes is indeed the catalyst type. Sutton et al. (2001) have summarized the following criteria for assessing the effectiveness of catalysts: effective tar removal, capability of generating a suitable syngas ratio, resistance to deactivation as a result of carbon fouling and sintering, simple regeneration, and low price. Catalysts used in gasification processes are divided into two classes including mineral and synthetic catalysts (El-Rub et al., 2004).

Calcined rocks are the mineral catalysts that contain alkaline earth metal oxides. Simell and Kurkela (1997) have classified them based on CaO/MgO ratio as: limestone (>50), dolomitic limestone (4–50), calcite dolomite (1.5–4) and dolomite (1.5). They found that improvement of the activity of these rocks was achieved by increasing the Ca/Mg ratio, decreasing the grain size, and increasing the active metal content such as iron. The most commonly used calcined rock catalyst is dolomites (El-Rub et al., 2004; Devi et al., 2003). Dolomites are most active in acting as a primary catalytic bed for the removal of heavy hydrocarbons prior to the reforming of the lighter hydrocarbons to produce syngas (Devi et al., 2003; Hu et al., 2006). Olivine was reported to eliminate tar as effectively as dolomite but its attrition resistance is higher than that of dolomite (Rapagná et al., 2000). Clays minerals can reduce tar quite effectively as they contain strong acid sites and have suitable pore diameters (El-Rub et al., 2004). In addition, it was noted that the reduction of iron oxide (Fe_2O_3) in clay to the more reactive form of magnetite (Fe_3O_4) can reduce C_2–C_3 content emissions during air/steam gasification of biomasses (Ross et al., 2007). For synthetic catalysts, alkali catalysts (Li, Na, K, Rb, Cs and Fr) can increase the rate of gasification dramatically and also reduce tar content in the gas product. However, the disadvantages associated with this type of catalyst are the difficulty in recovery, high cost and agglomeration problem at high temperatures (Sutton et al., 2001; El-Rub et al., 2004). For transition metal-based catalysts, nickel catalyst is sufficiently active, less expensive than

---

[*] Corresponding author. Tel.: +66 4422 3482; fax: +66 4422 4609.
E-mail address: piyarat.weerachanchai@gmail.com (P. Weerachanchai).

0960-8524/$ - see front matter Crown Copyright © 2008 Published by Elsevier Ltd. All rights reserved.
doi:10.1016/j.biortech.2008.08.002

noble metal catalysts such as Ru, Pt, and Rh and considered to be the most important catalyst in hot gas cleaning processes. They are highly effective to remove tar and help improve the content of syngas. Deactivation of the nickel catalysts are mainly due to carbon deposition and nickel particle growth. Char is an attractive synthetic catalyst due to its low price, being the direct by-product from gasification processes. Char has ample catalytic activity to eliminate tar but it can be deactivated by coke formation and loss of char mass in steam and dry reformation reactions (El-Rub et al., 2004).

As mentioned above, steam gasification can provide high H_2 content, but the undesirable products such as CO_2 and tars are also simultaneously generated. To enhance the efficiency of steam gasification, considerable efforts have been devoted to produce high yield of H_2 with simultaneous capture of CO_2. It has been reported (Florin and Harris, 2006) that the CaO introduced could capture CO_2 via Eq. (1) during gasification reaction, thus shifting the equilibrium reactions of the water–gas reaction by Eq. (2), methane reforming by Eq. (3) and water–gas shift reaction by Eq. (4) to promote a H_2-rich gas product.

$$CaO + CO_2 \rightarrow CaCO_3, \quad \Delta H_{298} = -170.5\ \text{kJ/mol} \tag{1}$$

$$C + 2H_2O \rightarrow CO_2 + 2H_2, \quad \Delta H_{298} = +100\ \text{kJ/mol} \tag{2}$$

$$CH_4 + 2H_2O \rightarrow CO_2 + 4H_2, \quad \Delta H_{298} = +165\ \text{kJ/mol} \tag{3}$$

$$CO + H_2O \rightarrow CO_2 + H_2, \quad \Delta H_{298} = -41\ \text{kJ/mol} \tag{4}$$

Lin et al. (2002, 2003, 2006) have developed HyPr-RING (hydrogen production by reaction-integrated novel gasification) which used calcium oxide (CaO) and/or calcium hydroxide ($Ca(OH)_2$) as the CO_2 adsorbent. However, it was found that this process had to be operated at a high steam pressure. From the limitations of capital and operating costs for high pressure processes, hydrogen production with CO_2 capture at atmospheric pressure should be more desirable. Hughes et al. (2005) have shown that at atmospheric pressure, the optimum temperature for carbonation of CaO should be in the range 650–750 °C. Furthermore, the capability of $CaCO_3$ formation at the respective temperature depended on the CO_2 partial pressure; CO_2 can be best adsorbed at a suitable partial pressure for a given temperature (Xu et al., 2005).

It should be noted that CaO is an attractive material that can play the combined roles of catalyst and adsorbent in a steam gasification process. Limestone is a commonly used material in the gasification process and CO_2 adsorption. However, it was reported that there were particle attrition and deactivation problems for long operation time and at temperatures higher than 650 °C (Florin and Harris, 2008). In this study, we propose to use waste concrete as another potential bed material in a steam gasification process. It is a material left for disposal after the concrete structures such as buildings, bridges, dams, road surfaces are demolished. Generally, the concrete contains CaO in the forms of tricalcium silicate ($3CaO \cdot SiO_2$), dicalcium silicate ($2CaO \cdot SiO_2$), tricalcium aluminate ($3CaO \cdot Al_2O_3$) and tetracalcium aluminoferrite ($4CaO \cdot Al_2O_3 \cdot Fe_2O_3$) (Mindess et al., 2003).

In this work, the steam gasification of biomass (larch) was performed in a batch bubbling fluidized bed reactor. The effects of gasification conditions including types of bed material (silica sand, calcined lime stone and calcined waste concrete), temperature (650 and 750 °C) and gasifying agents (steam and N_2) on gasification products were investigated. Analytical techniques of thermogravimetric analysis (TGA), X-ray diffraction (XRD) and scanning electron microscope (SEM) were used to investigate CO_2 adsorption and physical deterioration of bed material at the end of gasification operation. In addition, the combined use of calcined limestone and calcined waste concrete as a new bed material in the steam gasification process was also studied.

2. Experimental

2.1. Preparation of raw materials

Biomass feedstock used in this study was larch, which is one species of coniferous tree classified in the genus Larix of the family Pinaceae. Larch was supplied by Kuzumaki-Ringyo Co., Ltd. in the form of pellet (0.7 cm in diameter and 4.0 cm long). It was milled, sieved to the size fraction of 250–600 μm (20 × 60 mesh) and packed into a cellulose capsule (Matsuya Corporation: size no. 3 and weighing 0.05 g). Four alumina balls (2 mm in diameter) were also put inside the cellulose capsule to make the capsule sufficiently heavy to sink quickly downward in the fluidized bed after being fed into the gasifier, thus avoiding overbed gasification of the biomass. The larch pellet and the cellulose capsule were analyzed for their elemental compositions (A JM10 Micro Corder-CHN analyzer: J-Science Laboratory Co., Ltd.), proximate analysis for moisture content (ASTM D2867-95), volatile content (ASTM D5832-95), ash content (ASTM D2866-94) and fixed carbon content (by difference), and calorific values (Gallenkamp Bomb Calorimeter, Weiss Gallenkamp Ltd.).

Silica sand, limestone and waste concrete were used as bed materials in this study. Silica sand and limestone were acquired from Toyoura Keiseki Kogyo Co., Ltd. and Chichibu lime industry Co., Ltd., respectively. The waste concrete abandoned from remnants of the residential structures was received from a waste recycling company (Jobu Eco-Clean Co., Ltd.). These bed materials were crushed and sieved to obtain the particle size in the range of 150–250 μm (60 × 100 mesh). In addition, for limestone and waste concrete, they were further calcined at the temperature of 900 °C for 3 h prior to running the gasification experiments. Apparently, there was no observed change in the particle sizes of the bed materials after the calcination treatment. The physical properties of bed materials including particle density, pore volume, and surface area, were analyzed by a mercury porosimeter (Pore Sizer 9310: Micromeritics). Chemical compositions of the bed materials were identified and quantified by inductively coupled plasma emission spectroscopy (ICP-ES) (ICPS-7500 Sequential plasma spectrometer: Shimadzu Corporation).

2.2. Biomass gasification

Biomass gasification was performed in a fluidized bed gasifier at atmospheric pressure. Fig. 1 shows the schematic diagram of the experimental apparatus. Each bed material (125 g of calcined limestone, 125 g of calcined waste concrete, 125 g of a 50:50 wt% mixture of calcined limestone and calcined waste concrete, and 225 g of silica sand) was packed to the height of 8.0 cm inside a heated fluidized bed column made of stainless steel pipe (4.2 cm ID and 57.5 cm high). A mixture of 85 vol% steam and 15 vol% N_2 was introduced into the outer stainless steel pipe, and then flowed upwardly through the distributor (a sintered porous plate) with the superficial gas velocity of about five times the minimum fluidizing velocity ($U_0 = 5U_{mf}$) to ensure intense mixing and uniform bed temperature. The minimum fluidizing velocities for various gasification conditions were estimated by both visual observation and the traditional pressure drop-velocity diagram measured at the gasification temperatures. When the system was heated from room temperature to the desired gasification temperature at 650 or 750 °C, capsules containing biomass were dropped one by one into the gasifier through the nitrogen purged lockhopper at the rate of 0.21 g/min for a total of 3 g of biomass. In all experimental runs the total reaction time was 60 min. Over the course of steam gasification, the product gases passed through two tar trapping tubes packed with 2 mm of alumina balls and maintained at 200

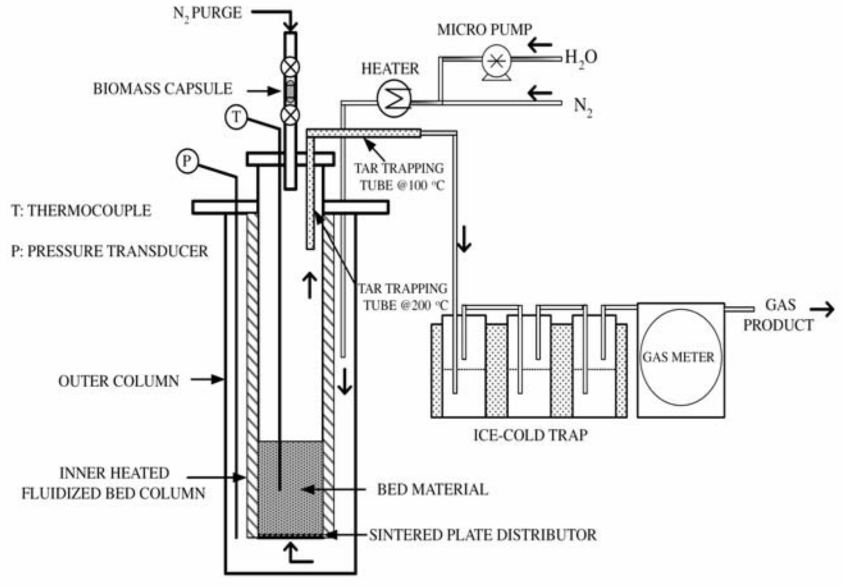

Fig. 1. Experimental fluidized bed gasification system.

and 100 °C, respectively. Subsequently, steam and tar of some light molecular weights were condensed in the three bottles connected in series. A volume of 300 cm^3 of distilled water was filled in each bottle and the temperature was controlled at 0–5 °C. Non-condensable gases were collected in teflon sample bags for subsequent gas composition analysis. The experimental gasification conditions used are listed in Table 1.

2.3. Product analyses

After the gasification test was completed, total gas product collected was analyzed by Micro GC (Agilent 3000, Agilent Technology) with a thermal conductivity detector; the micro GC consists of two independent capillary columns of PoraPLOT Q for CO_2, C_2H_4 and C_2H_6 and Molecular Sieve 5A with PoraPLOT U pre-column for H_2, O_2, N_2, CH_4 and CO. Knowing the product gas compositions and the volume collected, the cold gas efficiency (% LHV) can be computed as the percentage ratio of lower heating value (LHV) of the gas product and that of the starting feedstock.

Char (250–650 μm) and the bed material (150–250 μm) were first separated by careful hand sieving using a 60 mesh (250 μm) screen. Char retaining on the screen with a small amount of bed material adhering on the char particles were weighed and ground to fine sizes and its total carbon content was determined by using a CHN analyzer (JM10 Micro Corder: J-Science Laboratory). Materials passing the screen which consisted mainly of the bed material plus little amount of fine char particles were distributed uniformly on a tray and about 100 g of the sample was randomly collected for determining carbon content in the bed material by CHN analyzer. No attempt was made to separate completely the bed material and the char particles in the oversize and undersize screen fractions for the contamination in each fraction was considered to be insignificantly small. Total volume of condensed water was measured and its carbon content was analyzed by total organic carbon analyzer (TOC-2000, Hiranuma). The spent alumina balls packed in the 200 and 100 °C tar trapping tubes were combusted at 800 °C in a horizontal tube furnace. The generated CO_2 was then collected in a teflon gas bag and the amount of CO_2 was quantified by a micro GC. From the known gas volume of CO_2 and its composition, the carbon contents of tar at 200 and 100 °C were thus determined. As a result, carbon distributions of gasification products in gas, char and tar (collected in bed material, trapped tar at 200 and 100 °C and condensed water) could be determined.

Evidence for CO_2 adsorption by the bed materials was evaluated by XRD technique (RINT-2000-XRD, Rigaku Corporation) and a thermogravimetric analyzer (TG-DTA 2000S, Material analysis

Table 1
Experimental conditions used in fluidized bed steam gasification of biomass

Run no. Bed material	1 Silica sand	2 Calcined limestone	3 Calcined waste concrete	4 Calcined limestone (100% N_2)	5 Calcined limestone	6 Calcined waste concrete	7 Mixed bed material[a]
Temperature (°C)	650	650	650	750	750	750	750
Steam (vol%)	85	85	85	–	85	85	85
Minimum fluidizing velocity U_{mf} (m/s)	0.0216	0.0197	0.0203	0.0147	0.0179	0.0184	0.0181
Superficial gas velocity U_0 (m/s)	0.1016	0.0997	0.1003	0.0947	0.0979	0.0984	0.0981
Biomass feed rate (g/min)	0.21	0.21	0.21	0.21	0.21	0.21	0.21
Total feedstock (larch and capsule) (g)	3.00	3.00	3.00	3.00	3.00	3.00	3.00
Bed height (cm)	8.0	8.0	8.0	8.0	8.0	8.0	8.0

[a] About 50:50 wt% mixture of calcined limestone and calcined waste concrete.

and characterization). For thermogravimetric analysis, a sample of 10–15 mg of spent bed material was heated from room temperature to 1000 °C with the heating rate of 30 °C/min under a nitrogen flow rate of 100 cm^3/min. Physical deterioration of bed materials after gasification was examined by a field emission scanning electron microscope (FE-SEM) (JSM-6330FS, JEOL).

3. Results and discussion

3.1. Raw material properties

3.1.1. Feedstock

Table 2 shows the basic chemical compositions and calorific values of the feedstocks used in this work. The elemental compositions of larch and capsule are relatively similar; carbon and oxygen are the major elements with the values varying between 44 and 49 wt%. However, the results of proximate analysis show that cellulose capsule contains much higher volatile and lower fixed carbon than those of larch pellet. The lower heating values of both feedstocks are approximately 20 MJ/kg.

3.1.2. Bed material

The physical properties of the three bed materials are shown in Table 3. Their particle densities are in the range of 2600–2800 kg/m^3. The bulk density of silica sand is highest (~1900 kg/m^3) and that of calcined limestone and calcined waste concrete are approximately the same of 1100 kg/m^3. The magnitude of pore volume and surface area of the three bed materials are in the following order: calcined limestone > calcined waste concrete > silica sand. The pore size distribution data of the bed materials are shown in Fig. 2. It indicates that the pore sizes of all bed materials distribute mostly within the macro pore size range (>50 nm). Silica sand shows almost no pore volume distribution and total pore volume is extremely low, indicating that it is almost non-porous. The pore sizes of calcined waste concrete vary widely in the range of 20–40,000 nm with a bimodal distribution characteristic. Calcined limestone shows a much narrower distribution between 50 and 10,000 nm with the smallest average pore size. The order of average pore size for the three bed materials is as follows: calcined waste concrete (933 nm) > calcined limestone (192 nm) > silica sand (181 nm).

Table 2
Feedstock properties

Properties	Materials	
	Larch	Cellulose capsule
Elemental analysis (wt%)		
C	44.18	48.83
H	6.38	6.71
N	0.12	0.17
O (by difference)	49.32	44.29
Chemical formula	$CH_{1.723}N_{0.002}O_{0.837}$	$CH_{1.816}N_{0.003}O_{0.749}$
Proximate analysis (wt%)		
Moisture	8.16	2.51
Volatile	76.86	96.13
Ash	0.12	0.51
Fixed carbon (by difference)	14.86	0.85
Lower heating value (MJ/kg)	19.45	20.16

Table 3
Properties of bed materials

Properties	Silica sand	Calcined limestone	Calcined waste concrete
Physical properties			
Particle density (kg/m^3)	2790	2551	2623
Bulk density (kg/m^3)	1900	1089	1106
Pore volume (cm^3/g)	0.01	0.28	0.19
Surface area (m^2/g)	0.19	5.86	1.72
Average pore diameter (nm)	181	192	933
Chemical composition			
CaO	0.52	99.26	14.80
SiO_2	92.64	0.00	69.61
Al_2O_3	3.71	0.36	5.34
Fe_2O_3	0.73	0.00	4.05
MgO	0.19	0.37	1.80
Total	97.79	100.00	95.60

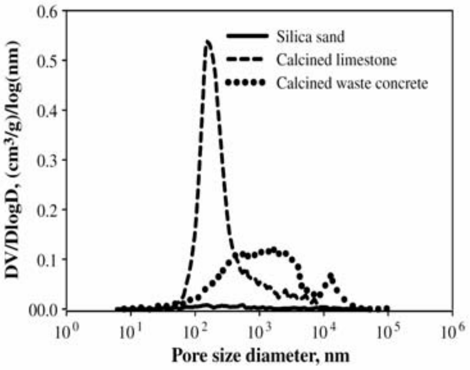

Fig. 2. Pore size distributions of the test bed materials.

The chemical compositions of bed materials were identified by inductively coupled plasma emission spectroscopy (ICP-ES). The oxide compositions of the three bed materials are shown in Table 3. Silica sand consists mainly of SiO_2 (92.64 wt%), as expected. Calcined limestone consists virtually of CaO (99.26 wt%) with trace amounts of Al_2O_3 and MgO. The major compositions of calcined waste concrete are SiO_2 (69.61 wt%) and CaO (14.80 wt%).

3.2. Biomass gasification

3.2.1. Effect of bed material types

The three bed materials including silica sand, calcined limestone and calcined waste concrete were used to study the effect of bed materials on the produced gas compositions, carbon distribution of products and cold gas efficiency (% LHV) for steam gasification at 650 °C. The results are presented in Fig. 3 and Table 4.

As observed, the type of bed material had a strong influence on the yield and composition of gas produced from the gasification process. Silica sand provided the lowest amount of gas (18.39 mmol/g or 412 cm^3/g) with CO having the highest content (8.28 mmol/g or 45.0 vol%). The largest volume of gas (47.53 mmol/g or 1065 cm^3/g) was produced from gasification by using calcined limestone as the bed material. For this case, the major components of product gas were H_2 (30.21 mmol/g or 63.56 vol%) and CO_2 (11.77 mmol/g or 24.75 vol%). Overall, calcined waste concrete gave intermediate amount of produced gas of 33.18 mmol/g or 743 cm^3/g and yielded similar major gases of H_2 (15.57 mmol/g or 46.94 vol%) and CO_2 (10.14 mmol/g or 30.55 vol%) but with a higher concentration of CO (4.70 mmol/g or 14.18 vol%) compared with calcined limestone. Also from Fig. 3, the effect of bed material on the cold gas efficiency (% LHV) followed the same trend as the effect on the amount of gas produced. The following order of % LHV was observed: calcined limestone (56.47%) > calcined waste concrete (39.40%) > silica sand (33.37%).

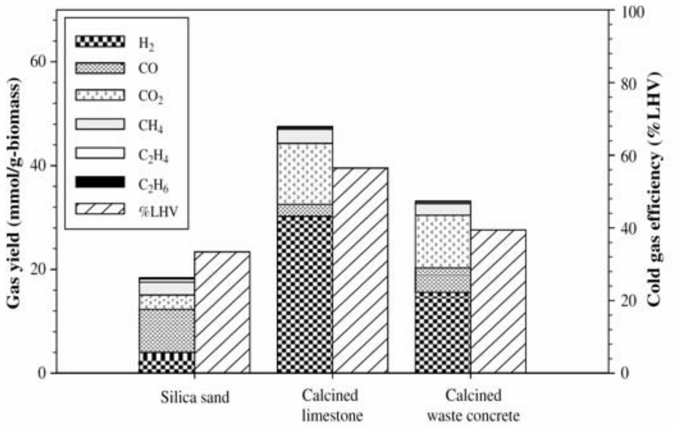

Fig. 3. Effect of bed materials on gas compositions for steam gasification at 650 °C.

Table 4
Gasification results obtained under various conditions

Bed material		Silica sand	Calcined limestone	Calcined waste concrete	Calcined limestone (100% N_2)	Calcined limestone	Calcined Waste concrete	Mixed bed material[a]
Temperature (°C)		650	650	650	750	750	750	750
Steam (vol%)		85	85	85	–	85	85	85
[Ca]/[C] mole ratio		–	19.83	2.94	19.39	20.01	2.99	11.58
Gas composition (vol%)	H_2	21.84	63.56	46.94	38.03	55.97	48.26	55.68
	CO	45.00	4.85	14.18	35.54	7.71	15.17	7.40
	CO_2	14.99	24.75	30.55	12.16	29.23	27.14	29.57
	CH_4	13.61	5.75	6.81	9.93	5.72	7.18	5.91
	C_2H_4	3.34	0.66	1.05	1.74	1.06	1.85	1.10
	C_2H_6	1.22	0.43	0.46	2.59	0.32	0.41	0.35
H_2/CO mole ratio		0.49	13.12	3.31	1.07	7.28	3.18	7.53
Gas formation (cm^3/g)		412	1065	743	692	1549	1194	1470
Lower heating value MJ/kg)		6.49	10.98	7.66	10.35	15.48	13.32	14.76
Cold gas efficiency (% LHV)[b]		33.37	56.47	39.40	53.19	79.61	68.46	75.88
Carbon distribution (wt%)	Gas products	39.75	47.91	48.95	52.78	78.75	76.09	79.91
	Char	26.37	20.85	23.87	20.61	3.05	2.32	3.51
	Bed material	6.68	19.68	11.52	23.36	14.97	11.96	12.13
	Tar at 200 °C	3.47	2.16	2.57	0.33	0.35	2.83	0.93
	Tar at 100 °C	4.00	1.16	1.19	0.38	0.34	2.07	0.86
	Condensed water	19.73	8.24	11.89	2.55	2.54	4.72	2.67
Carbon conversion (%)		73.63	79.15	76.13	79.39	96.95	97.68	96.49

[a] Combination of bed materials (50:50 wt% of calcined limestone and calcined waste concrete).

[b] Cold gas efficiency (% LHV) = (lower heating value of gas product/lower heating value of feedstock) × 100.

It has been reported that CaO could act as a catalyst to produce the H_2-rich gas (Florin and Harris, 2006; Franco et al., 2003; Rapagná et al., 2002; Ross et al., 2007). It can be observed from Table 3 that the three bed materials used in this study contain different contents of CaO and this could affect the compositions of gas products (Table 4). As observed from the above results, the bed material containing higher content of CaO could produce higher content of H_2 and CO_2 and lower amount of CO, presumably because of the catalytic role of CaO in converting CO to H_2 and CO_2 via water gas shift reaction of Eq. (4) (normally the reaction is appreciable at above 1000 °C (Lin et al., 2003)). The H_2/CO ratio derived from using different bed materials followed the sequence: calcined limestone (13.12) > calcined waste concrete (3.31) > silica sand (0.49). Moreover, it was observed that the content of light hydrocarbons of C_2H_4 and C_2H_6 derived from calcined limestone and calcined waste concrete was less than that of using silica sand as the bed material. This may result from the presence of CaO in calcined limestone and calcined waste concrete that could facilitate the conversion of these light hydrocarbon gases to CO and H_2 by the following equation (Wang et al., 2007).

$$C_nH_m + nH_2O \rightarrow nCO + \left(n + \frac{m}{2}\right)H_2, \quad \Delta H_{298} > 0 \tag{5}$$

As Table 4 shows, the types of bed material exerted relatively little influence on the carbon distribution in the char and tar. Percentage of carbon distributing in the char for the three bed materials varied in the range of 20.85–26.37 wt%, whereas total tar yield (carbon in bed material, condensed water and trapped tar at 200 and 100 °C) were 27.17–33.88 wt%. The results also indicate that calcined limestone is the most effective catalyst for carbon conversion with less tar emission (lowest %carbon in condensed water and trapped tar at 200 and 100 °C). This is consistent with the results of previous works (Franco et al., 2003; Mahishi and Goswami, 2007; Simell et al., 1992) which suggested that CaO enhanced the conversion of char and tar in steam gasification. Moreover, calcined limestone showed the highest percentage of tar removal by bed adsorption (19.68 wt% of carbon in bed material),

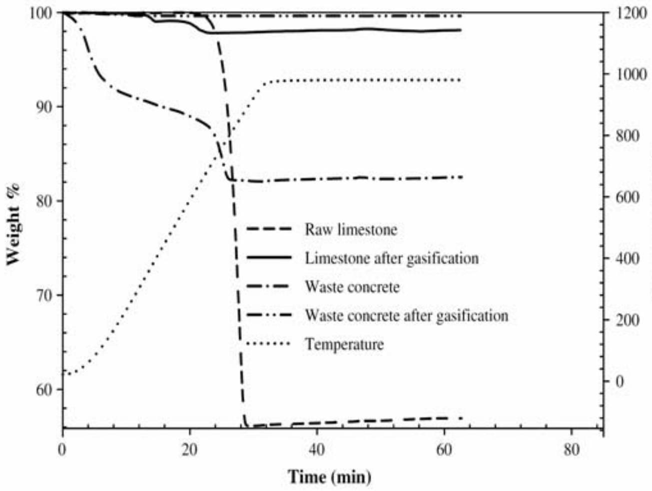

Fig. 4. TGA curves of bed materials after steam gasification at 650 °C.

as compared to 11.52 wt% for calcined waste concrete and 6.68 wt% for silica sand. The work of Ito et al. (2003) has shown that tar capture in the bed material depends on specific pore surface area and pore volume of the particle. Therefore, the significantly improved adsorption capacity of calcined limestone over the other two bed materials is obviously due to its larger pore volume and surface area.

The evidence of CO_2 adsorption by the bed material may be traced from examining the content of CO_2 in the gas products. During gasification, CO_2, H_2 and CO were generated simultaneously by several reactions such as the reactions of pyrolysis, water gas (Eq. (2)), steam reforming (Eqs. (3) and (5)) and water gas shift (Eq. (4)). According to these reactions, the higher H_2 contents observed with the use of calcined limestone (Fig. 3) was expected to be accompanied by the correspondingly higher CO_2 contents. It was noted, however, that the use of calcined limestone produced relatively the same amount of CO_2 in the gas product as in the case of calcined waste concrete although its H_2 content is higher (63.56% vs 46.94%). Thus, the disappearance of CO_2 during gasification in the fluidized bed using calcined limestone might be due to the effect of gas adsorption by the limestone bed. This hypothesis was tested by examining the XRD-patterns of calcined limestone and calcined waste concrete after gasification. The XRD-pattern of calcined limestone after gasification at 650 °C showed the existence of some additional peaks of $CaCO_3$ and $Ca(OH)_2$, indicating the possible incorporation of CO_2 and H_2O by the bed material. Furthermore, TG curves of Fig. 4 demonstrates that there were weight losses of calcined limestone after gasification at the temperature of 300–370 °C and 550–700 °C, conforming to the decomposition of $Ca(OH)_2$ and $CaCO_3$, respectively (Lin et al., 2006). Therefore, the ability of calcined limestone in capturing CO_2 during gasification was substantiated. In comparison, no capture of CO_2 by calcined waste concrete was observed from XRD results. This may be reasoned that calcined waste concrete contains much less content of CaO and lower available surface area and pore volume for CO_2 capture (cf. Table 3).

3.2.2. Effect of gasification temperature

Typically, biomass gasification in a fluidized bed system is operated at temperatures in the range of 800–900 °C (Saxena et al., 2008). However, for the purpose of studying the effect of CaO on the inbed capture of CO_2 to affect the gas yield and composition, it is necessary to operate the gasifier at a lower temperature range (Hughes et al., 2005). For this reason, the gasification temperatures of 650 and 750 °C were chosen in the present work. Fig. 5 and Table 4, respectively, show results on gas compositions and carbon distribution of the gasification products. The increase of gasification temperature from 650 to 750 °C had considerable effect on the gas yield and composition, carbon distribution of products and cold gas efficiency (% LHV). The increase in gas yield either with calcined limestone or calcined waste concrete was about 21 mmol/g biomass as the gasification temperature was increased. The increase in % LHV was 23.14% and 29.05% for calcined limestone and calcined waste concrete, respectively. In addition, %carbon in the char product and total tars (in bed material, trapped tar at 200 and 100 °C and condensed water) decreased markedly when the gasification temperature was increased. The decrease in char production for the two bed materials was almost the same, 17.80% and 21.55% for calcined limestone and calcined waste concrete, respectively. However, the amounts of total carbon in tars decreased by about 13.04% for calcined limestone and 5.59% for calcined waste concrete. It should be observed that the lowering of tar and char production gave rise to the increased carbon content in the product gas when the temperature was increased, as anticipated from the gas production from endothermic reactions of char decompositions via Eqs. (2) and (6) and steam reforming of hydrocarbon tar via Eq. (7). Gasification using calcined limestone at 750 °C generated the least tar emission (condensed water and trapped tar at 200 and 100 °C) of 3.23 wt% among other conditions. However, the increasing of temperature did not affect tar contents of high molecular weight (trapped tar at 200 and 100 °C) obtained from using calcined waste concrete as the bed material. This may result from the fact that calcined waste concrete contains much less amount of CaO than limestone to affect the following catalytic tar reforming reaction.

$$C + H_2O \rightarrow CO + H_2, \quad \Delta H_{298} = +131\ \text{kJ/mol} \tag{6}$$

$$\text{Tars} + H_2O \rightarrow H_2 + CO_2 + CO + \text{lower hydrocarbons}+, \ldots, \quad \Delta H_{298} > 0 \tag{7}$$

Concerning the effect of temperature on the composition of gas product, it was found that calcined waste concrete provided similar gas composition at the two gasification temperatures of 650

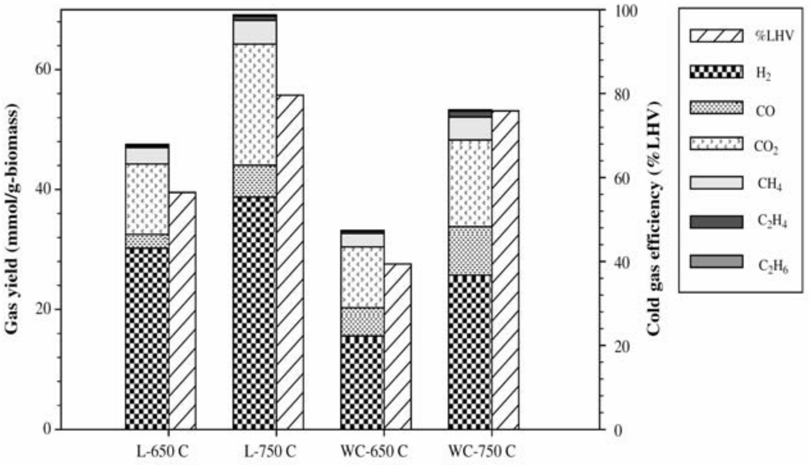

Fig. 5. Effect of gasification temperature on gas yield derived from using calcined limestone and calcined waste concrete (L: calcined limestone and WC: calcined waste concrete).

and 750 °C (cf. Table 4). In addition, for calcined waste concrete the H_2/CO ratio obtained at these two temperatures did not change much (3.18–3.31). When calcined limestone was used as the bed material, the H_2/CO molar ratios were 13.12 and 7.28 at the gasification temperatures of 650 and 750 °C, respectively (Table 4). This implies that the efficiency of converting CO to H_2 via water gas shift reaction (Eq. (4)) at 750 °C is lower than that at the lower temperature of 650 °C when calcined limestone was used. This result is in agreement with the work of Florin and Harris (2006) in that the exothermic water–gas shift reaction is favored at a lower temperature. In addition, the decrease of H_2 concentration may result from the deactivation of CaO sorbent at the temperature higher than 650 °C (Florin and Harris, 2008). When the lowering of CO_2 capture by CaO is observed, it means the lower capability of CaO to shift the equilibriums of the water–gas reaction via Eq. (2), methane reforming via Eq. (3) and water–gas shift reaction via Eq. (4). This was supported by the XRD results of both calcined limestone and calcined waste concrete at the higher gasication temperature of 750 °C, they did not adsorb much CO_2 at this higher temperature (no significant peaks of $CaCO_3$ were observed).

3.2.3. Effect of gasifying agents

Pure N_2 (pyrolysis) and the mixture of 85% steam and 15% N_2 (steam gasification) were used to compare the effect of gasifying agent by using calcined limestone as the bed material at 750 °C. It was found that the amount of total gas produced from steam gasification was higher than that obtained from pyrolysis process by about twofold (Fig. 6). A plausible explanation to this result could be the increased reaction conversion of lignocellulose biomass in the steam atmosphere (Haykiri-Acma and Yaman, 2008). Moreover, much lower carbon content of char and tar in bed material from steam gasification as compared to the pyrolysis process (Table 4) may be attributed to the contributions from char and tar decomposition reactions to produce more gas products when the steam was used. The carbon conversion in steam gasification

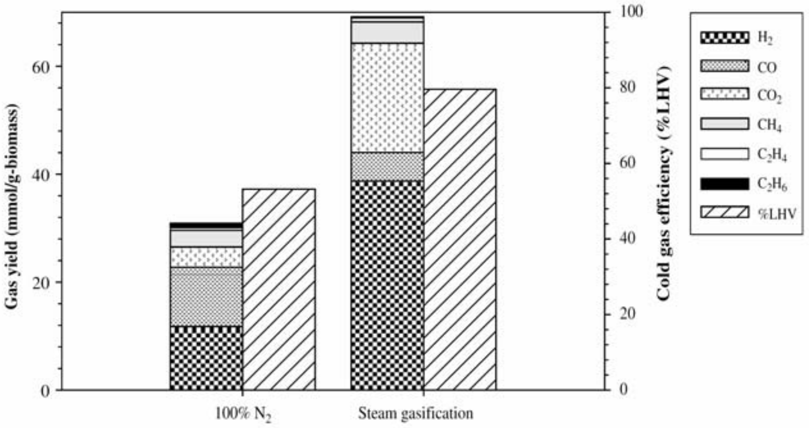

Fig. 6. Effect of gasifying agents on gas yield for 100% N_2 and steam gasification at 750 °C with calcined limestone as the bed material.

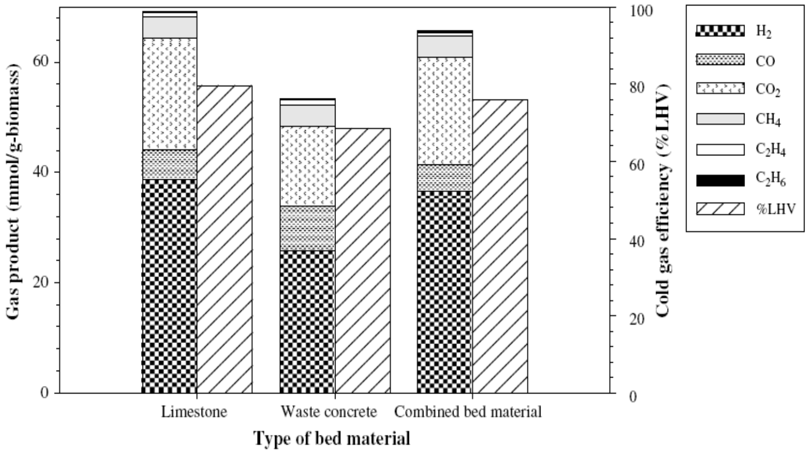

Fig. 7. Effect of mixed bed materials on gas yield for steam gasification at 750 °C.

reached 96.95%, whereas pyrolysis process could convert up to only 79.39% (cf. Table 4). In addition, percent of carbon in the bed material derived from steam gasification process was less than that of pyrolysis process by about 8.39%. Considering the tar emission, which was distributed in trapped tar at 200 and 100 °C and in condensed water, shows that there was almost no difference in the tar adsorption efficiency between the two processes.

As observed from Fig. 6, it was noted that there are differences in the gas compositions derived from the two different gasifying agents. The main gas product of steam gasification was H_2 (38.71 mmol/g) and CO_2 (20.21 mmol/g), while H_2 (11.76 mmol/g) and CO (10.99 mmol/g) were the major gas components in the pyrolysis process. For steam gasification, the significant increasing of H_2 and CO_2 content may be attributed to the char decompositions (Eqs. (2) and (6)), reforming of hydrocarbon gases and tars (Eqs. (3), (5), and (7)) and reactions of water–gas shift reaction (Eq. (4)). It may be also expected that the amount of CO should be increased through steam reforming reactions of hydrocarbon gases and tars (Eqs. (5) and (7)) and char decompositions (Eq. (6)). However, the lower content of CO derived from steam gasification was observed in this work and this may be due to the conversion of CO by water–gas shift reaction (Eq. (4)) to produce more H_2 and CO_2. In this study, steam gasification gave H_2/CO mole ratio about seven times higher than that obtained from the pyrolysis process (cf. Table 4).

3.2.4. Effect of mixed bed materials

As discussed earlier, the steam gasification with calcined limestone gave the highest cold gas efficiency (% LHV), H_2/CO ratio, and the lowest tar generation. However, limestone presented some disadvantages after being calcined and after steam gasification. It had a tendency to break, agglomerate and sinter; the resulting fine strong particle would cause the plugging and blocking of gas passage route such as parts of the trapped tar tubes used in this work. This problem could be intensified because of the increased temperature and higher contents of CO_2 and H_2O in the process (Florin and Harris, 2008). Evidence from SEM micrographs (not shown here) indicated the existence of small fragments of limestone particles after gasification while the breakage of waste concrete particles into smaller sizes did not occur even at the high gasification temperature of 750 °C. It is thus expected that calcined waste concrete can be applied at a high temperature and for a long period of gasification operation. In this respect, although waste concrete possesses the advantage of physical durability, it provides lower cold gas efficiency (% LHV) and higher tar emission than for the case of using calcined limestone.

To decrease the attrition and the agglomeration propensities during gasification operation and still maintaining reasonably high quality of gas product, the use of mixed bed materials was proposed in this work. An equal amount of calcined limestone and calcined waste concrete was mixed to give a 50:50 wt% mixture which was used in steam gasification at 750 °C. Fig. 7 and Table 4 show, respectively, the gas compositions and carbon distribution of products derived from using the mixture of calcined limestone and calcined waste concrete. It demonstrates that using the mixed bed materials gave comparable composition, amount of gas produced (65.62 mmol/g biomass or 1470 cm^3/g) and cold gas efficiency (75.88% LHV) to those of calcined limestone, but with less tar adsorption by bed material and slightly higher tar emission (trapped tar and condensed water). This can be explained on the ground that the use of mixed bed materials changed the [Ca]/[C] (see Table 4), which in turn affected the gas composition and tar emission. However, it is interesting to note that although mixed bed materials had lower [Ca]/[C] ratio but its H_2/CO molar ratio was still similar to that of calcined limestone (Table 4). In addition, in using the mixed bed material, the problems of attrition, sintering, and agglomeration became less than those of using calcined limestone alone. Therefore, a mixture of calcined limestone and calcined waste concrete should be a satisfactory bed material for steam gasification to provide high cold gas efficiency (% LHV) comparable to calcined limestone and yet giving longer physical durability.

4. Conclusions

The running of a shallow fluidized bed steam gasifier used in this study indicated that the gasification conditions had a strong influence on the gasification products derived from larch biomass. Major compositions of gas products observed from using calcined limestone or calcined waste concrete were H_2 and CO_2, while the highest CO concentration was obtained from using silica sand. Increasing gasification temperature from 650 to 750 °C caused the increase of % LHV by about 23.14–29.05% and the decrease of total tar by about 5.59–13.04%. However, the efficiency of CO_2

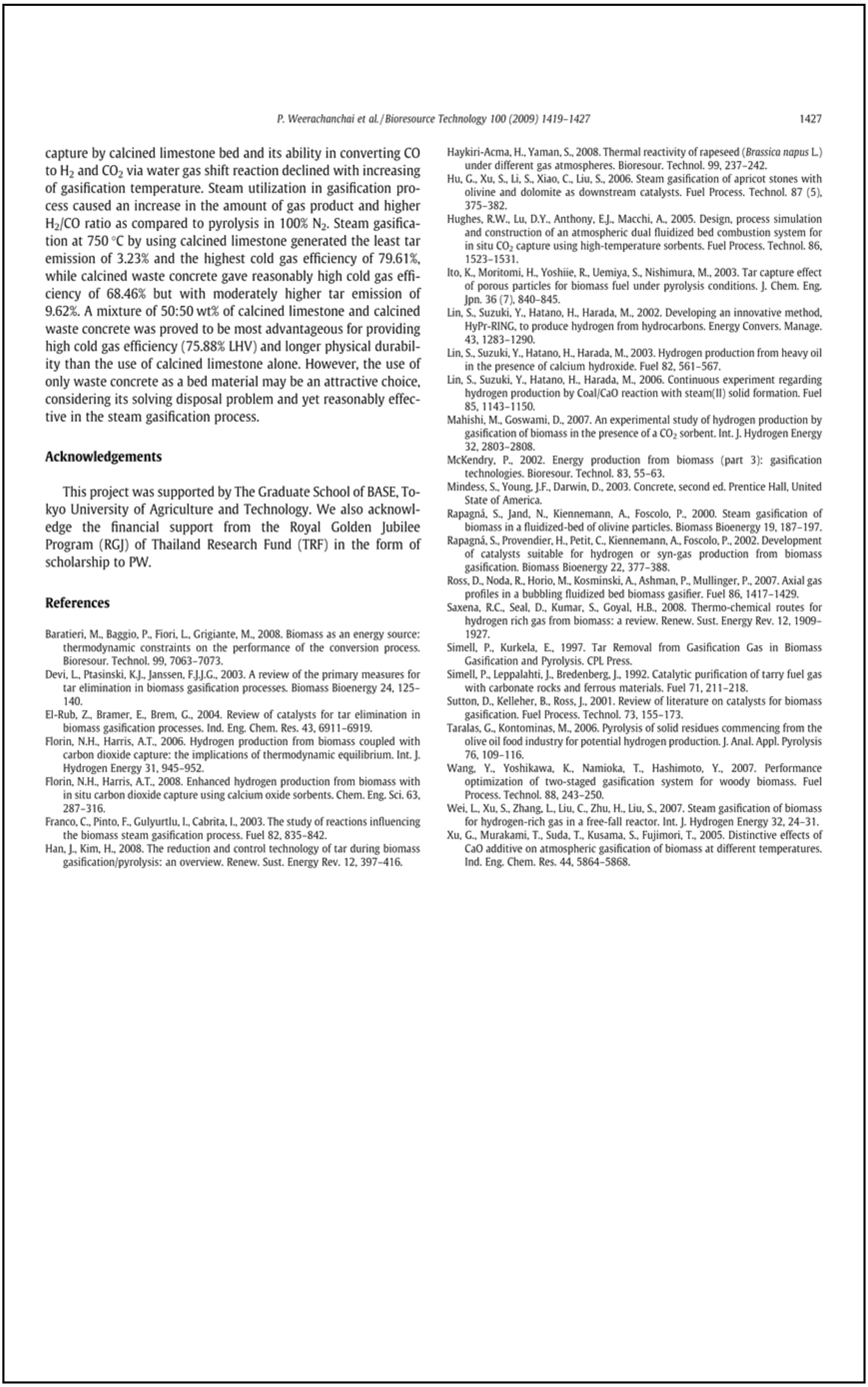

capture by calcined limestone bed and its ability in converting CO to H_2 and CO_2 via water gas shift reaction declined with increasing of gasification temperature. Steam utilization in gasification process caused an increase in the amount of gas product and higher H_2/CO ratio as compared to pyrolysis in 100% N_2. Steam gasification at 750 °C by using calcined limestone generated the least tar emission of 3.23% and the highest cold gas efficiency of 79.61%, while calcined waste concrete gave reasonably high cold gas efficiency of 68.46% but with moderately higher tar emission of 9.62%. A mixture of 50:50 wt% of calcined limestone and calcined waste concrete was proved to be most advantageous for providing high cold gas efficiency (75.88% LHV) and longer physical durability than the use of calcined limestone alone. However, the use of only waste concrete as a bed material may be an attractive choice, considering its solving disposal problem and yet reasonably effective in the steam gasification process.

Acknowledgements

This project was supported by The Graduate School of BASE, Tokyo University of Agriculture and Technology. We also acknowledge the financial support from the Royal Golden Jubilee Program (RGJ) of Thailand Research Fund (TRF) in the form of scholarship to PW.

References

Baratieri, M., Baggio, P., Fiori, L., Grigiante, M., 2008. Biomass as an energy source: thermodynamic constraints on the performance of the conversion process. Bioresour. Technol. 99, 7063–7073.

Devi, L., Ptasinski, K.J., Janssen, F.J.J.G., 2003. A review of the primary measures for tar elimination in biomass gasification processes. Biomass Bioenergy 24, 125–140.

El-Rub, Z., Bramer, E., Brem, G., 2004. Review of catalysts for tar elimination in biomass gasification processes. Ind. Eng. Chem. Res. 43, 6911–6919.

Florin, N.H., Harris, A.T., 2006. Hydrogen production from biomass coupled with carbon dioxide capture: the implications of thermodynamic equilibrium. Int. J. Hydrogen Energy 31, 945–952.

Florin, N.H., Harris, A.T., 2008. Enhanced hydrogen production from biomass with in situ carbon dioxide capture using calcium oxide sorbents. Chem. Eng. Sci. 63, 287–316.

Franco, C., Pinto, F., Gulyurtlu, I., Cabrita, I., 2003. The study of reactions influencing the biomass steam gasification process. Fuel 82, 835–842.

Han, J., Kim, H., 2008. The reduction and control technology of tar during biomass gasification/pyrolysis: an overview. Renew. Sust. Energy Rev. 12, 397–416.

Haykiri-Acma, H., Yaman, S., 2008. Thermal reactivity of rapeseed (*Brassica napus* L.) under different gas atmospheres. Bioresour. Technol. 99, 237–242.

Hu, G., Xu, S., Li, S., Xiao, C., Liu, S., 2006. Steam gasification of apricot stones with olivine and dolomite as downstream catalysts. Fuel Process. Technol. 87 (5), 375–382.

Hughes, R.W., Lu, D.Y., Anthony, E.J., Macchi, A., 2005. Design, process simulation and construction of an atmospheric dual fluidized bed combustion system for in situ CO_2 capture using high-temperature sorbents. Fuel Process. Technol. 86, 1523–1531.

Ito, K., Moritomi, H., Yoshiie, R., Uemiya, S., Nishimura, M., 2003. Tar capture effect of porous particles for biomass fuel under pyrolysis conditions. J. Chem. Eng. Jpn. 36 (7), 840–845.

Lin, S., Suzuki, Y., Hatano, H., Harada, M., 2002. Developing an innovative method, HyPr-RING, to produce hydrogen from hydrocarbons. Energy Convers. Manage. 43, 1283–1290.

Lin, S., Suzuki, Y., Hatano, H., Harada, M., 2003. Hydrogen production from heavy oil in the presence of calcium hydroxide. Fuel 82, 561–567.

Lin, S., Suzuki, Y., Hatano, H., Harada, M., 2006. Continuous experiment regarding hydrogen production by Coal/CaO reaction with steam(II) solid formation. Fuel 85, 1143–1150.

Mahishi, M., Goswami, D., 2007. An experimental study of hydrogen production by gasification of biomass in the presence of a CO_2 sorbent. Int. J. Hydrogen Energy 32, 2803–2808.

McKendry, P., 2002. Energy production from biomass (part 3): gasification technologies. Bioresour. Technol. 83, 55–63.

Mindess, S., Young, J.F., Darwin, D., 2003. Concrete, second ed. Prentice Hall, United State of America.

Rapagná, S., Jand, N., Kiennemann, A., Foscolo, P., 2000. Steam gasification of biomass in a fluidized-bed of olivine particles. Biomass Bioenergy 19, 187–197.

Rapagná, S., Provendier, H., Petit, C., Kiennemann, A., Foscolo, P., 2002. Development of catalysts suitable for hydrogen or syn-gas production from biomass gasification. Biomass Bioenergy 22, 377–388.

Ross, D., Noda, R., Horio, M., Kosminski, A., Ashman, P., Mullinger, P., 2007. Axial gas profiles in a bubbling fluidized bed biomass gasifier. Fuel 86, 1417–1429.

Saxena, R.C., Seal, D., Kumar, S., Goyal, H.B., 2008. Thermo-chemical routes for hydrogen rich gas from biomass: a review. Renew. Sust. Energy Rev. 12, 1909–1927.

Simell, P., Kurkela, E., 1997. Tar Removal from Gasification Gas in Biomass Gasification and Pyrolysis. CPL Press.

Simell, P., Leppalahti, J., Bredenberg, J., 1992. Catalytic purification of tarry fuel gas with carbonate rocks and ferrous materials. Fuel 71, 211–218.

Sutton, D., Kelleher, B., Ross, J., 2001. Review of literature on catalysts for biomass gasification. Fuel Process. Technol. 73, 155–173.

Taralas, G., Kontominas, M., 2006. Pyrolysis of solid residues commencing from the olive oil food industry for potential hydrogen production. J. Anal. Appl. Pyrolysis 76, 109–116.

Wang, Y., Yoshikawa, K., Namioka, T., Hashimoto, Y., 2007. Performance optimization of two-staged gasification system for woody biomass. Fuel Process. Technol. 88, 243–250.

Wei, L., Xu, S., Zhang, L., Liu, C., Zhu, H., Liu, S., 2007. Steam gasification of biomass for hydrogen-rich gas in a free-fall reactor. Int. J. Hydrogen Energy 32, 24–31.

Xu, G., Murakami, T., Suda, T., Kusama, S., Fujimori, T., 2005. Distinctive effects of CaO additive on atmospheric gasification of biomass at different temperatures. Ind. Eng. Chem. Res. 44, 5864–5868.

BIOGRAPHY

Miss Piyarat Weerachanchai was born on the 23rd of June 1981 in Muang District, Trang Province, Thailand. After completing her high school education from Kantangpittayakorn school, Trang, she moved to Nakhon Ratchasima for her undergraduate degree. She earned her Bachelor's degree in Chemical Engineering with second class honor from Suranaree University of Technology (SUT), Nakhon Ratchasima, in 2003. She has been awarded the Royal Golden Jubilee scholarship (RGJ) from the Thailand Research Fund (TRF) to study the Doctor of Philosophy (Ph.D.) Program in Chemical Engineering at SUT since the year 2003.